Universidade do Algarve

Faculdade de Ciências do Mar e do Ambiente

Functional analysis of bone related Gla proteins from bony fish during skeletal development

Paulo Jorge Travessa Gavaia

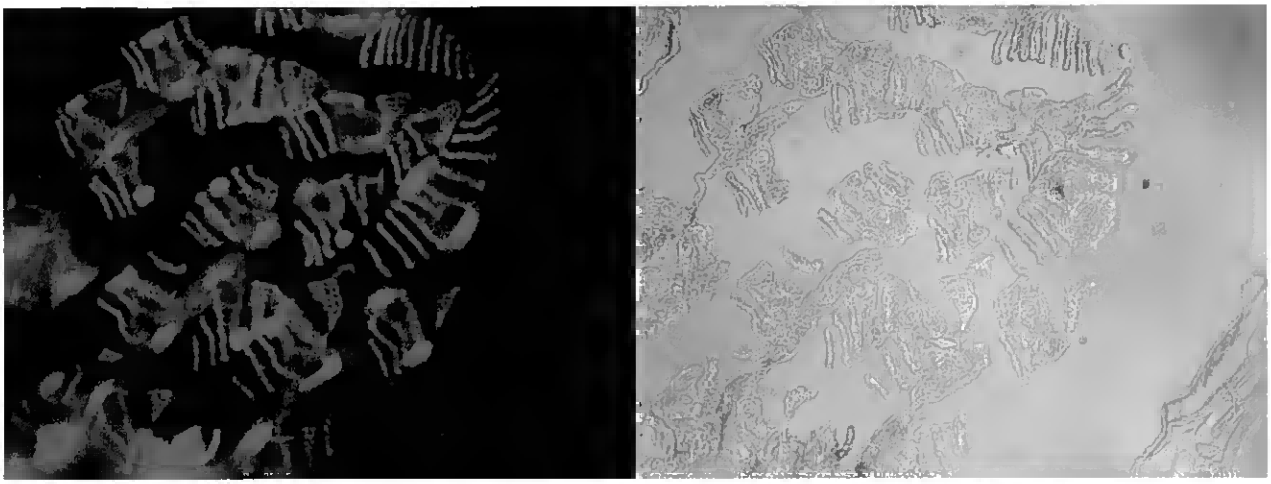

Faro, 2005

Universidade do Algarve

Faculdade de Ciências do Mar e do Ambiente

Functional analysis of bone related Gla proteins from bony fish during skeletal development

Paulo Jorge Travessa Gavaia

Dissertation presented at the University of Algarve, Portugal, to obtain the degree of Doctor in Biology, Area of Molecular Biology

Faro, 2005

The content of this dissertation is of the exclusive responsibility of the author

Paulo Jorge Travessa Gavaia

AGRADECIMENTOS

À Prof. Leonor Cancela, que foi a orientadora desta tese, por me ter transmitido todos os conhecimentos científicos, pelo apoio prestado ao longo da realização desta tese e pela amizade demonstrada.

À Dra Carmen Sarasquete Reiriz, directora do ICMAN-CSIC e minha orientadora externa por me ter proporcionado a oportunidade de realizar parte das experiências desta tese, por todos os ensinamentos na área da histologia e pela amizade que mantemos.

À Prof. Maria Teresa Dinis, cujos ensinamentos me motivaram a trabalhar na área da Aquacultura e por ter proporcionado a possibilidade de trabalhar em linguado.

Ao Dr. Robert Kelsh por me ter acolhido no seu laboratório e por todos os ensinamentos transmitidos na área da hibridação in situ.

Aos colegas de laboratório com quem iniciei a minha carreira científica, Eduardo Lopes, Nuno Henriques, J.P. Reia e Jorge Pinto com quem partilhei momentos inesquecíveis à descoberta das maravilhas do mundo da Biologia Molecular.

À Dra Dina Simes por me ter apoiado ao longo da realização de esta tese, por me ter cedido anti-corpos essenciais à realização do presente trabalho e por toda a amizade.

À Carla Viegas por toda a ajuda preciosa, sem a qual teria sido impossível realizar algumas experiências.

Aos meus colegas de laboratório com quem tenho partilhado estes últimos anos, Vincent Laize, Natércia Conceição, Ricardo Leite, Ricardo Afonso, António Pombinho, Juan Bosco, Sara Mira, Sandra Marques, Vera Fonseca, Susana Domingues e a todos os outros que de algum modo colaboraram directa ou indirectamente na realização deste trabalho.

A todos os meus colegas de trabalho do ICMAN, em especial à Isabel Viaña, José Luís Palazón e Eduardo Cargnin Ferreira de quem adquiri importantes conhecimentos na área da histologia e com quem partilhei agradáveis momentos.

Aos membros do grupo de Aquacultura da Universidade do Algarve pela preciosa ajuda e pelo material biológico cedido durante a realização de esta tese.

Aos meus amigos e colegas de curso que me acompanharam e apoiaram nos bons e maus momentos, dando-me força e estimulo para seguir em frente o meu trabalho.

Aos meus pais, pelo seu apoio e carinho demonstrados desde sempre.

À Elsa que me tem acompanhado e com quem partilho todos os meus momentos.

A realização deste trabalho teve o financiamento da Fundação para a Ciência e a Tecnologia, através da atribuição da bolsa de doutoramento PRAXIS XXI/ BD/19665/99.

Resumo

As proteinas dependentes da vitamina K, proteina Gla do osso (BGP ou osteocalcina) e proteina Gla da matriz (MGP) são pequenas proteinas que ligam o cálcio, tendo sido recentemente descobertas em peixe. Neste trabalho são descritas pela primeira vez as sequências dos ADNs complementares para as BGPs e as MGPs de peixe zebra (*Danio rerio*) e linguado (*Solea senegalensis*). Os padrões de expressão e acumulação destas proteinas foram investigados ao longo do desenvolvimento destes peixes, com particular interesse na altura da metamorfose do linguado. Em peixe zebra detectou-se a expressão e de *bgp* e *mgp* em todos os tecidos calcificados ou em calcificação, incluindo osso e a cartilagem calcificada dos arcos branquiais. Esta expressão foi confirmada através de RT-PCR e de PCR em tempo real em espécimes da mesma idade e estado de desenvolvimento. Em linguado verificou-se um acentuado aumento de expressão de BGP e MGP durante a metamorfose em paralelo com o desenvovimento de estruturas axiais e aumento de calcificação do esqueleto. A imunolocalização da BGP e da MGP revelou que estas proteinas se acumulam principalmente na matrix de estruturas calcificadas ou em calcificação, confirmando os resultados obtidos por hibridação *in situ*. Em contraste com o observado para outros peixes marinhos, em linguado e no peixe zebra a MGP apenas se acumula nos tecidos calcificados de forma semelhante ao descrito para mamíferos. Estes resultados sugerem diferenças nos padrões de acumulação de MGP entre peixes marinhos e de peixes de água doce. Através do uso do antagonista da vitamina K, a warfarina, pudemos observar a formação de calcificações ectopicas nos sistemas arteriais de peixe zebra e de charroco, à semelhança do observado para mamíferos. Estes resultados sugerem uma conservação da função da MGP entre peixes e mamíferos. De um ponto de vista evolutivo, estes resultados indicam que o peixe zebra se adequa como modelo para estudos de expressão genética da MGP e para determinar a sua função.

Foram investigados os padrões de desenvolvimento esquelético de peixe zebra e linguado através de coloração do esqueleto com azul de alcian e vermelho de alizarina. A avaliação da ocurrência de malformações em linguado, revelou um elevado número de malformações, que afectam 44% dos indivíduos em particular na coluna vertebral e no

complexo caudal. As causas para estas deformações não foram aqui estudadas, embora as elevadas incidências possam revelar problemas nas condições de cultivo ou na dieta.

Abstract

The vitamin K dependent bone Gla protein (BGP or osteocalcin) and matrix Gla protein (MGP) are small calcium binding proteins only recently discovered in fish. In this study we cloned for the first time the cDNAs for BGP and MGP of zebrafish (*Danio rerio*) and Senegal sole (*Solea senegalensis*) and investigated the tissue distribution and accumulation of BGP and MGP during larval development and in adult tissues of the zebrafish and throughout metamorphosis in Senegal sole. In zebrafish, the presence of *bgp* and *mgp* mRNA was revealed by *in situ* hybridization in all mineralized tissues during and after calcification, including bone and the calcified cartilage of branchial arches. This expression was confirmed by Real Time PCR in specimens of same age and developmental stages. Immunolocalization of BGP and MGP demonstrated that these proteins accumulate mainly in the matrix of skeletal structures already calcified or in the process of calcifying, confirming *in situ* hybridization results. Results obtained in Senegal sole further indicate that, during metamorphosis, there is an increase in expression of both *bgp* and *mgp*, in parallel with the calcification of axial skeleton structures. In contrast with results obtained for previously studied marine fishes, in sole as in the fresh water zebrafish, MGP accumulates in both calcified tissues and in vessel walls of the vascular system, as also seen previously in higher vertebrates. These results suggest a major difference in the pattern of MGP accumulation between marine and freshwater fishes, the latter being more reminiscent of those results obtained in mammals. Furthermore we were able to induce vascular calcification by treating zebrafish and toadfish with the vitamin K antagonist warfarin, obtaining results similar to the observed in mammalian system. From an evolutionary point of view, these results further indicate that zebrafish is a suitable model to conduct studies on *mgp* gene expression and function.

The normal skeletal development was followed in zebrafish and Senegal sole developmental stages by skeletal staining with alcian blue and alizarin red. An evaluation of the occurrence of skeletal malformations in Senegal sole revealed a high number of malformations with 44% of the individuals presenting malformations particularly in the caudal region and in the vertebral column. The causes for these malformations were not identified in this study, but the high incidence of malformations may reflect culture

problems due to rearing and/or feeding conditions that may affect the normal skeletal development.

Index

INTRODUCTION

MATERIALS AND METHODS

RESULTS

D- DISCUSSION

INTRODUCTION

Introduction

I1- General introduction

Since the discovery of bone Gla protein (BGP or osteocalcin) in 1976 and later matrix Gla protein (MGP) in 1985, a great effort has been done by the scientific community to characterize and understand the functions these proteins have in the skeleton as well as the mechanisms that regulate them. In the last decade, and in addition to results obtained in the classical mammalian systems, BGP and MGP have been purified from various teleost and cartilaginous fishes. Both amino acid and nucleotide sequences were obtained, providing the molecular tools to further investigate the patterns of expression and accumulation and to understand the functions that these calcium binding proteins exert in fish skeletal and vascular systems. Based on the existing information, the current information regarding BGP and MGP are overviewed in this introduction, with special interest on its regulation, expression and accumulation patterns. The current knowledge on the development of cartilaginous and bony structures in the fish skeleton will also be introduced.

I2- Vitamin K-dependent proteins

The family of gamma-carboxyglutamic acid (Gla) containing, vitamin K-dependent proteins is composed by three main groups (see table 1) comprising: 1) the proteins involved in blood coagulation, ,clotting factors II (prothrombin), VII, IX and X and plasma proteins C,S and Z; 2): those originally isolated from bone and cartilage, bone Gla protein (BGP) also called osteocalcin and matrix Gla protein (MGP); and 3) a group of less studied proteins including the vitamin K-dependent gamma-carboxylase.

Vitamin K was discovered by Dam in the 1930´s by finding that the hemorrhagic syndrome observed in chicks feed lipid free diets was associated with lower prothrombin activity and a reduction in the synthesis of factors VII, IX and X. It was later demonstrated that vitamin K is a cofactor for the hepatic vitamin k-dependent gamma-

glutamyl carboxylase, in the the post-translational conversion of the precursors of vitamin k-dependent proteins to their active forms (Suttie, 1990, Liu *et al.,* 1996, Vermeer and Braam, 2001). In fact the only known function of vitamin K is that it serves as a cofactor for gamma-glutamyl carboxylase promoting the conversion of selective protein-bound glutamate residues into gamma-carboxy glutamate (Gla) (Vermeer and Braam, 2001).

The first indications for vitamin K-dependent proteins involvement in bone metabolism came from the observation that babies born from women who had been treated with vitamin K antagonists during the first trimester of pregnancy displayed a serious bone malformation known as chondrodysplasia punctata or fetal warfarin syndrome (Pettifor and Benson, 1975). This deformity is characterized by hypoplasias of the nasal bridge and distal phalanges, ectopical calcifications in the growth plate and excessive bone calcifications (Pettifor and Benson, 1975, Vermeer and Braam, 2001; Simes, 2002).

The vitamin K-dependent gamma-glutamyl carboxylase is a microsomal enzyme which catalyzes the posttranslational conversion of glutamyl to gamma-carboxylglutamyl residues (Liu *et al.,* 1996) (see figure I1). The carboxylation reaction is vitamin K dependent and in the absence of vitamin K or in the presence of a vitamin K antagonist (e.g. warfarin) carboxylation *in vivo* is impaired (Suttie, 1985, Liu *et al.,* 1996) and it has also been observed that calcium binding capacity is altered with the degree of carboxylation (Poser and Price, 1979; Vermeer *et al.,* 1984). This reduction of activity is due to the discovery that the carboxylase also carboxylates itself in a reaction dependent on vitamin K (Berkner and Pudota, 1998). The presence of Gla residues has been associated with the ability of vitamin k-dependent proteins to bind divalent cations, hidoxyapatite and acid phospholipids (Vermeer, 1984, 1990; Lim *et al.,* 1977). The binding to mineral and mineral ions is mediated by the gamma-carboxylated glutamic acid residues, conferring the specific activity to the protein, since carboxylation affects their Ca^{2+}-mediated interaction with phospholipid bilayers (Berkner and Pudota, 1998).

From the identification of the cDNA sequences for these vitamin K-dependent proteins and comparative sequence analysis a homologous peptide was discovered, which is not observed in noncarboxylated proteins, and that subsequently was shown by mutation analysis to be a recognition sequence for the carboxylase (Jorgensen *et al.,*

1987). In most cases, this peptide is a propeptide that is cleaved from the vitamin K-dependent proteins while they follow their secretion pathway. There is also a limited amount of homology among the vitamin K-dependent proteins within the Gla domain, with a high conservation for clotting factors VII, IX, X, and proteins S, C, Z, prothrombin, and gas6 whereas MGP and BGP are more divergent (Berkner and Pudota, 1998). With the exception of MGP, all known vitamin K-dependent vertebrate proteins are initially synthesized as preproproteins. The hydrophobic prepeptide, or signal peptide, is cleaved during or shortly after protein translocation into the cisternae of the endoplasmic reticulum and the propeptide that is targeted to the carboxylase by a high-affinity carboxylase-binding site is removed after gamma-glutamyl carboxylation in the endoplasmic reticulum and prior to secretion. MGP is initially synthesized as a preprotein with a signal peptide, but the sequence corresponding to the propeptide is not removed prior to secretion (Engelke *et al.*, 1991; Rishavy *et al.*, 2004). In all Gla proteins, the carboxylase recognition sequence is adjacent to the vitamin K-dependent Gla domain and full carboxylation results in Ca^{2+}-binding by the Gla residues rendering the vitamin K-dependent proteins active in several different functions that include hemostasis, apoptosis, phagocytosis, signal transduction, and Ca^{2+} homeostasis (Rishavy *et al.*, 2004).

Table II- Resumed information concerning vitamin K dependent proteins previously described in mammals. All the information refers to mammals unless indicated otherwise.

Protein	Function(s)	Sites of expression	Number of Gla	Tissues of accumulation	References
BGP	Negative regulator of bone formation; maturation of hydroxyapatite crystals.	Bone, blood platelets, tooth	3	Calcified skeletal tissues, renal calculi, blood plasma.	Poser and Price,1979; Price *et al.*, 1977, 1983; Nishimoto *et al.*, 1992; Huq *et al.*, 1987; Cancela *et al.*, 1995; Shanahan *et al.*, 1999, 2000;
MGP	Inhibition of tissue calcification; modulation of BMP signaling	heart, kidney, liver, lung, cartilage, arterial walls (VSMC, macrophages)	5 [a]	Calcified tissues(bone, dentin, cartilage), plasma, atherosclerotic plates	Price *et al.*, 1985, 2002; Shanahan *et al.*, 1999, 2000; Luo *et al.*, 1995; Fraser and Price, 1988; Cancela *et al.*, 2001; Loeser *et al.*, 2001; Newman *et al.*, 2001; Hale *et al.*, 1988; Canfield *et al.*, 2000; Pinto *et al.*, 2003; Simes *et al.*, 2003.
Nephrocalcin	Inhibitor of calcium oxalate crystal formation	Kidney	2-3	Kidney, renal calculi	Nakagawa *et al.*, 1983, 1987, 1991; McKee *et al.*, 1995
Prothrombin	Blood coagulation; activation of factor IX	Liver	10	Blood plasma	Furie and Furie, 1988; Di Scipio *et al.*, 1977; Dowd *et al.*, 1995; Bajaj *et al.*, 1982; Bristol *et al.*, 1996)
Factor VII	Blood coagulation; activation of factor IX	Liver	10	Blood plasma	Furie and Furie, 1988; Larson *et al.*, 1996
Factor IX	Blood coagulation; convert prothrombin to thrombin; activation of factor X	Liver	12	Blood plasma	Di Scipio *et al.*, 1977; Furie and Furie, 1988; Larson *et al.*, 1996; Sommer *et al.*, 1994.
Factor X	Blood coagulation; convert prothrombin to thrombin	Liver	11	Blood plasma	Furie and Furie, 1988; Salte and Norberg, 1991

Table I1-continued

Protein Z	Coagulation	Liver	13	Plasma	Gundberg and Nishimoto, 1999; Yin *et al.*, 2000; Tabatabai *et al.*, 2001
Protein C	Anticoagulation	Liver	11	Blood	Furie and Furie, 1988; Suzuki, 1990; Stenflo *et al.*, 1990
Protein S	Anticoagulation, bone turnover	Liver, endothelial cells, brain, spleen, bone matrix	10	Blood plasma, cartilage, bone.	Di Scipio *et al.*, 1977; De Fouw *et al.*, 1986; Furie and Furie, 1988; Suzuki, 1990; Benzakour and Kanthou, 2000
PRGP1	Signal transduction	Spinal chord	12	Spinal chord	Kulman *et al.*, 1997, 2001
PRGP2	Signal transduction	Thyroid	9	Thyroid	Kulman *et al.*, 1997, 2001
TMG3	Signal transduction	Widespread	13	Skeletal muscle, heart	Kulman *et al.*, 2001
TMG4	Signal transduction	Widespread	9	Skeletal muscle, heart	Kulman *et al.*, 2001
Gas6	Cell growth and survival, growth factor,	VSMC, heart, liver, kidney, lung, cartilage	11-12	heart, liver, kidney, lung, cartilage, VSMC	Manfioletti *et al.*, 1993; Nakano *et al.*, 1995; Stitt *et al.*, 1995; Yanagita *et al.*, 2002
γ-glutamyl carboxylase	carboxylation of vitamin K-dependent proteins	Liver and other tissues	3	Endoplasmatic reticulum	Berkner and Pudota, 1998; Berkner, 2000; Wu *et al.*, 2001; Pudota *et al.*, 2001; Rishavy *et al.*, 2004

[a]- One of the five Gla residues in *Mus musculus* MGP is not conserved (Ikeda, *et al.*, 1991). Shark and teleost MGPs have only four Gla residues (Rice *et al.*, 1994; Simes *et al.*, 2003)

I3- Discovery and Purification of BGP

BGP was first purified from bovine bone by Price *et al.,* (1976a) and soon after, the primary structure of this protein was established by amino acid sequencing, revealing a 49 amino acid protein with three Gla residues located at positions 17, 21 and 24 and responsible for binding interactions with hydroxyapatite crystals.. It was also recognized a disulfide bond between two cystein residues and a proline rich sequence (Price *et al.,* 1976a, b). After this first identification, the potential involvement of BGP in calcium regulation and skeletal homeostasis was immediately recognized (Price *et al.,* 1981) and the protein was purified from several other vertebrate species ranging from human to fish indicating a conserved localization throughout evolution.

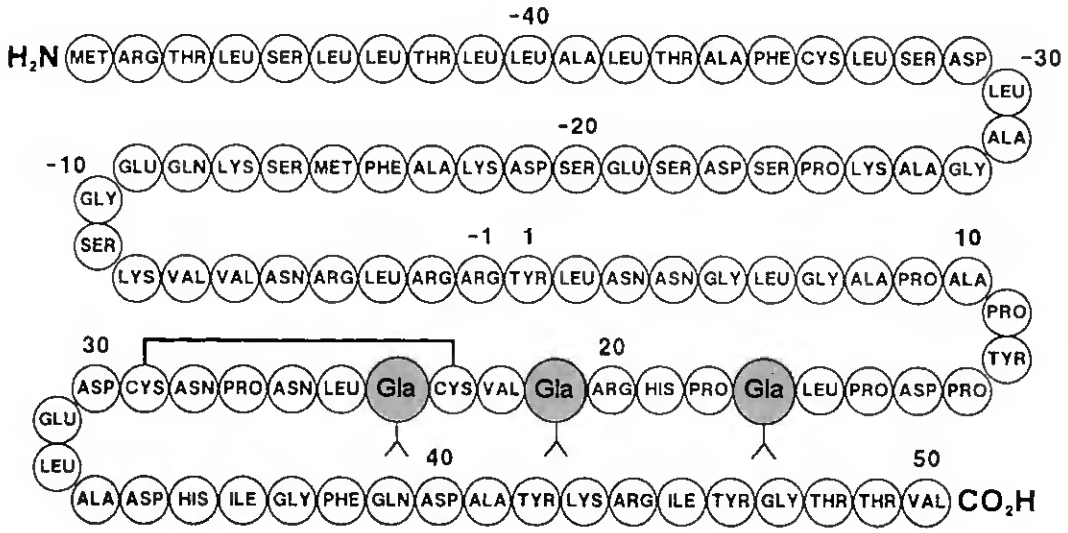

Figure I1- Amino acid sequence of the rat prepro bone Gla protein. The mature protein starts at position 1 and the propeptide ends at -1 (indicate in figure and in legend location of pre and propeptides). The residues marked in gray represent γ-carboxyglutamic acid. The solid line represents the disulfide-bond between Cys_{23} and Cys_{29}. Predicted amino acid sequence according to nucleotide sequence analysis (Pan and Price, 1985). (Modified after Price,1992).

I4-Discovery and purification of BGP in lower vertebrates

The presence of BGP in teleost fish has been known since Price et al (1977) first isolated BGP from the scales of swordfish and obtained the amino acid sequence (see Table I2 for summary of known BGP sequences). Other BGP amino acid sequences were obtained later from bluegill (Nishimoto *et al.,* 1992) and gilthead seabream (Cancela *et al.,* 1995). More recently the cDNA sequences for gilthead seabream and *Argirosomus regius* were obtained by reverse transcription- polymerase chain reaction (RT-PCR) of total RNA isolated from bone and branchial arches (Pinto *et al.,* 2001; Simes *et al.,* 2003).

Table I2- Summary of all known BGP sequences available and the bibliographic references where these sequences can be found.

Scientific name	(common name)	Accession	References
Rattus norvegicus	(Norway rat)	M25490	Pan and Price, 1985
Mus musculus	(house mouse)	L24429-31	Celeste *et al.*, 1986
Capra hircus	(goat)	1005180A	Huq *et al.*, 1984
Ovis aries	(sheep)	1010264A	Mende *et al.*, 1984
Bos taurus	(domestic cattle)	NM_174249	Price *et al.*, 1976a, Kiefer *et al.*, 1990
Sus scrofa	(pig)	AY129956	Huq *et al.*, 1984
Canis familiaris	(domestic dog)	AF205942	Colombo *et al.*, 1993
Felis catus	(domestic cat)	P02821	Shimomura *et al.*, 1984
Equus caballus	(horse)	P83005	
Homo sapiens	(Human)	X04143	Poser *et al.*, 1980, Kiefer *et al.*, 1988
Macaca fascicularis	(crab-eating macaque)	P02819	Hauschka *et al.*, 1982
Oryctolagus cuniculus	(European rabbit)	P39056	Virdi *et al.*, 1991
Setonix sp.	(wallaby)	1005180C	Huq *et al.*, 1984
Gallus gallus	(chicken)	U10578	Carr *et al.*, 1981, Neugebauer *et al.*, 1995
Dromaius novaehollandiae	(emu)	P15504	Huq *et al.*, 1987
Xenopus laevis	(African clawed frog)	AY043179	Cancela *et al.*, 1995; Viegas *et al.*, 2001
Rana catesbeiana	(bullfrog)	AB115667	Dohi *et al.*, 2004
Danio rerio	(zebrafish)	AY078413	Present study
Cyprinus carpio	(common carp)	A59458	PIR accession number.
Halobatrachus didactylus	(toadfish)	AF144707	Laizé *et al.*, 2005
Oncorhynchus mykiss	(rainbow trout)	AY233378	Laizé *et al.*, 2005
Solea senegalensis	(Senegal sole)	AF059349	Present study
Tetraodon nigroviridis	(green pufferfish)		Nishimoto *et al.*, 2003
Takifugu rubripes	(torafugu)		Nishimoto *et al.*, 2003
Argyrosomus regius	(meagre)	AF459030	Simes *et al.*, 2003
Sparus aurata	(gilthead seabream)	AF289506	Cancela *et al.*, 1995; Pinto *et al.*, 2001,
Lepomis macrochirus	(bluegill)	P28317 b	Nishimoto *et al.*, 1992
Xiphias gladius	(swordfish)	P02823 b	Price *et al.*, 1977
Oreochromis niloticus	(Nile tilapia)	AY294644	Laizé *et al.*, 2005

The BGP cDNA sequences for amphibians have also been recently described for xenopus (Viegas *et al.*,2002) and bullfrog (Dohi *et al.*, 2004). Interestingly, for bullfrog BGP two diferent mature protein forms were found, described as P-1 and P-2. These two forms have the same secondary structure except for P-2 lacking the four N-terminal amino acids (Dohi *et al.*, 2004). BGP is typically about 45-50 residues in length and presents a high degree of sequence homology throughout all the *taxon* with a strict conservation of position for Gla and cysteine residues (Laizé *et al.*, 2005). The BGP primary structure shows a large degree of conservation from fish to man, with amphibian BGPs being closer to mammalian than to fish sequences (Cancela *et al.*, 1995; Pinto *et al.*, 2001; Simes *et al.*, 2003; Viegas *et al.*, 2002; Dohi *et al.*, 2004).

I5- BGP in serum

The presence of BGP in blood plasma was initialy detected by radioimmunoassay in human and bovine using an antibody developed in rabbit against the COOH-terminal region of calf BGP (Price and Nishimoto, 1980). The reported presence of a protein with the same properties as the intact bone BGP suggested the possibility that this serum BGP originated from bone remodeling. However, it was later determined that the origin of serum BGP is from new cellular synthesis and not from the release of protein by bone matrix resorption. This fact was proven by analyzing the serum BGP of warfarin injected rats and verifying that, within 3 hours, serum BGP was mostly decarboxylated in contrast to bone BGP that was mainly γ-carboxylated, even 8 hours after treatment (Price *et al.*, 1981). Posteriorly a study by Sugiyama and Kaway (2001) proved that carboxylation of BGP is not dependent on bone turnover by determining the negative correlation of serum carboxylated BGP with serum bone formation markers.

The fact that BGP is a marker for osteoblastic proliferation and function makes the determination of serum BGP concentration a diagnostic tool for bone formation, with clinical relevance, reflecting bone formation at the systemic level (Sabatakos *et al.*, 2000). Following biosynthesis and cellular secretion, most of the BGP is bound to bone matrix hydroxyapatite, but about 20% of this *de novo* produced protein is released into the blood stream and is therefore available for detection by immunological techniques

(Knapen *et al.,* 1996). In addition, since the amino acid sequence of human BGP was determined, evidence for incomplete BGP γ-carboxylation (Poser *et al.,* 1980) was reported. Later, through N-terminal protein sequence analysis of the methyl-esterified protein, that allows the measurement of the percentage of γ-carboxylation at each glutamate residue, it was found that human BGP is incompletely γ-carboxylated (67 ±14%) in the Glu residue at position 17 (Cairns *et al.,* 1994). BGP appears both in normal form with the 3 Gla residues fully γ-carboxylated or with undercarboxylation of the Gla residue at position 17 (Poser *et al.,* 1980; Cairns *et al.,* 1994). Other studies showed that postmenopausal woman with lowest levels of plasma BGP hydroxyapatite binding activity have decreased bone mineral density in hip bones and are six times more likely to suffer subsequent osteoporotic fractures than postmenopausal woman with the highest plasma BGP binding activity, suggesting incomplete γ-carboxylation of BGP. To further support these findings, vitamin K supplementation was shown to restore normal hydroxyapatite binding activity to plasma BGP in these postmenopausal woman (Szulc *et al.,* 1993; Cairns *et al.,* 1994). This study showed that serum levels of decarboxylated BGP are a reliable indicator of the severity of osteoporosis in postmenopausal women (Szulc *et al.,* 1996) and supports the hypothesis proposed by Murshed *et al.* (2004) that similarly to thrombin (Furie and Furie, 1988), only decarboxylated BGP may have a diagnostic function.

I6- BGP in bone matrix

BGP is referred as being synthesized and secreted only by osteoblastic cells in late stages of bone maturation and mineralization, and is considered to be an indicator of osteoblast differentiation (Bortell *et al.,* 1993; Boguslawski *et al.,* 2000). It is the most abundant non-collagenous protein of bone extracellular matrix and is found essentially in mineralized bone matrix and dentine (Price, 1987, Price, 1990), being synthesized only by osteoblasts in bone, and cementoblasts and odontoblasts in tooth (Bronckers *et al.,* 1985, 1994, 1998; Price, 1990; Ducy and Karsenty, 1995; Ducy, *et al.,* 1996). In higher vertebrate models, BGP developmental appearance was first detected with the onset of mineralization, with an increase in protein synthesis during skeletal growth, in

concomitance with hydroxyapatite deposition (Hauschka and Reid, 1978; Lian *et al.*, 1982). Previous studies carried out in mammals reported that Bgp appears to be absent during early stages of osteoblast maturation, being undetectable in undifferentiated or recently differentiated osteoblasts near the growth plate but clearly detectable in mature osteoblasts (Mark *et al.*, 1988; Ikeda *et al.*, 1992; Liu *et al.*, 1994). Likewise, studies of the accumulation of Bgp protein in osteoblastic cells by immunolabeling could only detect this protein in cuboidal cells with a clear osteoblastic phenotype (Liu *et al.*, 1994)

The orientation of BGP binding to the bone mineral has been investigated by NMR spectroscopy (Dowd *et al.*, 2003). According to this study, the C-terminal pentapeptide (FYGPV in bovine BGP) is extending outward becoming accessible to neighboring cells. The carboxy terminus of BGP possesses chemotactic activity and the outward orientation allows it to carry out recruitment and signal transduction functions through binding to cell surface receptors on osteoclasts and osteoblasts (Dowd *et al.*, 2003; Hoang *et al.*, 2003). The calcium binding domain, comprising the three Gla residues at positions 17, 21 and 24, would project from the same face of the helical turns and be exposed to the calcified surface (Dowd *et al.*, 2003). Recent evidences for a BGP mediated modulation of hydroxyapatite crystal morphology and growth come from the identification of pig BGP structure since it was observed that it exists an excellent surface complementarity between the Ca^{2+} coordinating surface of BGP and the prism face of hydroxyapatite, suggesting that BGP may show selective binding characteristics to hydroxyapatite (Hoang *et al.*, 2003).

I7- Function of BGP

The evolutionnary conservation of BGP primary and tridimensional structure, in particular the calcium binding Gla containing motif, indicates that this protein has an important metabolic role in the matrix of calcified tissues. However, despite the large amount of information gathered since BGP was first discovered and the increasing number of known sequences for different species, its molecular mechanism of action in bone still remains uncompletely understood..

The most prominent in vitro properties of BGP are its affinity for hydroxyapatite and its ability to retard the crystallization of hydroxyapatite from supersaturated solutions of calcium phosphate (Price *et al.*, 1976a, Price, 1984, 1985) indicating a regulation of the rate of apatite crystal growth in solution (Romberg, *et al.*, 1986; Hunter *et al.*, 1996). These mineral binding properties are lost once γ-carboxyglutamic acid residues are thermally decarboxylated to glutamic acid residues (Poser *et al.*, 1979). The thermal decarboxylation of BGP generates an abnormal BGP similar to that produced by animals treated with warfarin (Price, 1984).

One of the approaches to determine the function of BGP was to produce a protein functionally inactivated using the vitamin K antagonist warfarin that inhibits the γ-carboxylation of Glu residues to Gla in newly synthesized BGP and thereby reduces its affinity for hydroxyapatite and consequently its bone levels (Price and Williamson, 1981, Price and Sloper, 1983). The major drawback of this *in vivo* approach is that vitamin K deficiency causes bleeding and death since synthesis of vitamin K dependent coagulation factors is also affected (Price and Williamson, 1981). In fact the major physiological effect of vitamin K deficiency is a prolonged coagulation time, caused by undercarboxylation of Gla residues in the N-terminal region of prothrombin and coagulation factors VII, IX and X produced in liver (Price and Kaneda, 1987). In order to have only an extra-hepatic effect of warfarin and counteract its effect on coagulation, a protocol for treating rats with warfarin was developed by Price and Williamson (1981) capable of reducing BGP levels to 2% of normal without effects in coagulation (Price and Kaneda, 1987). However, this did not prevent other extrahepatic Gla proteins from being inactivated thus masking the effect resulting only from a lack of functional BGP.

The most relevant clues about BGP function came through the use of mouse genetics coupled with genetic engineering, with the obtention of BGP deficient mice (knockout), where BGP genes were deleted. These mice showed no ectopic BGP expression and no effects on the expression of other non-collagenous proteins. The mice were normal at birth, with no skeletal defects and no changes in extracellular matrix and bone mineralization were detect along development. However a progressive increase in bone mass was observed, due to an increase in osteoblastic function but not in the number of osteoblasts. In addition, an increase in the number of osteoclasts was also observed but

without a significant increase in bone resorption. These experimental data provided strong evidences for BGP to be a negative regulator of bone formation (Ducy *et al.*, 1996). Later, in another in vivo experiment using BGP knockout mice, the bone mineral was analyzed by Fourier transform infrared microspectroscopy and it was demonstrated that in these knockout animals the absence of BGP acting on mineral-binding resulted in hydroxyapatite crystals that did not form correctly and the mineral phase remained immature when compared to wild type animals that presented bigger and more perfect crystals (Boskey *et al.*, 1998), suggesting that BGP may play a role in the maturation of hydroxyapatite crystals in the bone extracellular matrix.

I8- Regulation of BGP expression

The BGP gene is know to be regulated by a high number of signaling molecules. BGP gene transcription is controlled by the combined activity of nuclear factors binding to basal promoter regions and to positive and negative promoter elements in response to physiological mediators (Bortell *et al.*, 1992). The signaling and biological effects of steroids and other related hormones, including different forms of vitamins A and D_3, are mediated through their specific receptors. These receptors are members of a large group of ligand-activated proteins that bind specific sequences in the promoter regions of target genes, acting as transcriptional activators or repressors (Gou *et al.*, 1997). There are evidences that the transcription factor tumor necrosis factor (TNF) binds to a responsive element within the human BGP promoter resulting in a down-regulating the human BGP gene (Li *et al.*, 1993).

The mouse BGP cluster is composed by three genes, two of which (OG1 and OG2) encode for BGP and their coding sequences are 96% identical. OG1 and OG2 are expressed only in osteoblasts, whereas the third gene, BGP related gene (ORG), is expressed in kidney but not in bone (Desbois *et al.*, 1994a, Ducy *et al.*, 1996). The BGP gene cluster is regulated by *cys*-acting elements in the 5' flanking region of the gene promoter that are required for osteoblast specific expression of BGP (Ducy and Karsenty, 1995) in particular two elements specific to osteoblasts identified in the region between -147 and -34 [OSE1 (-64 to -47) and OSE2 (-146 to -132)], which are essential for

expression of OG2 (Ducy and Karsenty, 1995). It was later shown that a 1.3-kb fragment of the mouse *bgp* (OG2) promoter contains all the regulatory elements necessary to confer differentiated osteoblast- and postnatal- specific expression *in vivo* (Frendo et al. 1998).

The transcription factor Cbfa1 is expressed in cells of the osteoblastic lineage during development and regulates osteoblast-specific expression of *bgp* and osteopontin, being capable of inducing osteoblastic differentiation of nonosteoblastic cells (Ducy et al. 1997, 1999). In vitro studies revealed that Cbfa1 binds to OSE2-like elements in the promoter regions of BGP, α1(1) collagen, bone sialoprotein, and osteopontin genes, while enhancing the expression of levels of these genes (Ducy *et al.,* 1997; Komori *et al.,* 1997; Hoshi *et al.,* 1999). Further investigations using Cbfa1-deficient mice showed that *bgp* expression is decreased along with impaired osteoblastic differentiation, maturational arrest of hypertrophic chondrocytes and absence of bone formation (Ducy *et al.,* 1997; Komori *et al.,* 1997; Hoshi *et al.,* 1999; Kim *et al.,* 1999; Karsenty, 2000; Choi *et al.,* 2001). However it was shown *in vitro* that Cbfa1-deficient mice calvariae cultures, in the presence of BMP-2, had induced expression of *bgp* suggesting that other transcription factor may act over the expression of BGP under specific environments (Komori *et al.,* 1997)..

In normal diploid osteoblasts, expression of the BGP gene occurs only after cessation of proliferation, at the onset and during mineralization of the extra-cellular matrix, as reflected by transcription and mRNA accumulation in the cells and BGP protein biosynthesis (Bortell *et al.,* 1992; Gou *et al.,* 1997). In contrast, in vitro results indicate that in some cell lines, like ROS 17/ 2.8 osteosarcoma cells, BGP can be expressed during and after proliferation and in association with vitamin D3 treatment (Bortell *et al.,* 1992). In this transformed cell line, modifications in transcription factor binding at primary basal regulatory elements and in the vitamin D-responsive element (VDRE) leads to expression of BGP and other bone related genes in both proliferating and non-proliferating cells (Bortell *et al.,* 1993). The primary basal regulatory elements modified in these cells are i) the OC box that includes a CCAAT motif as a central core and ii) the TATA/ glucocorticoid-responsive element (GRE) domain. Two forms of vitamin D receptor (VDR) are present in proliferating osteoblasts but only one with lower

molecular weight is seen in osteoblasts after the down-regulation of proliferation (Bortell *et al.,* 1992; Bortell *et al.,* 1993). This down-regulation of proliferation is required to signal the induction of gene expression that is characteristic of post-proliferative stages of osteoblast differentiation (Bortell *et al.,* 1993) indicating a time and development/ dependent activation of transcriptional controling elements of osteoblast specific genes.

In human and rat, 1,25-dihydroxyvitamin D_3 (1-25 $(OH)_2D_3$) was shown to enhance BGP gene expression at three diferent levels i) transcription, ii) mRNA accumulation and iii) protein synthesis. The VDRE is a key component of steroid hormone–mediated transcriptional enhancement of the BGP gene expression, and is located between nt -466 and -437 in rat and between nt -512 and -485 in human BGP gene promoter regions (Bortell *et al.,* 1992). In contrast to the up-regulation of the BGP gene observed in human and rat, 1-25 $(OH)_2D_3$ inhibits the expression of BGP by both OG1 and OG2 genes in a concentration-dependent manner, both *in vitro* and *in vivo* (Zhang *et al.,* 1997). In addition the mouse BGP gene promoters contains a VDRE-like sequence that is inoperative due to a 2 bp substitution, when compared to rat VDRE, which abolishes VDR binding (Zhang *et al.,* 1997). This inhibition of mouse BGP was proposed to be due to an indirect effect of 1-25 $(OH)_2D_3$ by acting on a gene genetically located upstream of BGP, that abolishes binding of OSF2/Cbfa1 to OSE2, an osteoblast-specific *cis*–acting element that controls OG2 osteoblast-specific expression. The same 1-25 $(OH)_2D_3$ inhibition of BGP expression was also observed by Broess et al. (1995) in differentiated osteoblasts of chicken (Zhang *et al.,* 1997).

Molecular pathways like the cAMP-dependent protein kinase A (PKA) and protein kinase C (PKC) have been implicated in regulation of BGP expression. This regulation is made through mediation of the signaling action of molecules like cAMP, parathyroid hormone (PTH), insulin like growth factor I (IGF-I) and fibroblast growth factor (FGF), that have all been referred as having an effective activating action over the BGP promoter (Boguslawski *et al.,* 2000). It has also been found that BGP expression *in vitro* is upregulated with increasing calcium concentrations, along with Cbfa1, osteopontin and collagen I (Dvorak *et al.,* 2004). This increase can be due to Cbfa1 upregulation since BGP and osteopontin are the major genes downstream of Cbfa1 (Ducy *et al.,* 1997, 1999; Dvorak *et al.,* 2004).

In fish, there is very few data on the regulation of the BGP gene at the promoter level. It was recently shown that in zebra fish, Cbfa1 exerts a positive regulation on the zfBGP promoter, much in the same way as described for mammals. Furthermore, the mouse Cbfa1 was able to transactivate the fish BGP gene to a comparable extent as the fish Cbfa1 indicating a conservation in protein structure and function throughout evolution (Pinto *et al.*, 2005).

I9- Discovery and Purification of MGP

MGP is a 84 amino-acid protein (depending on species) with a MW of approximately 10 Kdal, that was initially purified from demineralized bovine bone powder (Price *et al.*, 1983; Price and Williamson,1985). Following this original report, MGP protein sequences and/or cDNA sequences have been identified in several other vertebrate species (for a review of all known MGP sequences consult Table I3). The MGP sequences allready available reveal a high conservation of structure observed troughout all the taxon, with particular conservation in the amino acid sequences for the phosphorilation domain, ANxF domain, Gla containing motif and disulfide bond position (Laizé *et al.*, 2005). After the discovery of MGP in bone matrix, it was later found to be present also in several cartilages including growth plate, costal tracheal cartilage, vertebral processes, nasal septum and auricular cartilage (Otawara and Price, 1986; Hale *et al.*, 1988; Fraser and Price, 1988). The protein isolated from bovine was originally described to be 79 residues in length. but later it was found that it was due to a C-terminal proteolytic cleavage and that effectively the mature protein had 84 amino acids (Price *et al.*, 1987; Kiefer *et al.*, 1988). MGP has the ability to bind mineral ions through the glutamic acid residues that have been carboxylated. Among the unique features that differentiate MGP from other vitamin K dependent proteins is the fact that MGP lacks a propeptide, having the gamma-carboxylase recognition sequence encoded within the mature protein (Price *et al.*, 1987). The absence of a propeptide in MGP shows that the gamma-carboxylation and secretion of this vitamin K-dependent protein is not directly linked to the proteolytic cleavage of a propeptide sequence (Price *et al.*, 1987).

In vivo MGP has been described to associate with the organic matrix of cartilage and bone. It has been found that MGP has little water solubility in the absence of denaturants which is a feature to be noticed given its high percentage of hydrophilic amino acids and its small size (Otawara and Price, 1986; Hale *et al.,* 1988; Price *et al.,* 1983).

Table I3- Summary of all known MGP sequences available and the bibliographic references where these sequences can be found.

Scientific name	(common name)	Accession	References
Rattus norvegicus	(Norway rat)	NM_012862	Otawara and Price, 1986
Mus musculus	(house mouse)	NM_008597	Ikeda *et al.*, 1991
Bos taurus	(domestic cattle)	NM_174707	Price *et al.*, 1994
Sus scrofa	(pig)	AF525316	Laizé *et al.*, 2005
Homo sapiens	(Human)	M55270	Kiefer *et al.*, 1988
Oryctolagus cuniculus	(European rabbit)	D21265	Sohma *et al.*, 1994
Gallus gallus	(chicken)	Y13903	Wiedemann *et al.*, 1998
Xenopus laevis	(African clawed frog)	AF234631	Cancela *et al.*, 2001
Galeorhinus galeus	(soupfin shark)	P56620 b	Rice *et al.*, 1994
Ictalurus punctatus	(channel catfish)	AF526377	Laizé *et al.*, 2005
Danio rerio	(zebrafish)	AY072811	Present study
Halobatrachus didactylus	(toadfish)	AY239015	Laizé *et al.*, 2005
Oncorhynchus mykiss	(rainbow trout)	AY182238	Laizé *et al.*, 2005
Salmo salar	(Atlantic salmon)	AY182239	Laizé *et al.*, 2005
Solea senegalensis	(Senegal sole)	AY113679	Present study
Takifugu rubripes	(torafugu)	AY112747	Laizé *et al.*, 2005
Tetraodon nigroviridis	(green pufferfish)	AF479081	Laizé *et al.*, 2005
Chilomycterus schoepfi	(striped burrfish)	AY298910	Laizé *et al.*, 2005
Argyrosomus regius	(meagre)	AF334473	Simes *et al.*, 2003
Sparus aurata	(gilthead seabream)	AY065651	Pinto *et al.*, 2003

MGP was found to be expressed in a wide variety of vertebrate tissues such as cartilage, kidney, lung, aorta, bone and tooth (Hao *et al.,* 1995; Hale *et al.,* 1988; Fraser and Price, 1988; Hashimoto *et al.,* 2001) and the cells responsible for MGP expression include osteoblasts, vascular smooth muscle cells (VSMC), chondrocytes, pneumocytes, kidney cells, fibroblasts and cementoblasts (Hale *et al.,* 1988; Fraser and Price, 1988; Fraser *et al.,* 1988; Hashimoto *et al.,* 2001; Cancela and Price, 1992; Shanahan *et al.,* 1993; Wallin *et al.,* 1999). Despite the broad range of cell types expressing MGP, it seems that only chondrocytes, endothelial cells and vascular smooth muscle cells synthesize significant levels of MGP *in vivo* (Luo *et al.,* 1997; Conceição, 2002; Simes *et al.,* 2003).

Although MGP mRNA is present in several tissues, MGP is a secreted protein and only accumulates to significant levels in the extracellular matrix of mineralized tissues including bone, cartilage, calcified cartilage and dentin (Hale *et al.,* 1988; Fraser and Price, 1988; Fraser *et al.,* 1988; Rice *et al.,* 1994; Cancela *et al.,* 2001; Hashimoto *et al.,* 2001; Simes *et al.,* 2003). Despite the low levels of MGP detected in normal blood vessels, MGP is increased in patients with atherosclerosis where it is associated with calcium and lipid in the intima (Canfield *et al.,* 2000). These findings suggested that MGP accumulates in sites of calcification and the protein produced in non calcified tissues is secreted and escapes to the plasma (Hale *et al.,* 1988; Rice *at al.*, 1994). The fact that MGP and other inhibitors of calcification are constitutively expressed in a wide range of soft tissues is consistent with the view that the prevention of calcification is an active function of soft tissues (Vermeer and Braam, 2001). During skeletogenesis, expression of the gene encoding MGP has been used as a reliable marker of the chondrogenic lineage, with osteoblasts appearing uniformly negative (Rice *et al.,* 1994; Luo *et al.,* 1995; Lawton *et al.,* 1999). In the cartilages that constitute the growth plate MGP expression was found to be associated to proliferating and hypertrophyc chondrocytes, being absent in early differentiated and maturing/early hypertrophyc chondrocytes (Luo *et al.,* 1995). In the rat, MGP was found to be present at high levels in newly formed bone at 2 days after birth, maintaining a high level of protein in bone until adulthood (Otawara and Price, 1986).

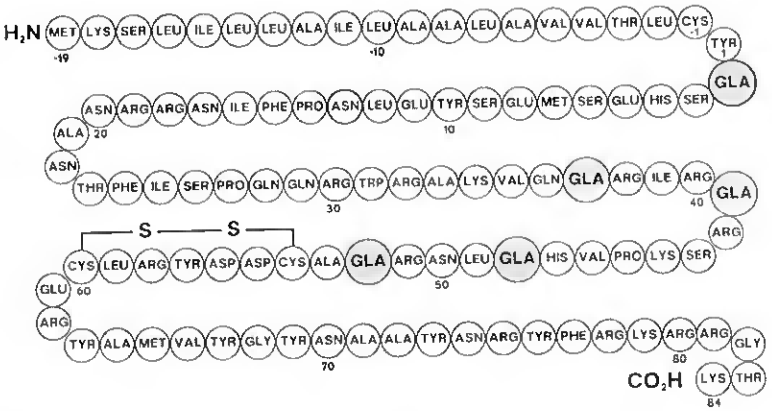

Figure I3- Amino acid sequence of the human matrix Gla protein. The residues marked in gray represent γ-carboxyglutamic acid. The solid line represents the disulfide-bond between Cys_{54} and Cys_{60}. Negative numbers corresponds to the pre peptide and mature protein starts at position 1. Adapted from Cancela *et al.* (1990).

I10- Regulation of MGP expression

The gene structure and regulatory promoter sequences for human MGP were obtained by Cancela *et al.* (1990). In the promoter, several structural consensus motifs that bind known transcription factors were identified including TATA and CAAT boxes, characteristic of polymerase II-transcribed genes and several putative binding sites for AP1, AP2, cAMP-dependent transcription factors and steroid hormone receptors including vitamin D3 and retinoic acid (Cancela *et al.,* 1990). The MGP gene is known to be regulated, in particular, by retinoic acid (RA) (Cancela and Price, 1992, Kirfel, *et al.,* 1997). Retinoids play an important role in development, cellular proliferation, and differentiation and are well-known inhibitors of cell growth. RA exerts biological effects by binding to at least two distinct classes of intracellular proteins including the RA receptors (RARs) and the retinoid X receptors (RXRs), both of which are members of the nuclear receptor superfamily. While both the RARs and RXRs are effective activators of some genes, RA is also known to repress MGP gene expression. It has been reported that RA is able to repress MGP gene expression in different cell lines (Kirfel, *et al.,* 1997; Sheik *et al.,* 1993). The inhibitory effects of RA on gene transcription can be exerted through various mechanisms such as competition between receptors and other transcription factors for overlapping binding sites or by competition for limiting cofactors (Kirfel, *et al.,* 1997). This comes in contrast to some other references that decribe RA as having a positive effect over expression of MGP in osteosarcoma cells (Fraser *et al.,* 1988) and in osteoblsts, chondrocytes and fibroblasts both in fetal and adult tissues (Cancela and Price, 1992).

Vitamin D_3 also has contradictory effects on the expression of MGP depending on the cell type or cell line analyzed. Shanahan *et al.* (1998) reported that 1,25-dihydroxyvitamin D_3 increases the levels of MGP expression on rat VSMC while in human VSMC it has the apposite effect. These differences in expression can be due to the MGP promoter specific properties in rat and human. In contrast, MGP is upregulated by vitamin D in rat and human osteosarcoma cells and in rat primary chondrocyte cultures (Fraser *et al.,* 1988; Fraser and Price, 1990; Barone *et al.,* 1991; Cancela and Price, 1992). In addition no effects over MGP expression were observed in human fibroblasts,

chondrocytes and osteoblasts when added alone, but when added together with RA it attenuated the stimulatory effects of RA on these cells. These decrease can be explained by the formation of heterodimers between RA and 1,25-dihydroxyvitamin D_3 receptors and in this way decreasing the availability of RA receptor to act over the MGP promoter (Cancela and Price, 1992).

Other molecules have been described to have an action over MGP expression like the parathyroid hormone (PTH), that stimulates MGP via a cAMP-dependent pathway, that may be balanced by reduced 1,25-dihydroxyvitamin D_3 dependent transcription (Tintut *et al.,* 1998). This stimulation of MGP expression can explain the inhibitory effects of PTH over mineralization (Gopalakrishnan *et al.,* 2001). It was observed that MGP levels increase as soon as three hours after addition of PTH to cell cultures and similar effects were also observed *in vivo* and correlated to PTH inhibition of calcification and osteoblast activity (Gopalakrishnan *et al.,* 2001). It has been recently reported that induction of Runx2 expression upregulated MGP expression in cell cultures of osteoblastic and fibroblastic lineages (Stock *et al.,* 2004)

I11- MGP function

In normal physiological conditions, MGP is present in the extracellular matrix of arteries and cartilage but not of bone and the fact that it was originally isolated from demineralized bone powder could be explained by the large number of arteries present in bone (Luo *et al.*, 1997). Although MGP null mutants were developed to study the effect of MGP deficiency on bone metabolism, the most important and unexpected information from these transgenic mice was the rapid calcification of a number of soft tissues, including the large arteries, bronchi, and trachea (Luo *et al.*, 1997). The profound impact of MGP deficiency was proved by the fact that null mutants were all healthy at birth, but developed massive calcifications of the large vessels within the first weeks of life, leading to death by internal haemorragy due to rupture of the thoracic and abdominal aortae within 8 weeks after birth (Luo *et al.*, 1997; Schinke and Karsenty, 2000). An increase in expression of MGP mRNA was observed in VSMC in culture and related to formation of calcification nodules and this increase in MGP was proposed to be a

feedback mechanism as cellular response to accumulation of calcium (Proudfoot *et al.*, 1998). A more recent study by Speer *et al.* (2002) revealed that MGP-knockout mice showed a strong up-regulation of osteopontin and when both MGP and osteopontin genes were inactivated simultaneously, this resulted in a significant increase in vascular mineralization, up to three times more at 4 weeks after birth. As a result, dead of these mice occurred significantly earlier than in MGP $^{-/-}$ mice. These results suggest an alternative mechanism for controling vascular calcification involving osteopontin (Speer *et al.*, 2002) eventually contradicting the hypothesis proposed by Proudfoot *et al.* (1998).

Recently Taylor *et al.* (2005) in a tentative search for relations between SNPs in MGP and osteopontin failed to find individual effects of the polymorphisms in coronary calcification, with weak and not statistically significant correlations. Similar vascular disorders to those obtained in MGP deletion studies were obtained by treating mice with warfarin injections, resulting in individuals that displayed calcifications at the elastic lamellae of the media in the aorta (Price *et al.*, 1998, 2000). Discrepancies exist on the relevance of MGP on serum since it was recently referred that decreased serum levels of MGP are correlated with increased severity of coronary arterial calcification (Jono *et al.*, 2004), however Braam *et al.* (2000) showed that serum MGP concentrations were found to be significantly increased in patients with severe atherosclerosis which seems more consistent with the high MGP mRNA expression observed in atherosclerotic vessels and plaques observed in other studies. In fact, a role for extracellular matrix proteins has previously been proposed in the pathogenesis of arterial calcification in the scenery of atherosclerosis, and a relation between osteoporosis and arterial calcification has been suggested (Doherty *et al.*, 2003). In humans, vascular calcification may occur in two distinct forms: calcification of the tunica media (also known as Mönckeberg sclerosis) and calcification of the intima wich is widely associated with atherosclerosis (Shanahan *et al.*, 1998, 1999). It has been shown that the calcifying vessel wall shares many similarities with bone, and that cells from the arterial wall are capable, in some circumstances, of assuming an osteoblast-like phenotype (Dhore *et al.*, 2001) with expression and accumulation of bone and cartilage proteins such as BGP, osteopontin, osteonectin, bone morphogenetic proteins, bone sialoprotein and MGP (Proudfoot *et al.*, 1998; Shanahan *et al.*, 1993, 1998, 1999; Engelse *et al.*, 2001). The regulation of the

processes leading to vascular calcification seems to be more complex in humans than in rodents, as becomes evident in studies envolving patients with Keutel syndrome, which is an autosomal recessive disorder characterized by abnormal cartilage calcification related to different mutations in the MGP gene (Munroe *et al.,* 1999). Keutel syndrome are therefore regarded as human models for MGP deficiency, but remarkably, Keutel syndrome patients do not develop massive arterial calcification has a common feature like observed in knockout mouse (Braam *et al.,* 2000, Wallin *et al.,* 2001; Doherty *et al.,* 2003) which can explain their long life spans.

A relation between MGP and chondrocyte differentiation was also suggested by Yagami *et al.,* (1999) who showed that in hypertrophyc chondrocyte cultures *in vitro* calcification was triggered by treatment with the vitamin K-antagonist warfarin but this did not affect immature chondrocytes and verified that MGP modulates chondrocyte matrix mineralization but mainly controls mineral quantity but not quality. Moreover, warfarin-induced calcification was counteracted by MGP overexpression in the presence of vitamin K. This work provided further support for an effect of MGP on cell differentiation since it is showed that overexpression of MGP in developing limbs delays chondrocyte maturation and blocks endochondral ossification (Yagami *et al.,* 1999). This is consistent with the results obtained by Newman *et al.,* (2001) demonstrating that overexpression of MGP in hypertrophic chondrocytes reduces mineralization. In addition, MGP expression is biphasic and stage-specific during chondrocyte differentiation and has an effect on chondrocyte viability since expression of MGP induces apoptosis in maturing chondrocytes, whereas decreased expression induces apoptosis in proliferative and hypertrophic chondrocytes. These results suggest that MGP is vital for hypertrophic chondrocyte survival (Newman *et al.,* 2001).

There are several evidences for a modulatory role of MGP on BMP2 action. BMP2 belongs to the TGF-β superfamily of growth factors, and it is a potent inducer of bone and cartilage (Ducy and Karsenty, 2000). When MGP was initially purified from bone, it was observed that BMP2 was strongly associated with MGP, and the two proteins could only be separate by the use of strong denaturants (Price *et al.,* 1983; Urist *et al.,* 1984). Like MGP, BGP and other bone matrix proteins, BMP2 has been detected in calcified atherosclerotic arteries and calcifying vascular cells (Bostrom *et al.,* 1993;

Dhore *et al.*, 2001). The capacity of interaction between the two proteins was demonstrated by Wallin *et al.* (2000), who studied the modulation of binding between MGP and BMP2 using ligand blotting. Posterior studies have demonstrated that MGP inhibits BMP2-induced osteogenic differentiation in the multipotent mesenchymal cell line C3H10T1/2 and in marrow stomal cells (Bostrom *et al.*, 2001; Zebboudj *et al.*, 2002). Bostrom *et al.* (2001) suggested that the probable *in vivo* scenario is that MGP binds BMP2, preventing its interaction with cell surface receptors and retaining BMP during integration with bone matrix, an hypothesis which is consistent with the previously described observation of BMP being tightly associated with MGP during protein purification. Further evidence was given by the observation that binding of BMP2 to its receptor, as well as Smad1 signaling system activation, is decreased in the presence of intermediate levels of MPG and that MGP promotes association of BMP-2 to the extracellular matrix (Zebboudj *et al.*, 2002).

The modulation of BMP2 by MGP was confirmed in human calcifying vascular cells with different relative expression of these proteins. It was reported that calcification in vascular cells with high relative expression of BMP2 was inhibited by MGP, while calcification in vascular cells with low relative expression of BMP2 was stimulated by MGP (Zebboudj *et al.*, 2003). It has also been demonstrated *in vitro* that both MGP and BMP2 accelerated nodule formation in vascular cells, but while MGP decreased nodule size BMP2 increased it, probably through a BMP2-induced decrease in MGP expression. This data suggest that MGP is a conditional enhancer or inhibitor of BMP2 induced calcification, and that enhancement or inhibition depends on the BMP2 level relative to that of MGP (Zebboudj *et al.*, 2003). It has been reported the presence of a gradient of MGP on the normal vessel wall, with MGP expression high at the luminal side and declining toward the center of the media. This gradient is also observed in atherosclerotic vessels revealing that calcification occurred in areas where MGP is absent, toward the center of the wall (Engelse *et al.*, 2001). The fact that MGP is expressed does not reflect the percentage of MGP that is properly γ-carboxylated since there are references to a marked reduction of about 70% in γ-carboxylase activity in atherosclerotic vessels (Deboervanderberg *et al.*, 1986). This has been observed by immunohistochemistry in aortic wall calcified lesions of aging rats, revealing that although there were increased

concentrations of MGP, it did not bind to BMP2. This was observed to be due to the fact that MGP was poorly γ-carboxylated, providing evidences that the Gla containing region mediates binding between BMP2 and MGP only when the calcium-induced conformer of the Gla region is present (Sweatt *et al.,* 2003). In this way it seems possible that age related arterial calcification may be a consequence of partial γ-carboxylation of MGP, allowing unopposed BMP2 activity in the calcified arteriosclerotic lesions to induce precursor cells to becoming calcifying osteoblastic cell. Since one function of MGP as a matrix protein is to bind BMP2 via its vitamin K-dependent Gla region, we predict that the N- or C-terminal part of the protein is attached to the matrix leaving the Gla region free for BMP-2 binding (Wajih *et al.,* 2004).

Recently the study of developmental appearance of MGP in xenopus identified the presence of two different gene transcripts, one of them being maternally inherited while the other was transcribed only when transcription was activated from the genome of the zygote. This indicated a different temporal expression of the two MGP transcripts during early development and suggests another function for MGP, possibly in relation with embryo patterning and localization of BMP2, which is known to be required for normal embryo development (Conceição *et al.,* 2005).

I12- Relationship between posttranslational modifications of Bgp and Mgp and function.

I12.1 Effect of gamma-carboxylation

BGP and MGP both serve as substrates for the enzyme gamma-carboxylase, which converts glutamic acid to γ-carboxyl-glutamic acid (Gla) (Kirfel, *et al.,* 1997). This post-translational modification confers to these proteins a high affinity for hydroxyapatite crystals, which form the principal mineral crystal present in the extracellular matrix of mineralized tissues (Roy and Nishimoto, 2002; Hoang *et al.,* 2003) and is also essential for stabilizing the tertiary structure of these proteins (Spronk *et al.,* 2001). The complexity of calcium binding to BGP was demonstrated by determining the X-ray crystal structure for pig BGP, showing a proteic structure with 3 α–helices and a

negatively charged surface centring on helix α 1 that comprises all 3 Gla residues and coordinates five calcium ions in a hydroxyapatite lattice (Hoang *et al.,* 2003). These results were confirmed for fish BGP confirming its evolutionary conservation (Frazão *et al.,* 2005).

The importance of Gla residues for calcium binding has been shown by replacing them in mouse MGP by aspartic acid residues, thus establishing that Gla residues are required for MGP anti-mineralization function. There have been reports of increased expression of MGP associated with vascular calcification of vessels wall, revealing a translational control mecanism as response to calcification. However the presence of mRNA in normal and diseased arterial vessels does not mean that the resulting protein product is functional, particularly if these are Gla containing proteins, whose function depends on the post-translational processing by the gamma-carboxylase on the vessel wall (Urist *et al.,* 1984). The activity of MGP is not dependent of hepatic gamma-carboxylase, since it was demonstrated by Wallin *et al.* (1999) that the vessel wall has a different gamma-carboxylation system than that observed in the liver. The mechanism for the selectivity of vitamin K as an antidote for warfarin in liver but not in the arterial wall is unknown and in order to understand this difference, it is imperative that the gamma-carboxylation system in the vessel wall is understood (Wallin *et al.,* 1999).

It has been shown that the levels of circulating undercarboxylated BGP are a valuable nutrition marker reflecting skeletal provision of vitamins K and D (Sokoll *et al.,* 1981; Vergnaud *et al.,* 1997; Zofková *et al.,* 2003) and that there is a strong correlation of this parameter with the risk of fractures in elderly women (Szulc *et al.,* 1993, 1996). Low levels of vitamin K intake have been related to calcification on the aortic valves of elderly women (Jie *et al.,* 1995), and it was also found that the levels of vitamin K and gamma-carboxylase decrease with increasing age and with the progression of vascular disease (Vermeer, 1990). In addition, supplementing the diets with vitamin K reduces the risk of vertebral and hip fractures without increasing bone mass in patients with osteoporosis, suggesting that vitamin K affects bone quality (Sugiyama and Kawai, 2001).

Treatments with the vitamin K antagonist warfarin are currently used in medicine to prevent risk of thromboembolism since it inhibits Gla-containing clotting factors, but

this also contributes to increase non-functional MGP and BGP (Conceição, 2002). Treatments with warfarin in rats are known to cause excessive calcification in the skeleton and vascular system (Price *et al.,* 1982; 1998; 2000). It was also demonstrated by Caraballo *et al.,* (1999) that regular intake of vitamin K antagonists is correlated with low bone mass.

I12.2 Effect of phosphorylation

Another posttranslational mechanism of regulation of MGP is phosphorylation of three serine residues. Phosphoserine residues were identified in the motif Gla-Ser-X-Glu-Ser-X-Glu-Ser-X-Glu near the N-terminus of all known MGPs (Price *et al.,* 1994; Conceição *et al.,* 2002; Simes *et al.,* 2003). Phosphoserine was identified in residues 3, 6 and 9 of xenopus (Cancela *et al.,* 2001), shark, lamb, human, rat and bovine (Price *et al.,* 1994) MGPs. Simes *et al.* (2003) identified phosphoserine in residues 3, 6, 7 and 9 of *A. regius* MGP. The first Gla residue in the motif is not conserved in shark, *A. regius* and xenopus (Cancela *et al.,* 2001; Simes, 2002; Simes *et al.,* 2003). Other secreted proteins like milk caseins or salivary proteins have the same motif for phosphorylation, but show different secretion properties depending on the degree of phosphorylation (Price *et al.,* 1994). MGP tends to be only partially phosphorylated when secreted to the extracellular matrix, in contrast to milk or saliva proteins. It has been proposed that the degree of serine phosphorylation regulates the activity of the secreted protein, and that change in phosphorylation levels and protein activity can be induced by action of the secretory protein kinase pathway (Akhoundi *et al.,* 1994) and by extracellular phosphatases. However no evidences have been presented correlating changes in MGP function with the degree of phosphorylation. A possible involvement of phosphorylation as a sorting signal for MGP and the relevance of the signal for MGP function have been recently proposed but is still under more detailded investigation (Wajih *et al.,* 2004).

I12.3 Effect of proteolytic cleavages of the mature proteins

A C-terminal proteolytic processing was determined in bovine, human and shark MGPs (Hale *et al.,* 1991; Rice *et al.,* 1994). Two forms of MGP were isolated from demineralized and urea extracts of bovine cortical bone, one with 79 residues and C-terminus Phe-Arg-Gln and other with 83 residues and C-terminus Phe-Arg-Gln-Arg-Arg-Gli-Ala. The 84 residue structure of bovine MGP predicted from the mRNA sequence (Kiefer *et al.,* 1988) was not detected in the bone extracts and it was proposed that the lysine at position 84 was removed by the action of a carboxypeptidase B-like enzime prior to secretion (Hale *et al.,* 1991; Price, 1992). A model has been proposed for the generation of the 79 residue protein, in which a sequence of proteolitic cleavages would include a trypsin-like cleavage at Arg_{80}-Arg_{81} or Arg_{81}-Gly_{82} followed by a carboxypeptidase B-like cleavage to remove the remaining C-terminal Arg (Hale *et al.,* 1991; Price, 1992). It has been proposed that this cleavage is a mechanism for insolubilizing MGP, and in this way retain it in bone tissue (Braam, *et al.,* 2000).

A cleaving site for plasmin was described in the C-terminus of BGP at residues Arg_{43} and Arg_{44} of the bovine protein (Novak *et al.,* 1997). Cleavage by plasmin ocurred both in serum and in mineral bound BGP that was released into solution, sugesting that plasmin could play a role in the regulation of bone remodeling (Novak *et al.,* 1997).

Another cleavage site was identified recently in fish MGP (Simes *et al.,* 2003). The presence of an Ala-Asn-Ser-Phe (ANSF motif, residues 20-23 of *A. regius* MGP) was identified as a conserved proteolytic cleavage site also present in mammalian and shark MGPs (Price, unpublished results), results confirmed in all cases by the isolation, during the purification process of MGP, of this shorter form (revised in Simes *et al.,* 2003). More recently, the comparison of all known sequences of MGP has confirmed that the presence of this sequence motif (ANXF, where X can vary) is a conserved feature of all MGPs, from shark to human, and 100% conserved throughout more than 400 million years of evolution (Laizé *et al.,* 2005). However, the functional relevance of this cleavage site is not known.

N-terminal cleavage of the transmembrane signal peptide occurs in MGP and BGP. In rat and bovine MGP, which is syntesized as a pre-protein, this cleavage is

predicted to occur after the cysteine residue at position -1, becoming tyrosine at position + 1 the first residue in the N-terminal sequence of mature rat and bovine MGP (Price *et al.*, 1987). In BGP, the initial primary structure of the translated product has been determined by sequencing its cDNA from human, rat and mouse (Pan and Price, 1985; Celeste *et al.*, 1986) and revealed the presence of a transmembrane signal, a propeptide and a mature protein identical to the one extracted from bone. Treatment of rat osteosarcoma cells with warfarin and vitamin K simultaneouly showed that the N-terminal sequence of secreted BGP into the culture media was identical to the BGP extracted from rat bone establishing that the proteolytic processing of pro-BGP takes place prior to secretion and is independent of gamma-carboxylation (Pan *et al.*, 1985; Price, 1992). BGP cleavage products have been identified by RIA in serum of normal adults and patients with bone methabolic disease (Garnero *et al.*, 1994). This study allowed the identification of four serum reactive forms of BGP other than the normal molecule, including one form resulting from the cleavage of BGP at residues 43-49 that was found in large amounts in patients with bone metabolic disease. This molecule was proposed to have been generated by proteolytic cleavage of BGP in circulation (Garnero *et al.*, 1994). It was recently found that avian bone contain multiple isoforms of BGP as well as bone sialoprotein, osteopontin, osteonectin and dentin matrix protein-1 due to differences in post-translational modifications in these proteins, since only single transcripts were observed with Northern blotting (Wang *et al.*, 2005).

Recently two different forms of BGP were isolated from bullfrog, with one of the forms corresponding to the intact mature BGP and the other form lacking the first 4 N-terminal residues (SNLR). The two different forms have different increases in alpha-helix content when binding to Ca^{2+} or Cd^{2+}, with the form that is missing four N-terminal amino acids leading to a more compact conformational change upon metal binding (Dohi *et al.*, 2004).

I13- Chromosomal assignment of MGPs and BGPs

The structure of the human MGP gene and promoter regions and its chromosomal assignment was accomplished in 1990 by Cancela *et al.*, describing a 3,9 kilobases (Kb)

gene located in the short arm of chromosome 12 (12p). This localization was confirmed and its precise site of insertion within 12p determined following the complete sequencing of the human genome (www.sangerinstitute.com/humangenome/). In mouse and rat, MGP was localized in chromosomes 6G1 (Johnson *et al.*, 1991) and 4q (www.genome-www5.stanford.edu), respectively, regions known to shown syntheny with the human chromosome 12p. The localization of BGP was determined to be in chromosome 1q for human (Puchacz *et al.*, 1989) in chromosome 3 for mouse (Johnson *et al.*, 1991; Desbois *et al.*, 1994b) and 2q for rat with a high homology observed between human chromosome 1q and chromosome 3 and 2 from mouse and rat. The only fish for which MGP and BGP localization was specifically determined was zebrafish. In contrast to mammals, both genes are located within the same chromosome LG3. (Gavaia *et al.*, submitted). However, the regions where they are included also show some syntheny with the previously identififed mammalian locations.

Danio rerio mgp and *bgp* were found to be located on the same chromosome (LG3) in zebrafish, a result that differs from what is known in mammals, where the two genes are located in different chromosomes [chromosome 12 for *mgp* (Cancela *et al.*, 1990) and chromosome 1 for *bgp* (Puchacz *et al.*, 1989), in human; chromosome 6 for *mgp* and chromosome 3 for *bgp* in mouse (Johnson *et al.*, 1991; Desbois *et al.*, 1994b)].

I14- The structure of the fish skeleton

The skeleton is highly diversified throughout the different fish and the vast array of habitats in the aquatic media. The skeleton is responsible for body shape, movement and muscle attachment, feeding habits, protection, reproduction and in some cases calcium and phosphate reservoir (Marshal and Hugues, 1985; Lagler *et al.*, 1987; Walker and Liem, 1994; Du *et al.*, 2001). In the great majority of fish there is a big variety of elements that compose the skeleton, both in shape, composition and function. The cartilaginous and osseous tissues are well differentiated from those in higher vertebrates (Bertin, 1958). Another particularity of fish skeleton is that it has a continuos growth throughout the life of the animals, with interruptions or lower rates depending on the feeding period (Bertin, 1958).

The fish skeleton is composed of bone, cartilage, notochord, connective tissues, scales and tooth components such as enamel and dentin (Lagler *et al.,* 1987). The skeleton, like every organ, has specific developmental and functional characteristics that define its identity in biologic and pathologic terms (Ducy and Karsenty, 1998; Karsenty, 1999). The shapes of cartilages and bones are of particular interest because skeletal function, acted upon by natural selection, is directly related to skeletal morphology (Kimmel *et al.,* 1998). In the generality of vertebrates the skeleton is composed of multiple elements of various shapes and origins spread throughout the body. Most of these skeletal elements are formed by two different tissues, cartilage and bone, and each of these two tissues have its own specific cell types: chondrocytes in cartilage; osteoblasts and osteoclasts in bone. Each of these cell types has its own differentiation pathway, physiological functions, and therefore pathological conditions (Ducy and Karsenty, 1998; Karsenty, 1999).

In teleosts, the cells involved in bone formation and remodeling are described as being similar in many aspects to those found in the mammalian system, with the presence of bone forming osteoblasts and both mononucleated and multinucleated bone resorbing osteoclasts (Witten *et al.,* 2001) although little is known on how these cells interact to modulate bone matrix formation and remodeling (Witten *et al.,* 2001). Cartilages and bones develop from multiple embryologic origins, with the craniofacial skeleton in the first branchial arch and other regions of the forming head developing largely from neural crest cells originating from the dorsal neural tube, while other cranial bones originate from the cephalic mesoderm (Couly *et al.,* 1993; Köntges and Lumsden, 1996). In the axial skeleton the ribs and vertebrae form from the sclerotomal part of the somites, and the appendicular skeleton is derived from the lateral mesoderm. Despite the different embryologic origin of the various skeletal elements, the precursor cells will eventually differentiate into the same specific cell types. The origin of the cells is also different: chondrocytes have a mesodermal origin, the osteoblasts are from neural crest or mesodermal origin, and the osteoclasts or bone resorbing cells originates from the macrophage monocyte linkage (Karsenty, 1998). One example of genes involved in differentiation of skeletal tissues are the bone morphogenetic proteins that are known to stimulate mesenchymal cells to follow the osteo-chondrogenic pathway and differentiate

into chondrocytes and osteoblasts, which deposit the bone matrix and regulate the pattern of skeletal formation (Derynck, 1999).

In the begining of vertebrate skeletogenesis there is a migration of undifferentiated mesenchymal cells into areas destined to become bone, forming condensations that have the general shape of the future skeletal elements. This process provides the anlagen or templates of the future skeleton (Hall and Miyake, 1992; Ducy and Karsenty, 1998; Karsenty, 1998). The cells present in the anlagen initially express collagens of both type I and type IIa (a transcript of the α1(II) collagen gene that is not chondrocyte specific). Cells that differentiate along the chondrocytic pathway are genetically characterized by the expression of type IIb collagen, type α1 (II) collagen, type IX, XI collagen, matrix gla protein (Luo *et al.*, 1995) and several other matrix genes.

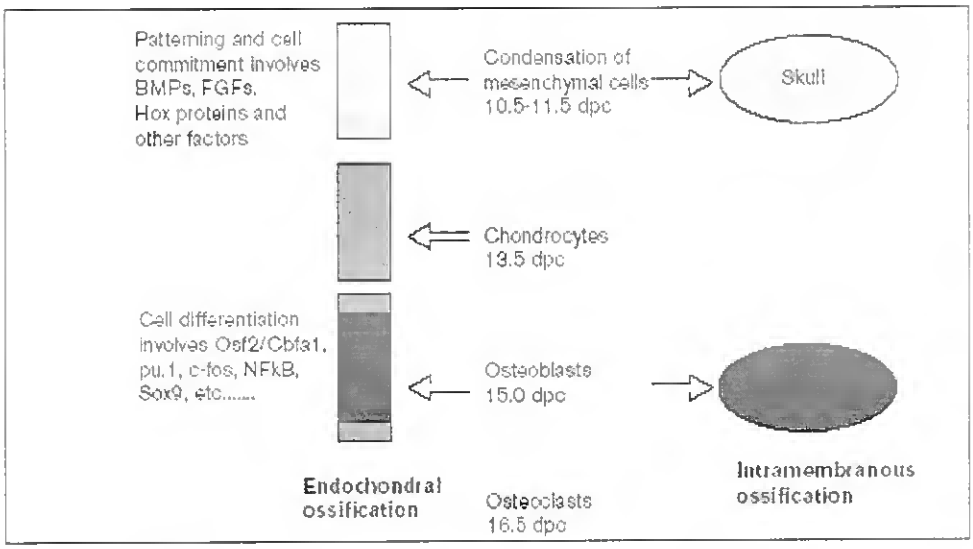

Figure I4- Proposed model for the different cell differentiation pathways during skeletogenesis in the mouse (adapted from Ducy and Karsenty, 1998).

The differentiating chondrocytes undergo a program of differentiation including hypertrophy, expression of type X collagen and a decrease in expression of type II collagen (Ducy and Karsenty, 1998; Karsenty, 1998). The cartilage is mostly replaced by bone in the majority of fishes and other vertebrates (Bond, 1979). In a process called endochondral ossification, the matrix surrounding hypertrophic chondrocytes calcifies and vascular invasion of the perichondrium of calcified cartilage brings in osteoblasts that gradualy replace cartilage by bone. At the time of vascular invasion from the

perichondrium, the hypertrophic chondrocytes die through apoptosis, and the osteoblasts brought in by the blood vessels begin depositing bone tissue (Bertin, 1958; Walker and Liem, 1994; Karsenty, 1998). This type of ossification can more accurately be divided into: endochondral ossification when calcification begins within the cartilage and perichondral ossification when bone begins to form around the periphery of the cartilage (Bertin, 1958; Walker and Liem, 1994; Junqueira *et al.*, 1995). Instead of a replacement by osteoblasts there are references to transdifferentiation during developmet of chick skeleton, where in some areas chondrocytes transform into, or are replaced by, bone-producing cells and osteoid is observed within the chondrocyte lacunae (Roach and Shearer, 1989). Another mechanism of ossification that occurs in some cranial bones, clavicle (mammals) and pelvic girdle (fish) is called dermal or intramembranous ossification. In this type of ossification bone develops directly from the connective tissue. It starts when mesenchymal cells condense, the tissue vascularizes, and cells differentiate directly into osteoblasts (Bertin, 1958; Walker and Liem, 1994; Junqueira *et al.*, 1995; Ducy and Karsenty, 1998; Karsenty, 1998). The vertebral centra develop primarily from the direct deposition of bone around the notochord by sclerotomal cells that form the continuous perichordal tube and perichordal sheath in a process called perichordal ossification (Walker and Liem, 1994).

Besides bone and cartilage, the fish skeleton also has chondroid bone, described as transition stage between bone and cartilage and is composed of chondrocyte like cells enclosed in bone-like matrix. This tissue is observed in the synovial joints, articular surfaces and in association with parallel fibred bone (Benjamin and Ralphs, 1991; Benjamin *et al.*, 1992). Bertin (1958) described this mixed tissue as similar to cartilage with normal chondrocyte-like cells in the center but with cells becoming fusiform towards the periphery as the matrix becomes fibrous and calcified. The chondrocytes end up resembling osseous cells once the matrix is calcified.

I15- General bone structure

Bone is a highly vascular, mineralized, specialized connective tissue that constitutes the main component of the skeleton of most adult vertebrates and is composed of a calcified extracellular matrix and three cell types: 1) osteoblasts, that synthesize the

organic components of the matrix; 2) osteocytes, located in cavities or lacunae within the matrix that affect mineralization; and 3) osteoclasts, that are giant multinucleated cells involved in bone resorption and remodeling (Marshal and Hugues, 1985; Walker and Liem, 1994; Junqueira *et al.*, 1995). Although bone forms hard, resilient structures, it is a dynamic tissue that has the capacity of changing as a result of the forces applied on the body (Gartner and Hiatt, 1999). Bone is formed when osteoprogenitor cells differentiate into osteoblasts (bone forming cells) that produce the components of the extracellular matrix, which then becomes calcified by binding of calcium phosphate (hydroxyapatite-$[Ca_{10}(PO_4)_6(OH)_2]$ crystals to collagen fibers, forming the osteoid (Walker and Liem, 1994; Gartner and Hiatt, 1999). The formation of hydroxyapatite crystals from calcium and phosphates present in the body fluids is possible due to the hydrolysis of pyrophosphate by the bone forming cells (Marshal and Hughes, 1980). As the matrix continues to be produced, some osteoblasts become trapped as osteocytes within spaces, called lacunae. The osteocytes are star-shaped cells that have radiating processes within minute canaliculi radiating the matrix (Walker and Liem, 1994). These cells are absent in accelular bone in which non ramified osteoblasts always retreat from the mineralizing front and localize in the periphery of the tissue, never becoming trapped (Bertin, 1958; Weiss and Watabe, 1979; Parenti, 1986).

It is apparent that most regulatory factors or pathways that control bone formation have been highly conserved in vertebrates during evolution, and signaling molecules required for embryonic skeletal development are also important for adult homeostasis (Du *et al.*, 2001).

In teleost fish the osseous tissues can be divided into two distinct bone types: acellular or anosteocytic bone, does not contain osteocytes and has a vascularized woven structure with chemical composition similar to other vertebrates; cellular or osteocytic bone, contains osteocytes and is similar to bone in mammals except for the absence of osteon (Ekanayake and Hall, 1988; Weiss and Watabe, 1979; Witten, 1997; Witten and Villwock, 1997; Witten *et al.*, 2001). Accelular bone is generally referred as characteristic of modern teleosts, while cellular bone is present in more primitive teleosts such as chondrosteans and dipnoans (Bertin, 1958; Weiss and Watabe, 1979; Ekanayake and Hall, 1988). However, some controversy has arisen from this classification. Hughes

et al., (1994) suggested that the bones of sparids, usually referred as acellular, cannot be classified as such only based on the absence of visible osteocytes and lacunae. Another major difference between the bone of teleosts and higher vertebrates is the presence of collagen type II and chondroitin sulphate that are characteristic components of cartilage (Benjamin and Ralphs, 1991).

As known from higher vertebrates, the skeletal development involves bone formation by osteoblasts along with cartilage degradation and bone resorption by osteoclasts (Lewinson and Kogan, 1995). Bone resorption and the presence of osteoclasts in fish has been motif for some controversy. The osteoclast belongs to the monocyte/macrophage cell lineage but phenotypically they are distinct from other cells in this lineage. They are giant multinucleated cells (up to 50 nuclei per cell depending on species) found in contact with calcified bone surfaces (Karsenty, 1999). Osteoclasts form by fusion of mononuclear precursor cells, which derive from an early haemopoietic stem cell. Osteoclasts are highly specialised cells, capable of breaking down both the inorganic (hydroxyapatite) and organic (collagen and multiple-non-collagenous proteins) matrix of bone, dentine and mineralised cartilage, in a process of matrix resorption that occurs largely extracellularly. To dissolve hydroxyapatite, the cells secrete large amounts of protons, and to dissolve organic components of bone, the cells secrete a number of proteolytic enzymes, including cathepsin K, tartrate resistant acid phosphatase, and collagenase (Helfrich, 2003).

Investigations on the skeleton of teleosts with cellular and acellular bone revealed that osteoclasts are present in the developing skeleton regardless of the fact that they are often referred as scarce or not observed in fish bone (Sire *et al.,* 1990). For some time multinucleated osteoclasts were not detected in fish and it was suggested that bone resorption was made by mononucleated cells (Witten, 1997; Sire *et al.,* 1990) and that a shift from mononucleated to multinucleated cells could occur during development (Sire *et al.,* 1990). It was also suggested that osteocytes could be capable of bone resorption (Hughes *et al.,* 1994). However it is now known that in teleost fish with acellular and cellular bone there is resorption by osteoclasts. Persson et al. (1998, 1999) detected in scales the presence of tartrate resistant acid phosphatase (TRAP) positive cells, identified as salmonid osteoclasts. Their activity was found to increase throughout sexual

maturation and spawning migration and it was proposed that the scales are resorbed in order to provide calcium for the growing ovaries. These resorbing cells were later characterized as two morphologically distinct osteoclast populations: type 1 and type 2 cells (Persson *et al.,* 1999). The identification of multinucleated cells, resembling the mammalian giant multinucleated osteoclasts, were found to be responsible for bone resorption in cichlids (Witten, 1997; Sire *et al.,* 1990) and salmonids (Persson *et al.,* 1999). More recently it was discovered that the zebrafish has both mononucleated and multinucleated resorbing cells (Witten *et al.,* 2001). The first were referred as appearing early in skeletogenesis and persistent until adulthood and the later appearing only in more advanced stages of bone resorption. Although multinucleated osteoclasts are the predominant form in adult zebrafish, mononucleated resorbing cells are the only type observed in neural arches and other thin skeletal elements, whereas multinucleated osteoclasts are responsible for resorption in the remaining bones (Witten *et al.,* 2001).

The bone extracellular matrix is composed by inorganic and organic components. The inorganic phase is composed mainly by calcium and phosphate complexed in hydroxyapatite crystals and other less abundant minerals like bicarbonate, citrate, magnesium, sodium and potassium as well as amorphous calcium phosphate (Debois *et al.,* 1994; Junqueira *et al.,* 1995; Gartner and Hiatt, 1999). The organic components of bone extracellular matrix are composed by polysacharides, collagen fibers, and two principal types of proteins that can be divided into two main groups: the collagens, mostly type I collagen, which accounts for 90% of the bone matrix proteins, and the noncollagenous proteins, including BGP, osteopontin, osteonectin and bone sialoprotein (Hauschka *et al.,* 1989; Denhardt and Guo, 1993; Ducy *et al.,* 1999; Gartner and Hiatt, 1999). Type I collagen is the most abundant protein synthesised in bone and consists of a heterotrimeric complex of two alpha-I (Col 1A1) and one alpha-2 (Col 1A2) molecules that are coordinately expressed and synthesised in a tissue- and development-specific manner (White *et al.,* 1998).

The production of bone extracellular matrix by osteoblasts requires a strict control of the balance between bone deposition and resorption, to allow skeleton growth to occur and to replace bone resorbed by the osteoclasts throughout life (Ott, 1996; Asou *et al.,*

2001). In an analogous way, bone resorption requires strict control of the balance against bone formation to avoid excessive loss of bone in normal individuals.

I16- Cartilage structure

Cartilage, like bone, is a dense connective tissue with an extracellular matrix rich in collagen, elastic fibers, mucopolysacharides and water (Walker and Liem, 1994; Marshal and Hughes, 1980; Gartner and Hiatt., 1999). The embryonic skeleton is mostly composed of cartilage that is substituted gradually by bone, remaining only in the growth zones (Storer *et al.,* 1986), the greater metabolic and structural flexibility of cartilage presumably being more suited to the requirements of the developing embryo. Cartilage is not vascularized, receiving nutrients through diffusion in the extracellular cartilaginous matrix. Cartilage is also not innervated and normal mechanisms of tissue repair, involving the recruitment of cells to the site of damage do not occur (Hardingham *et al.,* 2002). The chondroblasts, responsible for cartilage formation and production of the components of its extracellular matrix, are.derived from fibroblasts recruited from the connective tissue that covers cartilage, the perichondrium, and internally by mitotic division (Junqueira *et al.,* 1995; Gartner and Hiatt, 1999). Once differentiated chondroblasts start producing the components of cartilage, they become chondrocytes and are located in lacunae within the matrix they have secreted (Gartner and Hiatt, 1999). The extracellular matrix is composed by type IIb, IX, X and XI collagen, agrecan (composed of proteoglycans covalently linked to chondroitin sulphate molecules), chondronectin and chondroitin sulphate (Gartner and Hiatt, 1999). Three main types of cartilage can be found in vertebrates: hyalin cartilage, with chondrocytes well separated by water-rich extracellular matrix and with collagen II as principal protein; elastic cartilage, with a reduced extracellular matrix rich in elastin; and fibrous cartilage, with chondrocytes disposed in alined series and with a dense web of collagen type I as major extracellular matrix component (Junqueira *et al.,* 1995; Gartner and Hiatt, 1999).

In teleosts there appears to be different types of cartilage not previously recognized in higher vertebrates. These cartilages were identified in several teleost species by histological and immunohistochemical observations (Benjamin, 1989;

Benjamin and Ralphs, 1991; Benjamin *et al.,* 1992). The localization and morphological characteristics of these cartilage types are summarized in Table I4.

Morphologically, two different types of hyaline cartilage were identified either cell- or matrix-rich, depending on the percentage of tissue volume occupied by the extracellular matrix (if less than 50% is cell-rich and if more is matrix-rich), but they shown no differences at the immunological level. This cartilage is permanently present on the neurocranium and forms endochondral bone anlagen (Benjamin, 1989; Benjamin and Ralphs, 1991). One other type of cartilage present only in gill filaments is termed *Zellknorpel* and is characterized by piles of chondrocytes separated by a thin layer of matrix. This cartilage is normally surrounded by perichondral bone. The cartilage that forms articular tissue like the menisci is called fibro-cell-rich cartilage while elastic-cell-rich cartilage is found on the barbells. Surprisingly, this type of cartilage lacks collagen II. Hyaline-cell cartilage is characterized by abundant chromophobic cartilage and finally scleral cartilage is a thin sheet of cartilage that supports the eyes and is composed of lined chondrocytes sandwiched by peripheral layers of matrix (Benjamin and Ralphs, 1991; Benjamin *et al.,* 1992).

Table I4- Resumed information on the different cartilage types described for teleost fishes from the orders perciformes and cypriniformes. Cartilage types were identified by histological and immunohistochemical observations (Benjamin, 1989; Benjamin and Ralphs, 1991; Benjamin *et al.*, 1992).

Cartilage type	Localization	Characteristics
cell-rich hyaline cartilage (CRHC)	Gill arches, neurocranium, caudal and dorsal fins	Less than 50% of extracellular matrix; present only in structures under endochondral ossification
matrix-rich hyaline cartilage (MRHC)	Gill arches, neurocranium, caudal and dorsal fins	More than 50% extracellular matrix; same immunohistochemical characteristics as CRHC; present only in structures under endochondral ossification
Zellknorpel	Gill filaments	Chondrocytes organized in piles, separated by a thin layer of matrix; normally surrounded by perichondral bone
fibro-cell-rich cartilage	Articular tissue like the *menisci*	Cells shrunken in lacunae; matrix rich in collagen fibers
elastic-cell-rich cartilage	Barbells	Cells shrunken in lacunae Lack of collagen type II
Hyaline-cell cartilage	Oromandibular region; caudal fin and trunk	Cells with abundant chromophobic cytoplasm cartilage
scleral cartilage	thin sheet of cartilage supporting the eye	lined chondrocytes sandwiched by peripheral layers of matrix

I17- The biological models

I17.1- Zebrafish (*Danio rerio rerio*)

The zebrafish (*Danio rerio)* is a small tropical teleost with cellular (osteocyte containing) bone, which has become a model of choice for developmental biologists (Du *et al.*, 2001) and has emerged as an important organism for the study of early development in vertebrates (Streisinger *et al.*, 1981). For this study the zebra fish was chosen as the fresh water fish model because it has many of the advantages of invertebrate models *C. elegans* and *Drosophila* including high fecundity with a single female laying hundreds of eggs every week, a short generation time of 3-4 months, rapid development; external fertilization, translucent embryos which enable the investigator to examine its development readily with the dissecting microscope, and easy maintenance (Streisinger *et al.*, 1981; Rawls *et al.*, 2001; Nusslein-Volhard and Dahm, 2002). The fast

and syncronous embryonic development facilitates phenotypic analysis and large-scale experimental approaches. The fact that the egg is transparent and the embryo is easily accessible along with its robustness makes it an ideal model for micromanipulation and in vivo observations (Nusslein-Volhard and Dahm, 2002). Also zebrafish has advantages over the mouse model, since mouse developmental genetics is impeded by high maintenance costs of animals and by the fact that embryonic development is intrauterine (Driever *et al.,* 1996). Therefore, this model enables both modern molecular and genetic studies to be carried out to identify genes involved in a wide variety of developmental processes (Du *et al.,* 2001). In addition to the referred developmental advantages, recent studies have indicated the usefulness of the zebrafish as a model for human disease. Its genome provides an easily accessible source for identification of homologs for human genes, and the fish model can be helpfull in the functional analysis of these genes (Barut and Zon, 2000). However, research utilizing the zebrafish system in bone and bone diseases remains still scarce (Zhang *et al.,* 2002). The large scale screening of mutants generated by ENU (N-ethyl-N-nitrosourea) during the late 90's allowed the identification and characterization of a large number of mutants (Haffter *et al.,* 1996). This suitability for systematic mutagenesis studies to identify genes regulating the development of various tissues and organs, including the skeletal system (Vogel, 2000; Schilling, 1997; Schilling *et al.,* 1996a,b) led to the identification of several mutations affecting cartilage (Neuhauss *et al.,* 1996; Schilling *et al.,* 1996a; Schilling *et al.,* 1996b; Piotrowski *et al.,* 1996) and some genes acting over morphogenetic pathways leading to cartilage development have already been identified (Kimmel *et al.,* 1998).

Another advantage to the usage of the zebrafish, is the increasing number of tools and techniques that have been developed for this model in the last years (Nusslein-Volhard and Dahm, 2002) including the strategies for gene knockdown by the use of morpholino oligonucleotides (Morcos, 2001) and the production of zebrafish germ-line chimeras from cultured embryonic cells and techniques to transfer zigotic mutations through zebrafish germ line by cell transplantation (Ma *et al.,* 2001; Ciruna *et al.,* 2002). These findings raises the possibility that *in vitro* transgenesis and gene targeting technologies will become feasible in the fish and will allow the generation of chimeric transgenic lines and the use of reverse genetic approaches to determine gene function.

The targeted 'knockdown' technologies permit to generate phenocopies of mutations of zebrafish genes that have human homologues and contribute to the systematic development of models of human disease, using reverse-genetic approaches in zebrafish embryos (Nasevicius and Ekker, 2000).

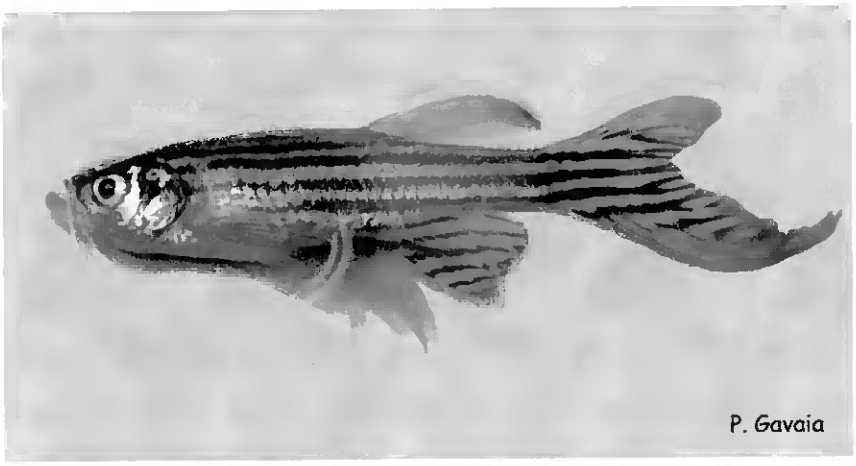

Figure I5- Adult male zebrafish (*Danio rerio*)

Taxonomical classification:

Kingdom Animalia
Phylum Chordata
Subphylum Vertebrata
Superclass Gnathostomata
Class Osteichthyes
Division Teleostei
Subclass Actinopterygii
Superorder Neopterygii
Order Ostariophysi
Family Cyprinidae
Genus *Danio*
Species *Danio rerio* (Hamilton, 1822)

This classification was based on the information obtained from www.fishbase.org, www.zfin.org and from Hickman *et al.,* 1993.

I17.1.1- The zebrafish skeleton

The description and analysis of the development of various zebrafish skeletal elements has been the subject of several previous studies. However, most of them have focused either on very early stages of development or in the formation of particular structures (Cubbage and Mabee, 1996; Schilling and Kimmel, 1997; Fisher *et al.,* 2003) and in general are consistent with observations for other vertebrates. In what regards the dentition, the zebrafish is classified as a polyphyodont species (i.e., with tooth replacement throughout life) and similarly to other cyprinids, teeth are restricted to the modified fifth branchial arches, or the pharyngeal jaws, and start formation as early as 2 dpf (Huysseune *et al.,* 1998; Van der Heyden and Huysseune, 2000; Van der heyden *et al.,* 2001; Wautier *et al.,* 2001). The early development of the neural crest cell-derived pharyngeal skeleton, that includes the branchial arches and jaw and the craniofacial skeleton, were described in detail by Piotrowski *et al.* (1996), Schilling *et al.* (1996 a, b) and Schilling and Kimmel (1997). These studies identified and described some of the mutations affecting jaw and branchial arch development such as *schmerle, sucker, hoover* and *sturgeon* that have reduced ventral structures in the mandibular and hyoid arches, the *jellyfish* mutant that presents severe reduction of all cartilaginous elements (Piotrowski *et al.,* 1996) or the *chinless (chn)* that is required for the formation of pharyngeal cartilages and of cranial muscles (Schilling *et al.,* 1996b). Grandel and Schulte-Merker (1998) described the structure and normal development of the zebrafish paired fins, referring the different endoskeletal development in the pectoral and pelvic fins. The authors observed that while most of the endoskeletal girdle develops within the fin bud mesenchyme, the pelvic fins have a pattern of chondrogenic condensations that directly reflect the adult internal skeleton pattern.

Some skeletal deformities affecting the axial skeleton were detected in zebrafish by radiography of specimens older than 2 months, and the gene responsible for the *chihuahua* mutation was identified as collagen I (α1), causing severe skeletal deformities

since growth and mineralization are both abnormal. The *chihuahua* mutants present irregular vertebrae with short dorsal spinous processes and bones with areas of uneven mineralization and accurately model human *osteogenesis imperfecta*, being an important resource for studies on the pathophysiology of this disease (Fisher *et al.*, 2003).

I17.2- Senegal sole (*Solea senegalensis*)

The Senegal sole (*Solea senegalensis*, Kaup) is a pleuronectiform fish characteristic of the South Atlantic and Mediterranean coasts and exploited in extensive aquaculture production allong the south coasts of Portugal and Spain (Dinis, 1986; Dinis, 1992; Dinis and Reis, 1995; Dinis *et al.*, 1999; Fernández-Díaz *et al.*, 2001). Because of the high commercial value that this species can reach on the market and promising rearing and reproduction results, it has a high potential for the diversification of aquaculture industry (Dinis, 1992; Dinis and Reis, 1995; Dinis *et al.*, 1999; Dinis *et al.*, 2003). The investigation on this species has been maynly focused on the development of digestive traits and enzimes (Sarasquete *et al.*, 1996; Martínez *et al.*, 1999; Ribeiro *et al.*, 1999*a*, *b*) and several studies that have addressed different aspects of its development, endocrinology and reproductive biology (Pendón *et al.*, 1994*a,b*; Rodriguez-Gómez *et al.*, 2000*a,b*; Fernández-Díaz *et al.*, 2001; Bedui, 2003). The Senegal sole is characterized by a flat oval body with the two eyes on the right (ocular) side of the head. The color on the ocular side is brownish with blue spots in fresh specimens, interradial pigments and with a black membrane in the pectoral fin (Arias & Drake, 1990; Muzavor *et al.*, 1993) as seen in Figure I6 . Senegal sole larvae at hatching are transparent, have a large yolk sac with several oil globules and present three melanophores in the primordial fin (Dinis, 1986; Ribeiro, 2003). The larvae have initially a pelagic life style for the first two weeks after hatching, but then metamorphosis starts with the left eye initiating its migration while the body suffers a torsion leading to its settling on the bottom, with acquisition of a benthic life style (Dinis, 1986). This species are gonochoric, and females mature at age 3+ for *S. senegalensis* and when total lengths are 32 cm (Dinis, 1986). The wide spawning season occurs from late winter to early summer and sometimes a small

season occurs during the autumn (Dinis, 1986; Andrade, 1990; Ribeiro, 2003), allowing the observation of larvae and post-larvae all year (Arias & Drake, 1990)

In flatfishes the metamorphosis is characterized by the dramatic anatomical transformation involving rotation in body position from a bilaterally symmetrical to an asymmetrical morphology and the migration of one eye to the ocular upper side (Tanaka *et al.*, 1996). Metamorphosis accompanies the transition from pelagic to a benthic life style by the settlement of the larvae on the substratum and consequently implying drastic changes in food habits and in digestive physiology (Tanaka *et al.*, 1996; Fernández-Díaz *et al.*, 2001). These dramatic changes in shape, morphology and physiology come together with a different ecological niche occupation by the fish (Blaxter, 1998; Ribeiro, 2003).

The Senegal sole was chosen as model organism in this study because of its interesting osteological development leading to a radical change in skeletal morphology during larval stages, which is crucial for its later survival and life style. In addition, there were also some practical reasons including i) availability of eggs and larvae in our institution; ii) fast growth rate during the larval period when fed live prey (Dinis and Reis, 1995 Ribeiro *et al.*, 1999*b*)d ;and iii) resistance to manipulation during larval stages.

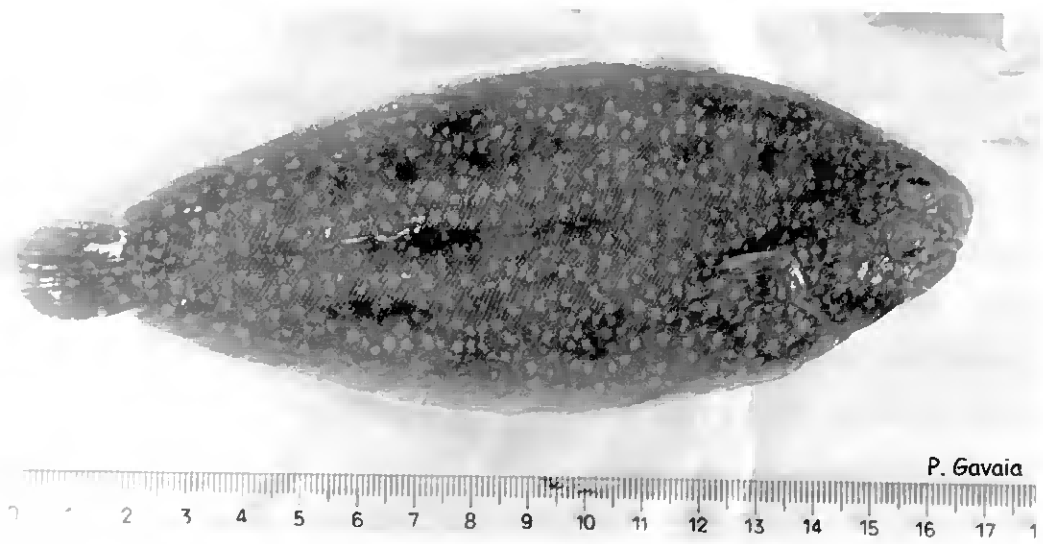

Figure 16- Juvenile individual of Senegal sole raised in the experimental laboratory for marine organisms (LEOA) of the University of Algarve.

Taxonomical classification:

Kingdom Animalia
Phylum Chordata
Subphylum Vertebrata
Superclass Gnathostomata
Class Osteichthyes
Division Teleostei
Subclass Actinopterygii
Superorder Neopterygii
Order Pleuronectiformes
Family Soleidae
Genus *Solea*
Species *Solea senegalensis* (Kaup,1858)

This classification was based on the information obtained from www.fishbase.org and from Hickman *et al.*, 1993.

I17.2.1- The Senegal sole skeleton

The Senegal sole is a teleost fish with acellular bone and the development of its axial skeleton was described for the first time, within the scope of this thesis, for individuals ranging from larvae to juvenile specimens (Gavaia *et al.*, 2002 and results section).

I18- Proposed objectives

The major objective of this work was to determine the spacio-temporal localization of BGP and MGP gene expression and protein accumulation during skeletal development of a fresh water and a marine fish and to initiate studies towards understanding its function in fish.

To achieve this goal, the skeletal developmental of sole and zebra were followed in a systematic way using both morphological and histological approaches and required the optimization of histological detection of bone and cartilage, to be able to detect structures with thicknesses within the micron range. To detect the onset of BGP/MGP gene expression the corresponding cDNAs were cloned from zebrafish and Senegal sole. In order to generate probes that, along with antibodies generated against teleost BGP and MGP permitted to investigate the patterns of expression and accumulation for BGP and MGP during development of the two model species chosen.

The effect of liposoluble vitamin A, that is known to have an effect on BGP and MGP in mammals, was investigated *in vivo* by supplementing the animal's diets with retinol palmitate. The effects of vitamin K and, its antagonist, warfarin were also investigated in order to provide the first evidence towards understanding if the function of those two skeletal Gla proteins has been conserved between fish and mammals.

MATERIALS AND METHODS

Materials and Methods

M1- *Solea senegalensis* larval rearing and maintenance

Solea senegalensis eggs were obtained from natural spawning of a broodstock adapted to captivity and gently provided by the aquaculture group of the University of Algarve. Fertilized eggs were selected through separation of buoyant eggs at a salinity of 35‰ and transferred to 80 l cylindro-conical tanks for incubation at a density of 350 eggs per liter. The incubation was done under the same environmental conditions of the broodstock tank. Larvae hatched after a period of 48-56 hours of incubation and first feeding was supplied at mouth opening (2 days after hatching) with addition to the rearing tanks of microalgii (green water technique) and rotifers (*Brachionus plicatilis*) enriched overnight with *Tetraselmis suessica* (clone T Chui) and *Isochrisys galbana* (clone T Iso), at a concentration of 5 rotifers per ml. Newly hatched artemia nauplii at a concentration of 2 nauplii per ml were supplied from day 5 to day 10, 24 h metanauplii from day 11 to the end of metamorphosis and 48 h metanauplii until juvenile stage. The metanauplii were enriched with microalgii *Tetraselmis suessica* (clone T Chui) and *Isochrisys galbana* (clone T Iso).

M2- Establishment of a zebrafish rearing system

Due to the complete absence of a zebrafish research laboratory in Portugal, it was necessary to establish a simple, but functional rearing system, that allowed us to obtain the larvae, juveniles and adults necessary for the realization of the present studies. One initial stock of zebrafish adults was purchased at a local aquarium shop and separated into 3 rearing groups and maintained in isolated 40 liter aquaria at low density. The aquariums were equipped with a heater to maintain a constant 28 °C temperature and a biological sand filter to maintain a good water quality. Water changes were done every month with dechlorinated tap water. Illumination was supplied by fluorescent day light lamps, programmed to ensure a photoperiod of 14 hour light and 10 hours dark.

The rearing stocks were fed twice a day. During periods when fish were intended to breed and produce high quality eggs the diet was composed of a morning meal with freshly hatched artemia nauplii, in a proportion of a full 3 ml pipette for each

group of 5 fish, and an afternoon meal composed of Tetramin® flakes. For periods of normal fish maintenance the morning meal with artemia *nauplii* was given only twice a week, being replaced in the other days by Tetramin® flakes.

M3- *Danio rerio* larval rearing and maintenance

D. rerio eggs were obtained from natural spawning of wild type breeding fish, maintained at 28.5 ± 0.5°C on a 14 hour light/10 hour dark photoperiod. Matting pairs were isolated and maintained overnight in a net cage. Eggs were recovered from the bottom of the spawning tanks, cleaned, recovered in a mesh and separated from dead or unfertilized eggs by visual examination under a stereomicroscope Leica MZ6 before transferring to 2 liter incubation tanks with dechlorinated water containing 0.001% methylene blue. Eggs were cleaned and water changed once a day during the incubation period. Hatching occurred 48-56 hours after fertilization under similar culture conditions. Larvae were maintained and raised by standard methods, according to Westerfield (1995) in the zebra fish book. Initial larval feeding was done with rotifers raised in *Tetraselmis suessica* (clone T Chui) supplied 4 times a day until day 7 post fertilization. Then rotifers were gradually substituted by newly hatched artemia nauplii. When larvae reached a total length of ~10 mm, feeding was substituted by a mixture of frozen artemia and Tetramin flakes.

M4- Sample collection

Samples of larvae and juvenile individuals were randomly collected at regular intervals throughout all developmental period, from hatching through metamorphosis and up to juvenile stages. Developmental stages were identified by direct observation under the stereomicroscope and by comparison with stages of embryonic development described by Kimmel et al (1995). The larvae and juvenile individuals were anaesthetized with 0.1 % 2-phenoxyethanol (Sigma, St Louis, MO) and either collected into TRIZOL reagent (Gibco BRL™) for subsequent RNA purification or fixed in buffered 4% paraformaldehyde (pH 7,4 in PBS) for 24 h at 4°C. After fixation, samples were washed twice for 10 min in PBS and immediately used for preparation of paraffin or glycol-methacrylate blocks. These were either sectioned and used in the different methodologies described bellow, or conserved in methanol at –20°C until further

processing. All sampling procedures and preparation of solutions used were performed in RNase free conditions to allow using the same tissues for *in situ* hybridization, immunohistochemistry detections and histological stainings.

M5- Histological procedures

M5.1- Whole-mount staining of the skeleton

Development of *Danio rerio* and *Solea senegalensis* skeletal structures was followed from hatching to juvenile stages in both species by detecting the appearance of calcified and cartilaginous structures as *t* previously described (Gavaia *et al.*, 2000). Fixed and preserved specimens were hydrated through a decreasing alcohol series (100%, 95%, 70%, 50%, 30% and 2x H_2O) followed by cartilage staining with Alcian blue 8 GX (Sigma, St Louis, MO) 0.01% in a 70:30 ethanol / glacial acetic acid solution at a pH ranging 1-2. After staining, the specimens were washed in absolute ethanol to remove excess dye and hydrated again as before. Maceration was done in 1% potassium hydroxide (KOH) for a period ranging from 6 hours in small larvae to several days in larger specimens. After transparency of muscle and fading of pigments were achieved, calcified structures were stained with Alizarin red S (Sigma, St Louis, MO) in 0.5% KOH. After staining, the specimens were submitted to a final maceration period with 1% KOH to which was added one drop of hydrogen peroxide (H_2O_2) to increase transparency of soft tissues and removal of all pigments. The stained specimens were submitted to an increasing series of glycerol and water and finally stored in glycerol with a crystal of phenol to prevent development of bacteria or fungi contamination.

M5.2- Histological slides

Some individuals of same age and developmental stage as those used for whole mount skeletal staining, and samples submitted to experimental treatments were included either in paraffin or in Historesin Plus (Jung). Specimens to be included in paraffin blocks were placed in a carrousel and dehydrated in a series of methanol and xylene baths until paraffin (methanol 2x 90 min; xylene 3x 60 min; paraffin 2x 90 min). Immediately after paraffin inclusion, blocks were prepared in a Leica histological station. Paraffin sections of 6-8 μm were prepared in a microtome, floated in sterile distilled water, collected in TESPA (3-aminopropyltriethoxysilane, Sigma)-coated slides and dried over night at 37°C. Specimens with a large portion of their skeleton

already calcified were included in the hydrophilic resin Historesin Plus. After methanol preservation, specimens were dehydrated with several changes of ice cold acetone for 1 hour and transferred to embedding media for 6-12 hour at 4°C. Samples were placed on plastic moulds with inclusion media and covered with plastic to avoid any contact with air. Polymerization took place at 4°C for 12 hours, after which blocks were mounted in supports for sectioning and kept in the refrigerator. Historesin Plus sections of 2-5 μm were obtained in a JUNG supercut 2065 microtome and collected in Poly-L-Lysine (Sigma) coated slides. Sections were stored at 4°C in a dry box with silica gel until processing for *in situ* hybridization or immunostaining.

For detection of mineral deposition, some sections were stained either with Alizarin red S and haematoxylin or with Silver nitrate by the von Kossa's method. Corresponding structures were determined by staining comparable slides with haematoxylin-eosin (HE) or Toluidine blue.

M5.3- Deparaffination of histological slides

The sections were deparaffined in two baths of xylene for 10 min each, and hydrated in a decreasing ethanol series of 10 min baths (2x 100%, 90%, 70%, 50% ethanol and 2x distilled H_2O).

M5.4- Von Kossa's method

Deparaffined and hydrated sections were covered with a 1% silver nitrate solution and placed under ultra-violet light for 45 minutes. Sections were washed in distilled H_2O and treated with 5% sodium thiosulphate for 5 minutes and again washed in water. Counterstaining was made with neutral red 0.5% in 70% ethanol, toluidine blue or Harry's haematoxilin. Stained sections were cleared with increasing ethanol and xylene series (70%, 90%, 100% ethanol and 2x xylene) and mounted in Eukitt (Merck).

M5.5- Haematoxilin-eosin

Deparaffined and hydrated sections were placed over a crystallizer and covered with Harry's haematoxilin for 6 min then washed under running tap water for 10 min. The sections were then stained with eosin for 2 min and washed again in distilled water. Stained sections were cleared with increasing ethanol and xylene series (70%, 90%, 100% ethanol and 2x xylene) and mounted in Eukitt (Merck).

M5.6- Toluidine blue method

Plastic sections were covered with a 0.5% toluidine blue in 1% sodium tetraborate solution for 30 sec. followed by washing in distilled H_2O to remove excess dye. Stained sections were air dried over a heated plate and mounted with Eukitt (Merck).

M5.7- Alizarin red-Haematoxilin

Deparaffined and hydrated paraffin sections or dried plastic sections were placed over a crystallizer and covered with a solution of alizarin red in 0.05% KOH (2 ml of 0.1% alizarin red stock in 18 ml of distilled water) for 30 min. After staining, sections were washed in distilled water for 5 min, incubated in 0.05 KOH for 5 min to remove excess dye and then submitted to another washing step with distilled water for 5 min. Sections were counterstained with Harris' haematoxilin for 6 min followed by a washing step under running tap water for 10 min. Plastic sections were cleaned in distilled water, dried over a heated plate and mounted in Eukitt. Paraffin sections were cleared using increasing ethanol and xylene series (70%, 90%, 100% ethanol and 2x xylene) and mounted in Eukitt (Merck).

M5.8- Detection of acid phosphatase activity

Tartrate-resistant acid phosphatase (TRAP) detection was performed using a modification of a previously established method (Burstone, 1959). Freshly prepared plastic sections of mineralizing larvae and juveniles were incubated in a working solution containing Naphthol-ASBI-phosphate, sodium nitrite, hexazotized pararosanilin and 50 mM sodium tartrate in veronal acetate buffer at pH 5, for 1 hour at 37°C. Sections were carefully washed for 10 min in distilled water and 10 min more in tap water. Counterstaining was performed with Harry's haematoxilin for 6 min followed by a washing step under running tap water for 10 min. Sections were cleaned in distilled water, dried over a heated plate and mounted in Eukitt (Merck). Control sections were prepared without sodium tartrate and in sections incubated for 2 hours at 45 °C.

M5.9- Detection of Alkaline phosphatase activity

Alkaline phosphatase activity was demonstrated in freshly prepared plastic sections of mineralizing larvae and juveniles, by incubating samples for 1 hour at 37°C in a working solution containing Naphthol AS-MX phosphate, Fast blue BB, and magnesium sulfate, in 0.1M Tris buffer (pH 8). Samples were washed for 5 min in distilled water and counterstaining was performed with Nuclear fast red for 10 minutes followed by 2 min washing in distilled water. After staining, the sections were dehydrated by air drying over a heated plate and mounted with EUKIT (Merck).

M6- Purification of Bgp and Mgp from *D. rerio* and *S. senegalensis* mineralyzed tissues

Fifty five *D. rerio* specimens (0.7-1.0 g wet weight per fish) and two adult *S. senegalensis* (1.0 and 1.5 kg wet weight per fish) were sacrificed and used for the purification of Bgp and MgpP. The entire *D. rerio* mineralized skeleton, including head and fins, and vertebra from *S. senegalensis* were freed from adhering soft tissues as much as possible, extensively washed in water and acetone, dried and ground to fine particles in a mortar with liquid nitrogen. The resulting powder (1.1 g for *D. rerio* and 12 g for *S. senegalensis*) was washed three times with a 10-fold excess of 6 M guanidine HCl (v/w) to remove the organic matrix, washed extensively first with water then with acetone, and air dried. Protein extraction was performed using a modification of a previously described procedure (Cancela *et al.*, 1995; Simes *et al.*, 2003). In brief, demineralization was done with a 10-fold excess of 10% formic acid (v/w) at 4°C for 4 hours with continuous stirring. The crude acid extract obtained was dialyzed against 50 mM HCl, using a 3,500 molecular weight cut-off tubing (SpectraPor 3, Spectrum, Gardena, CA), freeze-dried, re-suspended in 6 M guanidine-HCl, 0.1 M Tris-HCl pH 9, 10 mM EDTA and further dialyzed (SpectraPor 3) against 5 mM ammonium bicarbonate. The dialyzed material was freeze-dried and dissolved in 500 µl of 5 mM ammonium bicarbonate. Both proteins were then size separated by ultrafiltration using a Centricon YM10 (Amicon, Millipore, Bedford, MA, USA) with 10kDa molecular weight (MW) cut-off and further desalted and concentrated using a centricon YM-3 (3,000 MW cut-off). Purity of the filter-retained protein was further analyzed by SDS and native polyacrylamide gel electrophoresis (PAGE).

M7- Bgp and Mgp antibodies

Rabbit polyclonal antiserums against either Bgp or Mgp from *A. regius* (Ar) were obtained from Strategic BioSolutions (Ramona, CA), using the purified proteins from *Argyrosomus regius* branchial arches as described (Simes *et al.*, 2003).

These antibodies were validated for detection of Bgp and Mgp from other teleost fishes, including the Zebrafish and Senegal sole (Simes *et al.*, 2004).

M8- Identification of Bgp and Mgp by SDS/PAGE and Western blotting

Samples of each purified protein (circa 10 μg total protein) were dissolved in SDS sample buffer containing reducing agent (NuPage, Invitrogen), applied to a 12% polyacrylamide precast gel containing 0.1% SDS (NuPage, Invitrogen) and run at constant 140 volts. After electrophoresis, the gel was cut in three identical sections. One was stained with 0.2% Comassie Brillant Blue R-250 (C.I. 42660, Bio-Rad, Richmond, CA), 10% trichloroacetic acid, 10% 5-sulfosalicylic acid as described (Simes *et al.*, 2003). A second section was stained with a DBS-staining solution specific for Gla-containing proteins [(8.5 mM 4-diazobenzene sulfonic acid (DBS) (Sigma, St Louis), 6.4 mM NaNO2 in 2 M acetate buffer, pH 4.6)], as described (Simes *et al.*, 2003). The third section of the gel was used to determine, by Western blot analysis, the specificity of detection for Bgp and MGP from *D. rerio* and *S. senegalensis* using the polyclonal antibodies previously developed against the *A. regius* proteins (Simes et al, 2003). As secondary antibody, alkaline phosphatase-labeled goat anti-rabbit IgG antibody (Gibco-BRL, Paisley, UK) was used, with NBT/BCIP as substrate solution (Sigma), as described in detail elsewhere (Simes *et al.*, 2004). Bgp and Mgp purified from *A. regius* (Simes *et al.*, 2003) were used as positive controls and negative controls consisted in the substitution of the primary antibody with normal rabbit serum.

M9- N-Terminal protein sequence analysis

Intact purified proteins obtained from *D. rerio* and *S. senegalensis* were directly deposed on a polybrene-coated glass fiber filter. Automatic Edman degradations were performed as described (Rice *et al.*, 1994) using an Applied Biosystems Model 494 gas phase sequencer equipped with a model 120 on-line HPLC and employing the standard

program supplied by the manufacturer. Phenylthiohidantoin amino acid derivatives were separated using a 2.1 mm × 22 cm C-18 reverse-phase HPLC column (Applied Biosystems) and the gradient conditions recommended by Applied Biosystems. All protein sequences were performed by the laboratory of Professor Paul Price at the Division of Biological Sciences, University of California San Diego, Ca, USA.

M10- RNA purification

Total RNA from zebrafish and Senegal sole was purified using TRIZOL® Reagent (Gibco BRL™), as suggested by the supplier. RNA was purified from individuals ranging from early embryonic stages to fully calcified juveniles and adults.

The larger specimens and bone samples were minced in liquid nitrogen (N_2), transferred into extraction tubes, weighed and 10 vol. (w/v) of TRIZOL were added and mixed by vortexing. Small larvae were collected directly into 1.5 ml eppendorf tubes, weighed and 10 vol. (w/v) of TRIZOL were added. The larvae and TRIZOL were then homogenized by passing several times through a 19G needle fitted to a 2 ml syringe. After 5 min incubation at room temperature 0.2 ml of chloroform:isoamil alcohol (49:1) were added per 1 ml of TRIZOL Reagent used. The tubes were homogenized for 15 sec. and incubated at room temperature for 5 minutes. The samples were then centrifuged at 12,000 x g for 15 minutes at 4°C for phase separation. The upper aqueous phase was transferred to a fresh tube and the RNA was precipitated by adding 1 vol. (v/v) of isopropyl alcohol to the tubes. After 30 min incubation at -80°C, the tubes were centrifuged at 12,000 x g for 10 min at 4°C and an RNA pellet was obtained. The pellet was washed with 75% ethanol, air dried and resuspended in DEPC treated water. Purity and quantity of the extracted RNA were evaluated in a Genequant spectrophotometer (Promega) and the integrity of the RNA was assessed by fractionating 1µg into a 1.4 % agarose / 0.4 M formaldehyde gel (Appendix 1).

M11- Molecular cloning of *D. rerio* and *S. senegalensis bgp* cDNAs

Dr*bgp* and Ss*bgp* cDNAs were cloned following amplification by RT-PCR from total RNA extracted from the vertebral columns and heads of adult wild-type zebra fish and Senegal sole. 1µg of RNA was reverse transcribed using MMLV-Reverse

transcriptase (Gibco, BRL) and amplified by PCR with Taq DNA polymerase (Promega) in a DNA thermal cycler (Perkin Elmer, Foster City, CA, USA) using as forward primers either the ZbBGP 6F, designed based on the Dr*bgp* sequence obtained from N-terminal amino acid analysis or the SBG5F, designed on a consensus region based on alignments of all *bgp* cDNA sequences previously known. In both cases the reverse primer used was the universal adapter PCR products were resolved in a 1.5 % agarose gel by electrophoresis and expected size fragments were extracted from the gel, inserted into the plasmid pGem T-easy (PROMEGA) and inserted into supercompetent *E.Coli* DH 5α cells (Gibco BRL). Plasmid DNA was purified from positive clones using a standard procedure (NucleoSpin Plus Plasmid Miniprep kit, Clonetech) and sequenced with the T7 sequencing kit (Amersham-Pharmacia Biotech, USA). For the identification of the 5' ends of *D. rerio* and *S. senegalensis bgp* cDNAs, polyA+ RNA was purified from 300 μg of total RNA extracted from either a whole zebra fish specimen or from the vertebral column, branchial arches, kidney and heart of a juvenile sole, with Quick Prep Micro messenger RNA (mRNA) Purification Kit (Amersham-Pharmacia Biotech, USA). 1 μg of mRNA was reverse transcribed and used to amplify the 5'ends of *D. rerio* or *S. senegalensis bgp* cDNAs by 5'rapid amplification of cDNA ends (RACE) with the MarathonTM cDNA Amplification Kit (Clonetech), using Advantage Klen Taq polymerase (Clonetech), the AP1 primer (Clonetech) and specific reverse primers designed based on cDNA sequences from either *Drbgp* (ZbBGP1R) or *Ssbgp* (SseBGP1R). Amplification conditions used were those suggested by the supplier.

M12- Molecular cloning of *D. rerio* and *S. senegalensis mgp* cDNAs

A partial Dr*mgp* cDNA sequence (accession number BF938148) was obtained by TblastN search on the NCBI gene bank (EST: fm73a11.y1). One forward primer, designed based on this sequence (DrMGP1F), and the universal adapter as reverse primer were used to amplify the 3' end of Dr*mgp* sequence using 1 μg of total RNA obtained from zebrafish heads and vertebral columns. A partial *Solea senegalensis mgp* cDNA sequence was amplified by RT-PCR from 1 μg of total RNA isolated from Senegal sole head bones and vertebral column. The forward primer used was designed from a consensus region based on alignments of all fish *mgp* sequences previously

known (CorvMGP3F, Simes *et al.*, 2003) and the universal adapter was used as reverse primer. PCR products were resolved in a 1.5 % agarose gel by electrophoresis and expected size fragments extracted from the gel, inserted into the plasmid pGem T-easy (Promega), cloned and sequenced (T7 sequencing kit, Amersham-Pharmacia Biotech, USA). The 5' ends of Dr*mgp* and Ss*mgp* cDNAs were amplified by 5' RACE-PCR as described for *bgp* cDNAs using 1 μg of mRNA, the same Marathon cDNA libraries and specific reverse primers based on the previously obtained partial 3' end sequences (DrMGP1R) and (SsMGP1R).

M13-Quantitative Real Time -PCR

In order to determine the expression levels of both *bgp* and *mgp* in a quantitative manner, we have started by using 1 μg of total RNA isolated from different larval and juvenile stages of *D. rerio* (ranging from 32 hours post-fertilization (HPF) to 45 days post-hatching (DPH)) or from *Solea senegalensis* (ranging from 1DAH to juvenile stage) that was reverse transcribed using an oligo (dT) adapter. Real-time PCR was performed in a iCycler iQ real-time PCR detection system (Bio-Rad), using the following primer sets for amplification of *bgp*, *mgp* and 28S ribosomal RNA in zebrafish and *bgp*, *mgp* and *beta-actin* in senegal sole respectively: ZBGP 8F and ZBGP 2R; DrMGP 4F and DrMGP 2R; Dr28SRib 1F and Dr28SRib 1R; SsBGP 3F and SsBGP 2R; SsMGP 2F and SsMGP 2R; SsACT 1F and SsACT 1R.

The PCR reactions were set up by adding 2 μl of a 1:10 cDNA dilution to 18μl reaction mix containing 0.5 μM of each primer, and 10 μl of iQ SYBR green Supermix (Bio-Rad). The PCR program contained an initial cycle of 3 min at 95 °C followed by 50 cycles comprising a denaturation step at 95°C for 30 sec, followed by annealing and extension at 68°C for 30 sec. The fluorescence was measured at the end of each extension cycle in the FAM-490 channel. Relative levels of expression were determined using as control levels those found for the youngest specimen analyzed in each species.

Table M1- Sequences for the primers used in these work.

Amplified cDNA	Primer name	Primer Sequence [a]
Dr BGP	ZbBGP 6F [b]	TGYGARCAYATGGCNGAYAC
Dr BGP	ZbBGP1R	ACAGTCAGCTACTCTTCACTGCTGGTGTG
Dr BGP	ZBGP 8F	GCCTGATGACTGTGTGTCTGAGCG
Dr BGP	ZBGP 2R	AGTTCCAGCCCTCTTCTGTCTCAT
Dr mgp	DrMGP1F	TGTGTGTCTCCTCAGTGTGTGTT
Dr mgp	DrMGP1R	GAGCAGATGCAGGATCAGTGTCATTCACA
Dr mgp	DrMGP4F	AACACAACCCCTACATCTACCGAA
Dr mgp	DrMGP2R	GCGGGCTGAAGAAGGTCTGATAGG
Sse bgp	SBG5F	TGTGAGCACATGATGGATACGGAGGGAATC
Sse bgp	SseBGP1R	TTGGTCCATAGTAGGTGGTGTAGGCAGCG
Sse bgp	SsBGP3F	AACTTTGTCCGTCCTGGTTCTCTG
Sse bgp	SsBGP2R	GGACGCCTGCTCCTGCTCCACAAA
Sse mgp	CorvMGP3F	AGGCGTGCAGAGACCTGCGAGGACTAT
Sse mgp	SseMGP1R	TCTGTGGCTGACTCCGGGCACCAAAGTA
Sse mgp	SsMGP2F	TGTCAGTCTGTCAAAGGCAGGGTT
Sse mgp	SsMGP2R	CCTGAGAAAACACAAGAGATGGGC
Sse β-actin	SsACT1F	GACACTGACATCCGCCAAGACCT
Sse β-actin	SsACT1R	CTGCTGGAAGGTGGACAGGGAGG
*Dr*18S Ribosomal[c]	Dr28SRib1F	TCGGTCCTAAGGGATGGG
*Dr*18S Ribosomal[c]	Dr28SRib1R	CCGGGTTGGTTTGCGTCA
Dr β actin	ZBACT1F	CGTTTACCACTTTGCCCTCCTCAC
Dr β actin	ZBACT1R	GGACATCCCTTATTCACATACCCTA
	dT Adapter	$(T)_{21}$ACGCGTCGACCTCGAGATCGATG
	Universal adapter	ACGCGTCGACCTCGAGATCGATG

[a] All sequences are described in the 5' to 3'direction.
[b] Y, pyrimidine; R, purine; N, G + a + T + c.
[c] Based on the available partial sequence for *Danio rerio* 28S ribosomal RNA gene (AF398343)

M14- Northern blot hybridization

From each sample 10 µg of total RNA were fractionated in a 1.2% agarose / 0.4 M formaldehyde/ MOPS gel in MOPS 1x running buffer (Appendix 1) and then transferred by capillarity to a Nytran super charge nylon membrane (Amersham-Pharmacia) using 10x SSC (Appendix 1). The transfer apparatus was set-up according to the described in Sambrook *et al.*, (1989). Transfer was done overnight and RNA was blocked into the membrane by drying at 80 °C for 2 hours.

The membrane was prehybridized for 3 hours at 42°C with Ultrahyb solution (Ambion). Hybridization was performed overnight at 42°C with specific *S. senegalensis mgp* and *beta-actin* cDNA probes. The full length *S. senegalensis mgp* cDNA (see Fig. R11) and a 451 bp *S. senegalensis beta-actin* partial cDNA were labeled with [α–^{32}P] dCTP with the ReadyprimeII random priming labeling system (Amersham-Pharmacia). Unincorporated nucleotides were separated with Microspin S-200HR columns. The probe was denatured for 5 min in boiling water, ice cooled, then added to the Ultrahyb solution, pre-warmed to 42°C, and introduced into the hybridization bottles containing the membranes. After hybridization the membranes were washed twice for 15 min with 2x SSC / 0.1% SDS at room temperature, once for 15 min with 1x SSC / 0.1% SDS at 50°C and one last time for 30 min with 0.5x SSC /0.1% SDS at 50°C. For autoradiography the membranes were exposed to Kodak X-OMAT films at –70°C with two intensifying screens. The relative intensities of the bands for *mgp* and *beta-actin* on the radiographic film were analyzed using a Quantity One phosphoimager (BioRad).

M15- Detection of *D. rerio* and *S. senegalensis bgp* and *mgp* gene expression by RT-PCR coupled with Southern blot hybridization

After cloning the complete cDNAs, a 241 bp partial sequence of the *Drbgp* cDNA sequence was amplified by PCR, from reverse transcribed total RNA extracted from different larval and juvenile stages of *D. rerio* (ranging from 32 HPF to 45 DPH), using one specific forward primer starting at nucleotide 190 (ZBGP 7F) and extending to the polyadenylation signal with the universal adapter reverse primer. PCR reaction was set to a final volume of 50 µl as follows: 5 µl of 10x PCR reaction buffer; 1 µl of dNTPs (2.5 mM) 2 µl of 25 mM $MgCl_2$; 5 µl of RT product; 0.5 µl of 10 µM forward primer; 0.5µl of 10 µM reverse primer, 35.5 µl water and 0.5 µl Taq DNA polymerase

(Promega). Amplification was performed in a Perkin Elmer thermocycler set with temperatures of 58°C for annealing and 68°C for extension during 20 cycles. A partial 212 bp sequence of the zebrafish beta-actin was amplified with two primers designed based on the sequence published by Robinson et al (1993) (accession number: NM 131031). The sequence spans from bp 1398 (forward primer ZBACT1F) to bp 1610 (reverse primer ZBACT1R). Amplification conditions were the same as used for the *Drbgp* fragment. In both cases RT-PCR amplification was performed using 1µg of total RNA. PCR products were transferred to a Nytran Super Charge nylon membrane (Amersham-Pharmacia) by capillarity (Sambrook *et al.*, 1999) and hybridized with specific *Drbgp* and *Drbeta-actin* cDNA probes labeled with [^{32}P] dCTP as described above. The membrane was prehybridized for 3 hours and hybridized over night at 48 °C using the Ultrahyb system (Ambion). After hybridization the blots were washed for 30 min each with 2x SSC/ 0.1% SDS at room temperature and 1x SSC /0.1% SDS at 50°C followed by a final wash with 0.5x SSC / 0.1% SDS at 50°C for 1 hour. Membranes were exposed to Kodak X-OMAT films at –70°C until signal was clearly present.

M16- Immunohistochemistry

Immunohistochemical staining was performed using rabbit polyclonal primary antibodies against *Bgp* and *Mgp* from *A. regius*, following the procedure described by Rodriguez-Gómez *et al.*, (2000). Endogenous peroxidase activity was blocked in the dark with 3% hydrogen peroxide in Coons buffer (CBT- 0.01 M veronal, 0.15 M NaCl, 0.1% Triton X-100) for 30 minutes and endogenous phosphatase activity was blocked with 15% glacial acetic acid for 15 minutes. Before immunostaining, sections were transferred for 5 min to CBT and then saturated in CBT with 0.5% Bovine Serum Albumin, BSA (Fluka) for 30 min. Sections were then incubated overnight with rabbit anti-*Bgp* or anti-*Mgp* polyclonal antibodies (1:500) diluted in CBT / 0.5% BSA, in a humidified chamber at room temperature. Sections were washed in CBT and incubated for 120 min at room temperature with goat anti rabbit-IgG FITC conjugated (Sigma, St Louis, MO), goat anti rabbit-IgG peroxidase conjugated (Sigma, St Louis, MO), or goat anti rabbit-IgG phosphatase conjugated (Sigma, St Louis, MO) and diluted in CBT. The sections were washed again in CBT then in Tris–HCl (0.05 M, pH 7.4). Peroxidase activity was detected in the dark with 0.025% 3-3´ Diamino benzidine

tetrahydrochloride (Sigma, St Louis, MO) in Tris–HCl 0.05 M, pH 7.6 containing 0.05% hydrogen peroxide. Phosphatase activity was developed with Sigma fast red / Naphtol TR AS-MX. Reaction was stopped in distilled water when background signal started to be visible and the sections were mounted with aqueous mounting medium for optic microscopy (Aquatex, Merck). To confirm the specificity of the immunostaining, controls were performed by replacement of primary antibody with pre-immune serum or BSA and by omission of primary and secondary antibodies.

M17- *In situ* hybridization

M17-1 Generation of riboprobes for in situ hybridization

Partial cDNAs for both *D. rerio* and *S. senegalensis bgp* (250bp and 198bp DNA fragments respectively) and *mgp* were cloned into pGem T-Easy (Promega). 5 µg of each plasmid were linearized with appropriate endonucleases (Apa I for anti-sense probe and Pst I for sense probe) for two hours at 37°C. The reaction was stopped by adding a mix of phenol/chloroform (24:1) and incubating for 5 min. After centrifuging for 15 min at 13,000 g, the aqueous upper layer was transferred and precipitated with ethanol at -80 °C for 30 min, followed by centrifugation for 5 min at 13,000 g. The pellet was washed with RNAse-free 70% ethanol, air dried and resuspended in 25 µl of DEPC water. To confirm linearization an aliquot of each digestion product was size fractionated on a 1.2% agarose gel.

Digoxigenin (DIG)-labeled sense and anti-sense RNA-probes were synthesized with bacteriophage T7 and SP6 RNA polymerases, according to manufacturer specifications:

The following was mixed in an eppendorf tube and incubated for 2 h at 37°C:

- 1 µg linearized DNA, denatured for 5 min at 95 °C and cooled on ice.
- 10x Transcription buffer (SP6 or T7 RNA polymerase) - 2 µl
- NTP-DIG-RNA labeling mix - 2 µl
- RNAse inhibitor (35 units/µl) -1 µl
- SP6/T7 RNA polymerase (20 units/µl) - 1 µl
- RNAse free water to achieve a 20 µl total volume

The reaction was stopped by adding 2 µl of EDTA 0.5 M (pH 8) and the presence of the synthesized probe was confirmed by electrophoresis using a 1.2% agarose gel.

M17-2 Hybridization procedure

The hybridization procedure was in general performed as previously described (Pinto *et al.*, 2001; Simes *et al.*, 2004). 5-7 µm sections were dewaxed in 2x 10 min xylene, followed by 2x 8 min methanol, 5 min 75% methanol, 5 min 50% methanol, 5 min 25% methanol+75% PBT (PBS + 0.1% Tween 20) and 2x 10 min PBT. The sections were postfixed in 4% paraformaldehyde, washed for 2x 10 min in PBT and treated with proteinase K for 5 minutes, washed for 3 min in PBT, postfixed again for 30 min and washed 2x 10 min in PBT. The sections were then incubated at 50 °C for 3 hours covered with prehybridization solution (50% deionized formamide, 5x SSC, 1x Denhardt's, 100 µg/ml yeast tRNA, 100 µg/ml heparin, 0.05% CHAPS [(3-Cholamidopropyl) dimethylamonium-1-propanesulfonate]). The probes were heat denatured for 5 min and diluted 1:500 in prehybridization solution. The diluted probes were added to the sections (~50 µl per slide), covered with parafilm and incubated overnight with the same conditions of prehybridization, in a humidified chamber saturated with 20x SSC.

Following hybridization, the sections were washed 3x 20 min with 2x SSC and 2x 20 min with 2x SSC / 0.6% CHAPS at 55 °C. The sections were then washed 5 min in PBT, 5 min in PBT / maleic acid 100mM, blocked in 1% blocking reagent (Boehringer Mannheim) in maleic acid buffer for 1 hour and incubated with anti-digoxigenin antibodies (Boehringer Mannheim) at a dilution of 1:2000 in blocking solution for 2 hours at room temperature. After washing excess antibodies with 3x 10 min in PBT, slides were placed for 10 minutes in color buffer (100 mM Tris-HCl, 50 mM magnesium chloride, 100 mM sodium chloride, 0.1% Tween 20) and developed for 12-24 hours in the dark with color reagent [22.5 µl of 100 mg/ml 4-nitroblue tetrazolium chloride (Sigma) and 35 µl of 50 mg/ml 5-bromo-4-chloro-3-indolyl phosphate (Sigma) in color buffer], with constant agitation. The sections were observed regularly to check for appearance of signal and color reaction was stopped in PBT. The slides were rinsed in distilled water and mounted in AQUATEX (Merck).

M18- Treatments with vitamin K and sodium warfarin [3-(α-acetonylbenzyl)-4-hydroxycoumarin]

To access the effects of warfarin, larvae of zebrafish and adults of toadfish (*Halobatrachus didactylus*) were submitted to daily treatments with different concentrations of vitamin K and/or its antagonist sodium warfarin. Larvae were submitted to treatments by immersion and adult toadfish were treated by injection of vitamin K and/or warfarin following a procedure modified from the ones developed by Price *et al.*, (1999) and Howe & Webster (2000) for mice.

M18.1- Solutions for injection

Vitamin K1 (phylloquinone): A 10 mg/ml injection solution of vitamin K1 (Sigma, Madrid) was prepared by dissolving the vitamin K1 in Emulfor (alkamuls EL-620, Rhone-Poulenc) and subsequently used to prepare an emulsion with 3.75% dextrose. The solution was aliquoted in injection vessels and stored protected from light and air, at 4°C.

Sodium warfarin: A 100 mg/ml sodium warfarin (Sigma, Madrid) solution was prepared in 0.15 M NaCl. The solution was aliquoted in injection vessels and stored at 4°C.

M18.2- Injection protocol

Twelve adult toad fish were purchased from local fisherman. Upon arrival, the fish were weighed, measured and separated in four groups of 3. Each group was placed in 100 liter tanks in a closed recirculating circuit, with a photoperiod of 12 hours light and 12 hours dark, a stable temperature of 16 ± 1°C and salinity of 35‰. The fish were maintained in the circuit 3 weeks for aclimatation before treatment, and feed *ad-libitum* once a day with squid or mussels. After this period the fish were anesthetized with 0.1% 2-phenoxyethanol, weighed and measured again before beginning the treatments. Each group was injected once every 48 hours with: 100 µl / Kg 0.15 M NaCl + 100µl /Kg 7% Emulfor; 3.75% dextrose (control group); 1.5 mg Vit. K_1 / 100 g weight + 15 mg / 100 g weight (Group II); 1.5 mg Vit. K_1 / 100 g weight (Group III); 15 mg warfarin / 100 g weight (Group IV). The treatment was continued during 3 weeks. Weight, total length and survival were registered before every injection cycle. After the completion of the

treatment period, the fish were sacrificed and samples of vertebral bone, branchial arches and heart were collected both for RNA purification and for histological purposes.

At the end of the experimental period the hearts of sacrificed specimens were fixed as previously mentioned and stained with alizarin red S 0.001% in 0.5% KOH for 2 hours. After staining, hearts were macerated for 24 hours in 0.5% KOH, washed twice for 1 hour in distilled water, then passed through a series of baths of water and glycerol (3:1; 1:1; 1:3) for 1 hour each and preserved in glycerol.

M18.3- Immersion treatments

M18.3.1- Preliminary approach

Experiment 1: 150 larvae of zebrafish at 5 DPF were separated into 5 triplicates of 10 fish each and submitted to an initial preliminary treatment by immersion in different concentrations of sodium warfarin and vitamin K3 (menadione) as follows: O mg/l warfarin + 0 mg/l Vit. K3; 0 mg/l warfarin + 1 mg/l Vit. K3; 10 mg/l warfarin + 0 mg/l Vit. K3; 10 mg/l warfarin + 1 mg/l Vit. K3; 10 mg/l warfarin + 10 mg/l Vit. K3. Mortality was recorded daily during the 2 weeks of treatment.

Experiment 2: 150 larvae of zebrafish with 5 DPF were separated into 5 triplicates of 10 fish each and submitted to a treatment by immersion in different concentrations of sodium warfarin) as follows: O mg/l warfarin; 5 mg/l warfarin; 25 mg/l warfarin; 50 mg/l warfarin; 100 mg/l warfarin. Mortality was recorded daily during the 3 weeks of treatment.

In each experiment larvae were feed artemia nauplii 2 times a day. Samples were collected at the end of each week of treatment for both RNA extraction and histological purposes.

Detection of differences in calcium deposition patterns between treated animals were determined using the histological techniques of Von Kossa and alizarin red. Detection of differences in the accumulation of *Bgp* and *Mgp* proteins were determined by immunohistochemistry. *bgp* and *mgp* gene expression were analyzed by transferring 5 µg of total RNA to a Nytran super charge nylon membrane and performing northern hybridization as described above.

M19- Treatment with Vitamin A

M19.1- Methods

Vitamin A treatment: Solea senegalensis larvae and juveniles were submitted to different concentrations of vitamin A through feeding with artemia enriched with oil emulsion containing defined amounts of the vitamin. This approach to deliver the treatments to larvae has followed the protocols successfully used by other authors (Dedi *et al.*, 1995; 1998; Takeushi *et al.*, 1998). The use of commercial lipids to enrich artemia (Selco, Kurios super lipids) allows the inclusion of liposoluble vitamins added to the oil emulsions and the load of artemia which will deliver it to the larvae once these feed on the enriched artemia.

Artemia cists were incubated overnight at a density of 1g/liter in cylindroconical tanks with constant illumination, temperature of 24 °C and salinity of 30‰. After hatching the nauplii were harvested in a 125 µm mesh and separated into four groups of 100,000 in 2 liter glass beakers for enrichment. Vitamin A (Retinol palmitate, Sigma) was mixed with Selco at concentrations of 0, 100, 1,000 and 10,000 IU in 0.6 g of Selco. An emulsion of Selco was prepared with salt water and added to the enrichment containers. The enrichment media was changed 2 hours before supplying the artemia to the treatment cages

Four groups of 30 fish with 19 DPF were separated into floating cages with 250 µm mesh walls, placed inside two 100 liter tanks in a closed recirculating circuit with a photoperiod of 12 hours light and 12 hours dark, a stable temperature of 16 ± 1°C and salinity of 35‰. The treatment groups were feed daily with 100,000 artemia metanauplii enriched with Selco (control), or Selco + 100, 1,000 or 10,000 IU. The remaining artemia was removed by siphoning before supplying newly enriched artemia.

Fish were treated for 2 weeks and collected at 7 day intervals for RNA preparation and immunohistochemistry. *bgp* and *mgp* expression were analyzed by transferring 5 µg of total RNA to a Nytran super charge nylon membrane and performing northern hybridization as described.

RESULTS

Results

R1- Establishment of a zebrafish rearing system

The rearing system implemented, composed of independent aquaria, allowed us to properly maintain adults and obtain the larvae and juveniles required for the realization of the present studies. The temperature was maintained stable at 28 ± 1 °C and the biological parameters $NH4^+$, $NO3^-$, and $NO2^-$ were kept below detectable levels.

R2- Skeletal development

R.2.1- Zebrafish

The nomenclature used for description of head structures followed that presented by Piotrowski *et al.*, (1996) and Schilling *et al.*, (1996a) for the description of early branchial arches and cranium skeletal development. Specimens of zebrafish collected during the hatching period (between 52-56 hours post fertilization) presented an underdeveloped skeleton, composed only of cartilaginous elements and the otoliths. Structures present in the head skeleton were the basihyal and the first branchial arches, ceratohyal and ceratobranchials 1, 2 and 3, Meckel's cartilage, palatoquadrate, hyosymplectic, ethmoid plate and trabeculae. The notochord was the only axial support element and the paired pectoral fins appeared as cartilaginous plates, attached to a cartilaginous coraco-scapular complex. No calcified structures were visible at this stage, beside the otoliths. At 72 HPF the larvae presented a similar distribution of skeletal elements, although an elongation of the structures was observed and the number of ceratobranchials had increased to 5. Meckel's cartilage had migrated forward and the mouth was already opened. At this stage a calcified cleithrum becomes visible, supporting the coraco-scapular complex. The first calcified pharyngeal teeth appeared at 96 HPF (Fig. R1A) attached to the fifth pair of ceratobranchials as ventral elements. At this same age the process of perichordal calcification of the basioccipital articulatory process (BOP) had started, and this was the first structure of the axial support skeleton to mineralize. At 5 DPF calcification continued to increase in the cleithrum, pharyngeal teeth and BOP and extended to the opercular bones (Fig. R1B). At 6 DPF the hyosymplectic started to mineralize in a perichondral manner (Fig. R1C), and the zones

on the periphery of the opercula started to calcify. The ceratohyal cartilage began to mineralize in a median region at 8 DPF (Fig. R1D) extending subsequently to both extremities. The first two cartilaginous hypural plates appeared ventrally at the posterior extremity of the notochord (Fig. R1E). The first forming vertebrae were observed at 9 DPF as a mineral deposition on the notochord envelope (Fig. R1F), starting on the dorsal zone and then extending ventrally. The first vertebrae to form were 3, 4, 5 and 6, followed shortly by vertebrae 1 and 2. Calcification process continued in the head structures and the cartilaginous hypural 3 appeared. Vertebral formation continued towards the posterior end and at 12 DPF all individuals observed showed vertebrae surrounding the notochord to the level of caudal vertebrae 20-25 (Fig. R1G). The five hypurals, parhypural and modified haemal arches were already present (Fig. R1H) and the first calcified rays of the caudal fin were forming by intra-membranous calcification. The ceratobranchial 5 was almost completely calcified and the first mineral deposits appeared in the basihyal, palatoquadrate and Meckel's cartilage. The first neural arches appeaedr at 14 DPF on the fourth vertebra, already with visible calcification (Fig. R1I) while the cartilaginous elements of the hypuralia were beginning endochondral mineralization (Fig. R1J). An almost completely formed vertebral column was visible at 19 DPF (Fig. R1K), with all structures calcified, except for the two most posterior vertebra that formed the urostyle, still undergoing calcification, and in the process of upwards inflexion. The first dorsal arches are modified to form the Weberian apparatus The caudal fin had achieved the total number of structures with all rays, hypurals, epurals and modified arches and spines. The dorsal and anal fins were already formed and largely mineralized while in pectorals, mineralization of the rays was just beginning. The head was largely mineralized although skull bones forming by intramembranous calcification and cartilage undergoing endochondral ossification were continuing to develop until late juvenile stages.

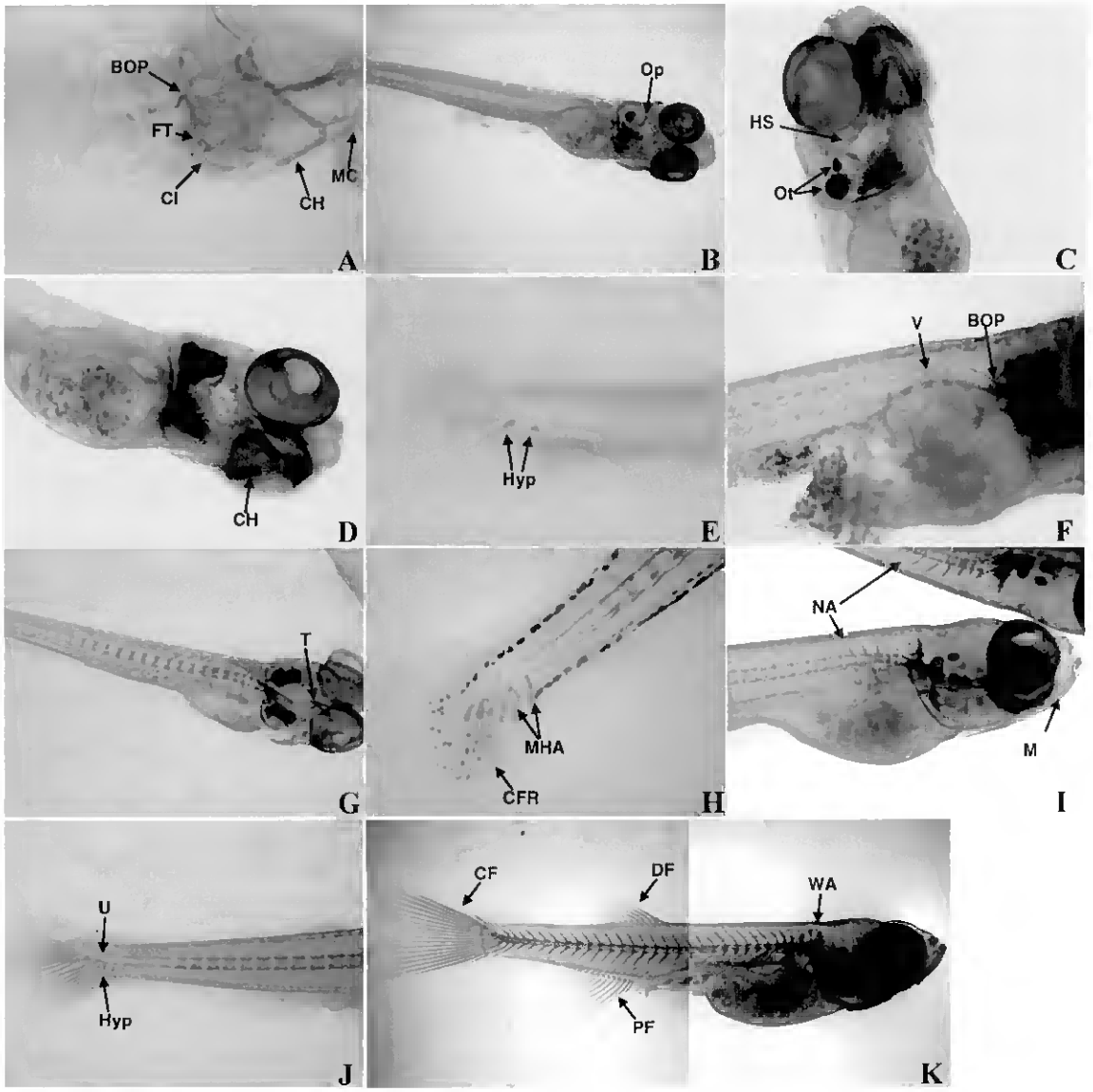

Figure R1- Observation of developmental appearance of skeletal structures in *Danio rerio* by Alcian blue-Alizarin red double staining. Whole mount double staining of the skeleton was used to follow ontogenic development of cartilaginous and calcified structures. A- 96 HPF *D. rerio* larvae head skeleton presenting calcified pharyngeal teeth (PT), cleithrum (Cl) and basioccipital articulatory process (BOP) while the remaining structures have a cartilaginous nature like Meckel's cartilage (MC) and ceratohyal (CH)(100X); B- 5 DPF *D. rerio* larva presenting calcification on the opercula (Op) 40x; C- Beginning of the calcification of the hyosyplectic (HS) in a 6 DPF larva 100x; D- Beginning of the calcification of the ceratohyal (CH) in a 8 DPF *D. rerio* 100x; E- First hypurals (Hyp) developed at 8 DPF (100x); F- The formation of the first vertebrae (V) is observed at 9 DPF 100x; G- Calcification of the trabeculae (T) is observed at 11 DPF, vertebrae continue to form (in an anterior-posterior direction) towards the posterior end of the notochord 40x; H- Caudal hypuralia acquires final number of structures and caudal fin rays appear at 12 DPF 100x; I- Formation of the first neural arches (NA) is observed dorsally in the anterior vertebrae at 14 DPF, the mandibula is already calcified (M) 40x; J- Beginning of the calcification of the hypurals at 14 DAF 40x; K- Composite image of a 19 DPF *D. rerio* with most of the skeletal structures present and calcified.

R.2.2- Senegal sole

For the examination of the skeletal structures used to study the ontogenic development of the skeleton and determination of skeletal abnormalities, 179 individuals ranging from 3.1 mm to 59.2 mm standard length were stained for cartilage and bone with alcian blue and alizarin red respectively, measured, observed and photographed.

R.2.2.1- General morphology of the axial skeleton in the adult Senegal sole

In the largest individual observed (5 months of age, 59.2 mm Lt), the vertebral and caudal skeleton were totally formed and mineralized, except for the cartilaginous islets in the base of the arches and the growth zones in the distal extremities of bones like the hypurals, epural and pterigophores that articulate with fin rays (Fig.2F and 2G).

The structures that articulated with fin rays on the caudal complex (Fig. 3F) were typically five hypurals, one parhypural, one epural, one modified neural spine from the first preural centrum and two modified haemal spines from preural centrum 1 and 2. The hypurals 1-4 were fused to the urostyle by their proximal bases, which in turn were fused with the base of each adjacent hypural, forming a unique plate (Fig. 2G and 3F). The hypural 5, parhypural and epural did not fuse to any structure. Branching was observed on the hypural plates 1-4 and parhypural that presented vertical ridges, extending from the distal to the proximal region of the structure. No branching was observed on the hypural 5, epural or on the modified spines. No free uroneurals were observed. The caudal fin had a total number of 20 soft rays, and no spiny rays were observed in the caudal or any other fin. The contribution of the internal skeleton structures was as follows: epural and the neural spines articulated with 3 rays, the hypural 5 with 2 rays, hypural 1-4 articulated with 10 rays and parhypural and the haemal spines articulated with 5 rays (Fig. R2G and R2F). The caudal fin was symmetrical, with 10 rays on each side of the lateral line that extended almost to the posterior tip of the caudal fin (Fig. 2G).

The vertebral column was composed of 45 ± 2 vertebrae, distributed into 8 abdominal (or pleural) and 37 caudal, including the urostyle (Fig. R4F). All abdominal vertebra (Fig. R5A) were equipped dorsally with a neural arch and neural spine and from the fourth to the eighth vertebrae a pair of parapophysis was observed ventrally. The first abdominal vertebra was articulated with the basioccypital articulatory process that connects the vertebral column to the skull (Fig. R4F). The first 5 neural spines were

thicker than all the others. The caudal vertebras (Fig. R5B) were equipped dorsally with a neural arch and neural spine and ventrally with a haemal arch and haemal spine except for the urostyle that lacks any complementary structures. The neural spines of preural vertebrae 1 and 2 and the haemal spine of the first preural vertebra were elongated and modified to help support the caudal fin rays (Fig. R3F and R4F). Both pleural and caudal vertebrae exhibited in the neural arch an anterior neural prezygapophysis and a posterior neural poszygapophysis. The haemal arches of the caudal vertebras exhibited an anterior haemal prezygapophysis and a posterior haemal poszygapophysis (Fig. R5).

R.2.2.2 - General skeletal development

At the yolk sac and early larval stages, Senegal sole showed as only visible support structure a straight notochord that extended for the entire length of the body (Fig. R2A and 4A). At these early stages, the only fin structures present were the primordial marginal fin fold and the pectoral cartilaginous plates (Fig. R2A). The caudal fin was the first fin to differentiate, with the appearance of internal support skeleton followed by the formation of fin rays by intramembranous ossification. Development of vertebral column elements occurred in parallel with caudal fin structures and eye migration. The dorsal and anal fins cartilaginous pterigophores appeared late in metamorphosis and developed in an anterior-posterior direction, followed by the formation of fin rays by intramembranous ossification (Fig. R2 D). By the time development of the vertebral column and formation of the caudal fin were completed, eye migration had also occurred and the dorsal and anal fins had extended dorsally until the caudal complex (fig 2D-G).

The dramatic morphological changes during metamorphosis imply acquisition of asymmetry and occur in parallel with changes in life style from pelagic to benthonic. These changes are 1) eye migration from left to right side and concomitant bending of the urostyle; and 2) torsion of internal organs that starts during the process of eye migration; This process initiated in larvae around 4.1mm Lst and ended when larvae reached approximately 8 mm Lst.

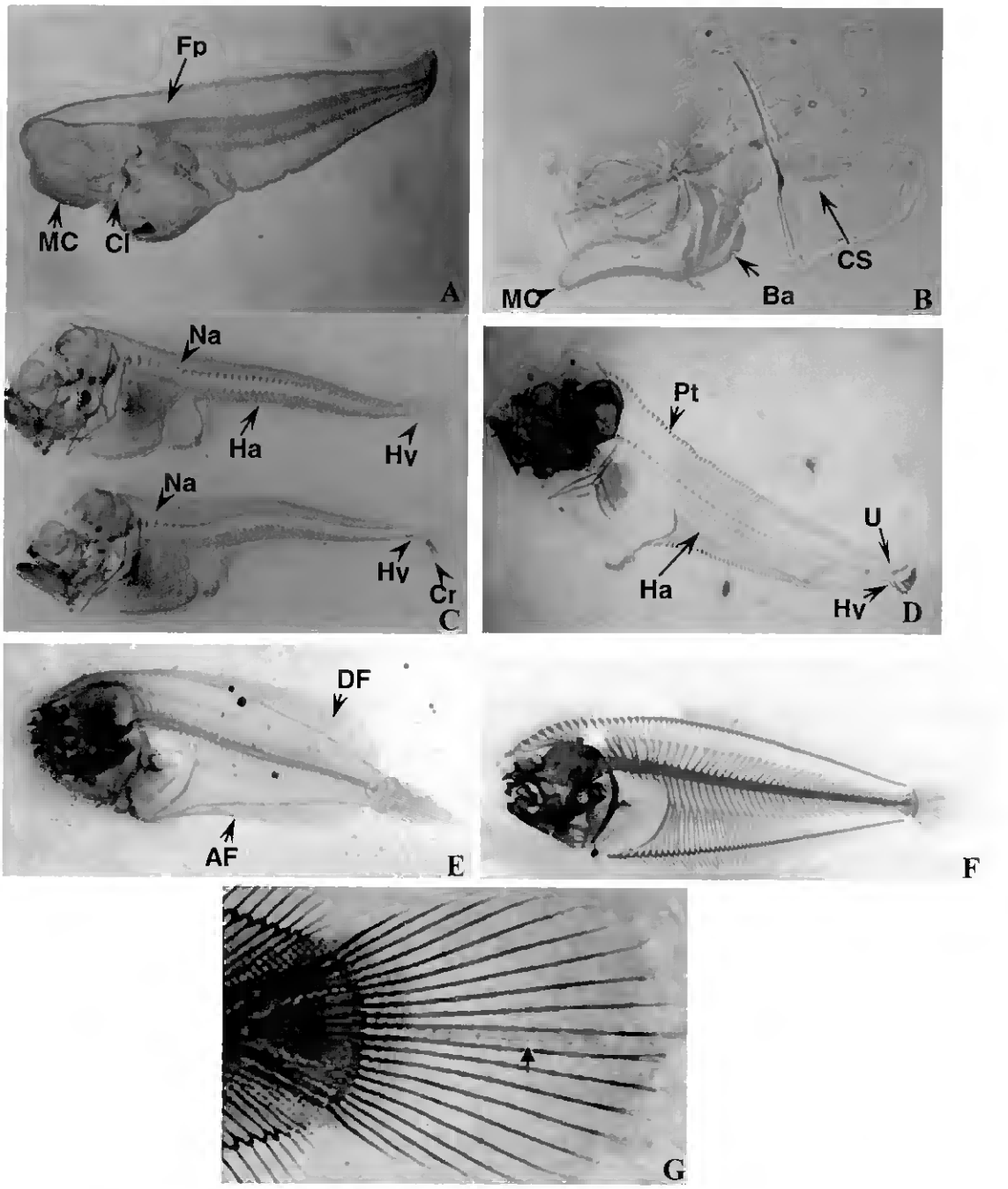

Figure R2- Developmental stages of skeletal development in the Senegal sole A- 2 dpf larvae (2.6 mm notochord length) displaying the non calcified Meckel's cartilage (MC), the already calcified cleithrum (Cl) and the fin plates (FP) still entirely cartilaginous; B- 7 dpf larvae with a well developed coraco-scapular complex (CS) and branchial arches (Ba); C- 15 dpf larvae at the beginning of metamorphosis, showing the developing first neural and haemal arches (Na and Ha) and first hypurals (Hy), and caudal fin rays appearing by intramembranous calcification (Cr); D- 17 dpf larvae showing the developing dorsal and anal fins and the inflected urostyle (Ur) E- *Solea senegalensis* post-larvae with an almost completely calcified skeleton; F- 75 dph juvenile with cartilage remaining only in growth zones; G- Caudal fin complex of a juvenile sole with 59.2 mm total length. Full development of skeletal structures and scales has been achieved. The caudal fin is exclusively composed of soft rays and symmetrically divided by the lateral line scales (arrow). The hypural plates are fused and present branching.

R.2.2.3- Vertebral column development

Vertebral column was formed by the vertebral centra, the neural and haemal arches and spines, the parapophyses and the ventral ribs. They were all formed by intramembranous ossification except for the arches and spines of the four preural centra, which appeared initially as cartilaginous structures and calcified by endochondral ossification. No vertebral elements were observed at hatching and in early stages of development, where the notochord was the only axial support structure observed (Fig. R2A).

The first calcified elements of the vertebral column to be observed were neural arches 2-6 in the first abdominal vertebrae of a 4.3 mm Lst larvae (Fig. R2C and R4B), at 13 DAH. The development of the arches initiated with the formation of two buds latero-dorsally on each side of the notochord by intramembranous ossification. These buds elongated dorsally until they joined together forming the arch (Fig. R4B). After the arches were formed, the neural spines also appeared by intramembranous ossification and elongated dorsally. Haemal vertebrae formed similarly but in ventral orientation. The vertebral development continued *caudad* for all the remaining neural arches and haemal arches except for the first neural arch, which formed *cephalad*.

The first haemal arches were observed in 4.55 mm Lst larvae, showing neural arches 2-8 and haemal arches 1-12 (Fig. R4C). In a 4.7 mm Lst specimen, 28 neural arches and 17 haemal arches were visible and the first neural arch was already completely formed (Fig. R4D). The cartilaginous buds of the arches in preural vertebra were already present near the urostyle, which had not yet begun bending upward. Parapophyses 3-5 were visible on pleural vertebrae at this stage (Fig. R4D). At 5.65 mm (Fig. R4E) the anterior vertebrae and arches were nearly formed and the notochord was completely surrounded by calcified tissue, while in the posterior caudal vertebrae, the calcified tissue was starting to spread around the notochord from the site of insertion of the arches. The urostyle had started bending upward, and was partially calcified. Only the modified arches and spines from preural vertebra 1 and 2 and the hypuralia were still present as cartilaginous structures.

At 45 DAH (8.3 mm Lst) the metamorphosis and flexion of the urostyle were already completed and all vertebral elements were formed and calcified (Fig. R4F). The vertebral centra completely surrounded the notochord and the adjacent arches were all closed around the ventral aorta in the haemal side and around the nervous chord in the

neural side. In larger animals, the vertebral elements and processes only increased in complexity and size, and the spines and fin rays elongated distally.

R.2.2.4- Caudal fin complex development

The elements that compose the caudal fin complex were formed either by endochondral or by intramembranous ossification. The first group included the hypurals, epural, and modified arches and spines; the second group included the urostyle, the preural centra and the caudal fin rays (lepidototrichia).

The first element to develop was the hypural 1, appearing in a cartilaginous form at 13 DAH in pre-flexion larvae ranging in size from 4.3 to 4.65 mm Lst. It was followed by hypural 2 (Fig. R3A) at 4.4 mm Lst and hypural 3 at 4.45 mm Lst, circa 15 DAH. Hypural 4 appeared generally in larvae larger than 4.5 mm Lst, during metamorphosis (Fig. R3B). At this stage the parhypural and the cartilaginous buds of the arches were visible. From the bases of these arches began to form the preural centra 1, 2 and 3, on each latero-dorsal face of the notochord, as seen in a larva with 4.7 mm Lst (Fig. R3C). At this stage the upward flexion of the urostyle was initiated and the caudal rays started to form by intra-membranous ossification within the primordial fin, in the area adjacent to the forming cartilaginous hypurals, with mineralization starting in the median zone and extending to the extremities of the soft rays (Fig. R2C and R3C). The epural appeared during flexion of the urostyle, between 5.2 and 5.65 mm Lst. The hypural 5 was the last structure to appear ventrally, next to the tip of the notochord, in 18 DAH larvae larger than 5.5 mm Lst (Fig. R3D), when flexion of the urostyle was almost concluded.

At 6.6 mm Lst, all the caudal plates had increased in size and calcification was visible in the urostyle, extending to the proximal bases of hypurals 1-4, which began to fuse with the urostyle. The neural and haemal arches and spines of the preural vertebrae started to calcify, as well as the corresponding centrum, which gradually surrounded the notochord, starting from the area of insertion of the arches. At this stage, all fin rays were already present, with alizarin red staining decreasing in intensity from the longer central to the shorter lateral rays. The caudal fin was still connected to the anal and dorsal fins by the primordial fin tissue (results not shown).

In a 7.8 mm Lst 34 DAH larvae (Fig. R2E and R3E), all the plates were largely ossified, with greater intensity of alizarin red staining observed in the proximal parts, and progressively decreasing in intensity towards the distal parts. The posterior end of

the hypurals was still cartilaginous and thus stained in blue. Calcification also extended to the spines in the preural vertebrae. At this stage, the caudal rays were all ossified and the caudal fin was totally separated from the anal and dorsal fins.

At 12.8 mm Lst, all the caudal fin elements were totally calcified and hypurals 1-4 were fusing to the urostyle and to each other by their proximal bases (results not shown). At 19.8 mm Lst, vertical fissures had appeared in the posterior regions of the parhypural and hypural 4, indicating the beginning of branching. Hypurals 1-4 were totally fused to the urostyle (results not shown). At the juvenile stage, in a 59.1 mm Lst individual, hypurals 1-4 and parhypural showed one vertical fissure each, extending from the posterior to the median zone of the plates (Fig. R2G and R3F).

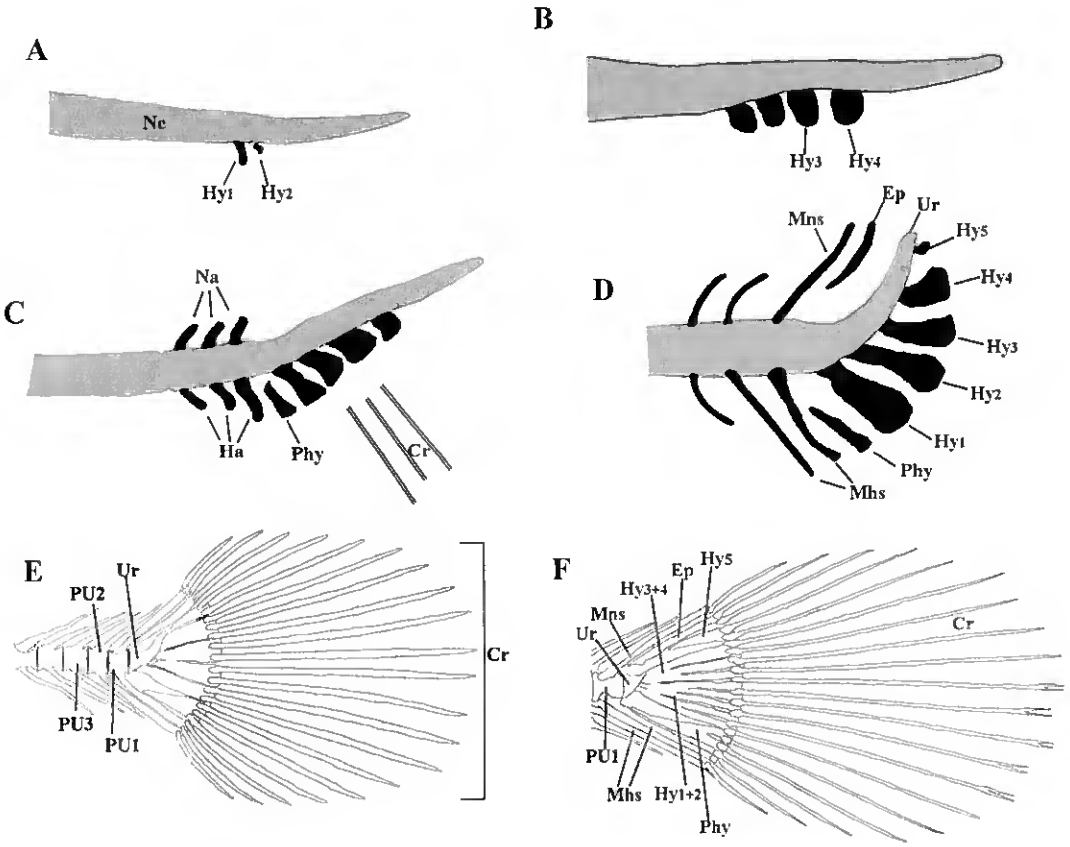

Figure R3- Schematic representation of the caudal fin complex development in Senegal sole. Calcified structures are presented in white and cartilaginous structures in black. Notochord is shown in gray. A- 13 DAH specimen (4.4mm Lst). B- 15 DAH specimen (4.55mm Lst). C- 18 DAH specimen (4.7mm Lst). D- 18 DAH specimen (5.6mm Lst). E- 34 DAH specimen (7.8mm Lst). F- 6 month old juvenile specimen (59.2mm Lst).

Cr- Caudal fin rays, DAH- Days after hatching, Ep- Epural, Hy- Hypural, Lst- Standard length, Mhs- Modified haemal spine, Mns- Modified neural spine, Nc- Notochord, Phy- Parhypural, PU- Preural vertebra, Ur- Urostile..

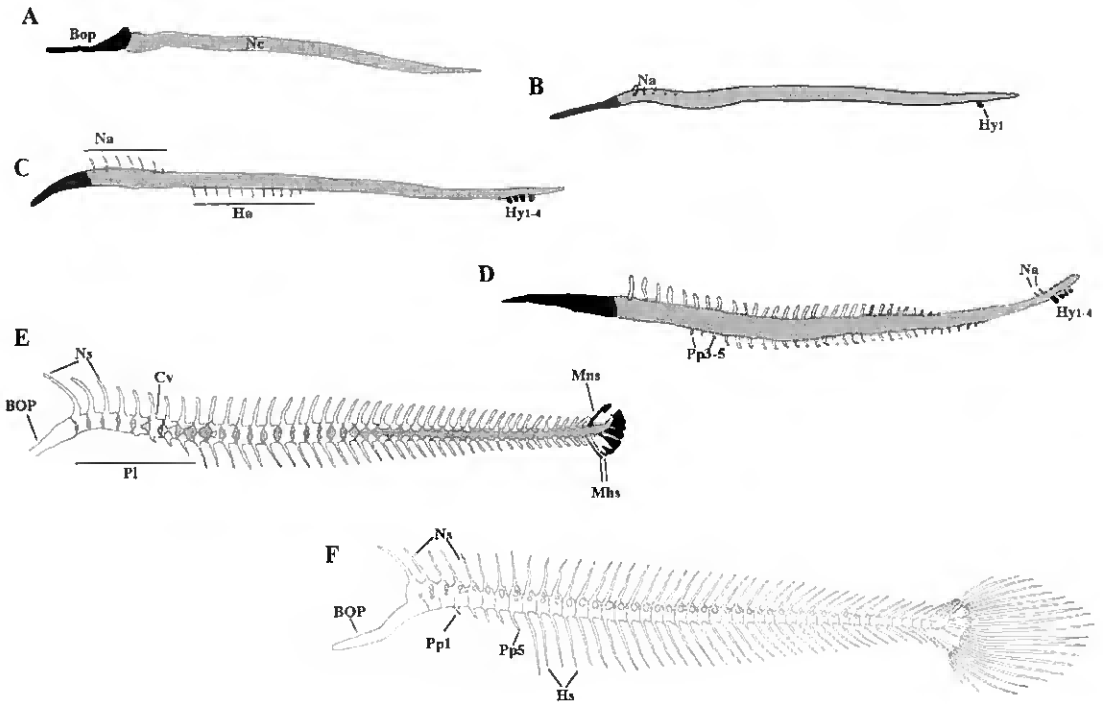

Figure R4- Schematic representation of the vertebral column development in Senegal sole. Calcified structures are presented in white and cartilaginous structures in black. Notochord is shown in gray. A- 0 DAH larva (3.4mm Lst). B- 13 DAH Lst larva (4.3 mm Lst). C- 15 DAH specimen (4.55mm Lst). D- 18 DAH specimen (4.7 mm Lst). E- 18 DAH specimen (5.65 mm Lst). F- 45 DAH specimen (8.3 mm Lst). Bop- basioccypital articulatory process, Cv- Vertebral centra, Hs- Haemal spine, Pl- Pleural vertebra, Pp- parapophysis, Na- Neural arch, Ns- Neural spine. For other abbreviations see Fig.2.

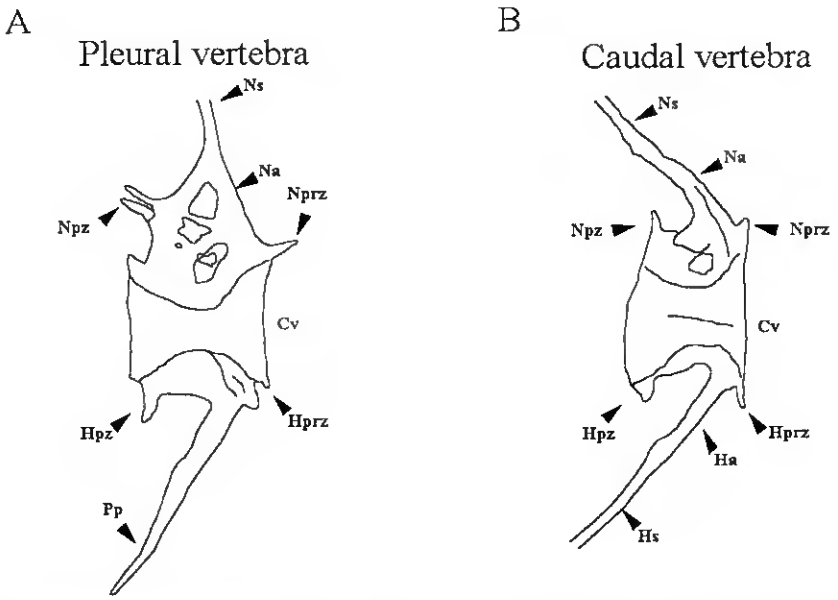

Figure R5- Schematic representation of an abdominal vertebra (**A**) and a caudal vertebra (**B**) from a Senegal sole juvenile.

Ha- Haemal arch, Hpz-Haemal poszigapophysis, Hprz- Haemal prezigapophysis, Npz- Neural poszigapophysis, Nprz- Neural prezigapophysis. For other abbreviations see Fig.R4.

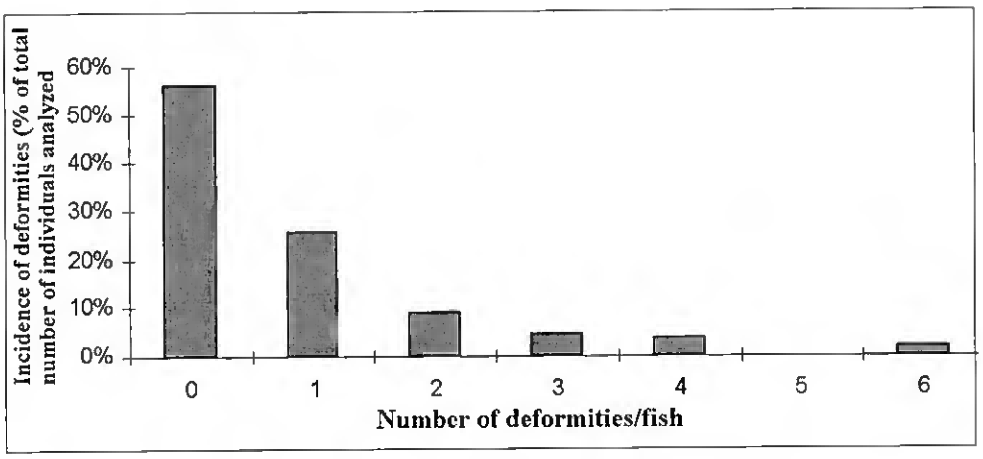

A

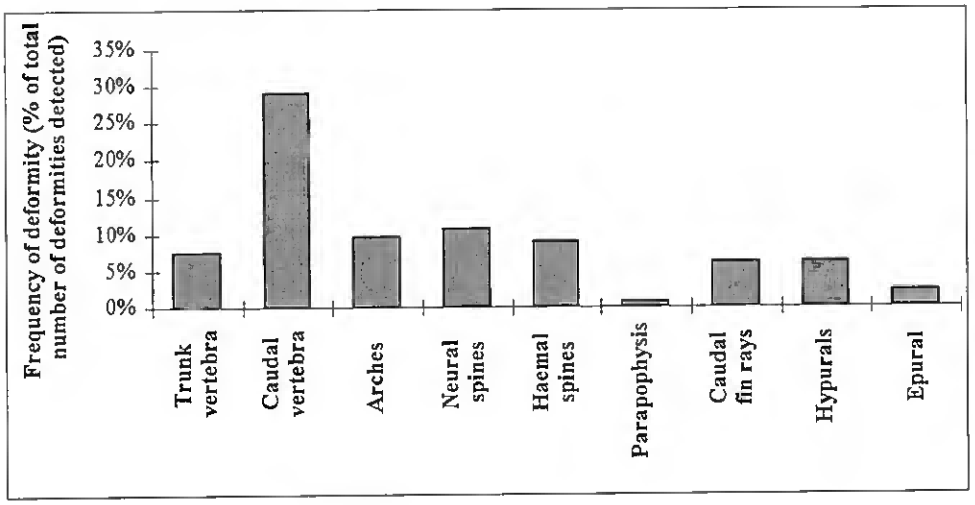

B

Figure R6- A- Distribution of analyzed fish according to the number of deformities observed in each individual. B- Distribution of the abnormalities detected according to the affected structures. All the skeletal structures studied are affected by deformities, with special incidence in the caudal vertebra and associated structures.

R.3- Skeletal malformations in hatchery reared Senegal sole

A large number of deformities were observed in the 179 individuals used for this study. The observed malformations ranged from fish with only one small anomaly in a fin ray to fish displaying multiple vertebral deformities with different degrees of

severity. From the specimens observed, 79 (44%) presented at least one deformity affecting any of the skeletal structures analyzed. From these deformed fish, more than half (25.6% of the individuals analyzed) presented only one deformity while 33 (18.4% of the individuals analyzed) presented multiple deformities (Fig. R6A).

Malformations where divided into 9 categories according to the place of incidence in the axial skeleton, as follows: trunk vertebra, caudal vertebra, arches, neural spines, haemal spines, parapophysis, caudal fin rays, hypurals and epural. The frequency observed for each type of deformity encountered is shown in Figure 6B. Caudal vertebra showed higher frequency of malformations (28%) but they also occurred in the neural (11%) and haemal spines (9%), trunk vertebra (7%), and vertebral arches (10%).

In Fig.7 are shown some examples of the most frequent deformities observed. Fig. R7A shows the caudal complex of a larva, presenting a large number of cartilaginous structures, with a supernumerary hypural (arrow) and abnormal fusion of the parhypural to hypurals 1 and 2. Vertebral deformities observed were frequently the result of partial or total vertebra fusions (arrow in Fig. R7B and R7C), sometimes accompanied by asymmetries to the vertebral axis (Fig. 7D and R7F). Another cause of deformation was caused by shortening of the vertebrae. Structures related to the abnormal centra, like the arches, were also found to present malformations, either in their general conformation or by fusing to adjacent structures (Fig. R7C, 7D and R7E). In the dorsal and anal fins, the observed deformities were normally fused fin rays and pterigophores as well as atrophied pterigophores, as show in Fig. R7E. Abnormal thickening of vertebrae was also observed, sometimes accompanied by asymmetries to the vertebral axis (Fig. R7F).

A schematic representation of the most common deformities observed in the axial skeleton is shown in Figure R8. The skeletal changes are shown in a diagram representing the axial skeleton of a 45 DAH individual, as follows: (1) fusion of caudal fin rays by their proximal portion (2) malformation of neural arch and spine of the preural vertebra 3; (3) fusion of hypurals 1-2, resulting in only one structure; (4) malformation of preural vertebra 2 with fusion of the correspondent haemal arch and spine with those of preural vertebra 3, (this type of deformity is also very common in preural vertebra 1 and 2); (5) malformation in a caudal vertebra partially fused with the adjacent vertebrae, resulting in absence of the haemal arch and spine and with the corresponding neural arch malformed and fused with the arch of the following vertebra,

exhibiting an atrophied neural spine; (6) fusion of the neural arches of two vertebras surrounding one that is deformed; (7) malformed caudal vertebra exhibiting no neural

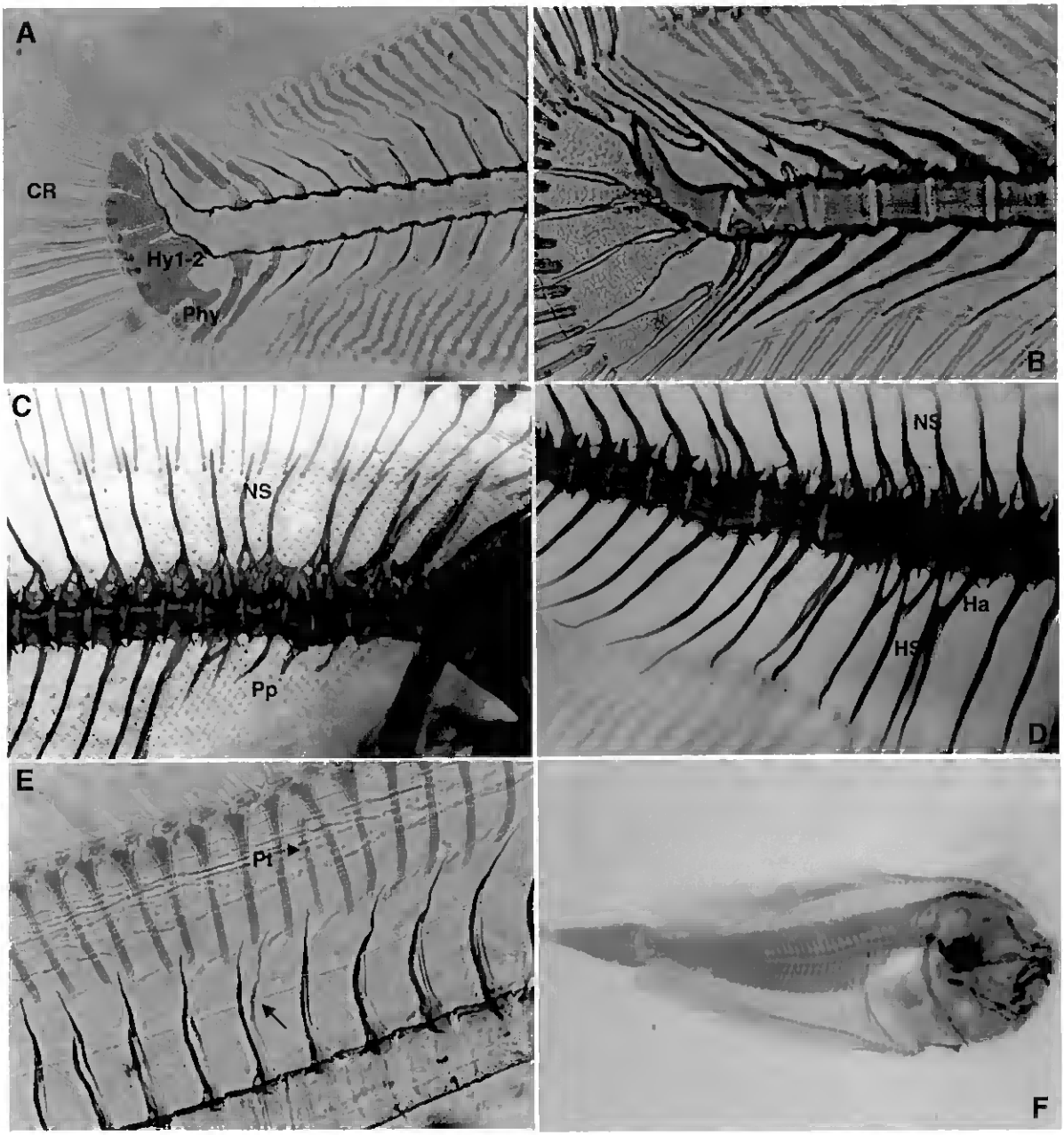

Figure R7- Some examples of the most frequently observed malformations. A- Fusion of the parhypural with the hypural plates 1 and 2, still in a cartilaginous form. Extra hypural plate near the tip of the urostyle (arrow) B- Abnormal formation and partial fusion of the preural vertebrae 1-3 (arrow) with an atrophied neural arch (arrow head) forming in PU3. C- Malformation of the pleural vertebrae and associated arches, spines and parapophysis. Partial fusion of pleural vertebrae 4-6 (arrow). D- Severe abnormalities affecting the caudal vertebrae and adjacent arches and spines and the symmetry of the vertebral column. E- Bifurcation of neural spine; abnormal dorsal pterigophore. For abbreviations see Fig. R2 and 3.

processes and an atrophied haemal spine; (8) compression of caudal vertebrae and of their corresponding processes, (this type of deformity is sometimes associated with deviations from the normal axis as shown in figure R7D); (9) malformation in the neural arch of the last pleural vertebra; (10) abnormal extra-numerary bony element connecting the parapophysis of the two last pleural vertebrae.

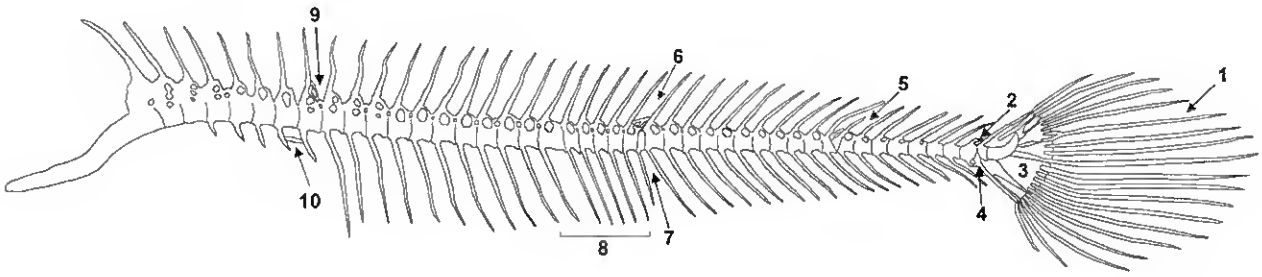

Figure R8- Schematic representation of the axial skeleton of a 45 DAH individual, presenting the major types of deformities described in this work. 1- Fusion of the proximal portion of caudal fin rays; 2- Malformation of neural arch and spine of preural vertebra 3; 3- Fusion of hypurals 1-2; 4- Malformation of preural vertebra 2 with fusion of the haemal arches of preural vertebra 2-3, resulting in one spine only; 5- Malformation in caudal vertebra associated with partial fusion with adjacent vertebrae resulting in absence of the corresponding haemal arch and spine. The corresponding neural arch is malformed and fused with the arch of the following vertebra, exhibiting an atrophied neural spine; 6- Fusion of the neural arches of two adjacent vertebras; 7- Abnormal caudal vertebra with atrophied haemal spine; 8- Compression in caudal vertebrae and corresponding processes; 9- Malformation in neural arch of the last pleural vertebra. 10- Abnormal presence of bony element connecting parapophysis.

R4- Cloning of zebrafish and Senegal sole *bgp* and *mgp* cDNAs

D. rerio and *S. senegalensis bgp* cDNAs: Taking advantage of the N-terminal amino acid sequence obtained for purified *Danio rerio* Bgp (P83238) (Simes *et al.*, 2004), the complete nucleotide sequence of the corresponding cDNA was obtained by a combination of RT-PCR and 5'RACE-PCR (Fig. R9).

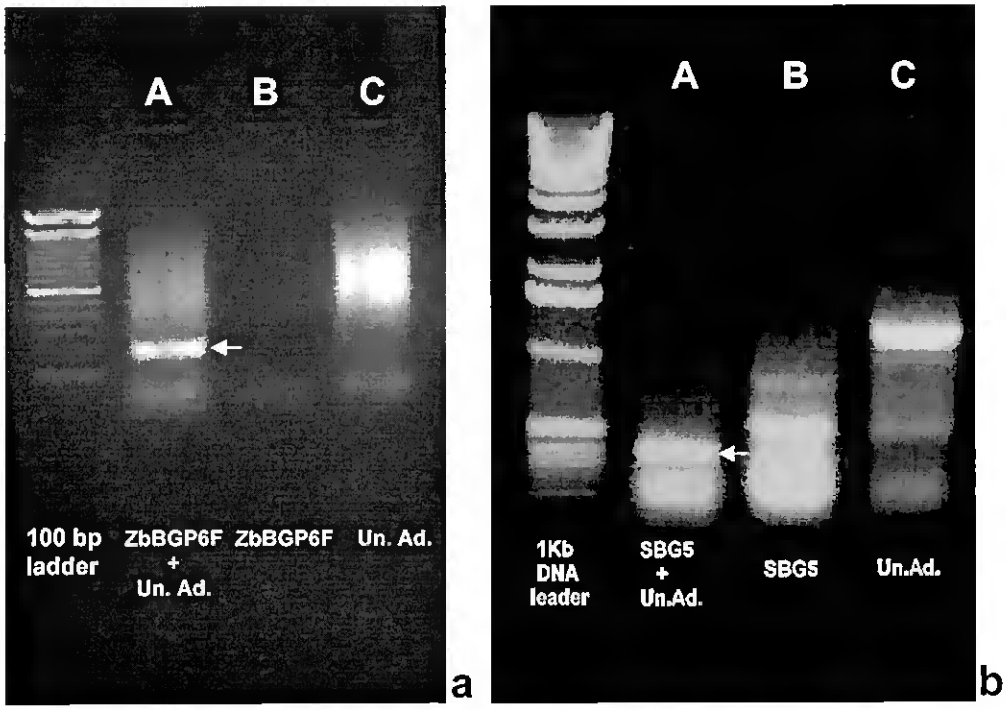

Figure R9 –RT-PCR amplification of partial *bgp* cDNA fragments for zebrafish (a) and Senegal sole (b). PCR was performed using in (a), a degenerated forward primer ZbBGP6F and the reverse primer Universal adapter for *D. rerio bgp* amplification and in (b), a specific forward primer SBG5 and the Universal adapter for *S. senegalensis bgp* amplification. The bands selected for sequence analysis are signalled by arrows. In lanes B and C of each figure are control PCR reactions with only forward or reverse primers, respectively.

The *Danio rerio bgp* cDNA (AY178836) spans 410 bp and contains an open reading frame (ORF) of 315 bp (Fig. R10) encoding a polypeptide with 104 aminoacids (AA) comprising a 56 residue pre-propeptide and a 48 residue mature peptide. The nucleotide sequence of the *Solea senegalensis bgp* cDNA, obtained by a similar approach as the *Danio rerio* cDNA, spans 635 bp and encodes a 45 residue mature protein, preceded by a pre-propeptide of 55 residues (Fig. R10). All pre-pro cleavage sites were deduced by comparison with other known Bgp sequences from mammals, birds, fish and amphibian. The first amino acid of each mature form was identified by comparison with results obtained following protein sequence analysis of Bgp purified from zebrafish and Senegal sole bone (Simes *et al.,* 2004). In both cases, the deduced N-terminal region was in full agreement with the sequence previously obtained by amino acid sequence analysis.

Zebrafish Bgp was found to contain three more amino acids than *S. senegalensis* Bgp at the N-terminus of its mature form. Out of the 45 AA present in the common region of the mature protein between the two species, 36 residues were 100%

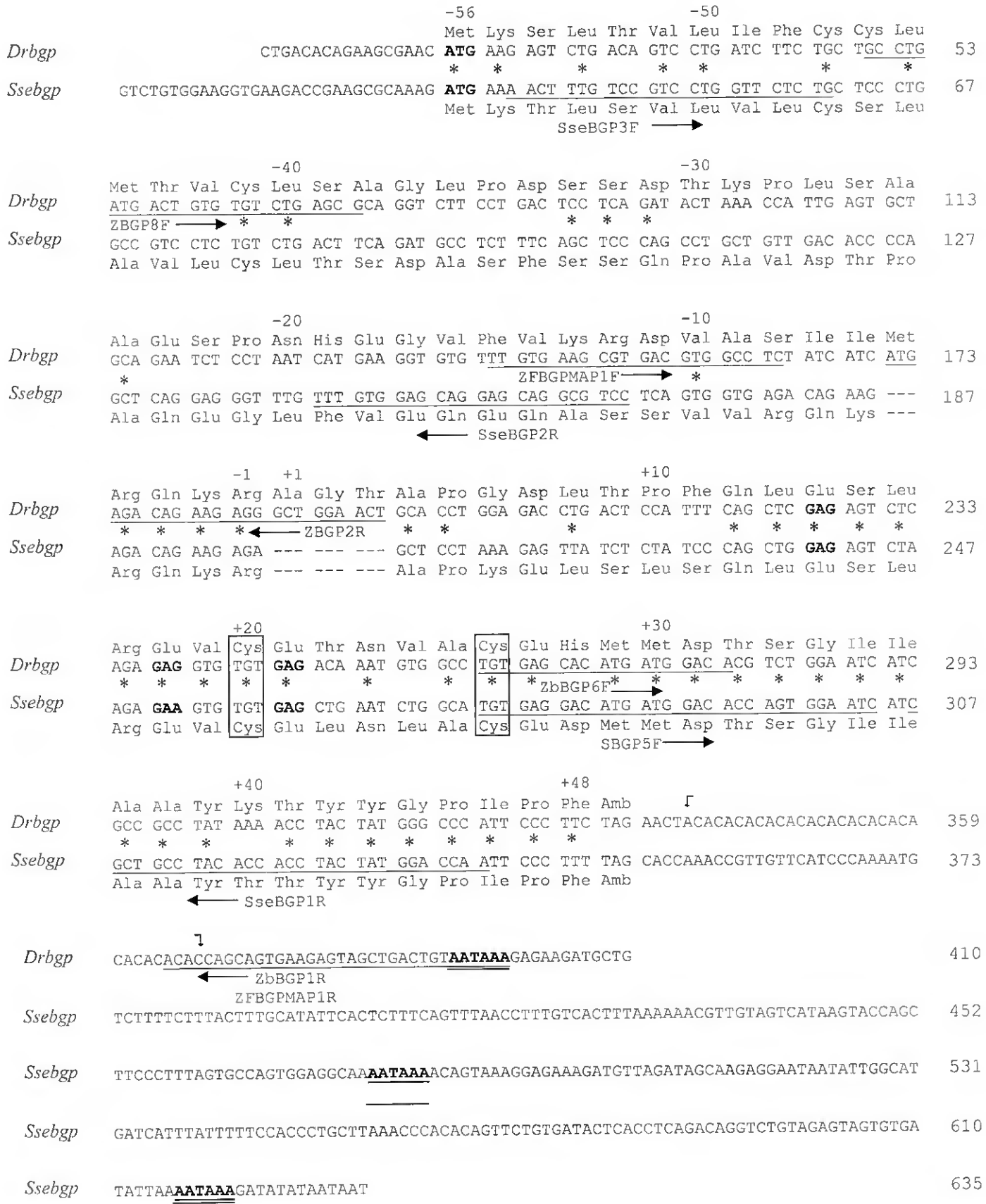
-56
-50
Met Lys Ser Leu Thr Val Leu Ile Phe Cys Cys Leu
Drbgp CTGACACAGAAGCGAAC ATG AAG AGT CTG ACA GTC CTG ATC TTC TGC TGC CTG 53
Ssebgp GTCTGTGGAAGGTGAAGACCGAAGCGCAAAG ATG AAA ACT TTG TCC GTC CTG GTT CTC TGC TCC CTG 67
Met Lys Thr Leu Ser Val Leu Val Leu Cys Ser Leu
SseBGP3F
-40
-30
Met Thr Val Cys Leu Ser Ala Gly Leu Pro Asp Ser Ser Asp Thr Lys Pro Leu Ser Ala
Drbgp ATG ACT GTG TGT CTG AGC GCA GGT CTT CCT GAC TCC TCA GAT ACT AAA CCA TTG AGT GCT 113
ZBGP8F
Ssebgp GCC GTC CTC TGT CTG ACT TCA GAT GCC TCT TTC AGC TCC CAG CCT GCT GTT GAC ACC CCA 127
Ala Val Leu Cys Leu Thr Ser Asp Ala Ser Phe Ser Ser Gln Pro Ala Val Asp Thr Pro
-20
-10
Ala Glu Ser Pro Asn His Glu Gly Val Phe Val Lys Arg Asp Val Ala Ser Ile Ile Met
Drbgp GCA GAA TCT CCT AAT CAT GAA GGT GTG TTT GTG AAG CGT GAC GTG GCC TCT ATC ATC ATG 173
ZFBGPMAP1F
Ssebgp GCT CAG GAG GGT TTG TTT GTG GAG CAG GAG CAG GCG TCC TCA GTG GTG AGA CAG AAG --- 187
Ala Gln Glu Gly Leu Phe Val Glu Gln Glu Gln Ala Ser Ser Val Val Arg Gln Lys ---
SseBGP2R
-1 +1
+10
Arg Gln Lys Arg Ala Gly Thr Ala Pro Gly Asp Leu Thr Pro Phe Gln Leu Glu Ser Leu
Drbgp AGA CAG AAG AGG GCT GGA ACT GCA CCT GGA GAC CTG ACT CCA TTT CAG CTC GAG AGT CTC 233
ZBGP2R
Ssebgp AGA CAG AAG AGA --- --- --- GCT CCT AAA GAG TTA TCT CTA TCC CAG CTG GAG AGT CTA 247
Arg Gln Lys Arg --- --- --- Ala Pro Lys Glu Leu Ser Leu Ser Gln Leu Glu Ser Leu
+20
+30
Arg Glu Val Cys Glu Thr Asn Val Ala Cys Glu His Met Met Asp Thr Ser Gly Ile Ile
Drbgp AGA GAG GTG TGT GAG ACA AAT GTG GCC TGT GAG CAC ATG ATG GAC ACG TCT GGA ATC ATC 293
ZbBGP6F
Ssebgp AGA GAA GTG TGT GAG CTG AAT CTG GCA TGT GAG GAC ATG ATG GAC ACC AGT GGA ATC ATC 307
Arg Glu Val Cys Glu Leu Asn Leu Ala Cys Glu Asp Met Met Asp Thr Ser Gly Ile Ile
SBGP5F
+40
+48
Ala Ala Tyr Lys Thr Tyr Tyr Gly Pro Ile Pro Phe Amb
Drbgp GCC GCC TAT AAA ACC TAC TAT GGG CCC ATT CCC TTC TAG AACTACACACACACACACACACACA 359
Ssebgp GCT GCC TAC ACC ACC TAC TAT GGA CCA ATT CCC TTT TAG CACCAAACCGTTGTTCATCCCAAAATG 373
Ala Ala Tyr Thr Thr Tyr Tyr Gly Pro Ile Pro Phe Amb
SseBGP1R
Drbgp CACACACACCAGCAGTGAAGAGTAGCTGACTGTAATAAAGAGAAGATGCTG 410
ZbBGP1R
ZFBGPMAP1R
Ssebgp TCTTTTCTTTACTTTGCATATTCACTCTTTCAGTTTAACCTTTGTCACTTTAAAAAACGTTGTAGTCATAAGTACCAGC 452
Ssebgp TTCCCTTTAGTGCCAGTGGAGGCAAAATAAACAGTAAAGGAGAAAGATGTTAGATAGCAAGAGGAATAATATTGGCAT 531
Ssebgp GATCATTTATTTTTCCACCCTGCTTAAACCCACACAGTTCTGTGATACTCACCTCAGACAGGTCTGTAGAGTAGTGTGA 610
Ssebgp TATTAAAATAAAGATATATAATAAT 635

conserved, including the three Gla residues and the two cysteines required for the disulphide bridge. This high level of identity contrasted with that observed between the pre-pro regions, where only 18 out of 55 residues were conserved. Comparison of the two cDNAs also identified a larger 3'-untranslated region (UTR) in *S. senegalensis bgp* cDNA with two consensus polyadenylation signals while the shorter 3'-UTR in zebrafish *bgp* contained a CA repeat four nucleotides downstream from the stop codon and only one polyadenylation signal.

Figure R10- *Danio rerio* and *Solea senegalensis bgp* cDNAs. Nucleotide sequence of the cDNAs encoding *D. rerio* and *S. senegalensis bgp*. The *bgp* cDNAs were obtained by a combination of RT-PCR and 5' RACE-PCR amplification. Numbering on right side corresponds to the nucleotides. Amino acid residues are numbered according to the first residue of the mature protein and are shown above (for *D. rerio Bgp*) corresponding codon in the DNA sequence. The polyadenylation signals are underlined twice and the stop codons are identified by their three letter code. Conserved Cys residues are boxed. An asterisk is used to show identity between *D. rerio Bgp* and *S. senegalensis Bgp* amino acid sequences. The sequences used for constructing primers are underlined and marked by horizontal arrows next to the name of the primer. Presumed Gla residues are shown in bold (based in homology with other *bgp* sequences). A 16 (AC) repetitive motif on *D. rerio bgp* 3'-UTR region is marked between curved arrows.

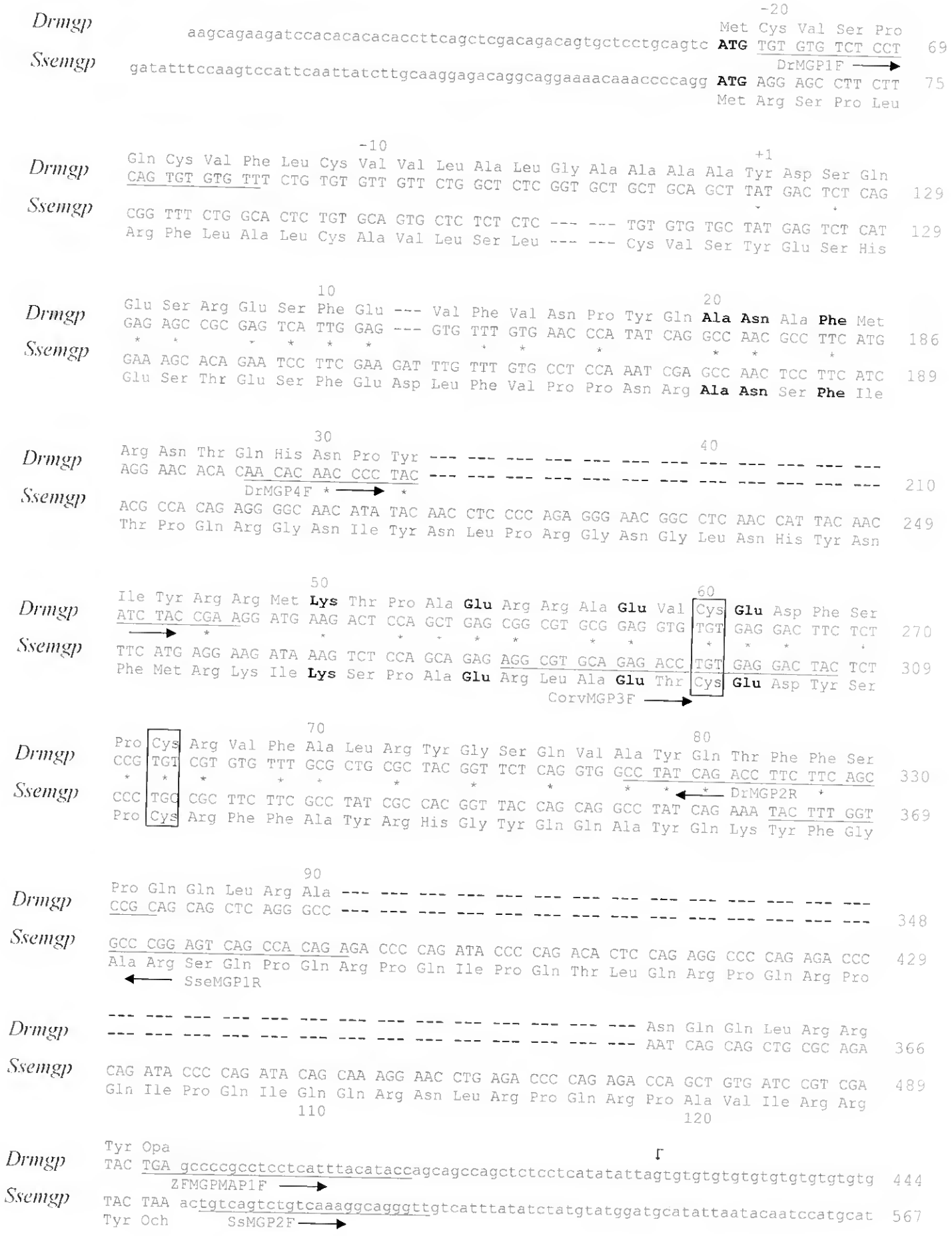
Drmgp
Ssemgp
-20
Met Cys Val Ser Pro
aagcagaagatccacacacaccttcagctcgacagacagtgctcctgcagtc ATG TGT GTG TCT CCT 69
DrMGP1F
gatatttccaagtccattcaattatcttgcaaggagacaggcaggaaaacaaaccccagg ATG AGG AGC CTT CTT 75
Met Arg Ser Pro Leu
-10
+1
Gln Cys Val Phe Leu Cys Val Val Leu Ala Leu Gly Ala Ala Ala Ala Tyr Asp Ser Gln
CAG TGT GTG TTT CTG TGT GTT GTT CTG GCT CTC GGT GCT GCT GCA GCT TAT GAC TCT CAG 129
CGG TTT CTG GCA CTC TGT GCA GTG CTC TCT CTC --- --- TGT GTG TGC TAT GAG TCT CAT 129
Arg Phe Leu Ala Leu Cys Ala Val Leu Ser Leu --- --- Cys Val Ser Tyr Glu Ser His
10
20
Glu Ser Arg Glu Ser Phe Glu --- Val Phe Val Asn Pro Tyr Gln Ala Asn Ala Phe Met
GAG AGC CGC GAG TCA TTG GAG --- GTG TTT GTG AAC CCA TAT CAG GCC AAC GCC TTC ATG 186
GAA AGC ACA GAA TCC TTC GAA GAT TTG TTT GTG CCT CCA AAT CGA GCC AAC TCC TTC ATC 189
Glu Ser Thr Glu Ser Phe Glu Asp Leu Phe Val Pro Pro Asn Arg Ala Asn Ser Phe Ile
30
40
Arg Asn Thr Gln His Asn Pro Tyr --- --- --- --- --- --- --- --- --- --- --- ---
AGG AAC ACA CAA CAC AAC CCC TAC --- --- --- --- --- --- --- --- --- --- --- --- 210
DrMGP4F
ACG CCA CAG AGG GGC AAC ATA TAC AAC CTC CCC AGA GGG AAC GGC CTC AAC CAT TAC AAC 249
Thr Pro Gln Arg Gly Asn Ile Tyr Asn Leu Pro Arg Gly Asn Gly Leu Asn His Tyr Asn
50
60
Ile Tyr Arg Arg Met Lys Thr Pro Ala Glu Arg Arg Ala Glu Val Cys Glu Asp Phe Ser
ATC TAC CGA AGG ATG AAG ACT CCA GCT GAG CGG CGT GCG GAG GTG TGT GAG GAC TTC TCT 270
TTC ATG AGG AAG ATA AAG TCT CCA GCA GAG AGG CGT GCA GAG ACC TGT GAG GAC TAC TCT 309
Phe Met Arg Lys Ile Lys Ser Pro Ala Glu Arg Leu Ala Glu Thr Cys Glu Asp Tyr Ser
CorvMGP3F
70
80
Pro Cys Arg Val Phe Ala Leu Arg Tyr Gly Ser Gln Val Ala Tyr Gln Thr Phe Phe Ser
CCG TGT CGT GTG TTT GCG CTG CGC TAC GGT TCT CAG GTG GCC TAT CAG ACC TTC TTC AGC 330
DrMGP2R
CCC TGC CGC TTC TTC GCC TAT CGC CAC GGT TAC CAG CAG GCC TAT CAG AAA TAC TTT GGT 369
Pro Cys Arg Phe Phe Ala Tyr Arg His Gly Tyr Gln Gln Ala Tyr Gln Lys Tyr Phe Gly
90
Pro Gln Gln Leu Arg Ala --- --- --- --- --- --- --- --- --- --- --- --- --- ---
CCG CAG CAG CTC AGG GCC --- --- --- --- --- --- --- --- --- --- --- --- --- --- 348
GCC CGG AGT CAG CCA CAG AGA CCC CAG ATA CCC CAG ACA CTC CAG AGG CCC CAG AGA CCC 429
Ala Arg Ser Gln Pro Gln Arg Pro Gln Ile Pro Gln Thr Leu Gln Arg Pro Gln Arg Pro
SseMGP1R
--- --- --- --- --- --- --- --- --- --- --- --- --- --- --- Asn Gln Gln Leu Arg Arg
--- --- --- --- --- --- --- --- --- --- --- --- --- --- --- AAT CAG CAG CTG CGC AGA 366
CAG ATA CCC CAG ATA CAG CAA AGG AAC CTG AGA CCC CAG AGA CCA GCT GTG ATC CGT CGA 489
Gln Ile Pro Gln Ile Gln Gln Arg Asn Leu Arg Pro Gln Arg Pro Ala Val Ile Arg Arg
110
120
Tyr Opa
TAC TGA gccccgcctcctcatttacataccagcagccagctctcctcatatattagtgtgtgtgtgtgtgtgtgtg 444
ZFMGPMAP1F
TAC TAA actgtcagtctgtcaaaggcagggttgtcatttatatctatgtatggatgcatattaatacaatccatgcat 567
Tyr Och
SsMGP2F

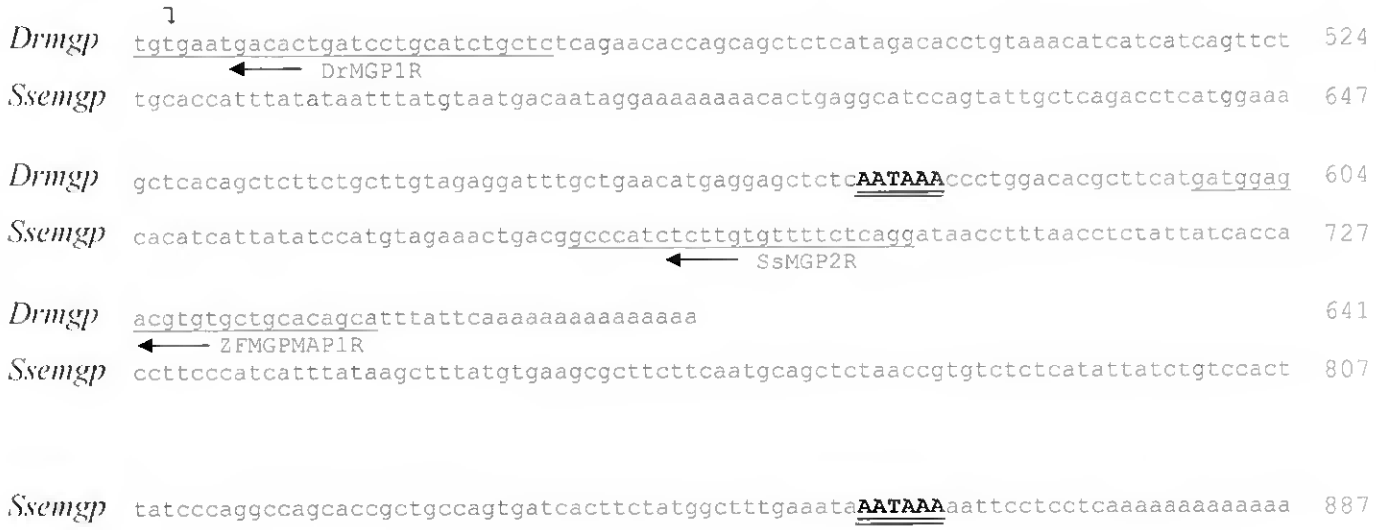

Figure 11- *Danio rerio* and *Solea senegalensis mgp* cDNAs. Nucleotide sequence of the cDNAs encoding *D. rerio* and *S. senegalensis mgp*. *Danio rerio mgp* and *Solea senegalensis mgp* cDNA sequences were obtained by a combination of RT-PCR and 5' RACE-PCR amplification. Numbering and labeling as in Figure 2. Amino acid residues are numbered according to the first residue of the mature protein and are shown above the corresponding codon in the DNA sequence, for *D. rerio*. A 13 (GT) repetitive motif on *Danio rerio mgp* 3'-UTR region is marked between curved arrows.

D. rerio and *S. senegalensis mgp* cDNAs: The *Danio rerio mgp* cDNA (*Dr*MGP-AY072811), cloned by a combination of RT- and 5'-RACE PCR, spans 628 bp (Figure 11) and comprises an ORF with 318 bp coding for a polypeptide of 105 residues comprising a pre-peptide of 21 residues and a mature protein of 84 residues. The 3'UTR includes a dinucleotide repeat motif (GT) and one canonical polyadenylation site. The *Solea senegalensis mgp* cDNA (AY113679) cloned by an analogous methodology, spans 874 bp and contains a 435 bp ORF encoding 144 residues (Figure 11) from which the first 19 constitute the pre-peptide. At the 3'-end is located a motif repeated three times within the coding region (consensus: CAGAGACCCCAGATACCCCAG, coding for Gln-Arg-Pro-Gln-Ile-Pro-Gln). Comparison between the two sequences show the conservation of the phosphorylation motif in the N-terminal region (Ser-Xxx-Glu-Ser-Xxx-Glu-Ser), the Ala-Asn-Xxx-Phe motif and the three putative Gla residues located within the region containing the two cysteines responsible for the disulphyde bridge (Gla-Xxx-Xxx-Xxx-Gla-Xxx-Cys-Gla-Xxx-Xxx-Xxx-Xxx-Cys). There is also a C-terminal extension in both fish sequences compared with mammalian *mgp*s, which is longer in Senegal sole than in zebrafish (Figure 11).

R5- Detection of *bgp* and *mgp* gene expression in *D. rerio* and *S. senegalensis* developing stages

R5.1- Detection of *bgp* and *mgp* gene expression by quantitative Real Time - PCR

Expression levels for mRNAs encoding *bgp* and *mgp* were determined in RNA samples from *D. rerio* and *S. senegalensis* larvae and juveniles, covering the main skeletal development stages for both species. *bgp* and *mgp* mRNA expression were observed in all developmental stages analyzed, but with a different pattern of expression for each species (Fig. R12). In *D. rerio*, *bgp* levels increase 13 fold from somitogenesis stage (29HPF) to complete embryo at 48 HPF followed by a strong upregulation at 120 HPF and returning to levels comparable to the reference sample or even moderately suppressed at 9 DPF (Fig. R12A). At 13 DPF and all stages thereafter *bgp* levels were observed to be 60 to 90 fold higher than the reference sample. *mgp* expression levels paralleled the *bgp* expression, being up regulated and down regulated at the same developmental stages. For *S. senegalensis*, *bgp* expression levels were stable from 72 HPF until 7 DPF and increased 43 fold at 10 DPF, 295 fold at 12 DPF and 87 fold at 14 DPF (Fig. R12B). A dramatic increase in expression was observed at 15 DPF corresponding to the stage of metamorphosis. At 20 DPF, the final stages of metamorphosis, *bgp* expression levels were similar to the pre-metamorphic stages, but again an increase of 10^3 was observed in juveniles. *mgp* had a reduction in expression levels in all developmental stages until 14 DPF but a dramatic increase was then observed at 15 DPF with a 430 fold increase. By the end of metamorphosis, at 20 DPF and in juveniles, the levels of *mgp* expression were decrease again but remained higher than in the reference sample.

In zebrafish, both *mgp* and *bgp* gene expression increased throughout larval development, and reached a stable level at late larval and juvenile stages. By contrast, in Senegal sole *bgp* expression started to increase after 10 DPF, and was found to be highly up-regulated during metamorphosis at 13-16 DPF. The *mgp* gene was down-regulated in larval stages before metamorphosis but highly up-regulated during metamorphosis. The graphics obtained for the amplification plotting are presented in Figures 12 A1 and 12 B1.

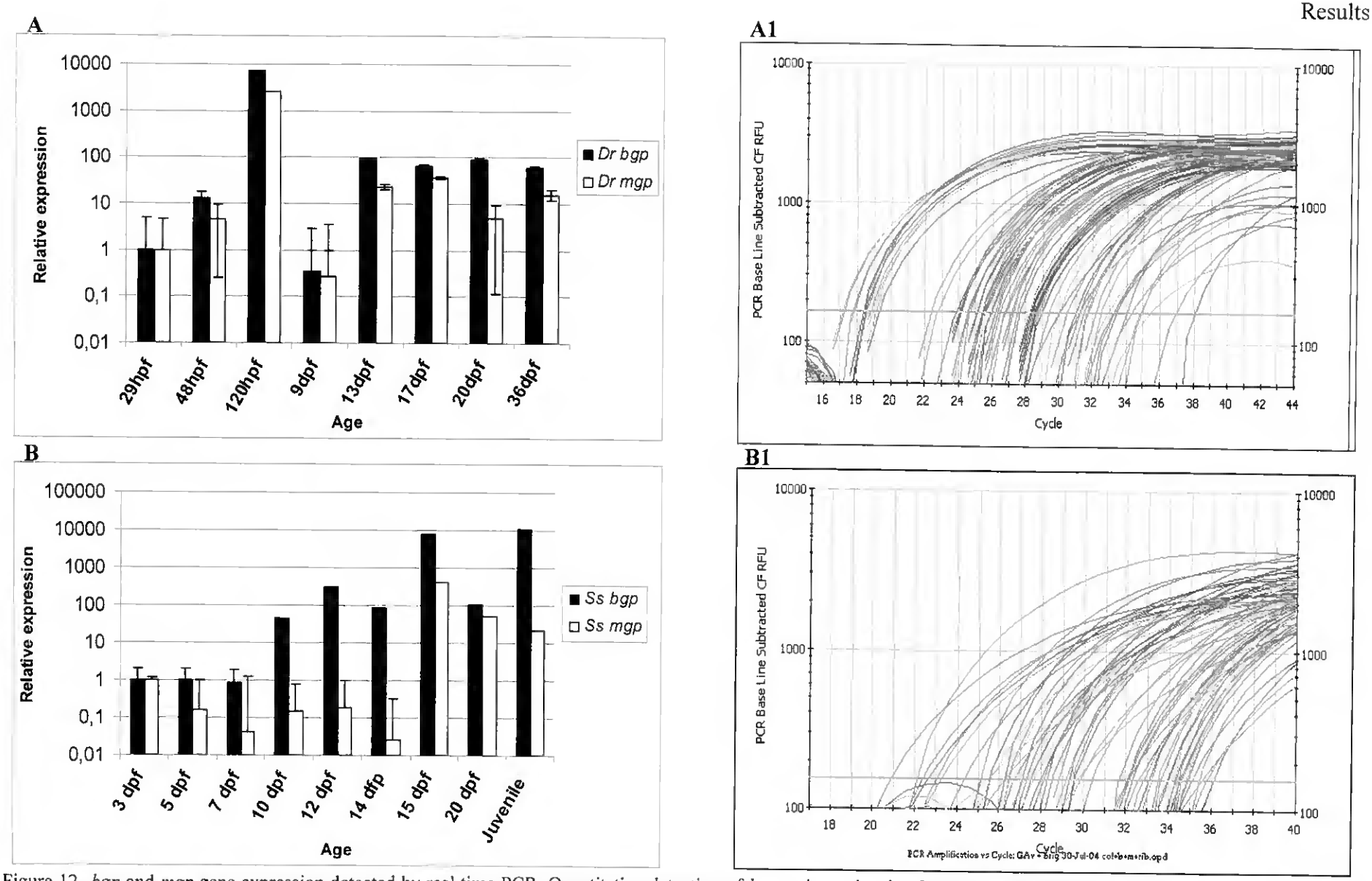

Figure 12- *bgp* and *mgp* gene expression detected by real time PCR. Quantitative detection of *bgp* and *mgp* levels of mRNA transcripts throughout development in *D. rerio* and *S. senegalensis*. The relative expression levels determined with respect to the youngest stage analyzed are presented in bar graphics for *D. rerio* (A) and for *S. senegalensis* (B) using logarithmic scales. A1 and B1 are the fluorescence graphics plotted for the PCR amplification.

R5.2- Detection of *bgp* and *mgp* gene expression in the zebrafish by RT-PCR and Southern hybridization

Detection of *bgp* and *mgp* mRNAs was performed in *D. rerio* total RNA samples extracted from whole larvae by a combination of RT-PCR coupled with Southern hybridization. *mgp* was observed in all developmental stages analyzed while *bgp* although not detectable at stage 48 hpf, corresponding to hatching, was detectable after 72 hpf and in all developmental stages ahead (Fig. R13).

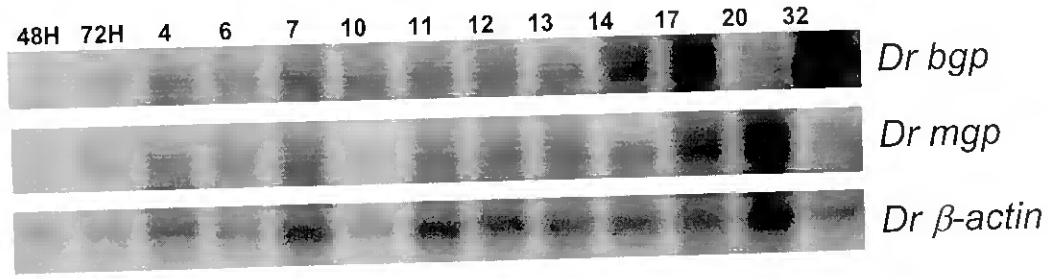

Figure R13- Detection of *bgp* and *mgp* gene expression in different developmental stages of zebrafish by RT-PCR coupled with Southern hybridization (Numbers above wells represent ages in hours (H) or days post fertilization)

R5.3- Detection of *bgp* and *mgp* gene expression in the Senegal sole by Northern hybridization

Northern hybridization was performed in samples of total RNA extracted from developmental stages and organs of Senegal sole. Both *bgp* and *mgp* mRNAs were first detected in larvae at 11 DPF (Fig. R14) and in all stages thereafter. No significant changes in mRNA levels were observed after normalization with ethidium bromide staining of ribosomal RNA.

Northern analysis of RNA from different organs revealed that, with this technique, *mgp* was only expressed at detectable levels in branchial arches, kidney and heart, being absent from vertebral bone and muscle (Fig. R15).

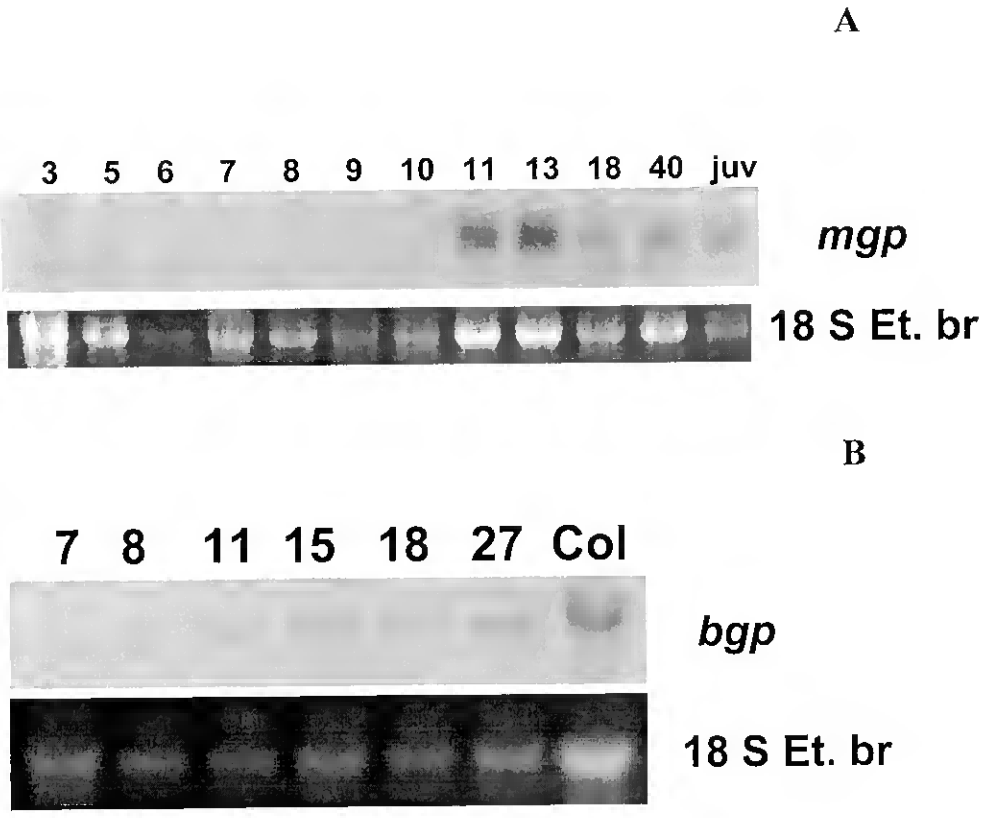

Figure R14- Detection of *S. senegalensis bgp* and *mgp* by Northern blotting

A- Northern hybridization of total RNA of larval and juvenile stages of *S. senegalensis* normalized by comparison with the 28S ribosomal RNA stained with ethydium bromide underneath. Juv corresponds to RNA extracted from an entire juvenile fish. B- Detection of *mgp* by Northern hybridization of total RNA from larvae of *S. senegalensis* at different developmental stages, normalized by comparison with the 18S ribosomal RNA stained with ethydium bromide underneath. The well marked with Col corresponds to RNA from vertebral column of a juvenile. Numbers above wells represent ages in days post fertilization.

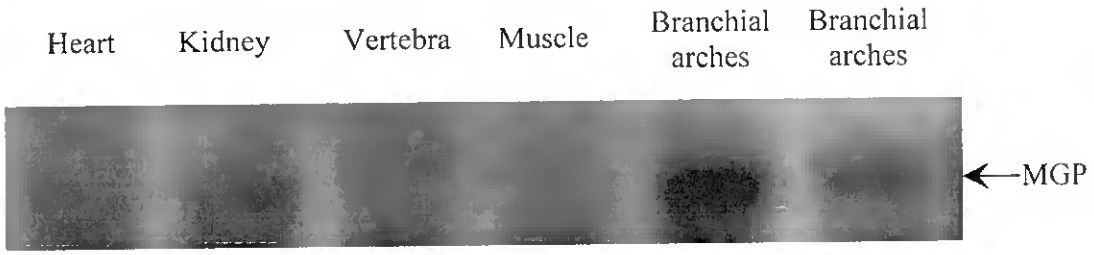

Figure R15- Detection of *Ssemgp* expression by northern hybridization of RNA from different tissues of Senegal sole. *mgp* was only expressed at detectable levels in branchial arches, kidney and heart.

R6- Detection of sites of *bgp* gene expression by *in situ* hybridization

R6.1- Detection of sites of *bgp* expression in zebrafish

In *D. rerio, bgp* gene expression was first observed by *in situ* hybridization at 7 DPF on the fifth ceratobranchial cartilage which already presented the calcified pharyngeal teeth. At 11 DPF both BOP and optic capsules presented *bgp*-positive cells, as well as the Meckell's cartilage (Fig. R16A). At 13 DPF vertebrae were developing around the notochord and hypertrophyc cells in the forming vertebral arches showed positive signal for *bgp* expression (Fig. R16B). At the same age, *bgp* expression was also observed in other structures undergoing calcification like the opercular bones, BOP and the fourth and fifth ceratobranchials (Fig. R16C). As the calcification of the BOP increased, expression appeared within the cells adjacent to the calcifying zones of the structure (Fig. R16D). At 24 DPF, *bgp* mRNA was observed in cells associated with the mineralizing cartilaginous pterigophores of the dorsal fin (Fig. R16E). As the number of structures undergoing mineralization increased in the head region, a more generalized expression was observed in the skeletal structures, as seen in the ceratobranchials, opercula, ceratohyal, BOP and jaw of a 24 DPF sample (Fig. R16F). In the adult fish, the proportion of matrix greatly increased relatively to the number of cells, and the positive signal indicating *bgp* expression became restricted to areas containing cells with a hypertrophyc phenotype.

R6.2- Detection of sites of *bgp* expression in Senegal sole

Localization of *bgp* gene expression in *Solea senegalensis* by *in situ* hybridization was first detected after the beginning of mineralization and in parallel with the onset of metamorphosis in the head structures, a process that initiated at around 12-13 DPF in the studied individuals. In 15 DPF larvae, *bgp* expression was detected in the first vertebra forming over the notochord (Fig. R17A), and once the vertebral arches are formed and mineralized, *bgp* expression was detected in cells within forming neural arches as observed in a 17 DPF larvae (Fig. R17B). At this same age *bgp* was found to be expressed by cells in the head skeletal structures, such as endochondral bones from the skull as shown in the hyosymplectic and basioccipital process and in the branchial arches

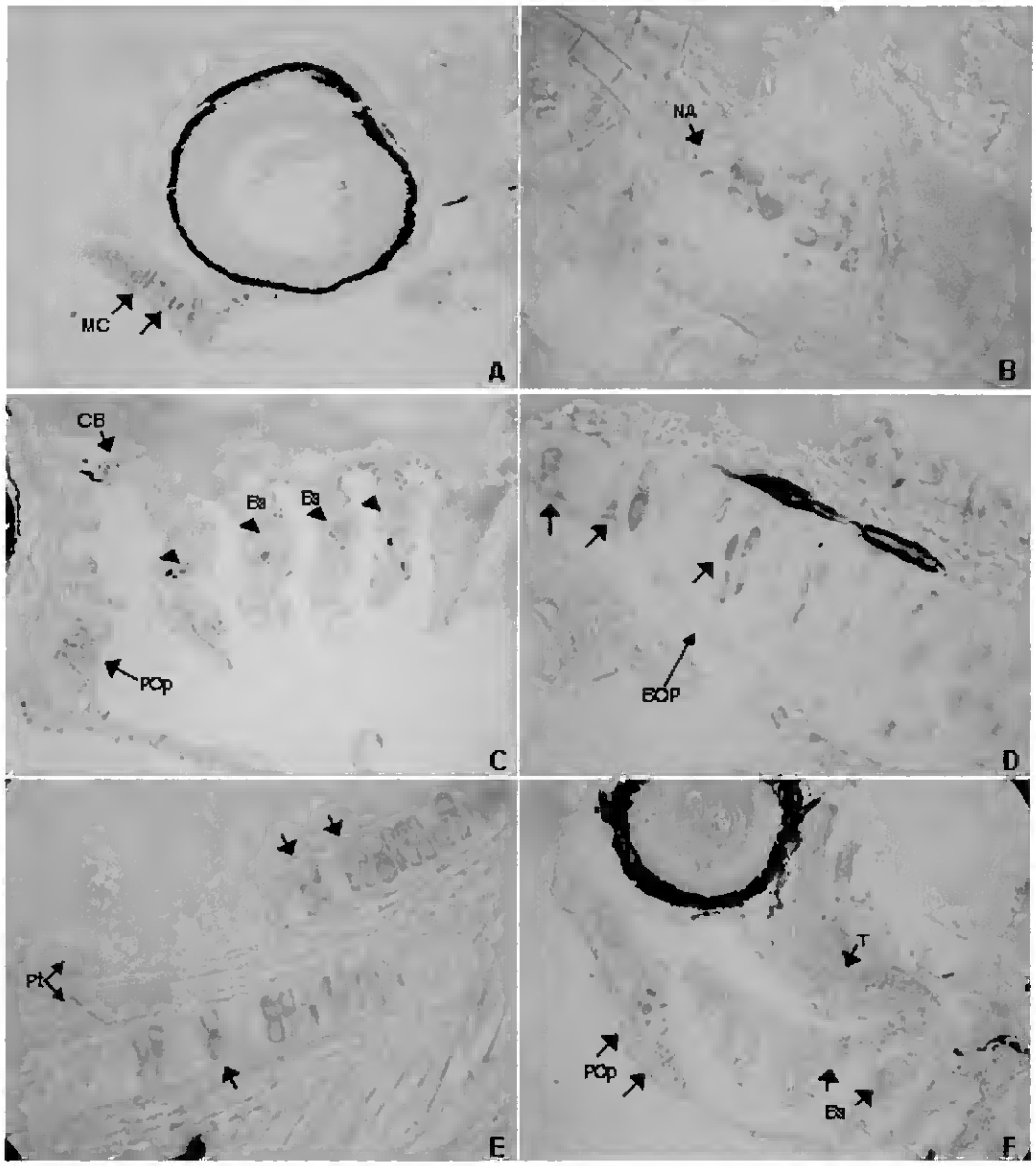

Figure R16- *In situ* localization of *D. rerio bgp* mRNA. *bgp* gene expression was detected by in situ hybridization in sections of zebra fish larvae at different ages and developmental stages. A- *bgp* expression in the calcifying Meckel´s cartilage (arrows) of a 9 DAH larvae (200x). B- Detection of *bgp* expression in a neural arch (arrowhead) at the beginning of formation (1000x). C- At 11 DAH *bgp* expression is detected at the branchial arches (arrowheads) and the calcifying preopercular bones (arrow) (100x). D- At 18 DAH *bgp* expression is detected at the BOP (arrows) (1000x). E- Expression is visible at the mineralizing internal fin support skeleton in this case the pterigophores of the dorsal fin of a 22 DAH zebra fish (1000x). F- At 22 DAH *bgp* expression is strongly detected in the calcifying preopercular bones (arrows), branchial arches (arrowheads) and trabeculae (small arrow) (100x).

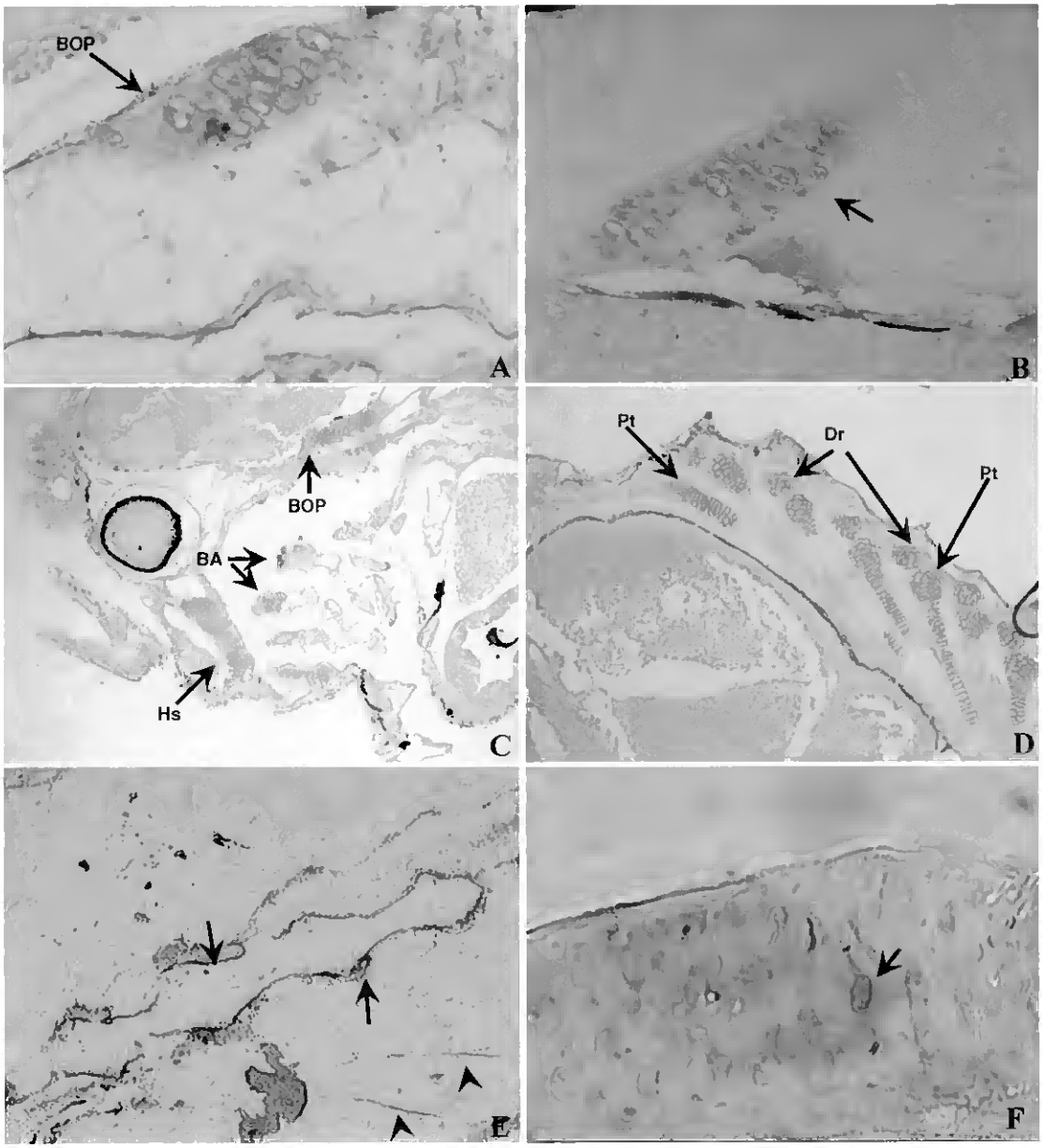

Figure R17- *In situ* localization of *S. senegalensis bgp* mRNA. Sites of *bgp* gene expression were detected by in situ hybridization in sections of Senegal sole larvae at different ages and developmental stages. (A)- First vertebra forming over the notochord (arrow) at13 DAH (400x). (B)- Cells expressing *bgp* in a forming neural arch (arrow) at15 DAH (400x). (C)- Head of a 15 DAH sole with *bgp* expression detected in the branchial arches (BA), basioccipital process (BOP) and hyosympletic (Hs) (100x) . (D)- Expression in the dorsal pterigophores (Pt) and distal radials (Dr) of a 18 DAH larvae (200x). (E)- Demonstration by radioactive in situ of *bgp* expression in the vertebral column (arrows) and haemal spines (arrowheads) of a 23 DAH sole (100x). F- Osteoblasts (arrowheads) expressing *bgp* in the mandibula of a 56 DAH juvenile sole (1000x)

of a 15 DAH sole (Fig. R17C). At 20 DPF larvae showed expression in the forming skeletal elements of the fins such as the dorsal pterigophores and distal radials (Fig. R17D) that are already undergoing endochondral calcification. Radioactive *in situ* hybridization revealed *bgp* expression in the calcified vertebral column and haemal spines in a post larval 25 DPH sole (Fig. R17E). At 58 DPF, juveniles had a completely differentiated skeleton and *bgp* expression was observed associated to osteoblasts, as seen in the mandibula of a juvenile sole (Fig. R17F).

R7- Detection of *mgp* gene expression by *in situ* hybridization

In *D. rerio, mgp* expression was first detected at 96 HPF on chondrocytes of the ethmoid plate (Fig. R18A). At 9 DPF, *mgp* expression was located in chondrocytes both from trabecular cartilage and ceratobranchial arches (Fig. R18B) as well as in the Meckel´s cartilage and quadrate (Fig. R18C). At 10 DPF, in cartilage from pectoral fin, *mgp* mRNA was detected in chondrocytes but was not observed in the cleithrum (Fig. R18D). At 13 DPF *mgp* gene expression was observed in ceratobranchials, mainly in hypertrophyc chondrocytes and in the BOP (Fig. R18E). In addition, *mgp* mRNA was also observed in hypertrophyc chondrocytes from Meckel´s cartilage and in chondrocytes of the hyaline cartilage from the basibranchial cartilage (Fig. R18F). At 16 DPF a positive staining for *mgp* mRNA was observed in chondrocytes from the BOP (Fig. R18G), within the cytoplasm of hypertrophyc chondrocytes from the Meckel´s cartilage and within chondrocytes of the ethmoid plate (Fig. R18H). At 17 DPF *mgp* expression was detected in chondrocytes of the optic capsules (Fig. R18I) and at 20 DPF in chondrocytes from the Zellknorpel catilage in the branchial filaments (Fig. R18J). At 25 DPF, the vertebrae were nearly formed with the notochord completely surrounded by calcified cartilage. At this stage, *mgp* expression was located in endosteal cells surrounding the vertebral centra. These cells were elongated in shape, with strong staining for *mgp* (Figures 18K and 18L). *mgp* expression was also located in chondrocytes from the pterigophores (Fig. R18L). In the adult fish, as mineralization of the skeleton increased, signal indicating expression of *mgp* was only detected in chondrocytes within the remaining cartilage islands.

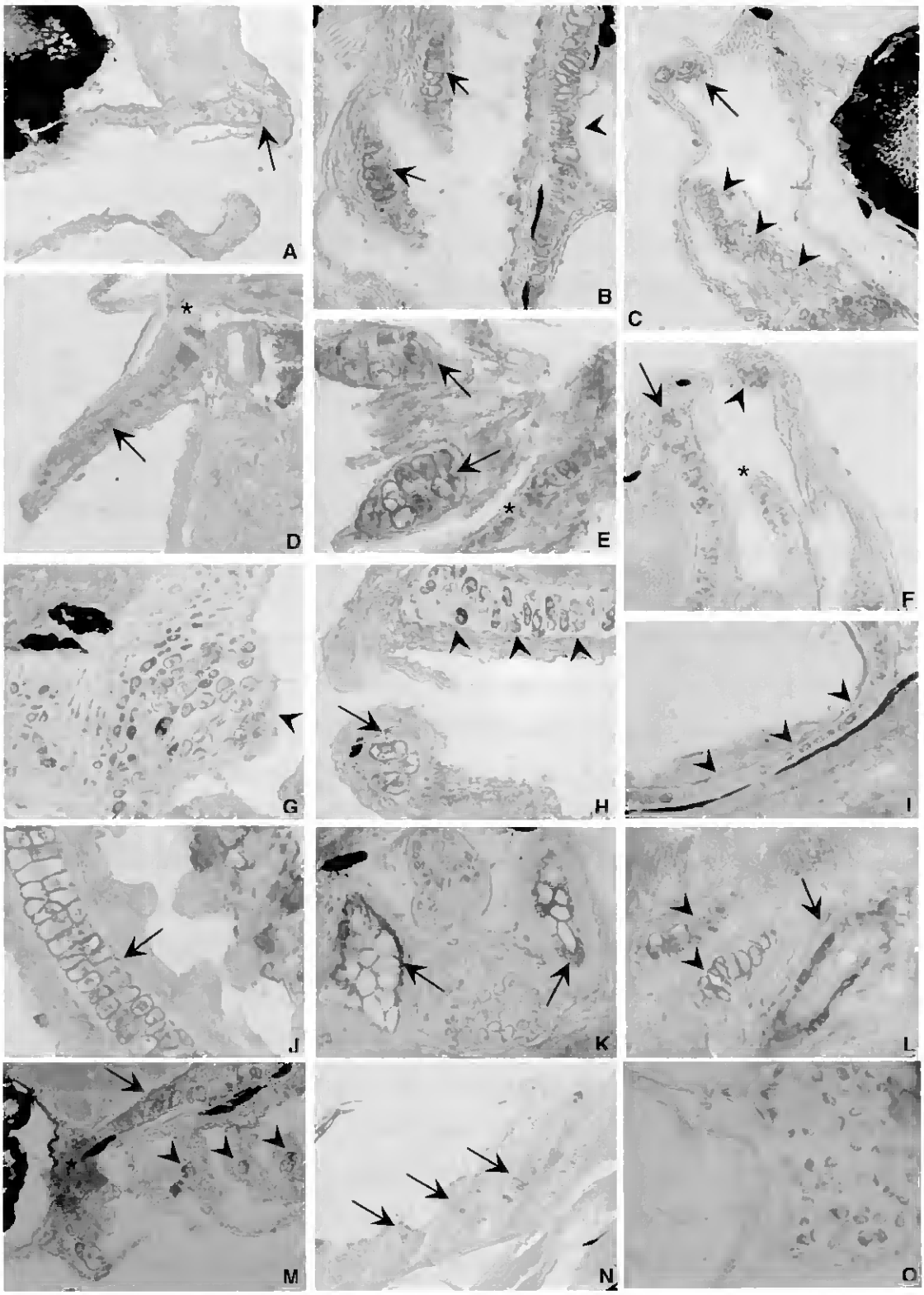

Figure R18

In *S. senegalensis*, *mgp* gene expression was observed mainly in skeletal structures both cartilaginous and calcified. At 11 DPF *mgp* mRNA was first observed in the chondrocytes of the branchial arches, trabeculae and hyosymplectic (Fig. R18M). At 15 DPF when vertebral structures are forming, *mgp* mRNA was observed in the chondrocytes at the base of the vertebral arches, and in the chondrocytes of the pterigophores from the developing dorsal and anal fins, as observed in the neural pterigophores of a 17 DPF larvae (Fig. R18N) under metamorphosis. In juveniles, *mgp* expression was present only in non-calcified skeletal structures, like the cartilage in the base of the vertebrae of a 47 DPF sole (Fig. R18O).

Figure R18- In situ localization of *D. Rerio* and *S. senegalensis mgp* mRNA. Sites of *mgp* gene expression were detected by in situ hybridization in sections of D. rerio larvae (A to L) and S. senegalensis larvae (M to O) at different ages and developmental stages. (A) *mgp* expression in the ethmoid plate of a 2 DAH larvae (arrow) (200x). (B) Detection of *mgp* expression in chondrocytes from the trabecular cartilage (arrowhead) and ceratobranchial arches from a 7 DAH larvae (arrows) (1000x). (C) *mgp* expression in Meckel's cartilage (arrowheads) and quadrate (arrow) in a 7 DAH larvae (100x). (D) Cartilage from the pectoral fin of a 8 DAH larvae showing *mgp* expression located within the chondrocytes (arrow). Note absence of signal in the cleithrum (asterisk) (1000x). (E) D. rerio larvae at 11 DAH showing *mgp* expression in the ceratobranchials (arrows) and in the BOP (asterisk) (1000x). (F) At 11 DAH, *mgp* expression was also evident in the hypertrophyc chondrocytes from the Meckel's cartilage (arrowhead), quadrate (arrow) and in chondrocytes from the basibranchial cartilage (asterisk) (200x). (G) *mgp* expression in a 14 DAH larvae, showing a positive staining in chondrocytes from the BOP (arrowhead) (1000x) (H) At 14 DAH *mgp* expression is also detected in hypertrophyc chondrocytes of the Meckel's cartilage (arrow), and in chondrocytes from the ethmoid plate (arrowheads) (1000x). (I) 15 DAH larvae showing *mgp* expression in chondrocytes from the optic capsules (arrowheads) (1000x). (J) D. rerio gill filaments showing *mgp* expression close to the cytoplasm membrane in chondrocytes from the Zellknorpel (arrow) (1000x). (K) *mgp* expression in endosteal cells surrounding the vertebral centra in a 23 DAH larvae (arrows) (1000x). (L) *mgp* expression in chondrocytes from the spines in a 23 DAH larvae (arrowheads). Note also the presence of fusiform cells surrounding the central core of the vertebra (arrow) (1000x). (M) *mgp* expression at the branchial arches (arrowheads), trabecula (arrow) hyosimpletic (asterisc) of a larval sole at 9 DAH (400x). (N) *mgp* expression is detected in the neural arches of sole at 13 DAH (400x). (O) *mgp* gene expression in the vertebral cartilage of a 45 DAH sole (1000x).

R8- Detection of sites of Bgp accumulation by immunohistochemistry

R8.1- Detection of sites of Bgp accumulation in zebrafish

Danio rerio Bgp was found to accumulate in the matrix of tissues undergoing calcification as determined by immunolocalization studies. This accumulation was first detected at 8 DPF in the BOP and calcified teeth of the branchial arch 5 and in the otolyths (Figures 19A and 19B). At 9 DPF accumulation was also observed in the cleithrum and in the BOP undergoing intra-membranous mineralization (Fig. R19C). At 13 DPF, Bgp accumulation was observed in the calcified upper jaw and in the mineralized matrix deposited by osteoblasts on the surface of Meckels cartilage undergoing perichondral mineralization (Fig. R19D). At 13 DPF Bgp was also detected in the developing calcified vertebral elements, with positive signal associated with the mineralized matrix of the forming vertebrae and arches on the surface of the notochord envelope, as observed in Fig. R19E for forming vertebra and haemal arches. At this age accumulation of Bgp was observed with stronger intensity in the growing structures, as observed in the teeth of branchial arch 5 and in the cleithrum (Fig. R19F). At 20 DPF the skeletal elements of the fin and of the internal fin support were mineralizing, and presented positive signal for Bgp accumulation, as observed in the coraco-scapular complex (Fig. R19G) from the pectoral fin associated with the mineralized matrix. As the calcified vertebrae and elements develop in an anterior-posterior manner along the notochord, Bgp was observed associated to the mineral matrix deposited as can be seen in Figure R19H. The last vertebral element, the urostyle, showed a strong positive signal for Bgp, observed by immunofluorescence within sites undergoing perichordal mineralization (arrows in Fig. R19H). The developing vertebrae, arches and spines of a 20 DPF specimen showed a strong signal for Bgp accumulation associated with a noticeable thickening of the mineralized tissue surrounding the notochord (Fig. R19I). At 31 DPF the hypurals and lepidotrichia of the caudal fin and the last vertebrae showed accumulation of Bgp. A strong increase in signal was observed as vertebra and arches became thicker (Fig. R19J). Bgp accumulated strongly in juvenile and adult calcified tissues, as seen in the supramandibular, trabeculae and skull bones (Fig. R19L) as well as in the branchial arches of a juvenile as seen by immunofluorescence (Fig. R19K). A clear

positive signal was also observed in the kidney of juveniles and adults, associated with the glomerulii (Fig. R19M).

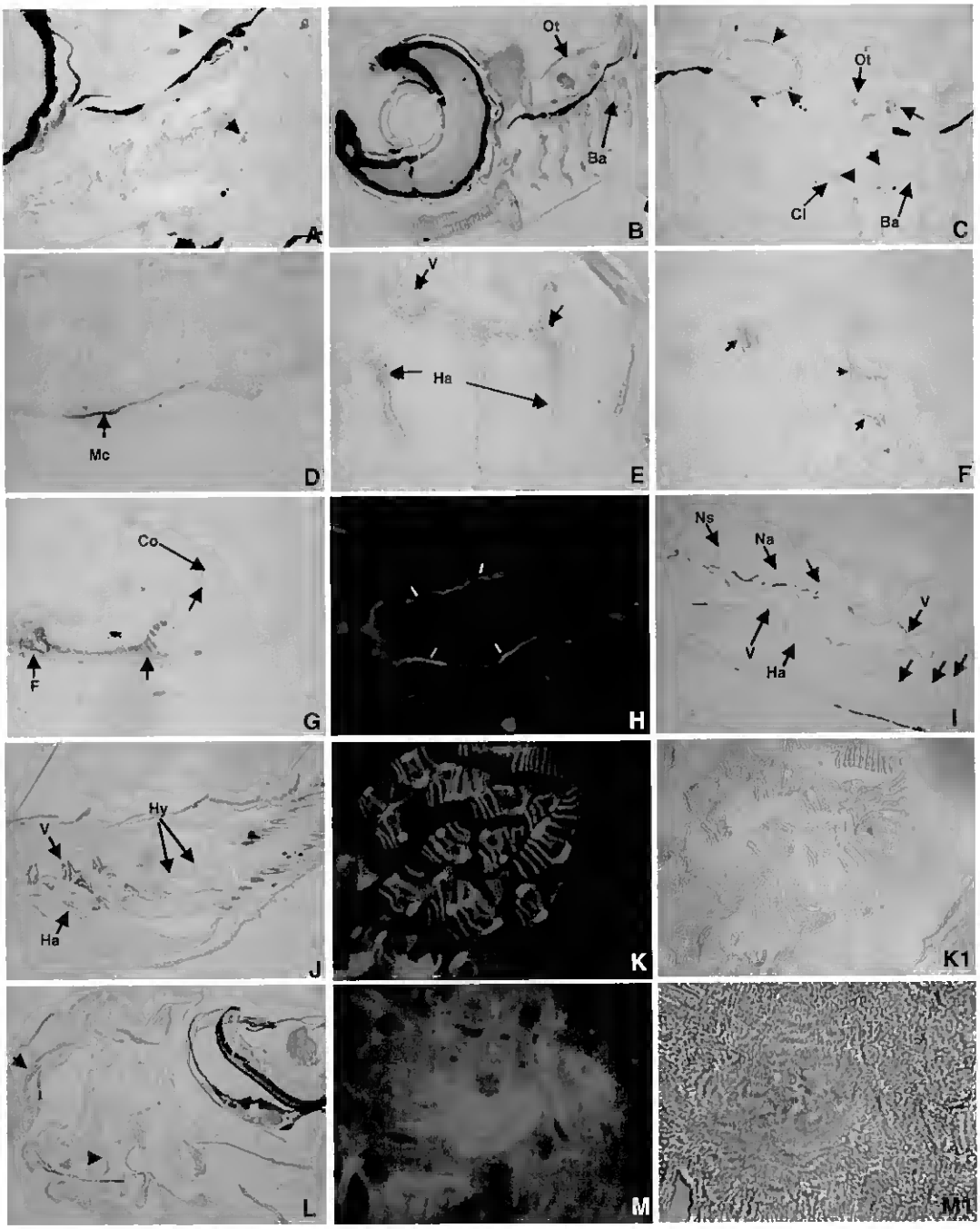

Figure R19

R8.2- Detection of sites of Bgp accumulation in Senegal sole

In *S. senegalensis*, Bgp was found to accumulate in mineralized skeletal structures but with a slight delay in respect to the appearance of mineralization. At 15 DPF larvae showed Bgp accumulation in the mineralized vertebrae forming around the notochord (Fig. R20A). At 17 DPF Bgp was found in the calcifying caudal vertebrae, and associated neural and haemal arches and at 25 DPF Bgp was observed in all the vertebral elements as revealed by immunofluorescence (Fig. R20B), showing strong accumulation of Bgp in calcified vertebral column and parapophysis of 25 DPF individuals with a completed metamorphosis. At this same age Bgp accumulation was also detected in the cartilaginous distal radials undergoing endochondral calcification (Fig. R20C). 41 DPF juveniles presented a strong signal for Bgp accumulation in all calcified structures, as observed in the calcified cartilages of the branchial arches (Fig. R20D). All the structures are formed at juvenile stage and Bgp is observed to accumulate in all bones, either from endochondral or intramembranous origin, and in all cartilages that present calcification.

Figure R19- Immunohistochemical detection of *D. rerio* Bgp accumulation in different developmental stages of zebra fish. A- Accumulation of Bgp in the teeth of branchial arch 5 and BOP of a 6 DAH larvae (400x). B- Accumulation of Bgp in the otholit of a 6 DAH larvae (200x). C- Accumulation of Bgp in the teeth of branchial arch 5, otholit and cleithrum of a 7 DAH larvae (400x).D- Accumulation of Bgp in Meckel's cartilage of a 11 DAH larvae (1000x). E- Accumulation of osteocalcin is first detected in calcifying vertebra and arches at 11 DAH (1000x). F- Accumulation of Bgp in the teeth of branchial arch 5 and in the cleithrum of an 11 DAH (1000x). G- Accumulation of Bgp in the calcifying pectoral fin e coracoscapular complex at 18 DAH (400x). Notice the accumulation at the periphery of the coracoid undergoing perichondral mineralization. H- Accumulation of Bgp in the mineralizing urostyle at 18 DAH (400x). I- Accumulation of Bgp in the vertebral column, neural arches and haemal arches at 18 DAH (200x). J- Bgp accumulation in the mineralizing perichondral matrix of the caudal vertebrae cartilages and in the mineralized arches in an 18 DAH juvenile (200x). K- Bgp accumulation in the caudal vertebrae, arches and spines in a 24 DAH juvenile (100x). L- Bgp accumulation in the mineralizing matrix of hypural plates of the caudal fin and in the mineralized fin rays of a 24 DAH juvenile (100x). M- Accumulation of Bgp is detected in the all the bones and calcifying cartilages of the head region, like the supramaxilary (arrow) and associated bones, the ethmoid plate (arrowhead) and the supra orbital cartilage that surrounds the eye (100x). N- Accumulation of Bgp is widely detected by immunoflourescence in the branchial arches of a juvenile zebra fish (200x). O- Epithelial cells from some renal tubules of the kidney appear with positive signal by immunoflourescence for Bgp in juvenile individuals (400x).

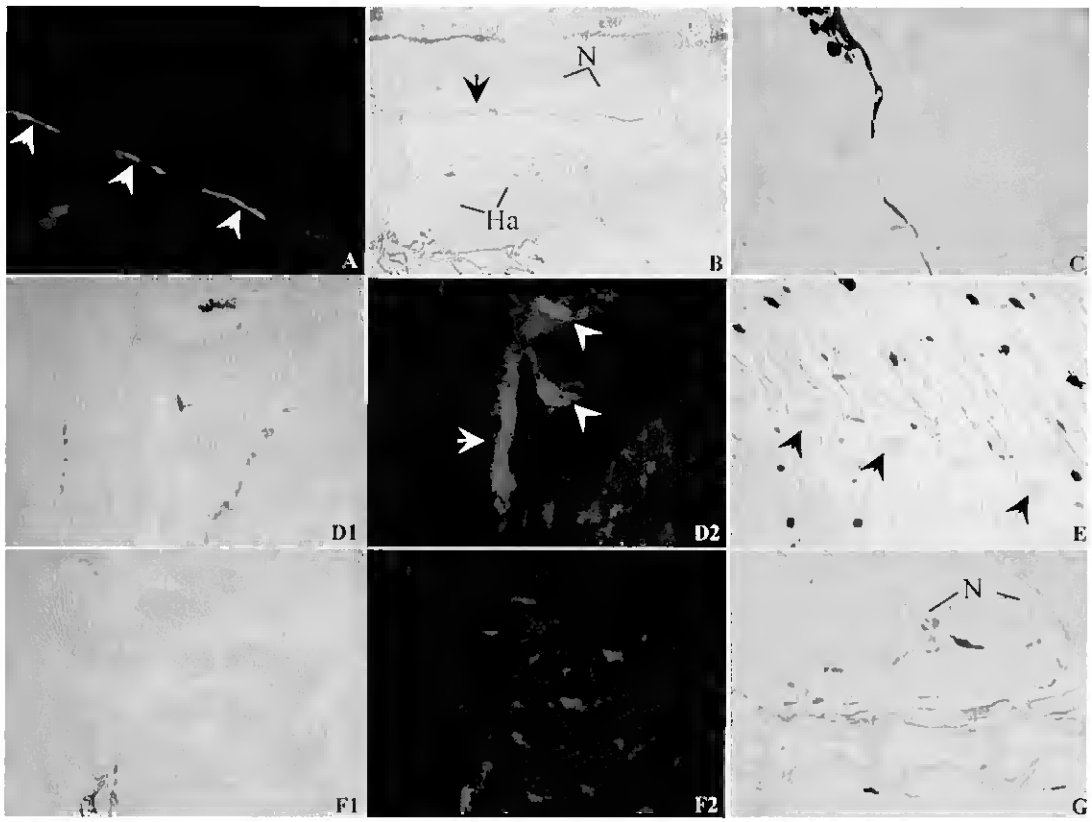

Figure R20- Immunohistochemical detection of *S. senegalensis* Bgp accumulation in different developmental stages of Solea senegalensis- Immunohistochemical detection of Bgp accumulation in different developmental stages of Senegal sole. A- Immunofluorescent detection of Bgp in the forming vertebra (Arrows) surrounding the notochord of a 13 DAH larvae (400x). B- Accumulation of Bgp in the calcifying caudal vertebra (Arrow), neural (Na) and haemal (Ha) arches at 15 DAH (200x). C- No staining observed in the head bones in a control with pre-immune serum of a 18 DAH larvae. D- Detection of Bgp accumulation in the vertebra (Arrow) and parapophysis (Arrowheads)at 23 DAH (D1 brightfield and D2 darkfield) (250x). E- Accumulation of Bgp in the calcifying distal radials (arrows) at 23 DAH. F- Bgp is strongly detected in the calcified branchial arches of a 39 DAH juvenile (F1 bright field and F2 dark field) (250x). G- Bgp strongly accumulates in the vertebra, arches and spines at 39 DAH (200x).

R9- Detection of sites of Mgp accumulation by immunohistochemistry

R9.1- Detection of sites of Mgp accumulation in zebrafish

Danio rerio Mgp accumulation was detected by immunohistochemistry throughout development of *D. rerio* and *S. senegalensis*. Accumulation of Mgp was first

observed in the mineralized otolyths at 96 HPF and the intensity of staining increased as the structure grew, as observed in a 6 DPF larvae (Fig. R21A). As new calcified structures appeared (see Fig. R1), accumulation of Mgp was observed in the mineralized matrix as soon as it formed, as can be observed in a 8 DPF larvae in the mineralized otholit and cleithrum (Figures 21B and 21C). At 13 DPF when vertebrae and arches are forming, Mgp was observed to accumulate in pleural vertebrae where mineralization of neural arches initiated, as seen in vertebrae 3-5 of a 13 DPF larva (Fig. R21D). At this same age, accumulation of Mgp was observed in the mineralizing branchial arches and pharyngeal teeth (Fig. R21E). At 20 DPF Mgp accumulation was present in the mineral layer over cranial cartilages undergoing endochondral ossification (Fig. R21F) and in the forming caudal vertebra and associated arches (Fig. R21G). In juveniles at 40 DPF a strong signal for Mgp accumulation was observed in the pre-opercular bones undergoing endochondral ossification (Fig. R21H) and in skull bones undergoing intra-membranous ossification (Fig. R21I). No staining was observed in control zebrafish vertebrae sections incubated with pre immune serum.

R9.2- Detection of sites of Mgp accumulation in Senegal sole

In *S. senegalensis*, Mgp accumulation was first detected at 8 DPF in the cartilaginous otic capsules (Fig. R21J) but not in the otholits. As calcification initiated, Mgp accumulation was observed in the mineralizing matrix of forming endochondral and intramembranous bones such as vertebrae and cranial structures, as can be observed in the the calcified matrix below the trabecula of a 17 DPF larvae (Fig. R21K). In 26 DPF post larvae, Mgp accumulation was observed mainly in calcified structures including mineralizing branchial arches, but also in the aorta and cardiac arterial bulbus (arrowhead in Fig. R21L).

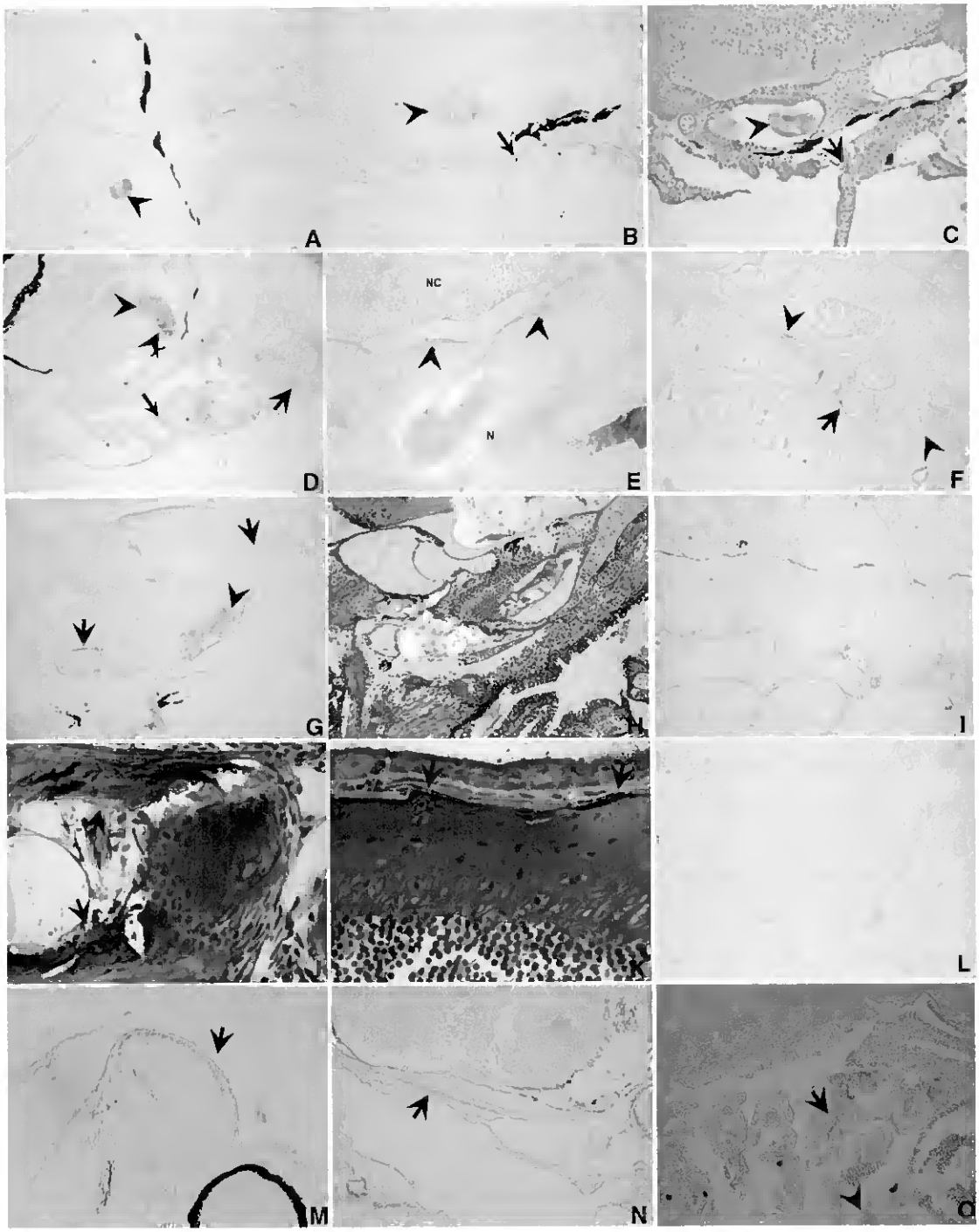

Figure R21

R10- Detection of ALP and TRAP enzymatic activity

The alkaline phosphatase (ALP) activity was determined in order to identify the cells responsible for bone deposition and tartrate resistant acid phosphatase (TRAP) activity was determined to identify cells responsible for bone resorption, both in *D. rerio* and in *S. senegalensis*. ALP was consistently detected in structures undergoing mineralization throughout skeleton development. In 13 DPF *D. rerio,* ALP activity is present in the mineralizing vertebrae (Fig. R22A). At 17 DPF is detectable around chondrocytes (arrow) and osteoblast like cells (arrowhead) in pre-opercular bones (Fig. R22B) undergoing intracartilaginous ossification and in the opercular bone undergoing intramembranous ossification. At the same age, TRAP activity indicative of ongoing resorption of mineralized matrix was detected in mineralizing branchial arches (Fig. R22C) and in skull bones undergoing intramembranous ossification (Fig. R22D).

Figure R21- Immunohistochemical detection of Mgp accumulation in different developmental stages of zebra fish (A-L) and Senegal sole (M-O) . A- Accumulation of Mgp in the otholit (arrowhead) of a 4 DAH larvae (400x); B- Accumulation of Mgp in the otholit (arrowhead) and cleithrum (arrow) of a 7 DAH (400x); C- Consecutive section of the otholit (arrowhead) and cleithrum (arrow) counterstained with toluidine blue (400x); D- Mgp accumulation in the otholit (arrowhead), cleithrum (arrow) and liver (large arrow) at 8 DAH (400x) E- Accumulation of Mgp at the zones initiating the mineralization (arrowhead) of neural arches in pleural vertebrae 3-5 of a 11 DAH larva (1000x); F- Accumulation of Mgp in the mineralizing branchial arches (arrowhead) and pharyngeal teeth (arrows) at 11 DAH; G- Mgp accumulation in the otholit (arrowhead) and cranial cartilages (arrow) undergoing ossification at18 dah (1000x); H- Consecutive section counterstained with toluidine blue (1000x); I- Mgp accumulation in the forming caudal vertebra at 18 DAH (250x); J- Mgp accumulation in the preopercular bones under endochondral ossification (arrows) in a 38 DAH juvenile (1000x); K- Mgp accumulation in skull bones undergoing intramembranous ossification (arrow) at 38 DAH (1000x); L- No staining observed in a control section with pre-immune serum (200x); M- Mgp accumulation in the othic capsule (arrow) of a 6 DAH sole (200x); N- Mgp accumulation in the mineralizing matrix under the trabecula of a 15 DAH larvae(400x); M- Mgp accumulation in the mineralizing branchial arches and pharyngeal teeth of a 24 DAH sole (200X)

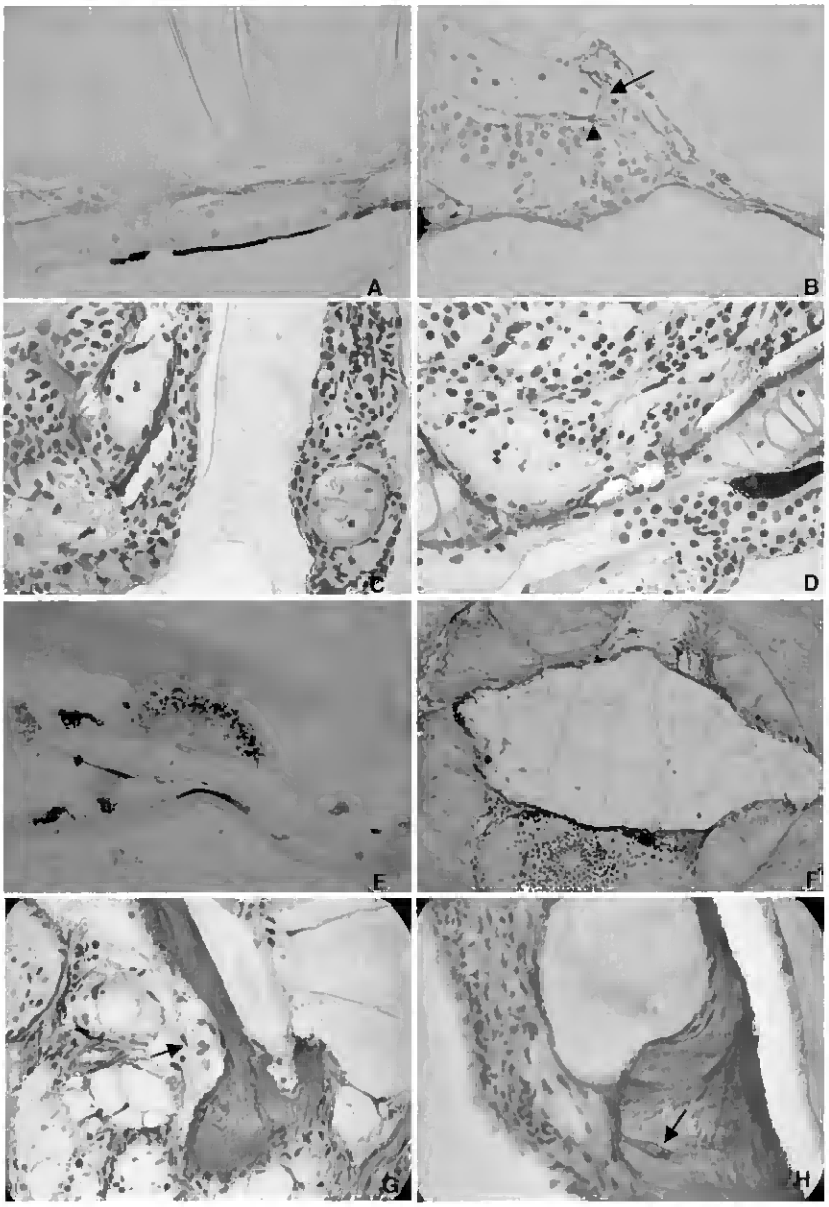

Figure R22- Alkaline phosphatase and TRAP activity in the developing zebra fish and Senegal sole skeleton. A- Alkaline phosphatase activity (in blue) detected in the forming vertebra surrounding the notochord in a 13 DPF zebrafish (1000x); and B- Alkaline phosphatase activity in the calcifying preopercular bones from zebrafish larvae at 17 DPF (1000x); C- TRAP activity (in red) detected in mineralizing branchial arches (1000x), and D- in skull bones undergoing intramembranous ossification from a 17 DPF zebrafish (1000x) E- Alkaline phosphatase activity is detected in the forming neural arches of a 17 DPF sole (1000x); F- TRAP activity is detected surrounding the vertebra, arches and spines in a 32 DPF sole .G and H- possible multinucleated osteoclast-like cells near areas of strong TRAP activity in young adult sole.

Only mononuclear cells were observed in larval and juvenile stages in sites where TRAP activity was detected. In *S. senegalensis*, ALP was also observed in various calcified structures like in the forming vertebrae of a 17 DPF individual (Fig. R22E). Resorption was observed in the vertebrae but not in head structures at this age (results not shown). Interestingly, although calcified structures were present in the head region, no resorption sites where detected by TRAP staining in the analyzed individuals undergoing metamorphosis, in which ocular migration occurs (15 DPF). In a 32 DPF juvenile, TRAP activity was strongly detected in the areas surrounding vertebrae, arches and spines (Fig. R22F). Young adult animals presented TRAP resorption in all skeletal structures and some multinucleated osteoclast-like cells were observed in the vicinity of areas of resorption or lacunae (arrows in Fig. R22G and R22H) but most of the cells observed in resorption areas were mononucleated.

R11- Effect of sodium warfarin treatment on survival and vascular mineralization of the zebrafish

R11.1- Effects of vitamin K and warfarin on larval survival.

On preliminary treatments we have determined that vitamin K has a toxic effect even at low concentrations, causing higher mortalities than warfarin alone in early stages of zebrafish larval development. On preliminary treatments using Vitamin K_3 and warfarin in early developmental stages of zebrafish, the mortality of all larvae treated with 10 mg/l vitamin K was observed until 7 dpf (Fig. R23A) as opposed to warfarin treated larvae. Warfarin alone allowed maintenance of treated fish for 2 weeks with concentrations ranging from 5 to 50 mg of warfarin per liter of media (Fig. R23B), as determined by the calculated LC50 of 26,07 mg/l. Treatment with warfarin in very early stages caused no noticeable mortality until 8 dpf, however at this age and until the end of the experiment, at 14 dpf, we observed a very high mortality at the concentration of 100 mg/l with just 3 surviving fish at the end, and a moderate mortality in the concentrations of 5 and 25 mg/l with 12 and 30 death fish respectively (Fig. R23B). The death larvae presented in some cases large hemorrhages, especially visible in the head. Based on these results subsequent warfarin treatments were administrated at concentrations ranging from

5 to 50 mg/l in fish after 15 dpf (Fig. R23C). A high mortality was observed in 50 mg/l treated individuals reaching 67% after three weeks of treatment, however there were still enough specimens for RNA purification and histological analysis. For the same period, the concentrations of 5 and 25 mg/l caused a mortality of 33% and 36% respectively, and no mortality was observed for the control (Fig. R23C).

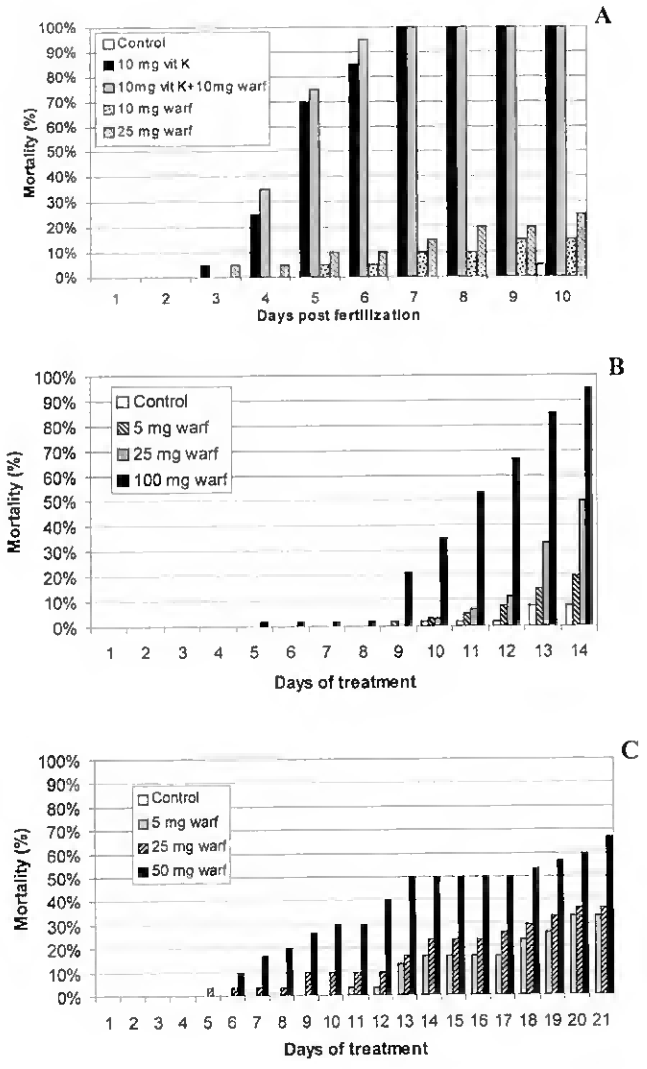

Figure R23- A- Mortality observed in vitamin K and warfarin treated zebrafish embryos starting at 9 hpf. High mortalities were observed in vitamin K treated groups. B– Mortality observed in warfarin treated zebrafish embryos starting at 9 hpf. High mortalities were observed in vitamin K treated groups. C– Mortality observed in warfarin treated zebrafish larvae starting at 15 dpf. Higher mortalities were observed in 50 mg treated group.

R11.2- Effects of warfarin on mineralization of the vascular system.

After 3 weeks of treatment by immersion in warfarin solutions, zebrafish juveniles were fixed, sectioned and stained by the von Kossa's method. No ectopic calcification was observed in the control specimens (Fig. R24A), that only presented

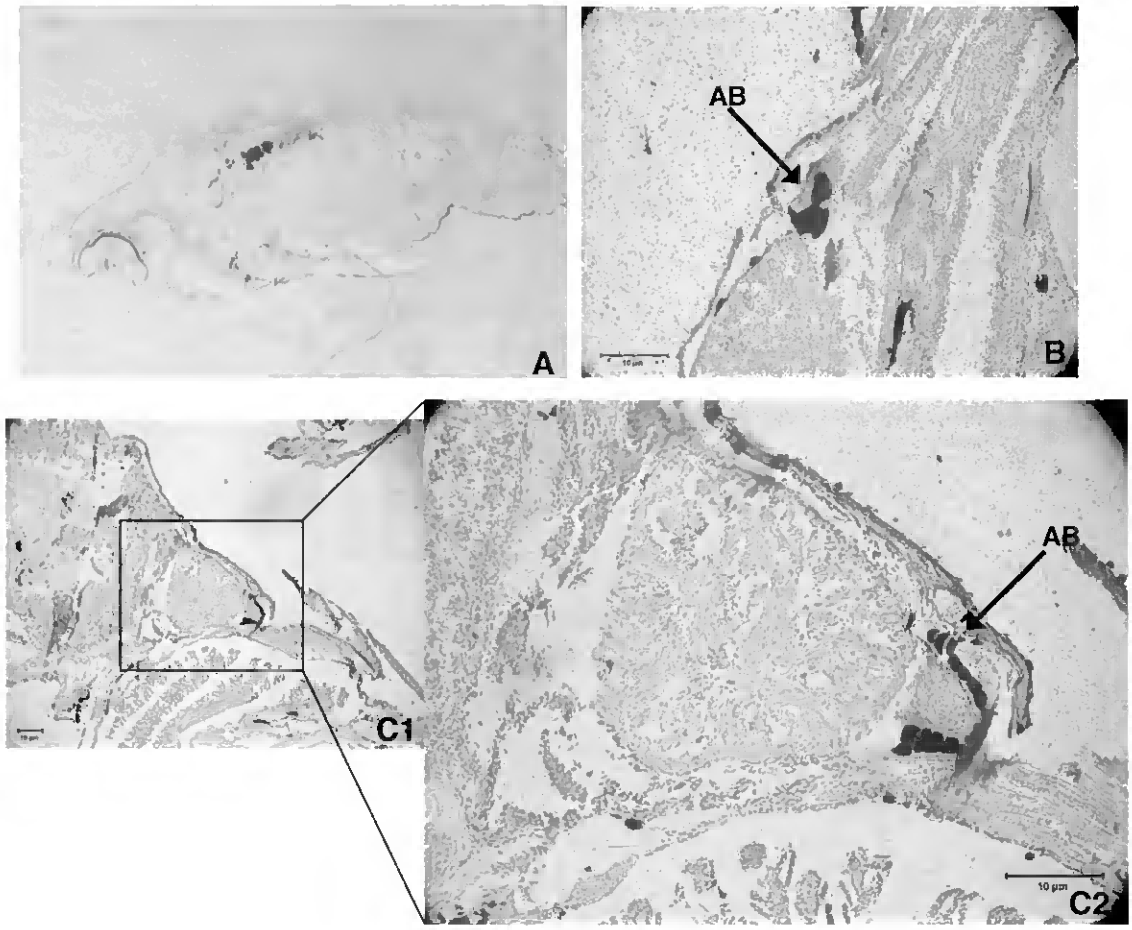

Figure R24 - Von Kossa' staining of zebrafish treated with warfarin for 3 weeks. A- Control with calcification only in skeletal tissues; B- Section of the heart region (ventral to top, head to the right) with pathological calcium accumulation in the aortic bulbus in a specimen treated with 25 mg/l warfarin; C- Calcification of the aortic bulbus in a specimen treated with 50 mg/l warfarin. C1- low magnification microphotography of the heart and , C2- high magnification microphotography with a detail of the calcified aortic bulbus.

calcification in the mineralized skeletal structures. Similar results were obtained for the specimens treated with 5 mg/l of warfarin. However, a strong accumulation of mineral was detected in the aortic bulbus (AB) of specimens treated with 25 mg/l and 50 mg/l of warfarin (Figures 24B and 24C) as observed by the von Kossa´s method. No ectopical calcifications were observed in the other cardiac chambers or in other vessels and organs.

R12- Effect of sodium warfarin treatment on *bgp* and *mgp* expression levels in zebrafish

Northern blot analysis of total RNA extracted from zebrafish treated with different concentrations of warfarin revealed that expression of *bgp* and *mgp* were detected in all stages and concentrations analyzed (Fig. R25). No noticeable differences in expression were detected during the period of time that the treatments were administered.

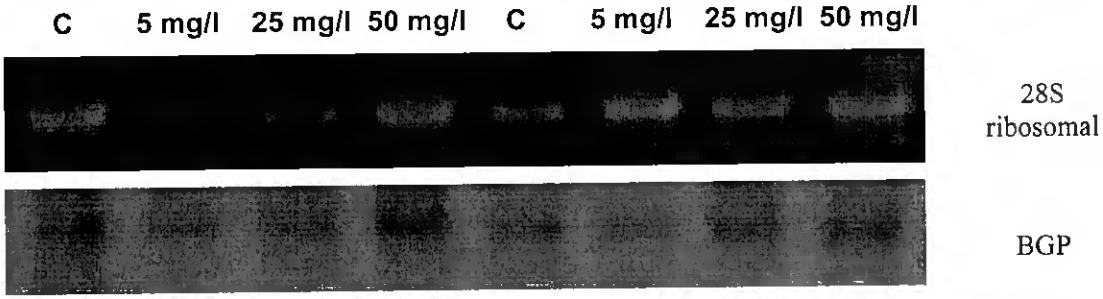

Figure R25- Effect of treatment with warfarin in zebrafish over *bgp* expression at the end of 15 and 21 days of treatment

R13- Effect of sodium warfarin treatment over vascular mineralization in toadfish

The toadfish (*Halobatrachus didactilus*) has been the model organism selected for administrating warfarin treatments by injection. The choice of this species is due to it´s high resistance to stress and manipulation allowing us to inject the fish 3 times a week, what would be impossible in the other species used in this study.

R13.1- Effect of sodium warfarin treatment over growth and survival

The toadfish specimens used in this experiment were maintained in the experimental circuit for 3 weeks before treatments initiated. During this period a small increase in weight was observed in the four groups (Fig. R26). During the treatment period a decrease in weight was observed in all individuals treated with warfarin. The fish treated with vitamin K alone or in conjunction with warfarin had small and divergent weight variation among individuals. The control group had a weight gain in both individuals, in particular specimen c1 that increased 20 g. During the first week of treatment two specimens died, one from the control group (c2) that asphyxiated and one from the vitamin K treatment group (k3) was found dead in the day after the second injection. After the beginning of manipulation and injections all the fish showed signs of stress and some fish reduced or even stopped feeding.

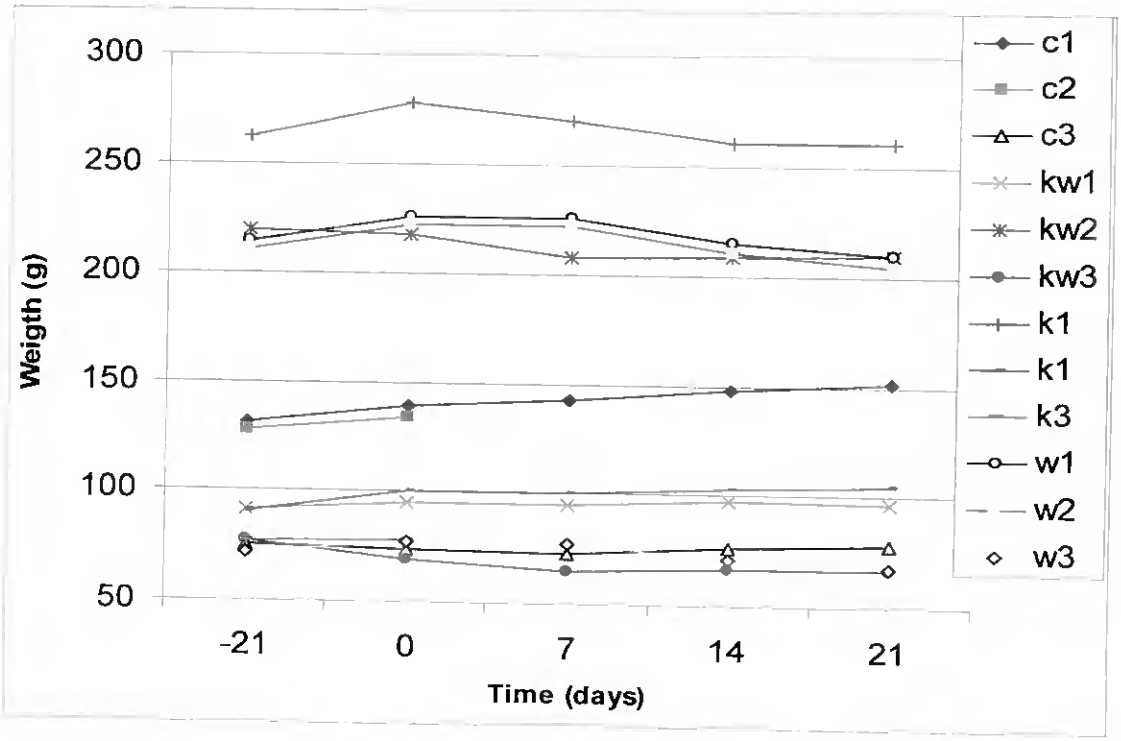

Figure R26 – Graphic of weight variation for toadfish groups treated with vitamin K and warfarin. Specimens c2 from control group and k3 (from vitamin K treatment group) died during the first week of treatment.

R13.2- Effect of sodium warfarin treatment in vascular mineralization

In a similar way to the observed for warfarin treated zebrafish, in toadfish after 3 weeks of treatment with warfarin by injection, the formation of a warfarin-induced ectopic calcification was observed in the aortic bulbus (AB) of hearths from specimens treated with 15 mg warfarin / 100g weight and stained with alizarin red, as can be seen in Fig. R27B. No abnormal calcium staining was observed in the arterial system of specimens from the control group (Fig. R27A) or in specimens that received vitamin K or a combination of vitamin K and warfarin.

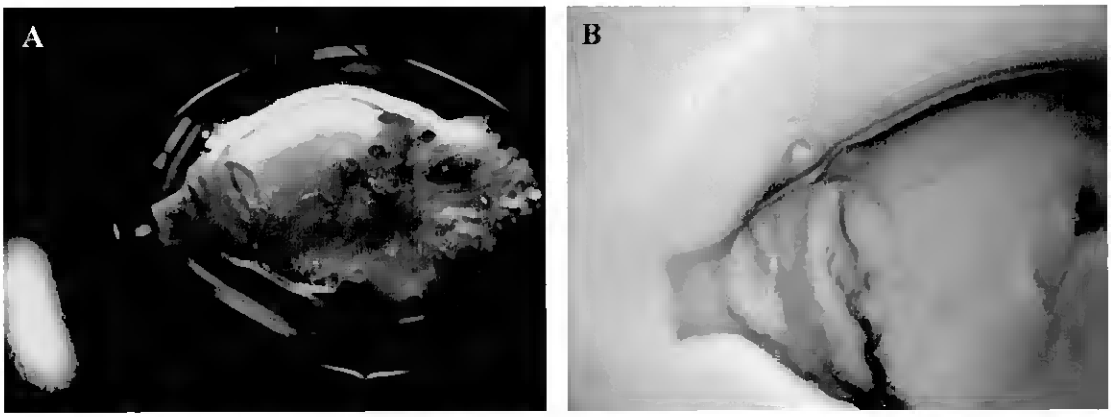

Figure R27– Whole mount alizarin red staining of hearts from toadfish injected with warfarin for 3 weeks. A- Control without any abnormal calcification in cardiac or arterial tissues. This individual displayed some calcium staining associated with endoparasites within the cardiac muscle; B- Heart from an individual treated with 15mg/kg of warfarin, showing pathological calcium accumulation in the aortic bulbus

R14- Effect of vitamin A treatments over *bgp* and *mgp* expression in the Senegal sole

The administration of Vitamin A treatments by feeding fish with retinol palmitate enriched artemia was tested in larval and juvenile stages at different times of exposure and at different concentrations of retinol palmitate in the enrichment media, with the purpose of verifying differences in *bgp* expression.

The administration of concentrations of 10^3, 10^4 and 10^5 IU vitamin A for 15 days did not induce any alterations in *bgp* expression in juvenile *S. senegalensis* as observed

by Northern hybridization of total RNA extracted at the end of the experimental period (Fig. R28 A).

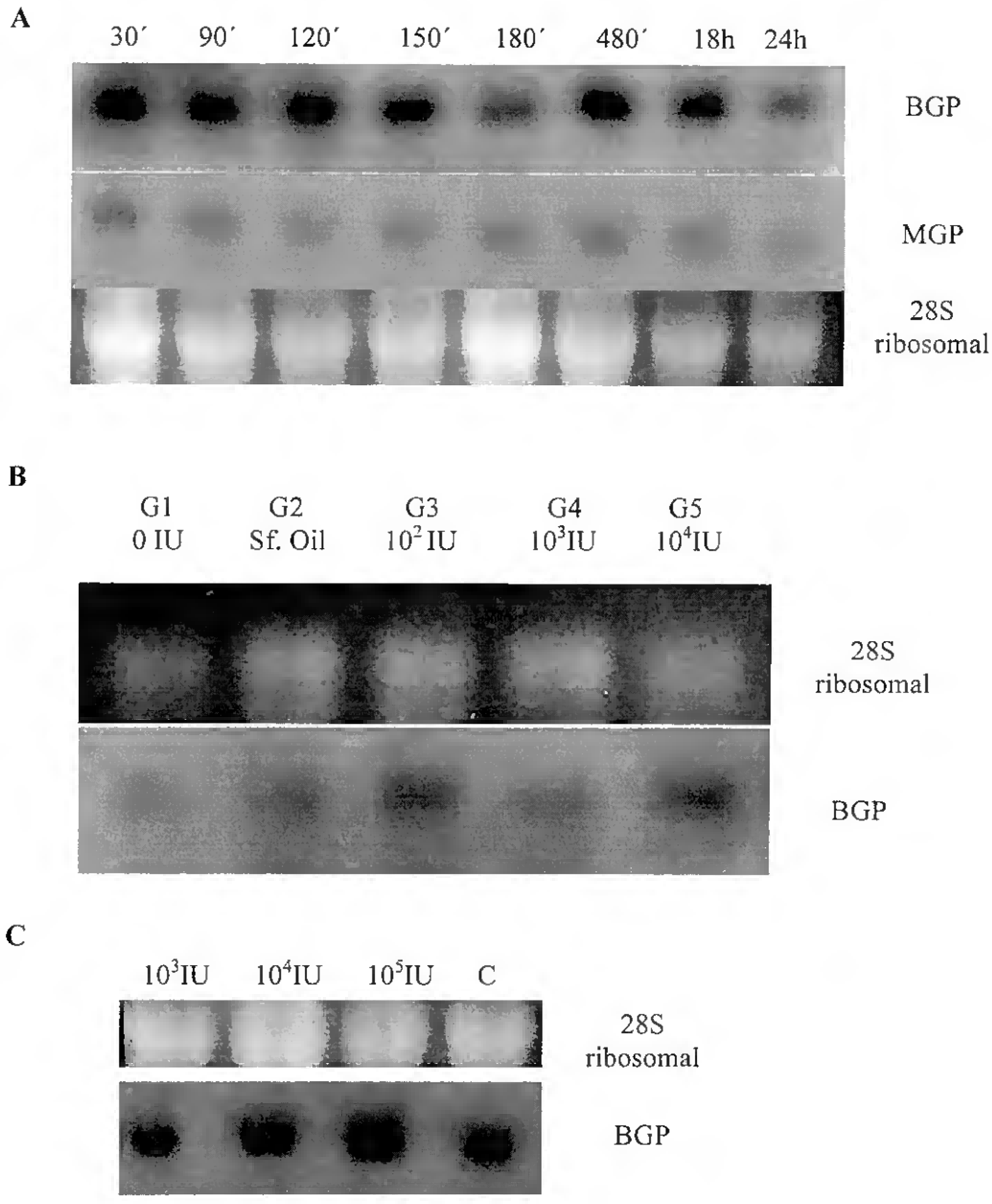

Figure R28- Northern hybridization to detect expression of *bgp* in RNA from Senegal sole fed vitamin A enriched artemia. A- Treatment with 10^4 IU vitamin A at different times after feeding in 6 month old sole; B- Treatment with 0 – 10^4 IU Vitamin A in sole from 15 to 30 DAH. Sf. Oil- Sunflower oil (vehicle); C- Treatment with 0 – 10^5 IU Vitamin A for 15 days in 6 month old sole. C- control treated with vehicle (Selco) only. IU- International units.

To verify if any alteration was induced in the time immediately after vitamin A administration, juvenile *S. senegalensis* were feed artemia enriched with 10,000 IU vitamin A and total RNAs were purified from specimens collected at intervals during the first 24 hours after feeding. No alterations on the expression of *bgp* or *mgp* were detected at any time point of the treatment, as observed by Northern hybridization (Fig. R28 B). Treatment of larval specimens with 100, 1,000 and 10,000 IU vitamin A resulted in a similar result, and no alterations on the expression of *bgp* were detectable after 15 days of treatment (Fig. R28 C). However some severe deformities were observed in the caudal vertebra and in the fin support structures of 10,000 IU vitamin A treated larvae (Fig. R28 A and B).

DISCUSSION

Discussion

D1- General overview

In this work we have cloned, for the first time, complete cDNAs for *bgp* and *mgp* in zebrafish and Senegal sole. We made a comprehensive study of gene expression and protein accumulation for these two important mineralization-related proteins during development of the skeleton in these fish species with different ecologies. These data, summarized in Tables D1 and D3, make an interesting comparison with our previous data for other fishes and with preexisting information for mammals. In addition, new data is presented indicating that in fish vascular calcification is under the control of Gla proteins, as shown by inhibiting Mgp from functioning with warfarin. This finding comes in agreement with the previously observed in mammals (Price *et al.,* 1998; 2000) revealing a conserved function from fish to man.

D2- Improved method for whole-mount double staining of the skeleton.

The improvements made on the alizarin red-alcian blue double staining method for cartilage and bone allows the visualization of the entire skeleton throughout vertebrate development and allows the easy detection of any deformities that may occur during the early developmental stages. Several authors have previously reported the application of whole-mount double staining of the skeleton for a large number of purposes and species (e.g. Inouye, 1976; Wassersug, 1976; Kimmel and Tramel, 1981; Francillon and Meunier, 1985; Parenti, 1986; Klymkowsky and Hanken, 1991; Webb and Byrd, 1994; Song and Parenti, 1995) and most of the references in fish are based on the protocols by Dingerkus and Uhler (1977) and by Taylor and Van Dyke (1985). Similar techniques have been used to localize bone and cartilage in froglets (Martìnez *et al.,* 1992), fetal mice (Webb and Byrd, 1994), and larvae and juveniles of marine fish such as sea bass (Daoulas *et al.,* 1991, Bogline *et al.,* 1993; Marino *et al.,* 1993), red seabream *Pagrus major* (Matsuoka, 1985) and gilthead sea bream (Faustino and Power, 1998, Koumoundouros *et al.,* 1997).

The improved technique is suitable to reveal even slight amounts of cartilaginous and calcified tissues even in small larvae where the calcified structures are

very small and prone to acid decalcification. The methodology used is also suitable for studying skeletal development since it allows the detection of small structures undergoing mineralization and in addition, this technique has also proven useful for the early detection of skeletal malformations in very young larvae (Gavaia *et al.*, 2000).

The best results for cartilage staining were obtained at lower pH since the specificity of Alcian blue for sulphated mucopolysaccharides is higher around pH 1.0 (between 0.5 and 1.0 it stains sulphated groups) while at pH greater than 2.0 the dye stains mostly carboxylated groups of mucopolysaccharides/glycoproteins (Pearse, 1985). However, in contrast to Alcian blue incorporated into soft tissues, which can be eliminated, dye incorporated into cartilage mucopolysaccharides cannot be washed out (Dingerkus and Uhler 1976).

The staining process with Alcian blue is the most critical step in this double staining technique since the acidity of this solution can rapidly and efficiently demineralize small structures undergoing calcification such as those observed in recently hatched fish larvae, where they can have a thickness of only a few microns. The staining time in Alcian blue is therefore a critical parameter since adequate dye penetration must be achieved without significant loss of mineralized structures by the action of the acidic staining media (Gavaia *et al.*, 2000). For small larvae up to 1cm the time of 12-24 hours proposed by Taylor and Van Dyke (1985) leeds to complete decalcification, whereas the times of 10-15 min proposed by our protocol were sufficient to adequately stain 3-4 mm larvae. We also proposed the use of a KOH / absolute ethanol solution rather then just KOH (Taylor and Van Dyke 1985) or just absolute ethanol washes (Dingerkus and Uhler, 1977; Hanken and Wassersug 1981) to neutralize the Alcian blue. This step helps prevent further decalcification by any remaining acidity within the specimen without allowing precipitation of the dye. If the neutralization is made only with KOH, the specimens may show high levels of non specific staining since Alcian blue precipitates at pHs above 6 (Kiernan, 1990)and is retained inside the sample, resulting in a more difficult and extended clearing process. On the other hand, using 100% ethanol washes removes the dye, but does not neutralize the samples.

This technique has been applied to several teleost species in different developmental stages and has given very good results for the detection of both cartilage and bone as well as for the detection of skeletal deformities in very early stages of development.

D3- Skeletal development and abnormalities of the Senegal sole.

In this work we have described for the first time the osteological development of the caudal complex and vertebral column in Senegal sole. In this species we have previously shown that the first calcified structures to appear are the appendicular elements (cleithrum) at 2 DAH (Gavaia *et al.,* 2000). Development of both caudal complex and vertebral column begins at 12-13 DAH, accompanying the urostyle torsion and acquisition of asymmetry by migration of the left eye. At this stage, larvae progressively change to a benthonic life style. Similar observations were made in the Japanese flounder, where the flexion of the notochord is closely related to the development of hypuralia (Hosoya and Kawamura, 1998). This parallelism can be explained by the importance of the described structures in the swimming and feeding capabilities of the larvae, especially in early stages of their development as reported for other species like red sea bream, rabbit fish or Asian sea bass (Kohno et al 1983, 1986, 1996). Knowledge of the normal pattern of development of skeletal structures is essential prior to identification of the factors responsible for the onset of skeletal deformities.

The caudal fin of Senegal sole is the first fin structure in the axial skeleton to develop, acquiring full meristic count after 6.1 mm Lst, followed by anal and dorsal and then paired fins. This same sequence of fin development has also been observed in the red sea bream (Konho *et al.,* 1983), the milkfish (Taki *et al.,* 1987), the common dentex (Koumoundouros *et al.,* 1999) and the Japanese flounder (Hosoya and Kawamura, 1998). In Senegal sole, there is a large variation in size and stage of development of larvae of the same age as can be seen in Figs. R1 (D, E) and R3 (C, D). The occurrence of high heterogeneity in growth has also been reported for the guilthead seabream (Faustino and Power, 1998). The caudal structure of the Senegal sole is less complex than in the majority of species already reported, lacking the uroneural processes visible in some sparid species (Matsuoka, 1985; Taki *et al.,* 1986, 1987; Koumoundouros *et al.,* 1997a, 1999). In addition, only one epural is found in the Senegal sole, a finding common only to the yellow tail, with all other species studied to date presenting two or more epurals, including the pleuronectiform Japanese_flounder (Hosoya and Kawamura, 1998).

The alizarin red-alcian blue double staining method for cartilage and bone allows the visualization of the entire skeleton throughout vertebrate development and

the easy detection of any deformities that may occur, as already done for Senegal sole (Gavaia *et al*, 2002). Similar techniques have been used to localize bone and cartilage in froglets (Martìnez *et al.,* 1992), fetal mice (Webb and Byrd, 1994), and larvae and juveniles from sea bass (Boglione *et al.,* 1993; Marino *et al.,* 1993) and gilthead sea bream (Faustino and Power, 1998, Gavaia *et al.,* 2000, Pinto *et al.*, 2001).

According to previous reports, the observation of deformities in wild specimens of teleost fish is rare (Hosoya and Kawamura, 1998) either because they are less abundant or due to decreased viability of the abnormal fish in their natural habitat. Nevertheless, skeletal malformations have been described in captured larval specimens of wild sea bass (Marino *et al.,* 1993), gilthead sea bream (Boglione *et al.,* 2001), common dentex (Koumoundouros *et al.,* 2001) and Japanese flounder (Hosoya and Kawamura, 1995, 1998) revealing, in all cases, a significantly lower incidence of deformities, when compared to those observed in specimens of the same species reared in hatchery conditions. In addition, we have recently analyzed very young larval stages of Senegal sole captured in the wild and found a significant incidence of skeletal malformations, suggesting that these malformations are also present in wild fish but likely to undergo a negative selection since they are rarely observed in captured adult fish (Gavaia *et al.*, 2003). The meristic characteristics also presented a higher variability in hatchery-reared than in wild captured specimens (Boglione *et al.,* 1993, 2001; Marino *et al.,* 1993; Koumoundouros *et al.,* 2001). These observations indicate that deviations to normal development are correlated to rearing conditions and may even be induced by them. Recently it was reported for Atlantic salmon that, although elevated incubating temperatures were the main factor causing bone deformities in the opercula, fins and jaw, there were no negative effects on development of spinal deformities (Ørnsrud *et al.,* 2004)

Our results show an overall incidence of deformities of 44% in hatchery reared Senegal sole, a value that is comparable to those observed in species already well adapted to intensive aquaculture conditions (Gavaia *et al.*, 2002). Accordingly, in seedlings of the flatfish Japanese flounder reared in captivity, malformations such as increase in hypural branches, fused spines and central fusions have been detected with an incidence of 30-60% of the total number of malformations observed in the caudal complex (Hosoya and Kawamura, 1995, 1998). For the gilthead sea bream, samples from individuals reared under intensive culture conditions presented a frequency of deformities of up to 100% while under semi-intensive culture conditions this frequency

decreased to 55% (Boglione *et al.,* 2001). In aquaculture-reared sea bass, a high number of deformities were also encountered in the axial skeleton and fins, with frequencies of incidence of up to 75 % in the vertebrae and 45% in the fins. In contrast, for common dentex it was found that only 6% of the individuals presented deformities, and from these the caudal fin region was not more affected than other regions of the skeleton (Koumoundouros *et al.,* 1999). The reason for such a discrepancy between species is not known and additional work is required in order to explain this fact.

Among the abnormalities observed in Senegal sole, the most common were vertebral fusions (Fig. 6) indicating that the development of these structures may be the most susceptible to rearing conditions in captivity. These deformities are among the most visible, since they can alter the shape and length of the fish depending on the severity and number of structures affected and consequently make it less attractive for the consumer. Nutritional factors, such as levels of vitamin A and its precursors, or levels of vitamin C, in the diet have also been shown to affect the development of skeletal structures. Low levels of dietary vitamin C were implicated in the development of severe deformities in rainbow trout (Madsen and Dalsgaard, 1999) while the number of malformations affecting the caudal region and vertebra of Japanese flounder larvae treated with vitamin A palmitate during metamorphosis, were shown to increase with increasing dietary levels of vitamin A (Dedi *et al.,* 1995; 1998). Similar effects of vitamin A on development of vertebral column elements were observed in turbot (Estevez and Kanazawa, 1995). Parasite infection has also been reported to be a possible factor in development of skeletal malformations (Taylor *et al.,* 1994). Shortness of the vertebral column described in Atlantic salmon was suspected to be related to an infectious etiology (Kvellestad *et al.,* 2000).

This work represents the first description of the skeletal structures in Senegal sole and their appearance during normal development. It provides therefore the basic knowledge required to easily identify the presence of skeletal malformations in this species, being of relevance for future studies. Since nearly half of the fishes observed had at least one deformity and given the very high commercial value of sole, it would be important to analyze the molecular events underlying the onset of such a high percentage of deformities when sole is reared in captivity.

Establishment of both nutritional and abiotic parameters involved in the mechanisms leading to the appearance of these deformities must be determined in order

to prevent a high incidence of malformations particularly under intensive culture conditions.

D4- Skeletal development of the zebrafish

Zebrafish has an accelerated development compared with other teleosts and, in general, structures develop earlier and faster than for the marine fish species examined here and elsewhere (Faustino *et al.,* 1998; Pinto *et al.,* 2003). In our work we used an improved histological procedure to detect sensitively development of the calcified and cartilaginous structures that compose the zebrafish skeleton by detecting both calcium deposition and cartilage with the histological markers alizarin red and alcian blue (Gavaia *et al.,* 2000). This method allowed us to follow the onset of skeletogenesis in more detail compared with previous studies using calcein as a fluorescent marker for calcium (Du *et al*, 2001) which do not allow cartilage visualization.

The skeletal development in zebrafish larval stages is described in detail up to the juvenile stage, when most skeletal elements are already present, and thus complements earlier studies describing the development of skeletal structures during specific periods. Schilling *et al.* (1996), Piotrovsky *et al.* (1996) and Schilling and Kimmel (1996) have described the chondrocranium in embryos up to 120 hours focusing in particular on the development of pharyngeal arches. Cubbage and Mabee (1996) describe skeletal development in larval and adult individuals, with special reference to the cranium and paired fins. Du *et al.* (2001) used calcein to describe the axial skeleton, in larvae up to 23 days post fertilization (dpf). Although their study only allowed visualization of calcified structures, our results concerning mineralisation are in good general agreement with those obtained by Du *et al.* (2001). We detect calcification one day sooner in the head region, although this may perhaps result from differences in the feeding regimes employed, but the timing of subsequent events of skeletal development remain similar.

D5- Identification of bone formation and resorption by the detection of ALP and TRAP enzymatic activity.

We where able to detect alkaline phosphatase (ALP) activity in the area surrounding the cells responsible for bone deposition and tartrate resistant acid

phosphatase (TRAP) activity in the proximity of cells responsible for bone resorption, both in *D. rerio* and in *S. senegalensis*. ALP was consistently detected during development in structures undergoing mineralization throughout the skeleton. TRAP activity was detected at the same developmental stages and structures as ALP activity, indicating that the formation and growth of skeletal elements in both zebrafish and Senegal sole are processes strictly regulated by a balance between calcium deposition and resorption. We where able to detect multinucleated cells associated with TRAP activity as reported by Witten *et al.* (2001), however the individuals used in our study were mostly larvae and juveniles that have mostly mononucleated cells, whereas according to Witten *et al.* (2001), the multinucleated resorbing cells are the predominant form in adult zebrafish. The variety of bone resorbing processes in teleosts is connected to the variety of different types of bone tissues, comprising cellular bone (like in zebrafish), acellular bone (like in sole) and the various stages between cartilage and bone (Witten *et al.*, 2001). No evidences have been presented to date regarding the mechanisms leading to osteoclast differentiation in fish. In mammals, it is known that osteoclastogenesis is controled by RANKL which is expressed on the surfaces of cells from the osteoblastic lineage. Cell-to-cell contact allows RANKL to bind to its physiologic receptor RANK, which is expressed on the surface of osteoclast lineage cells and induce differentiation. The action of RANKL action is opposed by osteoprotegerin (OPG) also produced by preosteoblastic marrow stromal cells and osteoblasts (Eghbali-Fatourechi, *et al.*, 2003). However recent evidences showed that the differentiation of osteoclasts is also controlled by the sympathetic system and leptin. Leptin acts via a dowstream β2-adrenergic receptor (Adrb2) present in osteoblasts that controls bone formation. Deleting Adrb2 in mice causes a sympathetic nervous system mediated induction of expression of the osteoclast differentiation factor RANKL by osteoblast precursor cells and increases bone resorption. Another mechanism involves CART ('cocaine amphetamine regulated transcript') a neuropeptide whose expression is controlled by leptin and which inhibits bone resorption by modulating RANKL expression (Elefteriou *et al.*, 2005). In this way leptin controls bone resorption through, at least, two distinct and antagonistic pathways: i) a sympathetic signalling via Adrb2 that promotes osteoclast differentiation and ii) CART-mediated inhibition of osteoclast differentiation, both pathways acting by regulating RANKL expression.

D6- Structure of zebrafish and Senegal sole *bgp* and *mgp* cDNAs

D6.1- *D. rerio* and *S. senegalensis bgp* cDNAs

The *Danio rerio bgp* cDNA and the *Solea senegalensis bgp* cDNA were cloned for the first time used as templates for generating the probes necessary for further characterization of the genes and localization of sites of expression.

In order to obtain the cDNA for *Danio rerio bgp* we have taken advantage of the N-terminal amino acid sequence previously purified from zebrafish bone (Simes *et al.*, 2004) in order to design degenerated primers. The complete nucleotide sequence of the *Danio rerio bgp* cDNA was obtained by a combination of RT-PCR and 5'RACE-PCR. (Figure R9). The sequence coding for *Danio rerio bgp* spans 410 bp and contains an open reading frame (ORF) of 315 bp (Figure R10) encoding a polypeptide with 104 aminoacids (AA) comprising a 56 residue pre-propeptide and a 48 residue mature peptide. The nucleotide sequence of the *Solea senegalensis* (*Sse*) *bgp* cDNA, obtained by a similar approach as the *Danio rerio* cDNA, spans 635 bp and encodes a 45 residue mature protein, preceded by a pre-propeptide of 55 residues (Figure R10). All pre-pro cleavage sites were deduced by comparison with other known *Bgp* sequences from mammals, birds, fish and amphibian (Viegas *et al.*, 2001) (Figure R10). The first amino acid of each mature form was identified by comparison with results obtained following protein sequence analysis of *Bgp* purified from zebrafish and Senegal sole bone (Simes *et al.*, 2004). Zebrafish *Bgp* was found to contain three more amino acids than *S. senegalensis Bgp* at the N-terminus of its mature form. Comparison between the two cloned Bgp sequences and other fish Bgps indicate that out of the 45 AA present in the common region of the mature protein between the two species, 36 residues were 100% conserved, including the three Gla residues and the two cysteines required for the disulphide bridge this features are shared with all mature fish Bgps that contain a large block of high identity (EXXXEXCEXXXXC motif), containing the three Gla residues involved in calcium binding and the two cysteines (Simes *et al.*, 2003). For both proteins, the deduced N-terminal region was in full agreement with the sequence previously obtained by amino acid sequence analysis (Simes, 2002; Simes *et al.*, 2004).

The high level of identity observed in the mature proteins contrasted with that observed between the pre-pro regions, where only 18 out of 55 residues were conserved. Comparison of the two cDNAs also identified a larger 3'-untranslated region (UTR) in *S. senegalensis bgp* cDNA with two consensus polyadenylation signals before the poly

A tail, on the other hand zebrafish *bgp* had a shorter 3'-UTR that contained a CA repeat four nucleotides downstream from the stop codon and only one polyadenylation signal in contrast to the two observed in sole.

D6.2- *D. rerio* and *S. senegalensis mgp* cDNAs

The *Danio rerio mgp* cDNA and the *Solea senegalensis mgp* cDNA were cloned for the first time and used as templates for generating the probes necessary for further characterization of the genes and localization of sites of expression.

The *Danio rerio mgp* cDNA, cloned by a combination of RT-PCR amplification and 5'-RACE PCR, spans 628 bp (Figure R11) and comprises an 318 bp ORF coding for a polypeptide of 105 residues comprising a pre-peptide of 21 residues and a mature protein of 84 residues. Surprisingly we found that the 3'UTR includes a dinucleotide repeat motif (GT) and one canonical polyadenylation site. The *Solea senegalensis mgp* cDNA that was also cloned by RT-PCR amplification and 5'-RACE PCR, spans 874 bp and contains a 435 bp ORF encoding for a 144 residue peptides (Figure 11) from which the first 19 constitute the pre-peptide. At the 3'-end is located a motif repeated three times within the coding region (consensus: CAGAGACCCCAGATACCCCAG, coding for Gln-Arg-Pro-Gln-Ile-Pro-Gln). Comparison between the two sequences shows a high conservation of the main phosphorylation motif in the N-terminal region (Ser-Xxx-Glu-Ser-Xxx-Glu-Ser) that is highly conserved in all known sequences (Price *et al.*, 1994; Simes *et al.*, 2003; Laizé *et al.*, 2005). Also the Ala-Asn-Xxx-Phe motif and the three putative Gla residues are located within the region containing the two cysteines responsible for the disulphyde bridge (Gla-Xxx-Xxx-Xxx-Gla-Xxx-Cys-Gla-Xxx-Xxx-Xxx-Xxx-Cys) that is a motif highly conserved among other known *mgp* sequences (Cancela *et al.*, 2001; Pinto *et al.*, 2003; Simes *et al.*, 2003, Laizé *et al.*, 2005). We have also found a C-terminal extension in both fish sequences when compared with mammalian Mgps (Price *et al.*, 1994), which is longer in the Senegal sole than in zebrafish Mgp. The two cysteine residues involved in the formation of the disulfide bridge are conserved in all known Bgps and Mgps.

D7- Expression of *bgp* and *mgp* during skeletal development.

As observed for other species like mouse (Desbois *et al.*, 1994a) and seabream (Pinto *et al.*, 2001) the accumulation of Bgp protein in zebrafish is detected soon after

the appearance of the first calcified structures. Although Bgp accumulation was clearly observed at 8 dpf in the otolyths, cleithrum and pharyngeal teeth, some was detectable at 96 hpf in the mineralized pharyngeal teeth. Thus Bgp is detected here within around a day of the onset of mineralisation although we note that Huysseune *et al.* (1998) and Van der heyden *et al.* (2000) report mineralisation slightly earlier than this, probably due to the methodology used by these authors, aiming to detect even the primordial cell condensations that lead to the formation of the structures.

The presence of *Danio rerio bgp* mRNA is first observed at 5 dpf by *in situ* hybridization in the pharyngeal teeth of the fifth ceratobranchial arch and in the cleithrum, consistent with RT-PCR amplification of *Danio rerio bgp* at this age and with these structures being the first to become mineralized. In *Solea senegalensis*, *bgp* is observed much later, at 15 dpf, and at a more advanced stage of skeletal development, when calcified structures are prominent in both the head and axial skeleton. At this age, sole were already mineralizing the vertebral column (Gavaia *et al.*, 2002) and there is extensive calcification in the head region. We suggest that in this slower growing species, *bgp* expression appears to initiate later than in the faster growing zebrafish. This is consistent with results obtained by others for *Sparus aurata* (Pinto *et al.*, 2001), where presence of mRNA is only detected at relatively late stages (39 dpf). *bgp* expression in *Danio rerio* is restricted to cells of mineralized structures or stuctures undergoing calcification like the cartilages undergoing endochondral calcification, in agreement with results obtained for other fish species (Pinto *et al.*, 2001; Simes *et al.*, 2003). Expression of *bgp* was mainly observed in hypertrophic chondrocytes during the early skeletogenesis events, when the cartilaginous structures are starting to present deposits of mineral (as observed by histological staining) and becoming calcified cartilages or bones. Although Bgp has been widely accepted as a bone marker and referred to as expressed mainly in osteoblastic and odontoblastic cells (Price, 1990, Papagerakis *et al.*, 2002), some references describe the presence of Bgp in cultures of hypertrophic chondrocytes from chicken (Neugebauer *et al.*, 1995) and from mouse (Strauss *et al.*, 1990). The observation of *bgp* gene expression in chondrocytes at a stage when cartilage calcification is occurring is in agreement with those observations and may reflect the fact that during cartilage calcification a number of structures calcify before osteoblasts have been observed. Bgp is thought to be required for the correct formation of hydroxyapatite crystals in the mineralizing matrix of developing skeletal structures, as previously described in mouse (Boskey *et al.*, 1998), a function that is

consistent with the data obtained from fish and which suggesting evolutionary conservation of gene function.

D8-Relationship between expression of *bgp* and *mgp* mRNAs and the onset of metamorphosis

The analysis of mRNA transcripts for *bgp* and *mgp* by quantitative real time PCR revealed expression of both transcripts in all developmental stages investigated, but with different patterns for the two species. *bgp* transcripts showed a tendency to increase in both species with a peak for *D. rerio* at 120 hpf, corresponding to the periods when calcification of cranial bones and initial formation of axial skeleton elements take place. The pattern of *mgp* levels closely matches that of *bgp* in zebrafish. In contrast, in *S. senegalensis* the levels of *mgp* are proportionately much lower until the beginning of metamorphosis at 14 dpf. In *S. senegalensis* a dramatic increase of *bgp* and *mgp* expression is observed at 14-16 dpf when metamorphosis is initiated, coincident with the time of dramatic rotation of the skeletal structures to the ocular (right) side. This increase may be related both to the high number of structures that form *de novo* and calcify during the metamorphosis and to the corresponding need for rearrangement of pre-existing structures, which must rotate and change morphology.

D9- Sites of Mgp accumulation in fish versus mammals

Our results show that Mgp in zebrafish and Senegal sole is accumulating mainly in sites where a calcified matrix is present, either bone or calcified cartilage, in contrast to the observations in *A. regius* where Mgp accumulates in cartilage matrix and in chondrocytes (Simes *et al.*, 2003). The results obtained for zebrafish are thus more in agreement to those found in mammals, where Mgp protein was found to accumulate only in the extracellular matrix of bone, cartilage and tooth cementum (Price *et al.*, 1983; Hashimoto *et al.*, 2001), despite the fact that *mgp* mRNA was present in cartilage and various soft tissues as described in rats particularly in heart, kidney, and arterial vessel wall (Fraser and Price, 1988).

Previous studies carried out in mammals reported that Bgp appears to be absent during early stages of osteoblast maturation, being undetectable in undifferentiated or recently differentiated osteoblasts near the growth plate but clearly detectable in mature

osteoblasts (Mark *et al.*, 1988; Ikeda *et al.*, 1992; Liu *et al.*, 1994). Likewise, studies of the accumulation of Bgp protein in osteoblastic cells by immunolabeling could only detect this protein in cuboidal cells with a clear osteoblastic phenotype (Liu *et al.*, 1994). The relationship between Bgp and mineralization remains unclear even within the same species, since some authors detect Bgp prior to mineralization (Bronckers *et al.*, 1987; Gerstenfield *et al.*, 1987; Mark *et al.*, 1988; Liu *et al.*, 1994) and others at the onset or after the beginning of mineralization (Groot *et al.*, 1986; Boivin *et al.*, 1990; Owen *et al.*, 1990, 1991; Pockwinse *et al.*, 1992, Pinto *et al.*, 2001). This discrepancy remains to be explained and is likely to be linked to the still unclear function played by Bgp during bone formation and/or mineralization. For the zebrafish and for Senegal sole Bgp was detected after the onset of mineralization in all the structures analyzed as summarized in Table D1 and D2.

D10- Effects of vitamin A treatment on *bgp* and *mgp* expression

We have submitted fish to treatments with vitamin A in the form of retinol palmitate in a protocol adapted from the one used by Dedi *et al.* (1998) in which retinol is added to artemia nauplii enrichment media resulting in high levels of retinoic acid in the nauplii has determined by HPLC (Dedi *et al.*, 1995, 1998). The analysis of total RNA isolate from Senegal sole treated with this retinoic acid rich artemia did not reveal any effect over the expression of *bgp* or *mgp* either at different times after the beginning of the treatment or in specimens treated with different concentrations of vitamin A for a longer period. It would be expected to observe an effect over the expression of these proteins since it has been reported that retinoic acid can regulate the expression of *mgp* both *in vitro* and *in vivo* (Cancela *et al.*, 1992, 1993; Kierfel *et al.*, 1997). The stimulating action of retinoic acid over the expression of human *bgp* is mediated by its ligand (RAR). In this promoter, RAR binds within the same responsive element (VDRE) as the vitamin D receptor, that also stimulates *bgp* expression, and as the receptors for c-Jun and c-Fos, that repress retinoic acid and vitamin D induced *bgp* expression. The fact that the VDRE mediates the regulation by these different receptors was designated as cross-coupling (Schüle *et al.*, 1990). In humans the information concerning the effects of retinoic acid over *mgp* expression are divergent since there are reports of a strong up-regulation of *mgp* in cultures of osteoblasts, articular cartilage chondrocytes, and fibroblasts treated with retinoic acid (Cancela and Price, 1992) and

on the other hand another work reports a down-regulation of *mgp* gene expression in different rat and human cell lines by interacting with the endogenous retinoid receptors: retinoic acid receptor (RAR) and retinoid X receptor (RXR) (Kierfel *et al.,* 1997). Co-transfection experiments in xenopus A6 cells made by Conceição (2002), using xenopus MGP promoter constructs in combination with expression vectors with mammalian RAR and other steroid hormone receptors failed to influence the expression of a Luc reporter gene. The expression levels of *bgp* have also been reported to be up-regulated by retinoic acid in human osteoblastic cells (Cancela and Price, 1992) and at the protein level (Evans *et al.,* 1988), in rat osteoblast like ROS cells treatment with 9-*cis* retinoic acid inhibits *bgp* expression. The modulatory effect of retinoic acid over vitamin D-induced *bgp* expression is exerted trough the formation of heterodimers between RXR and VDR (MacDonald *et al.,* 1963). The retinoic acid and retinoid X receptors have been cloned in zebrafish and are known to respond differently to different forms of retinoic acid (Jones *et al.,* 1995). The effects of retinoic acid have been studied in Japanese flounder, and shown that retinoic acid action is mediated through specific receptors localized in the nucleus of the target cells (Suzuki *et al.,* 2003) and have been shown to affect patched and collagen gene expression. In order to further elucidate the effects of retinoic acid on expression of *bgp* and *mgp* in fish we are going to take advantage of the osteblast like and chondroblast like cell lines recently developed (Pombinho *et al.,* 2004).

D11-Effects of vitamin A treatment on skeletal development

The oral administration of vitamin A resulted in a higher number of fish observed with skeletal deformations. These vitamin A treated fish presented some individuals with very severe skeletal deformations affecting the vertebral column and caudal fin complex. The fact that these structures were the most affected is probably due to the fact that by the time the treatment started these structures where not differentiating and so all the processes could be affected by retinoid signaling. Although in the head some skeletal structures were already developing, either with cartilaginous or bony nature, these were not affected so markedly by the treatment. Vitamin A supplementation in the diet have been reported to cause high levels of deformities in the Japanese flounder (Paralichthys olivaceus) vertebral column and caudal fin complex with an increasing number of deformities correlating with increasing dietary levels of

vitamin A palmitate administrated during metamorphosis (Dedi *et al.,* 1995; 1998; Takeuchi *et al.,* 1995). There are several reports of embryological deformities induced in fish after exposure of the eggs to high levels of vitamin A. Teratogenic effects of all-trans retinoic acid were observed in zebrafish early development causing oedema in the heart and malformations in the eyes, the brain, jaw, gill, fins and tail (Herrmann, 1995; Ellies *et al.,* 1997). The experimental induction of deformities by exposure of Japanese flounder to retinoic acid resulted in a shift of the growth direction of the pharyngeal cartilages posteriorly, and caused jaw deformities such as fusion of cartilage components in the mandibular and hyoid arches and absence of Meckel's cartilage (Suzuki *et al.,* 2000). Estevez & Kanazawa (1995) reported also the occurrence of skeletal deformities on turbot associated to hipervitaminosis A, although these high levels add a positive effect over pigmentation. Haga *et al.* (2002; 2004) also observed that a diet containing high levels of vitamin A caused hypermelanosis on the Japanese flounder. It seems probable that several of the deformities observed in the aquaculture industry may be linked to an embryonic vitamin A imbalance. The fact that incomplete formation of bony tissue in the craniofacial region is a characteristic trait of vitamin A teratogenicity in both fish and mammals (Ellies *et al.,* 1997; Suzuki *et al.,* 2000; Ørnsrud *et al.,* 2004) and the fact that the teratogenic effects observed are also related to the altered expression of genes such as *dlx* that causes malformation of craniofacial cartilages (Ellies *et al.,* 1997). Vitamin A controls a number of other genes involved in patterning of the skeleton such as sonic hedgehog (*shh*) required for growth and differentiation of cartilage precursor cells (Helms *et al.,* 1997) and found in the zone of polarizing activity of developing zebrafish fin buds (Akimenko and Ekker, 1995), Indian hedgehog (*Ihh*) which is involved in the regulation of proliferation and differentiation of chondrocytes and has a role in endochondral bone formation (St-Jaques *et al.,* 1999) and Hox genes that control the segmentation of pharyngeal arches and their regional identities (Kontges and Lumsden, 1996). Affecting the RAR signaling pathways that regulate both condrocyte and osteoblast activity are therefore responsible for the development of deformities. Haga *et al.* (2003) used specific vitamin A agonists that increased RAR expression and decreased the hedgehog receptor patched (*ptc*), being responsible for the development of jaw deformities in Japanese flounder.

D12-Effects of warfarin in fish vascular calcification

We have submitted fish to treatments with the vitamin K-antagonist sodium-warfarin that prevents the gamma-glutamyl carboxylation essential for calcium binding properties of Bgp and Mgp. Two different sets of experiments were undertaken in order to access the effects of warfarin on the calcium binding function and expression of Gla proteins. Warfarin was delivered either by immersion or by injection.

The analysis of the vascular system from zebrafish and toadfish submitted to warfarin treatment revealed that an abnormal accumulation of calcium was formed in the aortic bulbus and the ventral aorta. Abnormal calcification however was not observed in the cartilages or other skeletal elements. The absence of an effect of warfarin treatment on bone growth is in agreement with previous studies, which showed that warfarin only causes growth plate fusion in rats older than four months (Price *et al.*, 1982). The analysis of RNA purified from warfarin treated fish revealed no differences on expression of both *bgp* and *mgp*. No effects were observed for any of the concentrations or treatment duration. These results were not expected since it has been previously observed that in rats treated for four weeks with warfarin + vitamin k, the levels of *mgp* mRNA expression are significantly increased in the aorta when compared to vitamin K treated rats (Price *et al.*, 1998). It has also been observed that in cultured cells *mgp* expression is also increased as a result of treatment with warfarin (Marques *et al.*, unpublished). The reasons for the discrepancy between these results and our data remain to be investigated.

The presented data suggests that the mechanisms leading to vascular calcification in fish are under the control of Gla proteins, since treatment with sodium warfarin caused calcification of the aortic bulbus, probably due to loss of Mgp function by the fact that it is not carboxylated. Our results in what concerns vascular calcification come in agreement to what has previously been observed in the vascular system of rats treated with warfarin (Price *et al.*, 1998, 2000) where this drug caused calcification of the elastic lamellae in the media in major arteries and in aortic heart valves of treated rats. The warfarin-induced vascular calcification observed in our fish models is similar to that present in the Mgp–deficient mouse (Lou *et al.*, 1997) suggesting that warfarin induces arterial calcification in fish also by inhibiting γ-carboxylation of Mgp necessary for its calcium binding activity and thereby inactivating the putative calcification-inhibitory function of this protein. Spronk *et al.* (2001) showed that Mgp accumulates

strongly in the border regions of rat and human calcified arterial vessels, probably in an attempt to counteract calcium deposition. Besides affecting vascular calcification it has been shown that treatment of rats with warfarin results in excessive mineralization of bone and cartilage (Otawara and Price, 1986).

The previous studies with generation of MGP-deficient mice (Luo *et al.,* 1997) and warfarin-treated rats (Price *et al.,* 1998, 2000) provided strong evidence that, *in vivo*, Mgp functions as a calcification inhibitor. To support this comes the fact that calcification of arteries is very extensive in animals that either do not express MGP or have uncarboxylated Mgp. This argues strongly against the hypothesis that there is some other equivalently active inhibitor of calcification in vascular tissue and that Mgp has a mere backup function in preventing arterial calcification, seeming more likely that Mgp is central to the process by which the calcification of arteries is normally inhibited *in vivo* (Price *et al.,* 1998). An additive effect to the inactivation of Mgp was obtained by inactivating the genes for both Mgp and osteopontin (Speer *et al.,* 2002), revealing an increase of up to three times in vascular mineralization after 4 weeks, compared to Mgp $^{-/-}$ mice, and resulting in a more premature dead of the mice. These results suggest an alternative mechanism for controlling vascular calcification involving osteopontin (Speer *et al.,* 2002) although it does not seem to play a critical role since lack of osteopontin alone does not induce calcification in arteries.

It has been proposed that vascular calcification is a passive process that occurs if no regulatory action by inhibitors of mineralization is exerted (Schinke and Karsenty, 2000). Furthermore, the molecular mechanisms inducing extracellular matrix mineralization are the same regardless of whether they occur physiologically in bone, or pathologically in ectopic sites of calcification. In this manner it is necessary to elucidate why extracellular matrix mineralization occurs only in bone in order to better understand degenerative conditions such as osteoarthritis (Murshed *et al.,* 2005). Recent evidences showed that normal extracellular phosphate concentrations are required for bone mineralization and that lowering this concentration prevents mineralization. However due to the presence of pyrophosphate, an inhibitor of mineralization, extracellular matrix mineralization occurs only in bone because osteoblasts coexpress *Type I collagen* and *Tnap*, an enzyme that cleaves pyrophosphate. This strict coexpression in osteoblasts of these genes seems to be necessary and sufficient to induce bone mineralization (Murshed *et al.,* 2005). This work also shows that ectopic expression of *Tnap* in collagen expressing cells is sufficient to induce pathological

mineralization, suggesting that in diseases where TNAP is reduced ectopical calcifications may occur. *Tnap* is also coexpressed with collagen α1(X) collagen in hypertrophic chondrocytes of the growth plate cartilage (Takeda *et al.*, 2001) who do not calcify since hypertrophic chondrocytes also express Mgp that inhibits extracellular matrix mineralization (Luo *et al.*, 1997). This confirms the theory previously suggested that calcification of arteries involves ectopic expression of genes usually expressed by osteoblasts (Schinke *et al.*, 1998).

Taken together, the available data indicate that, given the overall high conservation of Gla protein function from fish to man, fish may represent valid model systems to study the role of these proteins in human diseases like Keutel syndrome, Mönckeberg disease and artherosclerosis.

Table D1- Summarized information on the development of skeletal structures of *Danio rerio* with times of cartilaginous appearance, mineralization and detection of *mgp* and *bgp* by *in situ* hybridization (▬) and immunolocalization(····). Age is expressed in days post fertilization (dpf).

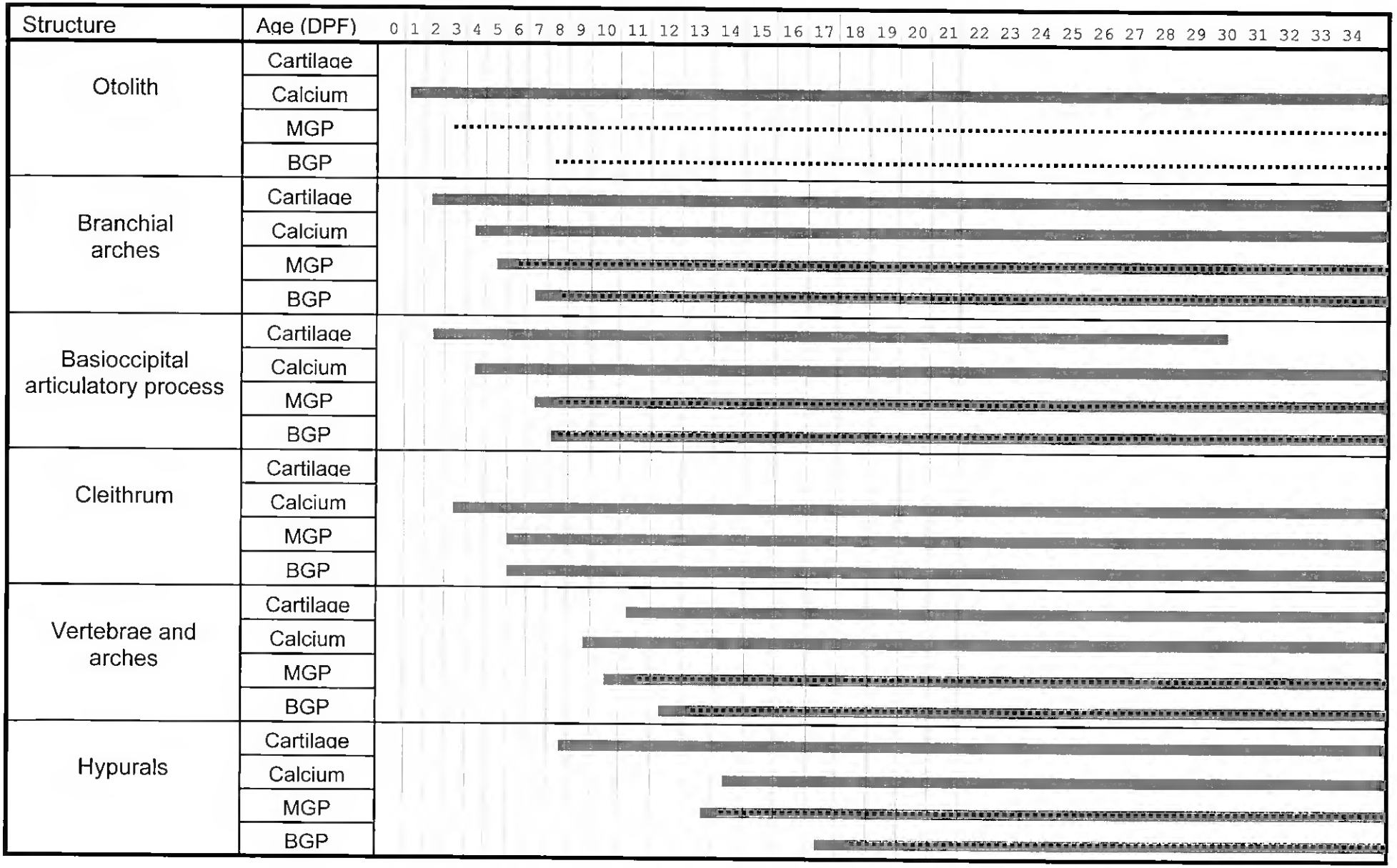

Table D2- Summarized information on the development of skeletal structures of *Solea senegalensis* with times of cartilaginous appearance, mineralization and detection of *mgp* and *bgp* by *in situ* hybridization (▬) and immunolocalization(····). Age is expressed in days post fertilization (dpf).

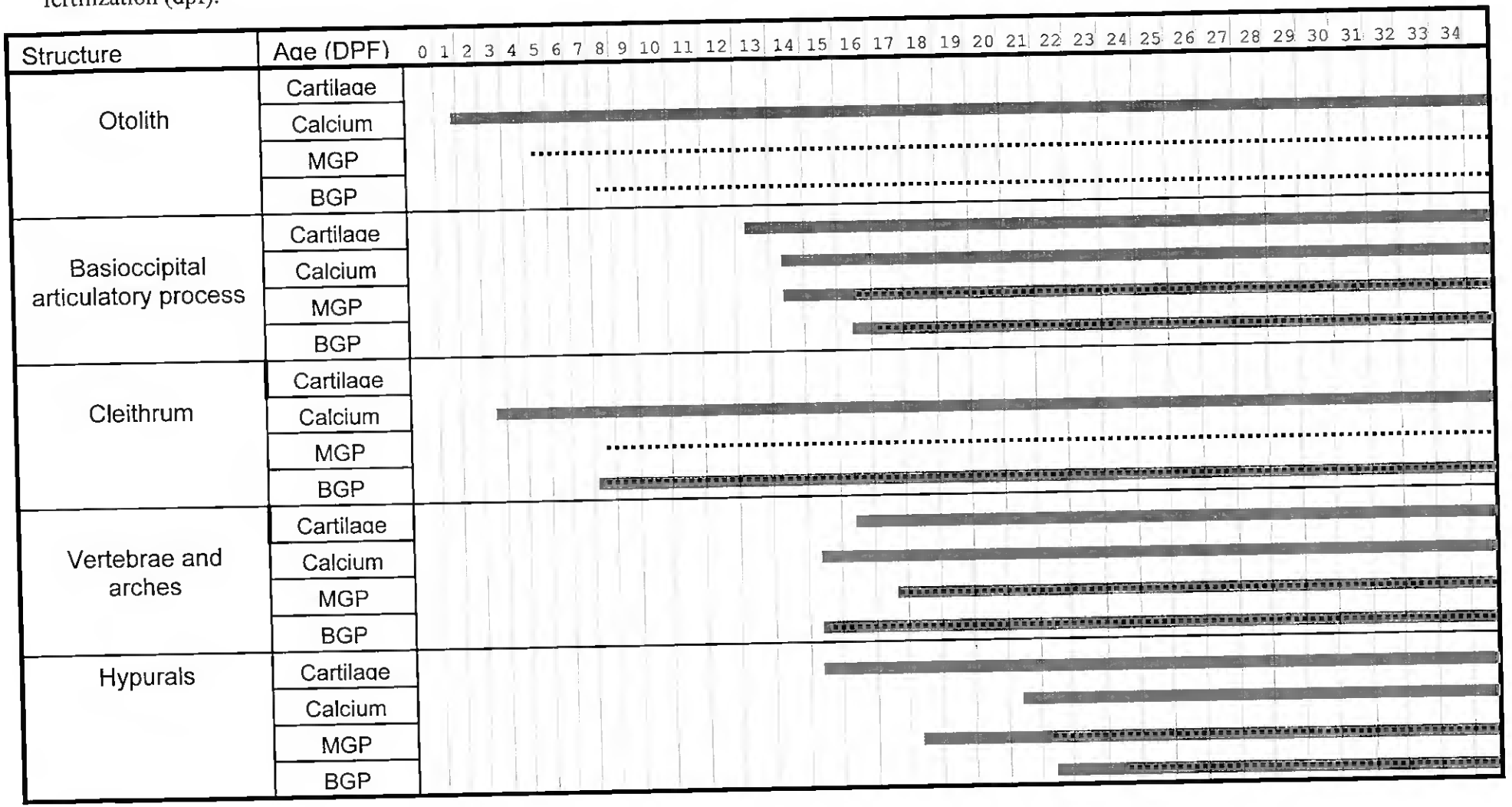

Final considerations and future perspectives

In order to better understand the events that occur during the skeletal development of teleost fishes and in particular the zebrafish and the Senegal sole, an improved skeletal staining method was developed in order to provide a more accurate method than conventional established methods to detect small changes in cartilaginous and calcified tissue formation, allowing the visualization of very small calcified structures during fish larval development.. This improved method was successfully used to study the development of skeletal structures in zebrafish and in Senegal sole larval and juvenile life stages. The formation of skeletal elements initiates in very early stages of differentiation, and newly hatched larvae already have present the otoliths, branchial arches, notochord and a calcified cleithrum. It was observed that zebrafish has a faster development than sole and most marine teleosts, acquiring calcified vertebral elements at 9 DPF and a fully formed and calcified skeleton in juvenile individuals with one month. In the Senegal sole the development of vertebral elements occurs later compared to zebrafish and in parallel with the process of metamorphosis and by the time the fish acquires a benthic life style all the vertebral elements and the fins are present although not completely formed yet. From the analysis of Senegal sole skeleton we have observed a high number of deformities affecting in particular the vertebral column and the caudal fin complex that can reflect problems not yet identified in the rearing conditions presently used for this species. The histological method of diagnostic we have optimized for small fish larvae should prove to be very useful to monitor the results of nutritional/rearing studies on the development of malformations in an effort to identify the causes.

We have cloned for the first time the full length cDNAs for *bgp* and *mgp* from zebrafish and Senegal sole, obtaining sequences with features highly conserved with other known Bgps and Mgps, suggesting that there is a conservation of function along the evolution of vertebrates.

I this study we made a comprehensive analysis of gene expression and protein accumulation for these two mineralization-related proteins during development of the skeleton of two fish species with different ecologies. The expression and accumulation patterns observed are in general agreement with the previously observed for mammalian species. Interestingly, Mgp accumulation patterns are contrasting with the observed for other marine fishes since we observed that in Senegal sole and zebrafish Mgp

accumulates either in bone or in calcified cartilage, in contrast with *A. regius* where Mgp accumulates in cartilage matrix and in chondrocytes.

To better understand the function of Gla proteins we undertook some experiments using warfarin to prevent gamma-carboxylation and to render MGP and BGP non functional. We were able to induce pathological vascular calcification in warfarin treated individuals from marine and freshwater fish, obtaining results similar to those observed in rat. Our data, together with all available information in mammals and fish provides further evidences that the role of Mgp in preventing vascular calcification is maintained from fish to mammals.

To further investigate the function of Bgp and Mgp in fish requires the use of reverse genetics techniques such as gene knockout or antisense technologies using, for example, morpholino oligos. We plan to continue this work by using those technologies and for some of them we have already obtained preliminary data.

Further investigation is also required in order to understand the effects of liposoluble vitamins over the expression of Bgp and Mgp in fish. The development of additional, homologous, in vitro cell systems should prove to be very useful to initiate these studies. A cell line derived from sole is already available and studies are being undertaken to develop cell lines derived from zebra fish bone.

BIBLIOGRAPHY

Bibliography

Akhoundi, C., Amiot, M., Auberger, P., Le Cam, A., Rossi, B. (1994). Insulin and interleukin-1 differentially regulate pp63, an acute phase phosphoprotein in hepatoma cell line. J. Biol. Chem 269: 15925-15930.

Akimenko, M.-A., Ekker, M., (1995). Anterior duplication of the *Sonic hedgehog* expression pattern in the pectoral fin buds of zebrafish treated with retinoic acid. Dev. Biol. 170, 243–247.

Andrade, J.P. (1990). A importância da Ria Formosa no ciclo biológico de *Solea senegalensis* Kaup 1858, *Solea vulgaris* Quensel 1806, *Solea lascaris* (Risso, 1810) e *Microchirus azevia* (Capello, 1868). Tese de doutoramento. Universidade do Algarve. 340p.

Arias, A.M., Drake, P.(1990). Estados juveniles de la ictiofauna en los canos de las salinas de la Bahia de Cadiz. Consejo Superior de Investigaciones Cientificas, Cadiz, Spain. 163p.

Asou, Y., Rittling, S.R., Yoshitake, H., Tsuji, K., Shinomiya, K., Nifuji, A., Denhardt, D.T., Noda, M. (2001). Osteopontin Facilitates Angiogenesis, Accumulation of Osteoclasts, and Resorption in Ectopic Bone. Endocrinology 142(3): 1325–1332.

Bajaj, S.P., Price,P.A., Russel, W.A. (1982). Decarboxylation of γ- Carboxyglutamic acid residues in human prothrombin. J. Biol. Chem 257: 3726-3731.

Barone, L.M., Owen, T.A., Tassinari, M.S., Bortell, R., Stein, G.S., and Lian, J.B. (1991). Developmental expression and hormonal regulation of the rat matrix gla protein (MGP) gene in chondrogenesis and osteogenesis. J. Cell. Biochem. 46: 351–365

Barut, B.A. and Zon, L.I. (2000). Realizing the potential of zebrafish as a model for human disease. Physiol. Genomics 2: 49–51.

Bedui, R. (2003). Elevage de *Solea senegalensis* (Kaup, 1958) en Tunisie. CIHEAM - Options Mediterraneennes.

Benjamin, M. (1989). The development of hyaline-cell cartilage in the haed of the black molly, Poecilia sphenops. Evidence for secondary cartilage on teleosts. J. Anat. 164: 145-154.

Benjamin, M. and Ralphs, J.R. (1991). Extracellular matrix of connective tissues in the heads of teleosts. J. Anat. 179: 137-148.

Benjamin, M., Ralphs, J.R. and Eberewariye, O.S. (1992). Cartilage and related tissues in the trunk and fins of teleosts. J. Anat. 181: 113-118.

Benzakour, O. and Kanthou, C. (2000). The anticoagulant factor, protein S, is produced by cultured human vascular smooth muscle cells and its expression is upregulated by thrombin. Blood 95: 2008-2014.

Berkner, K.L. (2000). The vitamin K-dependent carboxylase. J. Nutr. 130:1877-1880.

Berkner, K.L. and Pudota, B.N. (1998). Vitamin K-dependent carboxylation of the carboxylase. Proc. Natl. Acad. Sci. USA 95: 466–471.

Bertin, L. (1958). Tissus squeletiques. *in* Grassé, P.P. (1958). Taité de Zoologie-Anatomie, Systématique,Biologie. Tomo XIII, Fasciculo I. Masson et Cie editeurs, Paris. pp 532-550.

Blaxter, J.H.S. (1988). Pattern and variety in development. In: The physiology of developing fish. Vol XI – Part A, pp1-58. Hoar, W.S. and Randalls, B.J. editors.

Boglione, C., Marino, G., Bertolini, B., Rossi, A., Ferreri, F. and Cataudella, S. (1993). Larval and postlarval monitoring in seabass: morphological approach to evaluate finfish seed quality. Production, Environment and Quality. Bordeaux Aquaculture'92. European Aquaculture Society special publication 18:1-16.

Boguslawski, G., Hale, L.V., Yu, X-P, Miles, R.R., Onyia, J.E., Santerre, R.F, Chandrasekhar, S. (2000). Activation of Osteocalcin Transcription Involves Interaction of Protein Kinase A- and Protein Kinase C-dependent Pathways. J. Biol. Chem. 275(2): 999–1006.

Boivin, G., Morel, G., Lian, J.B., Anthione-Terrier, C., Dubois, P.M., Meunier, P.J. (1990). Localization of endogenous osteocalcin in neonatal rat bone and its absence in articular cartilage: effect of warfarin treatment. Pathol. Anat. 417:505–512.

Bond, C.E. (1979). Biology of fishes. Saunders College Publishing, USA. 514p.

Bortell, R., Owen, T.A., Bidwell, T.A., Gavazzo, P., Breen, E., van Wijnen, A.J., DeLuca, H.F., Stein, J.L., Lian, J.B., Stein, G.S. (1992).Vitamin D-responsive protein-DNA interactions at multiple promoter regulatory elements that contribute to the level of rat osteocalcin gene expression. Proc. Natl. Acad. Sci. 89: 6119-6123.

Bortell, R., Owen, T.A., Shalhoub, V., Heinrichs, A., Aronow, M.A., Egly, C.R., Lutz, Y., Stein, J.L., Lian, J.B., Stein, G.S. (1993).Constitutive transcription of the osteocalcin gene in osteosarcoma cells is reflected by altered protein-DNA interactions at promoter regulatory elements. Proc. Natl. Acad. Sci. 90: 2300–2304.

Bostrom, K., Watson, K.E., Horn, S., Wortham, C., Herman, I.M., Demer, L.L. (1993). Bone morphogenetic protein-2A expression in human atherosclerotic lesions. J Clin Invest 91: 1800–1809.

Bostrom, K., Tsao, D., Shen, S., Wang, Y., and Demer, L.L. (2001). Matrix Gla Protein Modulates Differentiation Induced by Bone Morphogenetic Protein-2 in C3H10T1/2 Cells. J. Biol. Chem. 276(17): 14044–14052.

Boskey, A.L., Gadaleta, S., Gundberg, C., Doty, S.B., Ducy, P., Karsenty, G. (1998). Fourier transform infrared microspectroscopic analysis of bones of osteocalcin-deficient mice provides insight into the function of osteocalcin. Bone 23: 187–196.

Braam, L.A.J.L.M., Dissel, P., Gijsbers, B.L.M.G., Spronk, H.M.H., Hamulya´k, K., Soute, B.A.M., Debie, W., Vermeer, C. (2000). Assay for human matrix gla protein in serum potential applications in the cardiovascular field. Arterioscler. Thromb. Vasc. Biol. 20: 1257-1261.

Bristol, J.A., Ratcliffe, J.V., Roth, D.A., Jacobs, M.A., Furie, B.C., Furie, B. (1996). Biosynthesis of prothrombin: intracellular localization of the vitamin K- dependent carboxylase and the sites of gamma-carboxylation. Blood 88: 2585-2593.

Broess, M., Riva, A., Gerstenfeld, L. C. (1995). J. Cell. Physiol. 57: 440–451.

Bronckers, A.L.J.J., Gay, S., Dimuzio, M.T., Butler, W.T. (1985).Immunolocalization of gamma-carboxyglutamic acid-containing proteins in developing molar tooth germs of the rat. Collagen Rel. Res. 5: 17–22.

Bronckers A.L.J.J., Farach-Carson, M.C., van Waveren, E., Butler, W.T. (1994). Immunolocalization of osteopontin, osteocalcin and dentin sialoprotein during dental root formation and early cementogenesis in the rat. J. Bone Miner. Res. 9: 833–841.

Bronckers A.L.J.J., Price, P.A., Schrijvers, A., Bervoets, T.J.M., Karsenty, G. (1998). Studies of osteocalcin function in dentin formation in rodent teeth. Eur. J. Oral. Sci. 106: 795–807.

Burstone, M.S. (1959). Histochemical demonstration of acid phosphatase activity in osteoclasts. J. Histochem. Cytochem. 7: 39-41.

Cairns, J.R., Price, P.A. (1994). Direct demonstration that the vitamin K-dependent bone Gla protein is incompletely γ-carboxylated in humans. J. Bone Miner. Res. 9: 1989-1997.

Cancela, M.L., Hsieh, C-L, Francke, U., Price, P.A. (1990). Molecular structure, chromosome assignment, and promoter organization of the Human matrix Gla protein gene. J. Biol. Chem. 256(25): 15040-15048.

Cancela, M.L. and Price, P.A. (1992). Retinoic acid induces matrix Gla protein gene expression in human cells. Endocrinology 130:102-108.

Cancela, M.L., Williamson, M.K., Price, P.A. (1993). Retinoic acid increases matrix Gla protein in rat plasma. Nutrition Res. 13: 87-91.

Cancela M.L., Williamson M.K., Price, P.A. (1995). Amino acid sequence of bone Gla protein from the African clawed frog *Xenopus laevis* and the fish *Sparus aurata*. Int. J. Pept. Protein. Res. 46: 419-423.

Cancela, M.L., Ohresser, M.C.P., Reia, J.P., Viegas, C.S.B., Williamson, M.K., Price, P.A. (2001). Matrix Gla Protein in *Xenopus laevis*: molecular cloning, tissue distribution and evolutionary considerations. J. Bone Min. Res. 16:1611-1622.

Canfield, A.E., Dohertya, M.J., Kellyb, V., Newmana, B., Farringtona, C., Grantb, M.E., Boot-Handford, R., P. (2000). Matrix Gla protein is differentially expressed during the deposition of a calcified matrix by vascular pericytes. FEBS Letters 487: 267-271.

Canfield, A.E., Farrington, C., Dziobon, M.D., Boot-Handford, R.P., Heagerty, A.M., Kumar, S.N., Roberts, I.S. (2002). The involvement of matrix glycoproteins in vascular calcification and fibrosis: an immunohistochemical study. J. Pathol. 196: 228–234.

Carr, S., Hauschka, P., Bieman, K. (1981). Gas chromatographic mass spectrometic sequence determination of osteocalcin, a γ-carboxyglutamic acid-containing protein from chicken bone. J. Bio: Chem. 256: 9944-9950.

Caraballo, P.J., Heit, J.A., Atkinson, E.J., Silverstein, M.D., O'Fallon, W.M., Castro, M.R., Melton, L.J. (1999). Long-term use of oral anticoagulants and the risk of fracture. Arch. Intern. Med. 159: 1750–1756.

Celeste, A.J., Rosen V., Buecker, J.L., Kriz, R., Wang, E.A., Wozney, J.M. (1986). Isolation of the human gene for bone gla protein utilizing mouse and rat cDNA clones. The EMBO journal 5 (8): 1885-1890.

Choi, J-Y., Pratap, J., Javed, A., Zaidi, S. K., Xing, L., Balint, E., Dalamangas, S., Boyce, B., van Wijnen, A.J., Lian, J.B., Stein, J.L., Jones, S.N., Stein, G.S. (2001). Subnuclear targeting of Runx/Cbfa/AML factors is essential for tissue-specific differentiation during embryonic development. Proc. Natl. Acad. Sci. 98 (15): 8650–8655.

Ciruna, B., Weidinger, G., Knaut, H., Thisse, B., Thisse, C., Raz, E., Schier, A.F. (2002). Production of maternal-zygotic mutant zebrafish by germ-line replacement. Proc. Natl. Acad. Sci. 99 (23): 14919–14924.

Colombo, G., Fanti, P., Yao, C., Malluche, H. (1993). Isolation and complete amino acid sequence of osteocalcin from canine bone. J. Bone. Min. Res. 8: 733-743.

Conceição, N. (2002). Regulation of matrix Gla protein gene expressio: comparative studies on fish and amphibians. Tese PhD. Universidade do Algarve. Portugal.

Conceição, N., Henriques, N.M., Ohresser, M.C.P., Hublitz. P., Schule, R., Cancela, M.L. (2002). Molecular cloning of the matrix Gla protein gene from *Xenopus laevis*: functional analysis of the promoter identifies a calcium sensitive region required for basal activity. Eur. J. Biochem. 269: 1947–1956.

Conceição, N., Silva, A.C., Fidalgo, J., Belo, J.A., Cancela, M.L. (2005). Identification of alternative promoter usage for the matrix Gla protein gene. Evidence for differential expression during early development in *Xenopus laevis*. FEBS J. 272: 1501–1510.

Couly, G.F., Coltey, P.M., Le Douarin, N.M. (1993). The triple origin of the skull in higher vertebrates: a study in quail-chick chimeras. Development 117: 409–429.

Cubbage, C.C. and Mabee, P.M. (1996). Development of the cranium and paired fins in the zebrafish *Danio rerio* (Ostariophysi, Cyprinidae). J. Morphol. 229: 121-160.

Daoulas. C.H., Economou, N.A., Bantavas, I. (1991). Osteological abnormalities in laboratory reared sea-bass (*Dicentrachus labrax*) fingerlings. Aquaculture 97: 169-180.

Dingerkus, G. and Uhler, L.D. (1977). Enzyme clearing of Alcian blue stained whole small vertebrates for demonstration of cartilage. Stain Technology 52 (4): 229-232.

Dam, H. (1935). The antihaemorrhagic vitamin in the chick. Biochem. J. 29: 1273–1285

De Boer van der Berg, M.A.G., van Haarlem, L.J.M., Vermeer, C. (1986). Vitamin K-dependent carboxylase in human vessel wall. Thromb. Res. S6:134.

Dedi, J., Takeuchi, T., Seikai, T., Watanabe, T. (1995). Hypervitaminosis and safe levels of vitamin A for larval flounder (Paralicthys olivaceus) fed Artemia nauplii. Aquaculture 133: 135– 146.

Dedi, J., Takeuchi, T., Hosoya, K., Watanabe, T., Seikai, T. (1998). Effect of vitamin A levels in Artemia nauplii on the caudal skeleton formation of Japanese flounder Paralicthys olivaceus. Fish. Sci. 64: 344–345.

De Fouw, N.J., Haverkate, F., Bertina, R.M. (1986) The cofactor role of protein S in the acceleration of whole blood clot lyses by activated protein C *in vitro*. Blood 67: 1189-1192.

Denhardt, D.T. and Guo, X. (1993). Osteopontin: A protein with diverse functions. FASEB J. 7: 1475–1482.

Derynck, R. (1999). Skeletal development in the zebrafish. Nature genetics 23: 379.

Desbois, C., Hogue, D.A., Karsenty, G., (1994). The mouse osteocalcin gene cluster contains three genes with two separate spatial and temporal patterns of expression. J. Biol. Chem. 269: 1183-1190.

Desbois, C., Seldin, M.F., Karsenty, G. (1994b). Localization of the osteocalcin gene cluster on mouse chromosome 3. Mamm. Genome 5: 321-322.

DiScipio, R.G., Hermodson, M.A., Yates, S.G.(1977). A comparison of human prothrombin, factor IX (christmas factor), factor X (stuart factor), and protein S. Biochemistry 16: 698-706.

Dinis, M.T. (1986). Quatre Solcidae de l'Estuaire du Tage. Reproduction et Croissance. Essai d'Elevage de *Solea senegalensis* Kaup 1858. These d'Etat es-Sciences Naturelles, Universite de Bretagne Occidentale, France.

Dinis, M.T. (1992). Aspects of the potential of *Solea senegalensis*, Kaup for aquaculture: larval rearing and weaning to an artificial diet. Aquacult. Fish Manag. 23: 515–520.

Dinis, M.T., Reis, J. (1995). Culture of *Solea* spp. Workshop on Diversification in Aquaculture Cyprus June. Cahiers Options Mediterranees 16, pp. 1–7.

Dinis, M. T., Ribeiro, L., Soares, F., Sarasquete, C. (1999). A review on the cultivation potential of *Solea senegalensis* in Spain and Portugal. Aquaculture 176: 27–38.

Dinis, M. T., Ribeiro, L., Conceição, L.E.C., Aragão, C. (2003). Larvae digestion and new weaning experiments in *Solea senegalensis.* CIHEAM - Options Mediterraneennes.

Dhore, C.R., Cleutjens, J.P., Lutgens, E., Cleutjens, K.B., Geusens, P.P., Kitslaar, P.J., Tordoir, J.H., Spronk, H.M., Vermeer, C., Daemen, M.J. (2001). Differential expression of bone matrix regulatory proteins in human atherosclerotic plaques. Arterioscler. Thromb. Vasc. Biol. 21: 1998–2003.

Doherty, T.M., Asotra, K., Fitzpatrick, L.A.; Qiao, J.-H., Wilkin, D.J., Detrano, R.C., Dunstan, C.R. Shah, P.K., Rajavashisth, T.B. (2003). Calcification in atherosclerosis: Bone biology and chronic inflammation at the arterial crossroads. Proc. Natl. Acad. Sci. USA 100 (20): 11201–11206.

Dohi, Y., Tabata, S., Yamaguchi, M., Ohgushi, H., Yonemasu, K. (2004). Characterization of the cDNA encoding bullfrog, *Rana catesbeiana*, osteocalcin and two forms of the protein isolated from bone. Biochimie 86: 471–480.

Dowd, P., Hershline, R., Ham, S.W., Naganathan, S. (1995).Vitamin K and energy transduction: a base strenght amplification mechanism. Science 269: 1684-1691.

Dowd, T.L., Rosen, J.F., Li, L., Gundberg, C.M. (2003). The three-dimensional structure of bovine calcium ion-bound osteocalcin using 1H NMR spectroscopy. Biochemistry 42: 7769–7779.

Driever, W., Solnica-Krezel, L., Schier, A. F., Neuhauss, S. C. F., Malicki, J., Stemple, D. L., Stainier, D. Y. R., Zwartkruis, F., Abdelilah, S., Rangini, Z., Belak, J., and Boggs, C. (1996). A genetic screen for mutations affecting embryogenesis in zebrafish. Development 123: 37–46.

Du, S. J., Frenkel, V., Kindschi, G., Zohar, Y. (2001). Visualizing normal and defective bone development in zebrafish embryos using the fluorescent chromophore Calcein. Dev. Biol. 238: 239-246.

Ducy, P. and Karsenty, G. (1995). Two distinct osteoblast-specific cis-acting elements control expression of a mouse osteocalcin gene. Mol. Cellular Biol. 15(4): 1858-1869.

Ducy, P., Desbois, C., Boyce, B., Pinero, G., Story, B., Dunstan, C., Smith, E., Bonadio, J., Goldstein, S., Gundberg, C., Bradley, A., Karsenty, G. (1996). Increased bone formation in osteocalcin-deficient mice. Nature 382: 448 –452.

Ducy, P., R. Zhang, V. Geoffroy, A. Ridall, and G. Karsenty (1997). Osf2/Cbfa1: A transcriptional activator of osteoblast differentiation. Cell 89: 747–754.

Ducy, P. and Karsenty, G. (1998). Genetic control of cell differentiation in the skeleton. Curr. Op. Cell Biol. 10: 614–619.

Ducy, P., Starbuck, M., Priemel, M., Shen, J., Pinero, G., Geoffroy, V., Amling, M., Karsenty, G. (1999). A Cbfa1-dependent genetic pathway controls bone formation beyond embryonic development. Genes Dev. 13: 1025–10236.

Ducy, P., and Karsenty, G. (2000). The family of bone morphogenetic proteins. Kidney Int. 57: 2207–2214.

Dvorak, M.M., Siddiqua, A., Ward, D.T., Carter, D.H., Dallas, S.L., Nemeth, E.F., Riccardi, D. (2004). Physiological changes in extracellular calcium concentration directly control osteoblast function in the absence of calciotropic hormones. Proc. Natl. Acad. Sci. USA 101 (14): 5140–5145.

Eghbali-Fatourechi, G., Khosla, S., Sanyal, A., Boyle, W.J., Lacey, D.L., Riggs, B.L. (2003). Role of RANK ligand in mediating increased bone resorption in early postmenopausal women. J. Clin. Invest. 111:1221–1230.

Ekanayake, S., Hall, B.K. (1988). Ultrastructure of the osteogenesis of acellular vertebral bone in the Japanese medaka, *Oryzias latipes* (Teleostei, Cyprinidontidae). Am. J. Anat. 182: 241–249.

Elefteriou, F., Ahn, J.D., Takeda, S., Starbuck, M., Yang, X., Liu, X., Kondo, H., Richards, W.G., Bannon, T.W., Noda, M., Clement, K., Vaisse, C., Karsenty, G. (2005). Leptin regulation of bone resorption by the sympathetic nervous system and CART. Nature 434: 514-520.

Ellies, D.L., Langille, R.M., Martin, C.C., Akimenko, M.A., Ekker, M. (1997). Specific craniofacial cartilage dysmorphogenesis coincides with a loss of dlx gene expression in retinoic acid-treated zebrafish embryos. Mechanisms of Development 61: 23–36.

Engelke, J.A., Hale, J. E., Suttie, J.W., P.A. Price (1991). Vitamin K-dependent carboxylase: utilization of decarboxylated bone Gla protein and matrix Gla protein as substrates. Biochim. Biophys. Acta 1078: 31-34.

Engelse, M.A., Neele, J.M., Bronckers, A.L.J.J., Pannekoek, H., de Vries, C.J.M. (2001). Vascular calcification: Expression patterns of the osteoblast-specific gene core binding factor α-1 and the protective factor matrix gla protein in human atherogenesis. Cardiovasc. Res. 52: 281–289.

Estevez, A. & Kanazawa, A. (1995). Effect of (n-3) PUFA and vitamin A Artemia enrichment on pigmentation success of turbot, *Scopthalmus maximus* (L.). Aquaculture Nutrition 1: 159–168.

Evans, D.B., Bunning, R.A.D., Russell, R.G.G. (1988). Studies on the interaction between retinoic acid and 1,25-(OH)gDa on human bone-derived osteoblast-like cells. In: Norman, A.W., Schaefer, K., Grigoleit, H.G., von Herrath, D. (eds.) Vitamin D: Molecular and Clinical Endocrinology. de Gruyter, Berlin and New York, pp 606- 607

Faustino, M. and Power, D.M. (1997). Development of osteological structures in the sea bream: vertebral column and fin complex. J. Fish Biol. 52: 11-22.

Fernández-Díaz, C., Yúfera, M., Cañavate, J.P., Moyano, F.J., Alarcón, F.J., Díaz, M. (2001) Growth and physiological changes during metamorphosis of Senegal sole reared in the laboratory. J. Fish Biol. 58: 1086–1097.

Fisher, S., Jagadeeswaran, P., Halpern, M.E. (2003). Radiographic analysis of zebrafish skeletal defects. Dev. Biol. 264: 64–76

Fleet, J.C., Hock, J.M. (1994). Identification of osteocalcin mRNA in nonosteoid tissue of rats and humans by reverse transcription-polymerase chain reaction. J. Bone Min. Res. 9: 1565–1573.

Francillon, H. and Meunier, F.J. (1985). Conservation et présentation des préparations coloreés au bleu alcian et a l'alizarine. Cybium 9(2): 121-126.

Fraser, J.D. and Price, P.A. (1988). Lung, heart, and kidney express high levels of mRNA for the vitamin K-dependent matrix Gla protein. J. Biol. Chem. 23: 11033-11036.

Frazão, C., Simes, D.C., Coelho, R., Alves, D., Williamson, M.K., Price, P.A., Cancela, M.L., Carrondo, M.A. (2005). Structural evidence of a fourth gla residue in fish osteocalcin: biological implications. Biochemistry 44(4): 1234-1242.

Frendo, J-L., Xiao, G., Franceschi, R.T., Karsenty, G., Ducy, P. (1998). Functional hierarchy between two OSE2 elements in the control of Osteocalcin gene expression *in vivo*. J. Biol. Chem. 273: 30509–30516.

Furie, B. and Furie, B.C. (1988). The molecular basis of blood coagulation. Cell 53: 505–518.

Garnero, P., Grimaux, M., Seguin, P., Delmas, P.D. (1994). Characterization of immunoreative forms of human osteocalcin generated *in vivo* and *in vitro*.. J Bone Miner Res 9: 255–264.

Gartner, L.P. and Hiatt, J.L. (1999). Tratado de histologia em cores 1st ed. Ed. Guanabara Koogan, Rio de Janeiro, Brazil. 426pp.

Gavaia, P.J., Sarasquete, C., Cancela, M.L. (2000). Detection of mineralized structures in early stages of development of marine *Teleostei* using a modified alcian blue-alizarin red double staining technique for bone and cartilage. Biotech. Histochem. 75(2): 79-84.

Gavaia, P.J., Dinis, M.T., Cancela, M.L. (2002). Osteological development and abnormalities of the vertebral column and caudal skeleton in larval and juvenile stages of hatchery-reared Senegal sole (*Solea senegalensis*). Aquaculture 211: 305–323.

Gavaia, P., Dominguez, S., Cancela, L. Sarasquete, C. (2003). Observacion del esqueleto de larvas de lenguado senegalés, *Solea senegalensis*, cultivadas y salvajes. IX Congreso Nacional de Acuicultura, May 3002, Cadiz, Spain.

Gavaia, P.J., Simes, D.C., Ortiz Delgado, J.B., Viegas, C.S.B., Pinto, J. P., Kelsh, R.N., Sarasquete, C., Cancela, M.L. (2005). Molecular cloning of osteocalcin and Matrix Gla Protein from zebrafish (*Danio rerio*) and Senegal sole (*Solea senegalensis*): Comparative gene and protein expression analysis from larval development through adulthood. Submited to Mechanisms of development - Gene expression patterns.

Gerstenfeld, L.C., Chipman, S.D., Glowacki, J., Lian, J.B. (1987). Expression of differentiated function by mineralizing cultures of chicken osteoblasts. Dev. Biol. 122: 49–60.

Gopalakrishnan, R., Ouyang, H., Somerman, M.J., Mccauley, L.K., Franceschi R.T. (2001). Matrix γ-Carboxyglutamic Acid Protein Is a Key Regulator of PTH-Mediated Inhibition of Mineralization in MC3T3-E1 Osteoblast-Like Cells. Endocrinology 142(10): 4379–4388.

Grandel, H. and Schulte-Merker, S. (1998). The development of the paired fins in the Zebrafish (*Danio rerio*). Mechanisms of Development 79: 99–120.

Groot, C.G., Danes, J.K., Blok, J., Hoogendijk, A., Hauschka, P.V. (1986). Light and electron microscopic demonstration of osteocalcin antigenicity in embryonic and adult rat bone. Bone 7: 379–385.

Guo, B., Aslam, F., van Wijnen, A. J., Roberts, S. G. E., Frenkel, B., Green, M.R., Deluca, H., Lian, J.B., Stein, G.S., Stein, J.L. (1997). YY1 regulates vitamin D receptor/retinoid X receptor mediated transactivation of the vitamin D responsive osteocalcin gene. Proc. Natl. Acad. Sci. 94: 121–126.

Gundberg, C.M. and Nishimoto, S.K. (1999). Vitamin K-deppendent proteins of bone and cartilage. *in* Dynamics of bone and cartilage metabolism. M.J. Seibel, S.P. Robins, J.P.Bilezikian editors. Academic press, San Diego USA. 672 p.

Hackeng, T.M., Rosing, J., Spronk, H.M.H., Vermeer C. (2001). Total chemical synthesis of human matrix Gla protein. Protein Science 10: 864–870.

Haffter, P., Granato, M., Brand, M., Mullins, M. C., Hammerschmidt, M., Kane, D. A., Odenthal, J., van Eeden, F. J. M., Jiang, Y.-J., Heisenberg, C.-P., Kelsh, R. N., Furutani-Seiki, M., Vogelsang, E., Beuchle, D., Schach, U., Fabian, C., and Nusslein-Volhard, C. (1996). The identification of genes with unique and essential functions in the development of the zebrafish *Danio rerio*. Development 123: 1–36.

Haga, Y., Suzuki, T., Takeuchi, T. (2002). Retinoids as potent teratogens in larval development of Japanese flounder, *Paralichthys olivaceus*. Fish. Sci. 68 (Supp. 1): 789–792.

Haga, Y., Suzuki, T., Kagechikac, H., Takeuchi, T. (2003). A retinoic acid receptor-selective agonist causes jaw deformity in the Japanese flounder, Paralichthys olivaceus. Aquaculture 221: 381–392.

Haga, Y., Takeuchi, T., Murayama, Y., Ohta, K., Fukunaga, T. (2004). Vitamin D3 compounds induce hypermelanosis on the blind side and vertebral deformity in juvenile Japanese flounder *Paralichthys olivaceus*. Fish. Sci. 70: 59–67.

Hale, J.E., Fraser, J.D., Price, P.A. (1988). The identification of matrix Gla protein in cartilage. J. Biol. Chem. 263: 5820–5824.

Hale, J.E., Williamson, M.K., Price, P.A. (1991). Carboxy-terminal proteolytic processing of matrix Gla-protein. J. Biol. Chem. 266: 21145–21149.

Hall, B.K. and Miyake, T. (1992). The membranous skeleton: the role of cell condensations in vertebrate skeletogenesis. Anat. Embryol. 186: 107–124.

Hanken, J. and Wassersug, R. (1981). A new double stain technique reveals the nature of the hard tissues. The Visible Skeleton 16 (4):22-44.

Hao, H., Hirota, S., Tsukamoto, Y., Imakita, M., Ishibashi-Ueda, H., Yutani, C. (1995). Alterations of bone matrix protein mRNA expression in rat aorta *in vitro*. Arterioscler. Thromb. Vasc. Biol. 15: 1474-1480.

Hardingham, T., Tew, S., Murdoch, A. (2002). Tissue engineering: chondrocytes and cartilage. Arthritis Res. 4 (suppl 3): S63-S68.

Hashimoto, F., Kobayashi, Y., Kobayashi, E.T., Sakai, E., Kobayashi, K., Shibata, M., Kato, Y., Sakai,H. (2001). Expression and localization of MGP in rat tooth cementum. Arch. Oral Biol. 46: 585–592.

Hauschka, P.V., Reid, M.L. (1978). Timed appearance of a calcium-binding protein containing gamma-carboxyglutamic acid in developing chick bone. Dev. Biol. 65: 426–434.

Hauschka, P.V., Carr, S.A., Bieman, K. (1982). Primary structure of monkey osteocalcin. Biochem. 21: 638-342.

Hauschka, P., Lian, J., Cole, D., Gundberg, C. (1989). Osteocalcin and matrix Gla protein: Vitamin K-dependent proteins in bone. Physiol. Rev. 69: 990–1047.

Helfrich, M. H. (2003). Osteoclast Diseases. Microsc. Res. Tech. 61: 514–532.

Helms, J.A., Kim, C.H., Hu, D., Minkoff, R., Thaller, C., Eichele, G., (1997). *Sonic hedgehog* participates in craniofacial morphogenesis and is down-regulated by teratogenic doses of retinoic acid. Dev. Biol. 187: 25–35.

Herrmann, K. (1995). Teratogenic effect of retinoic acid and related substances on the early development of the zebrafish (*Brachydanio rerio*) as assessed by a novel scoring system. Toxicol. in Vitro 9: 267–283.

Hickman Jr., C.P., Roberts, L.S., Larson, A (1993). Integrated principles of zoology. Ninth edition. Wm. C. Brown publishers. Dubuque, Iowa USA. 984p.

Hoang, Q.Q., Sicheri, F., Howard, A.J., Yang., D.S. (2003). Bone recognition mechanism of porcine osteocalcin from crystal structure. Nature. 425: 977–980.

Hoshi, K., Komori, T., Ozawa, H. (1999). Morphological Characterization of Skeletal Cells in Cbfa1-deficient Mice. Bone 25 (6): 639–651.

Hosoya, K., Kawamura, K. (1998). Skeletal formation and abnormalities in the caudal complex of the Japanese flounder, *Paralichthys olivaceus* (Temminck and Schlegel). Bull. Natl. Res. Inst. Fish. Sci. 12: 97-110.

Howe, A. M. and Webster, W. S. (2000). Warfarin exposure and calcification of the arterial system in the rat. Int. J. Exp. Path. 81: 51-56.

Hughes, D.R., Bassett, J.R., Moffat, L.A. (1994). Histological identification of osteocytes in the allegedly acellular bone of the sea breams *Acanthopagrus australis, Pagrus auratus* and *Rhabdosargus sarba* (Sparidae, Perciformes, Teleostei). Anat. Embryol. 190: 163–179.

Hunter, G.K. Hauschka, P.V., Poole, A.R., Rosenberg, L.C., Goldberg, H.A. (1996). Nucleation and inhibition of hydroxyapatite formation by mineralized tissue proteins. Biochem. J. 317: 59-64.

Huq, N., Teh, L., Christie, D., Chapman, G. (1984). The amino acid sequence of goat, pig and wallaby osteocalcins. Biochem. Int. 8: 521-527.

Huq, N., Tseng, L., Chapman, G. (1987). The amino acid sequence of emu osteocalcin: gas-phase sequencing of gla-containing proteins. Biochem. Int. 15: 271-277.

Huysseune, A., Van der heyden, C., Sire J.Y. (1998). Early development of the zebrafish (*Danio rerio*) pharyngeal dentition (Teleostei, Cyprinidae). Anat. Embryol. 198: 289–305.

Ikeda, T., Yamaguchi, A., Icho, T., Tsuchida, N., Yoshiki, S. (1991). cDNA and deduced amino acid sequence of mouse matrix gla protein: One of five glutamic acid residues potentially modified to gla is not conserved in the mouse sequence. J. Bone. Miner. Res. 6: 1013–1017.

Ikeda, T., Nomura, S., Yamaguchi, A., Suda, T., Yoshiki, S. (1992). *In situ* hybridization of bone matrix proteins in undecalcified adult rat bone sections. J. Histochem. Cytochem. 40 (8): 1079-1088.

Inouye, M. (1976). Differential staining of cartilage and bone in fetal mouse skeleton by alcian blue and alizarin red S. Congenital anomalies 16: 171-173

Jaillon, O., Aury, J. M., Brunet, F., Petit, J. L., Stange-Thomann, N., Mauceli, E., Bouneau, L., Fischer, C., Ozouf-Costaz, C., Bernot, A., Nicaud, S., Jaffe,

D., Fisher, S., Lutfalla, G., Dossat, C., Segurens, B., Dasilva, C., Salanoubat, M., Levy, M., Boudet, N., Castellano, S., Anthouard, V., Jubin, C., Castelli, V., Katinka, M., Vacherie, B., Biémont, C., Skalli, Z., Cattolico, L., Poulain, J., de Berardinis, V., Cruaud, C., Duprat, S., Brottier, P., Coutanceau, J.-P., Gouzy, J., Parra, G., Lardier, G., Chapple, C., Mckernan, K.J., Mcewan, P., Bosak, S., Kellis, M., Volff, J.-N., Guigó, R., Zody, M.C., Mesirov, J., Lindblad-Toh, K., Birren, B., Nusbaum, C., Kahn, D., Robinson-Rechavi, M., Laudet, V., Schachter, V., Quétier, F., Saurin, W., Scarpelli, C., Wincker, P., Lander, E.S., Weissenbach J., Crollius, H.R. (2004). Genome duplication in the teleost fish Tetraodon nigroviridis reveals the early vertebrate proto-karyotype. Nature 43: 946-57.

Jie, K.S., Bots, M.L., Vermeer, C., Witteman, J.C., Grobbee, D.E. (1995). Vitamin K intake and osteocalcin levels in women with and without aortic atherosclerosis: A populationbased study. Atherosclerosis 116: 117–123.

Johnson, T.L., Sakaguchi, A.Y., Lalley, P.A., Leach, R.J. (1991). Chromosomal assignment in mouse of matrix GLA protein and bone GLA protein genes. Genomics 11: 770-772.

Jono, S., Ikari, Y., Vermeer, C., Dissel, P., Hasegawa, K., Shioi, A., Taniwaki, H., Kizu, A., Nishizawa, Y., Saito, S. (2004). Matrix Gla protein is associated with coronary artery calcification as assessed by electron-beam computed tomography. Thromb. Haemost. 91: 790–794.

Jorgensen, M. J., Cantor, A. B., Furie, B. C., Brown, C. L., Shoemaker, C. B. & Furie, B. (1987). Recognition site directing vitamin K-deppendent gamma-carboxilation residues on the propeptide of factor IX. Cell 48: 185–191.

Junqueira L.C., Carneiro, J., Kelley, R.O. (1995). Basic histology, 8th edition. Appleton & Lange. USA. 488p.

Karsenty, G. (1998). Genetics of skeletogenesis. Dev. Gen. 22: 301–313.

Karsenty, G. (1999). The genetic transformation of bone biology. Genes Dev. 13: 3037–3051.

Karsenty, G., (2000). Role of Cbfa1 in osteoblast differentiation and function. Semin. Cell Dev. Biol. 11: 343-346.

Kiefer, M.C., Bauer, D.M., Young, D., Hermsen, K.M., Masiarz, F.R, Barr, P.J. (1988). The cDNA and derived amino acid sequences for human and bovine matrix Gla protein. Nucleic Acids Res. 16: 5213–5213.

Kiernan, J.A. (1990). Histological & histochemical methods: Theory and practice. 2nd Edition. Pergamon press. Oxford. 433p.

Kim, I.S., Otto, F., Zabel, B., Mundlos, S. (1999). Regulation of chondrocyte differentiation by Cbfa1. Mech. Dev. 80: 159-170.

Kimmel, C.A. and Trammell, C. (1981). A rapid procedure for routine double staining of cartilage and bone in fetal and adult animals. Stain Technol. 56(5): 271-273

Kimmel, C.B., Ballard, W.W., Kimmel, S.R., Ullmann, B. and Schilling, T.F. (1995). Stages of embryonic development of the zebrafish. Dev. Dyn. 203: 253-310.

Kimmel, C.B., Miller, C.T., Kruze, G., Ullmann, B., BreMiller, R.A., Larison, K.D., Snyder, H.C. (1998). The shaping of pharyngeal cartilages during early development of the zebrafish. Dev. Biol. 203: 245–263.

Klymkowsky, M.W. and Hanken, J. (1991). Whole mount staining of *Xenopus* and other vertebrates. Methods in cell biology 36: 419-441.

Kirfel, J., Kelter, M., Cancela, M.L., Price, P.A., Schule, R. (1997). Identification of a novel negative retinoic acid responsive element in the promoter of the human matrix Gla protein gene. Proc. Natl. Acad. Sci. 94: 2227–2232.

Knapen, M.H.J., Heisenwiener, H-G, Vermeer, C. (1996). Osteocalcin detection in aging serum and whole blood: stability of different osteocalcin fractions. Clin Chim Acta 256: 151-164.

Kohno, H., Taki, Y., Ogasawara, Y., Shirojo, Y., Taketomi, M., Inoue, M. (1983). Development of swimming and feeding functions in larval *Pagrus major*. Jap. J. Ichthyol. 30: 47-60.

Kohno, H., Hara, S., Gallego, A.B., Duray, M.N., Taki, Y. (1986). Morphological development of the swimming and feeding apparatus in larval rabbitfish, *Signatus guttatus. in* Maclean, J.L., Dizon L.B. and Hosillos LV (Eds.). The first Asian Fisheries Forum. Asian Fisheries Society, Manila, Philippines. P. 173-178.

Kohno, H., Ordonio-Aguillar, R. Ohno, A., Taki, Y. (1996). Osteological development of the feeding apparatus in early stage larvae of the sea bass, *Lates calcarifer*. Ichthyol. Res. 43: 1-9.

Komori, T., Yagi, H., Nomura, S., Yamagushi. A., Sasaki, K., Degushi, K., Shimizu, Y., Bronson, R. T., Gao, Y.-H., Inada, M., Sato, M., Okamoto, R., Kitamura, Y., Yoshiki, S., Kishimoto, T. (1997). Targeted disruption of Cbfa1 results in a complete lack of bone formation owing to maturational arrest of osteoblasts. Cell 89: 755–764.

Köntges, G., Lumsden, A. (1996). Rhombencephalic neural crest segmentation is preserved throughout craniofacial ontogeny. Development 122: 3229–3242.

Koumoundourous, G., Oran, G., Divanach, P., Stefanakis, S., Kentouri, M. (1997). The opercular complex deformity in intensive gilthead sea bream *Sparus aurata* L. larviculture. Moment of appearance and description. Aquaculture 156: 165–177.

Kulman, J.D., Harris, J.E., Xie, L., Davie, E.W. (2001). Identification of two novel transmembrane γ-carboxyglutamic acid proteins expressed broadly in fetal and adult tissues. Proc. Nati. Acad. Sci. USA. 98(4): 1370–1375.

Kulman, J. D., Harris, J. E., Haldeman, B. A. & Davie, E. W. (1997). Primary structure and tissue distribution of two novel proline-rich g-carboxyglutamic acid proteins. Proc. Natl. Acad. Sci. USA 94: 9058–9062.

Kvellestad, A., Høie, S., Thorud, K.,Tørud, B., Lyngøy, A., (2000). Platyspondyly and shortness of vertebral column in farmed Atlantic salmon *Salmo salar* in Norway-description and interpretation of pathologic changes. Dis. Aquat. Org. 39: 97-108

Lagler , K., Bardach, J., Miller, R., Passino, D.M. (1987). Ichthyology, 2nd edition. John Wiley & Sons, inc.USA. 506 p.

Laizé,V., Martel, P., Viegas, C.S. B., Price, P.A., Cancela, M. L (2005). Evolution of matrix and bone γ-carboxyglutamic acid proteins in vertebrates. J. Biol. Chem. (in press).

Larson, P.J., Stanfield-Oakley, S.A., VanDusen, W.J., Kasper,C.K., Smith, K.J., Monroe, D.M., High, K.A. (1997). Structural integrity of the γ-carboxyglutamic acid domain of human coagulation factor IXa is required ti its binding to coofactor VIIIa. J. Biol. Chem. 271: 3869-3876.

Lawton, D.M., Andrew, J.G., Marsh, D.R., Hoyland, J.A., Freemont, A.J. (1999). Expression of the gene encoding the matrix gla protein by mature osteoblasts in human fracture non-unions. J. Clin. Pathol.: Mol. Pathol. 52: 92–96.

Lewinson, D. and Kogan, Y. (1995). Ontogenesis of chondro/osteoclasts and their precursors in the mandibular condyle of the mouse. Bone 17: 293–299.

Li, Y., Chen, W., Stashenko, P. (1993). Characterization of a Tumor Necrosis Factor-responsive element wich down-regulates the human osteocalcin gene. Mol. cell. biol. 13 (9): 3714-3721.

Lian, J.B., Roufosse, A.H., Reit, B., Glimcher, M.J. (1982). Concentration of osteocalcin and phosphoprotein as a function of mineral content and age in cortical bone. Calcif. Tissue Int. 34 (Suppl. 2): 82–87.

Lim, T., Bloomfield, V., Nelseustuen, G. (1977). Structure of the prothrombine- and blood clotting factor X– membrane complexes. Biochemistry 16: 4177-4181.

Liu, F., Malaval, L., Gupta, A.K., Aubin, J.E. (1994). Simultaneous detection of multiple bone-related mRNAs and protein expression during osteoblast differentiation: polymerase chain reaction and immunocytochemical studies at the single cell level. Dev. Biol. 166: 220-234.

Liu, Y., Nelson, A.N., Lipsky, J.J.(1996).Vitamin K-Dependent Carboxylase: mRNA Distribution and Effects of Vitamin K-Deficiency and Warfarin Treatment Biochem. Biophys. Res. Comm. 224: 549–554.

Loeser, R., Carlson, C., Tulli, H., Jerome, G., Miller, L., Wallin, R. (1991). Articular cartilage matrix Gla protein: characterization and immunolocalization. Biochem J 287: 1-6.

Luo, G., D'Souza, R., Hogue, D., Karsenty, G. (1995). The matrix Gla protein gene is a marker of the chondrogenesis cell lineage during mouse development. J. Bone Miner. Res. 10: 325–334.

Luo, G., Ducy, P., McKee, M.D., Pinero, G.J., Loyer, E., Behringer, R.R., Karsenty, G. (1997). Spontaneous calcification of arteries and cartilage in mice lacking matrix GLA protein. Nature 358: 78–81.

Ma, C., Fan, L., Ganassin, R., Bols, N., Collodi, P. (2001). Proc. Natl. Acad. Sci. USA 98: 2461–2466.

Macdonald, P.N., Dowd, D.R., Nakajima, S., Galligan, M.A., Reeder, M.C., Haussler, C.A., Ozato, K., Haussler, M.R. (1993). Retinoid X receptors stimulate and 9-*cis* retinoic acid inhibits 1,25-Dihydroxyvitamin D_3 activated expression of the rat osteocalcin gene. Mol. Cell. Biol. 13 (9): 5907-5917.

Manfioletti, G., Brancolini, C., Avanzi, G., Schneider, C. (1993). The protein encoded by a growth arrest-specific gene (gas6) is a new member of the vitamin K-dependent proteins related to protein S, a negative co-regulator in the blood coagulation cascade. Mol. Cell. Biol. 13: 4976.

Madsen, L., Dalsgaard, I. (1999). Vertebral column deformities in farmed rainbow trout (*Oncorhynchus mykiss*). Aquaculture 171: 41-48.

Marino, G., Boglione, C., Bertolini, B., Rossi, A., Ferreri, F., Cataudella, S. (1993). Observations on development and anomalies in the appendicular skeleton of sea bass, *Dicentrarchus labrax* L. 1758, larvae and juveniles. Aquacult. Fish. Manage. 24: 445-456.

Mark, M.P., Butler, W.T., Prince, C.W., Finkelman, R.D., Ruch, J.V. (1988). Developmental expression of 44-kDa bone phosphoprotein (osteopontin) and bone

gamma-carboxyglutamic acid (Gla)-containing protein (osteocalcin) in calcifying tissues of rat. Differentiation 37: 123-136.

Marshal, P.T. and Hughes, G.M. (1980). Physiology of mammals and other vertebrates- 2nd edition. Saunders Colege ed., 755p.

Martínez, I., Álvarez, R., Herraéz, I., Herraéz, P. (1992). Skeletal malformations in hatchery reared *Rana perezi* Tadpoles. The anatomical record 233: 314-320.

Martínez, I., Moyano, F. J., Fernández-Díaz, C. & Yúfera, M. (1999). Digestive enzyme activity during larval development of the Senegal sole (*Solea senegalensis*). Fish Physiol. Biochem 21: 317–323.

Matsuoka, M. (1985) Osteological development in the red sea bream, *Pagrus major*. Japanese Journal of Ichthiology 32: 35-51.

McKee, M.D., Nanci, A., Khan, S.R. (1995). Ultrastructural immunodetection of osteopontin and osteocalcin as major components of renal calculi. J. Bone Miner. Res. 10: 1913-1929.

Mende, L., Huq, N., Matthews, H., Chapman, G. (1984). Primary structure of osteocalcin from ovine bone. Int. J. Peptide Protein Res. 24: 297-302.

Morcos, P.A. (2001). Achieving efficient delivery of morpholino oligos in cultured cells. Genesis 30: 94–102.

Munroe, P., Olgunturk, R., Fryns, J., van Maldergem, L., Ziereisen, F., Yuksel, B., Gardiner, R., Chung, E. (1999). Mutations in the gene encoding the human matrix Gla protein cause Keutel syndrome. Nat. Genet. 21:142–144.

Murshed, M., Schinke, T., McKee, M.D., Karsenty, G. (2004). Extracellular matrix mineralization is regulated locally; different roles of two gla-containing proteins. J. Cell Biol. 165: 625–630.

Murshed, M., Harmey, D., Millán, J.L., McKee, M.D., Karsenty, G. (2005). Unique coexpression in osteoblasts of broadly expressed genes accounts for the spatial restriction of ECM mineralization to bone. Genes & Development 19:in press.

Muzavor, S., Arruda, L.M.; Andrade, J.P. (1993). Roteiro ecológico da Ria Formosa. II-Peixes. Algarve em foco editora. Faro. Portugal. 167pp.

Nakagawa. Y., Abram, V., Kaiser, E., Coe, F.L. (1983). Purification and characterization of the principal inhibitor of alcium oxalate monohydrate crystal growth in human urine. J. Biol. Chem. 258: 12594-12600.

Nakagawa. Y., Ahmed, M., Hall, S.L., Deganello, S., Coe, F.L. (1987). Isolation of human calcium oxalate renal stones of nephrocalcin, a glycoprotein inhibitor of calcium oxalate crystal growth. J. Clin. Invest. 79: 1782-1787.

Nakagawa. Y., Renz, C.L., Ahmed, M. Coe, F.L. (1991). Isolation of nephrocalcin from kidney tissue of nine different vertebrate species. Am. J. Physiol. 263: F243-F248.

Nakano, T., Higashino, K., Kikuchi, N., Kishino, J., Nomura, K., Fujita, H., Ohara, O., Arita, H. (1995). Vascular smooth muscle cell-derived, Gla-containinggrowth-potentiation factor for Ca (2+)-mobilizing growth factors. J. Biol. Chem. 270: 5702–5705.

Nasevicius, A. and Ekker, S. C. (2000). Effective targeted gene 'knockdown' in zebrafish. nature genetics 26: 216-220.

Neugebauer, B.M., Moore, M.A., Broess, M., Gerstenfeld, L.C. and Hauschka, P.V. (1995). Characterization of structural sequences in the chicken osteocalcin gene: expression of osteocalcin by maturing osteoblasts and by hypertrophic chondrocytes *in vitro*. J. Bone Miner. Res. 10 (1): 157-163.

Neuhauss, S. C. F., Solnica-Krezel, L., Schier, A. F., Zwartkruis, F., Stemple, D. L., Malicki, J., Abdelilah, S., Stainier, D. Y. R., Driever, W. (1996). Mutations affecting craniofacial development in zebrafish. Development 123: 357–367.

Newman, B., Gigout, L. I., Sudre, L., Grant, M. E., Wallis, G. A. (2001). Coordinated expression of matrix Gla protein is required during endochondral ossification for chondrocyte survival. J. Cell Biol. 154: 659–666.

Nishimoto, S.K., Araki, N., Robinson, F.D., Waite, J.H. (1992). Discovery of bone γ-carboxyglutamic acid protein in mineralized scales. The abundance and structure of Lepomis macrochirus bone γ-carboxyglutamic acid. J. Biol. Chem. 267 (16): 11600-11605.

Nishimoto, S. K., Waite, J. H., Nishimoto, M., and Kriwacki, R. W. (2003). Structure, Activity, and Distribution of Fish Osteocalcin. J. Biol. Chem. 278: 11843-11848.

Novak, J.F., Hayes, J.D., Nishimoto, S.K. (1997). Plasmin-mediated proteolysis of osteocalcin. J. Bone Miner. Res. 12: 1035–1042.

Nüsslein-Volhard, C. and Dahm, R., editors (2002). Zebrafish, a practical approach. Volume 261. The practical approach series. Oxford University Press. Oxford, UK. 352 p.

Nusslein-Volhard,C.; Gilmour G.T.; Dahm, R. (2002). Zebrafish as a system to study development and organogenesis. i*n* Zebrafish-practical aproach. Nusslein-Volhard,C.and Dahm, R. eds. Oxford University Press, Oxford, UK. 352p.

Ørnsrud, R., Gil, L., Waagbø, R. (2004). Teratogenicity of elevated egg incubation temperature and egg vitamin A status in Atlantic salmon, Salmo salar L. J. Fish Diseas. 27: 213–223.

Ott, S.M. (1996). Theoritical and methodoligical approach. pp. 231–234. *in* Principles of bone biology. Bilezikian, J.P., Raisz, L.G., Rodan, G.A., eds.,. Academic Press, San Diego, CA.

Otawara, Y. and Price, P.A. (1986). Developmental appearance of matrix Gla protein during calcification in the rat. J. Biol. Chem. 261: 10828–10832.

Owen, T.A., Aronow, M., Shalhoub, V., Barone, L.M., Wilming, L., Tassinari, M.S., Kennedy, M.B., Pockwinse, S., Lian, J.B., Stein, G.S. (1990). Progressive development of the rat osteoblast phenotype *in vitro*: reciprocal relationships in expression of genes associated with osteoblast proliferation and differentiation during formation of the bone extracellular matrix. J. Cell. Physiol. 143: 420–430.

Owen, T.A., Aronow, M.A., Barone, L.M., Bettencourt, B., Stein, G.S., Lian, J.B. (1991). Pleiotropic effects of vitamin D on osteoblast gene expression are related to the proliferative and differentiated state of the bone cell phenotype: dependency upon basal levels of gene expression, duration of exposure, and bone matrix competency in normal rat osteoblast cultures. Endocrinology 128: 1495–1504.

Pan, L.C. and Price, P.A. (1985). The propeptide of rat bone y-carboxyglutamic acid protein shares homology with other vitamin K-dependent protein precursors. Proc. Nati. Acad. Sci. USA 82: 6109-6113.

Pan, L.C., Williamson, M.K., Price, P.A. (1985). Sequence of the precursor to rat bone gamma-carboxyglutamic acid protein that accumulates in warfarin-treated osteosarcoma cells. J. Biol. Chem. 260: 13398-13401.

Papagerakis, P., Berdal, A., Mesbah, M., Peuchmaur, M., Malaval, L., Nydegger, J., Simmer, J., Macdougall, M. (2002). Investigation of Osteocalcin, Osteonectin, and Dentin Sialophosphoprotein in Developing Human Teeth. Bone 30(2):377–385.

Parenti, L.R. (1986). The phylogenetic significance of bone types in euteleost fishes. Zool. J. Linn. Soc. 87 (1): 37-51.

Pearse, A.G.E. (1985). Histochemistry: Theoretical and Applied. Vol 2- analytical technology. 4th Ed.. Churchill –Livingstone, Edinburgh. pp 441-1055.

Pendón, C., Martínez-Barberá, J.P., Valdivia, M.M., 1994a. Cloning of a somatolactin-encoding cDNA from sole (*Solea senegalensis*). Gene 147: 227–230.

Pendón, C., Martínez-Barberá, J.P., Pérez-Sánchez, J., Rodríguez, R.B., Grenett, H., Valdivia, M.M., 1994b. Cloning of the sole (*Solea senegalensis*) growth hormone-encoding cDNA. Gene 147: 237–240.

Persson, P., Sundell, K., Björnsson, B.Th. and Lundqvist, H. (1998). Calcium metabolism and osmoregulation during sexual maturation of river running Atlantic salmon (*Salmo salar* L.). J. Fish Biol. 52: 334–349.

Persson, P., Björnsson, B.T. and Takagi, Y. (1999). Characterization of morphology and physiological actions of scale osteoclasts in the rainbow trout. J. Fish Biol. 54: 669–684.

Pettifor, J.M., Benson, R. (1975). Congenital malformations associated with the administration of oral anticoagulants during pregnancy. J. Pediatr. 86: 459–462.

Pinto, J.P., Ohresser, M.C.P., Cancela, M.L. (2001). Cloning of the bone Gla protein gene from the teleost fish Sparus aurata. Evidence for overall conservation in gene organization and bone-specific expression from fish to man. Gene 270: 77–91.

Pinto, J.P., Conceição, N., Gavaia, P.J., Cancela, M.L. (2003). Matrix Gla protein gene expression and protein accumulation co-localize with cartilage distribution during development of the teleost fish *Sparus aurata*. Bone 32: 201 –210.

Pinto, J.P., Conceição, N.M.,. Viegas, C.S.B., Leite, R.B., Hurst, L.D., Kelsh, R.N., Cancela, M.L. (2005). Identification of a new pebp2αA2 isoform from zebrafish runx2 capable of inducing osteocalcin gene expression *in vitro*. J. Bone Miner. Res. In press.

Piotrowski, T., Schilling, T. F., Brand, M., Jiang, Y.-J., Heisenberg, C.-P., Beuchle, D., Grandel, H., van Eeden, F. J. M., Furutani-Seiki, M., Granato, M., Haffter, P., Hammerschmidt, M., Kane, D. A., Kelsh, R. N., Mullins, M. C., Odenthal, J., Warga, R. M., Nusslein-Volhard, C. (1996). Jaw and branchial arch mutants in zebrafish. II. Anterior arches and cartilage differentiation. Development 123: 345–356.

Pockwinse, S., Wilming, L., Conlon, D., Stein, G.S., Lian, J.B. (1992). Expression of cell growth and bone specific genes at single cell resolution during development of bone tissue-like organization in primary osteoblast cultures. J. Cell Biochem. 49: 310–323.

Pombinho, A.R., Laizé, V., Molha, D.M., Marques, S.M.P., Cancela, M.L. (2004) Development of two bone-derived cell lines from the teleost Sparus aurata; evidence for extracellular matrix mineralization and cell-type specific expression of matrix Gla protein and osteocalcin. Cell & Tissue Res. 315: 393-406.

Poser, J.W., Price, P.A. (1979). A method for decarboxylation of gamma-carboxyglutamic acid in proteins. Properties of the decarboxylated gamma-carboxyglutamic acid protein from calf bone. J. Biol. Chem. 254: 431-436.

Poser, J.W., Esch, F.S., Ling, N.C., Price, P.A. (1980). Isolation and sequence of the vitamin K-dependent protein from human bone. J. Biol. Chem. 255: 8685-8691.

Price, P.A. (1984). Vitamin K-dependent bone gla proteins and the action of 1,25-dihydroxyvitamin D3 on bone. R XIV 73(4): 217-222.

Price, P.A. (1985). Vitamin K-dependent formation of bone Gla protein (osteocalcin) and its function. Vit. Horm. 42: 65–108.

Price, P.A. (1987). Vitamin K-dependent proteins. P419-425. *in* D.V. Cohn, T.J. Martin and P.J. Meunier (ed.). Calcium regulation and bone metabolism: Basic and clinical aspects. Elsevier Science Publishers, Amsterdam.

Price, P.A. (1990). Vitamin K-dependent bone proteins. *in* Saito H. and Suttie. J.W. Vitamin K-dependent proteins and their metabolic roles. New York, Elsevier. chapter 3: 49-70.

Price, P.A. (1992). Gla-containing proteins of mineralized tissues, *in* Slavkin, H. & Price, P. (1992) Chemistry and Biology of mineralized tissues. Eds. Excerpta Medica, Elsevier, Amsterdam, 169-176.

Price, P.A., Otsuka, A.S., Poser, J.W., Kristaponis, J., Raman, N. (1976a). Characterization of a gamma-carboxyglutamic acid-containing protein from bone. Proc. Natl. Acad. Sci. USA 73 (5): 1447-1451.

Price, P.A., Poser, J.W., Raman, N. (1976b). Primary structure of the gamma-carboxyglutamic acid-containing protein from bovine bone. Proc. Natl. Acad. Sci. 73 (10): 3374-3375.

Price, P.A., Otsuka, A.S., Poser, J.W. (1977). *in* Wasserman, R.H., Corradino, R.A., Carafoli, E., Kretsinger, R.H., Maclennan, D.H. and Siegel, F.L. (Eds.); Calcium-Binding Proteins And Calcium Function: 33-337; North-Holland, New York.

Price, P.A., and Nishimoto, S.K. (1980). Radioimmunoassay for the vitamin K-dependent protein of bone and its discovery in plasma. Proc. Natl. Acad. Sci. USA 77: 2234 – 2238.

Price, P.A., Williamson, M.K., Lothringer, J.W. (1981). Origin of the vitamin K-dependent bone protein found in plasma and clearance by kidney and bone. J. Biol. Chem. 256: 12760-12766.

Price, P.A. and Williamson, M.K. (1981). Effects of warfarin on bone. Studies on the vitamin K-dependent protein of rat bone. J. Biol. Chem. 256: 12745-12759.

Price, P.A., Williamson, M.K., Haba, T., Dell, R.B., Jee, W.S.S. (1982). Excessive mineralization with growth plate closure in rats on chronic warfarin treatment. Proc. Natl. Acad. Sci. USA 79: 7734 –7738.

Price, P.A. and Sloper, S. A. (1983). Concurrent warfarin treatment further reduces bone mineral levels in 1,25 dihydroxyvitamin D_3-treated rats. J. Biol. Chem. 258: 6004-6007.

Price, P.A., Urist, M.R., Otawara, Y. (1983). Matrix Gla protein, a new gamma-carboxyglutamic acid-containing protein which is associated with the organic matrix of bone. Biochem. Biophys. Res. Commun. 117: 765–771.

Price, P.A., and Williamson, M.K. (1985). Primary Structure of Bovine Matrix Gla Protein, a New Vitamin K-dependent Bone Protein. J. Biol. Chem. 260(28): 14971-14975.

Price, P.A. and Kaneda, Y. (1987). Vitamin K counteracts the effect of warfarin in liver but not in bone. Thromb. Res 46: 121-131.

Price, P.A, Fraser, J.D., Metz-Virca, G. (1987). Molecular cloning of matrix Gla protein: Implications for substrate recognition by the vitamin K-dependent y-carboxylase. Proc. Natl. Acad. Sci. USA 84: 8335-8339.

Price, P.A., Rice, J.S., Williamson, M.K. (1994). Conserved phosphorylation of serine in the Ser-X-glu/Ser (P) sequences of the vitamin K-dependent matrix Gla protein from shark, lamb, rat, cow and human. Protein Sci. 3: 822-830.

Price, P.A., Faus, S.A., Williamson, M.K. (1998). Warfarin causes rapid calcification of the elastic lamellae in rat arteries and heart valves. Arterioscler. Thromb. Vasc. Biol. 18: 1400–1407.

Price, P.A., Faus, S.A., Williamson, M.K. (2000). Warfarin-induced artery calcification is accelerated by growth and vitamin D. Arterioscler. Thromb. Vasc. Biol. 20: 317–327.

Price, P.A., Thomas, G.R., Pardini, A.W., Figueira, W.F., Caputo, J.M., Williamson, M.K. (2002). Discovery of a High Molecular Weight Complex of Calcium, Phosphate, Fetuin, and Matrix γ-Carboxyglutamic Acid Protein in the Serum of Etidronate-treated Rats. J. Biol. Chem. 277(6): 3926–3934.

Prockop, D.J. and Kivirikko, K.I. (1984). Heritable diseases of collagen. New Engl. J. Med. 311: 376–386.

Proudfoot, D., Skepper, J.N., Shanahan, C.M., Weissberg, P.L. (1998). Calcification of human vascular cells *in vitro* is correlated with high levels of matrix Gla protein and low levels of osteopontin expression. Arterioscler. Thromb. Vasc. Biol. 18: 379-388.

Puchacz, E., Lian, J.B., Stein, G. S., Wozney, J., Huebner, K., Croce, C. (1989). Chromosomal Localization of the Human Osteocalcin Gene. Endocrinology 124: 2648-2650.

Pudota, B.N., Hommema, E.L., Hallgren, K.W., McNally, B.A., Lee, S., Berkner, K.L. (2001). Identification of Sequences within the γ-Carboxylase That Represent a Novel Contact Site with Vitamin K-dependent Proteins and That Are Required for Activity. J. Biol. Chem. 276(50): 46878–46886

Rawls, J.F., Mellgren, S E., Johnson, M..L. (2001). How the zebrafish gets its stripes. Dev. Biol. 240: 301–314.

Ribeiro, L. (2003). Ontogeny of *Solea senegalensis*: digestive system and nutritional aspects. Tese doutoramento Universidade do Algarve. Faro. 170p.

Ribeiro, L., Sarasquete, C. & Dinis, M. T. (1999a). Histological and histochemical development of the digestive system of *Solea senegalensis* (Kaup, 1858) larvae. Aquaculture 171: 293–308.

Ribeiro, L., Zambonino-Infante, J. L., Cahu, C., Dinis, M. T. (1999b). Development of digestive enzymes in larvae of *Solea senegalensis* Kaup 1858. Aquaculture 179: 465–473.

Rice, J.S., Williamson, M.K., Price, P.A. (1994). Isolation and sequence of the vitamin K–dependent matrix Gla protein from the calcified cartilage of the soupfin shark. *J.* Bone Miner. Res. 9: 567–576.

Rishavy, M.A., Pudota, B.N., Hallgren, K.W., Qian, W., Yakubenko, A.V., Song, J.-H., Runge, K.W., Berkner, K.L. (2004). A new model for vitamin K-dependent carboxylation: The catalytic base that deprotonates vitamin K hydroquinone is not Cys but an activated amine. Proc. Natl. Acad. Sci. USA 101 (38): 13732–13737.

Roach, H.I. and Shearer, J.R. (1989). Cartilage resorption and endochondral bone formation during the development of long bones in chick embryos. Bone Miner. 6(3):289-309

Robson, P., Wright G.M., Keeley, F.W. (2000). Distinct non-collagen based cartilages comprising the endoskeleton of the Atlantic hagfish, *Myxine glutinosa*. Anat. Embryol. 202: 281–290.

Rodriguez-Gómez, F.J., Rendón-Unceta, M.C., Sarasquete, C., Muñoz-Cueto, J.A.. (2000a). Localization of tyrosine hydroxylase-immunoreactivity in the brain of the Senegalese sole, Solea senegalensis. Journal of Chemical Neuroanatomy 19: 17–32.

Rodriguez-Gómez, F.J., Rendón-Unceta, M.C., Sarasquete, C., Muñoz-Cueto, J.A.. (2000b). Distribution of serotonin in the brain of the Senegalese sole, *Solea senegalensis*: an immunohistochemical study. Journal of Chemical Neuroanatomy 18: 103–115.

Romberg, R.W., Werness, P.G., Riggs, B.L., Mann, K.G. (1986). Inhibition of hydroxyapatite crystal growth by bone-specific and other calcium-binding proteins. Biochemistry 25: 1176-1180.

Roy, M.E.and Nishimoto, S.K. (2002). Matrix Gla protein binding to hydroxyapatite is dependent on the ionic environment: calcium enhances binding affinity but phosphate and magnesium decrease affinity. Bone. 31: 296–302.

Sabatakos, G., Sims, N.A., Chen, J., Aoki, K., Kelz, M.B., Amling, M., Bouali, Y., SMukhopadhyay, K., Ford, K., Nestler, E.J., Baron, R. (2000). Overexpression of ΔFosB transcription factor(s) increases bone formation and inhibits adipogenesis. Nature Medicine 6 (8): 985-990.

Salte, R. and Norberg, K. (1991). Effects of warfarin on vitamin K-dependent coagulation factors in Atlantic salmon and rainbow trout with special reference to factor X. Thromb. Res. 63: 39-45.

Sambrook, J., Fritsch, E.F., Maniatis, T. (1989). Molecular cloning: a laboratory manual. Cold Spring Harbor Laboratory Press, New York.

Sarasquete, C., Gonzalez de Canales, M.L., Arellano, J.M., Muñoz Cueto, J.A., Ribeiro, L., Dinis, M.T. (1996). Histochemical aspects of the yolk-sac and digestive tract of larvae of the Senegal sole, *Solea senegalensis* (Kaup, 1858). Histol. Histopathol. 11: 881–888.

Schilling, T.F. (1997). Genetic analysis of craniofacial development in the vertebrate embryo. BioEssays 19: 459–468.

Schilling, T.F., Piotrowski, T., Grandel, H., Brand, M., Heisenberg, C.P., Jiang, Y.J., Beuchle, D., Hammerschmidt, M., Kane, D.A., Mullins, M.C., van-Eeden, F.J., Kelsh, R.N., Furutani-Seiki, M., Granato, M., Haffter, P., Odenthal, J., Warga, R. M., Trowe, T., and Nusslein-Volhard, C. (1996a). Jaw and branchial arch mutants in zebrafish. I. Brachial arches. Development 123: 329–344.

Schilling, T.F., Walker, C., Kimmel, C.B. (1996b). The *chinless* mutation and neural crest cell interactions in zebrafish jaw development. Development 122: 1417–1426.

Schilling, T.F. and Kimmel, C.B. (1997). Musculoskeletal patterning in the pharyngeal segments of the zebrafish embryo. Development 124: 2945-2960.

Schinke T, Karsenty G (2000). Vascular calcification: a passive process in need of inhibitors. Nephrol. Dial. Transplant. 15: 1272–1274.

Shanahan, C.M., Weissberg, P.L., Metcalfe, J.C. (1993). Isolation of gene markers of differentiated and proliferating vascular smooth muscle cells. Circ. Res. 73:193–204.

Shanahan, C.M., Proudfoot, D., Farzaneh-Far, A., Weissberg, P.L. (1998). The role of Gla-proteins in vascular calcification. Crit. Rev. Eukar. Gene. Expr. 8: 357–375.

Shanahan, C.M., Cary, N.R.B., Salisbury, J.R., Proudfoot, D., Weissberg, P.L., Edmonds, M.E. (1999). Medial localization of mineralization regulating proteins in association with Mönckeberg's sclerosis. Circulation 100: 2168–2176.

Shanahan, C.M., Proudfoot, D., Tyson, K.L., Cary, N.R.B., Edmonds, M., Weissberg, P.L. (2000). Expression of mineralization-regulating proteins in association with human vascular calcification. Z Kardiol 89: 63–68.

Sheik, M.S., Shao, Z., Chen, J., Fontana, J.A.(1993). Differential expression of matrix gla protein (MGP) gene expression by retinoic acid and estrogen in human breast carcinoma cells. Mol. Cell. Endocrinol. 92: 153-160.

Shimomura, H., Kanai, Y., Sanada, K. (1984). Primary structure of cat osteocalcin. J. Biochem. 96: 405-411.

Schinke, T., McKee M.D., Kiviranta, R., Karsenty, G. (1998). Molecular determinants of arterial calcification. Ann. Med. 30: 538–541.

Schinke, T. and Karsenty, G. (2000). Vascular calcification-a passive process in need of inhibitors. Nephrol. Dial. Transplant. 15: 1272-1274.

Schüle, R., Umesono, K., Mangelsdorf, D., Bolado, J., Pike, J., Evans, R. (1990). Jun-Fos and receptors for vitamins A and D recognise a commun response element in the human osteocalcin gene. Cell 61: 497-504.

Simes, D.C. (2002). Purification, biochemical characterization and localization at single cell resolution of matrix Gla protein (MGP) and bone Gla protein (BGP) in the teleost fish, *Argyrosomus regius*. Tese PhD. Universidade do Algarve. Portugal.

Simes, D.C., Williamson, M.K., Ortiz-Delgado, J.B., Viegas, C.S.B., Price, P.A., Cancela, M.L. (2003). Purification of matrix Gla protein from a marine teleost fish, *Argyrosomus regius*: calcified cartilage and not bone as the primary site of MGP accumulation in fish. J. Bone Min. Res. 18: 244-259.

Simes, D.C., Williamson, M.K., Schaff, B.J., Gavaia, P.J., Ingleton, P.M., Price, P.A., Cancela, M.L. (2004). Characterization of osteocalcin (BGP) and matrix Gla protein (MGP) fish specific antibodies: validation for immunodetection studies in lower vertebrates. Calcif. Tissue. Int. 74: 170 –180.

Sire, J.Y., Huysseune, A., Meunier, J. (1990). Osteoclasts in the teleost fish: light and electron-microscopical observations. Cell Tissue Res. 260: 85–94.

Sohma, Y., Suzuki, T., Sasano, H., Nagura, H., Nose, M., Yamamoto, T. (1994). Expression of mRNA for matrix gamma-carboxyglutamic acid protein during progression of atherosclerosis in aortae of Watanabe heritable hyperlipidemic rabbits. J. Biochem. (Tokyo) 116: 747–51.

Sokoll, L.J., Booth, S.L,, O'Brien, M.E., Davidson, K.W., Tsaioun, K.I., Sadowski, J.A. (1981). Changes in serum osteocalcin, plasma phylloquinone, and urinary gamma-carboxy glutamic acid in response to altered intakes of dietary phylloquinone in human subjects. Am. J. Clin. Nutr. 65: 779.

Sommer, S.S., Ricke, D.O., Thorland, E. And Buettner, V.L. (1994). The factor IX gene family in birds and fish: evidence for two novel members of the gene family. Blood 84: 194a.

Song, J. and Parenti, L.R. (1995). Clearing and staining whole fish specimens for simultaneous demonstration of bone, cartilage and nerves. Copeia 1: 114-118.

Speer, M.Y., McKee, M.D., Guldberg, R.E., Liaw, L., Yang, H.Y., Tung, E., Karsenty, G., Giachelli, C.M. (2002). Inactivation of the osteopontin gene enhances vascular calcification of matrix Gla protein-deficient mice: evidence for osteopontin as an inducible inhibitor of vascular calcification *in vivo*. J. Exp. Med. 196: 1047–1055.

Spronk, H.M.H., Soute, B.A.M. Schurgers, L.J., Cleutjens, J.P.M., Thijssen, H.H.W., De Mey, J.G.R., Vermeer, C. (2001). Matrix Gla protein accumulates at the border of regions of calcification and normal tissue in the media of the arterial vessel wall. Biochem. Biophys. Res. Comm. 289: 485–490.

Stenflo, J., Ohlin, A-K., Persson, E., Selander, M., Linse, S., Drakenberg, T. (1990). Calcium binding and B-hydroxyaspartic acid in thc first EGF-like domain of protein C and related vitamin K-dependent proteins. *in* K-dependent proteins and their metabolic roles. H. Saito and J.W. Suttie, editors. Elsevier, New York. Pp.95-110.

Stitt, T.N., Conn, G., Gore, M. Lai, c:, Bruno, J., Radziejewski, C., Mattsson, K., Fisher, G., Gies, D.R., Jones, P.F., Masiakowski, P., Ryan, T.E., Tobkes, N.J. Chen, D.H. DiStefano, P.S., Long, J.L., Basislico, C., Goldfarb, M.P., Lemke, G., Glass, D.J., Yancopoulos, G.D. (1995). The anticoagulation factor protein S and its relative, gas

6, are ligands for the Tyro3/Axl family of receptor tyrosine kinases. Cell 80: 661-670.

St-Jaques, B., Hammerschmidt, M., McMahon, A.P. (1999). Indian hedgehog signaling regulates proliferation and differentiation of chondrocytes and its essential for bone formation. Genes Dev. 13: 2072–2086.

Stock, M., Schäfer, H., Fliegauf, M., Otto, F. (2004). Identification of Novel Target Genes of the Bone-Specific Transcription Factor Runx2. J. Bone. Miner. Res. 19: 959-972.

Storer, T., Stebbins, R., Usinger, R., Nybakken, J. (1986). Zoologia general. Ediciones OMEGA, Barcelona. 955p.

Streisinger, G., Walker, C., Dower, N., Knauber, D. and Singer, F. (1981). Production of clones of homozygous diploid fish (*Brachydanio rerio*). Nature 291: 293-296.

Sugiyama, T, Kawai, S. (2001).Carboxylation of osteocalcin may be related to bone quality: a possible mechanism of bone fracture prevention by vitamin K. J. Bone Miner. Metab. 19: 146–149.

Suttie, J. W. (1985). Vitamin K-dependent carboxylase. Ann. Rev. Biochem. 54: 459–477.

Suttie, J.W. (1990). The role of Vitamin K-dependent microsomal gamma-carboxylase in clotting factor biosyntesis. *in* Saito H. and Suttie. J.W. Vitamin K-dependent proteins and their metabolic roles. New York, Elsevier. chapter 1: 1-35.

Suzuki, N. (1990). The role of the vitamin K-dependent protein C and protein S and C4b-binding protein in blood coagulation. *in* Vitamin K-dependent proteins and their metabolic roles. H. Saito and J.W. Suttie, editors. Elsevier, New York. Pp.11-134.

Suzuki, T., Srivastava, A.S. and Kurokawa, T. (2000). Experimental induction of jaw, gill and pectoral fin malformations in Japanese flounder, *Paralichthys olivaceus*, larvae. Aquaculture 185: 175–187.

Szulc, P., Chapuy, M.C., Meunier, P.J., Delmas, P.D. (1993). Serum undercarboxylated osteocalcin is a marker of the risk of hip fracture in elderly women. J. Clin. Invest. 91: 1769–1774.

Szulc, P., Chapuy, M.C., Meunier, P.J., Delmas, P.D. (1996) Serum undercarboxylated osteocalcin is a marker of the risk of hip fracture: a three year follow-up study. Bone 18: 487.

Sweatt, A., Sane, D.C., Hutson, S.M., Wallin, R. (2003). Matrix Gla protein (MGP) and bone morphogenetic protein-2 in aortic calcified lesions of aging rats. J. Thromb. Haemostas. 1: 178–185.

Takeda, S., Bonnamy, J.P., Owen, M.J., Ducy, P., Karsenty, G. (2001). Continuous expression of Cbfa1 in nonhypertrophic chondrocytes uncovers its ability to induce hypertrophic chondrocyte differentiation and partially rescues Cbfa1-deficient mice. Genes & Dev. 15: 467–481.

Takeuchi, T., Dedi, J., Ebisawa, C., Watanabe, T., Seikai, T., Hosoya, K., Nakazone, J.I., (1995). The effect of betacarotene and vitamin A enriched Artemia nauplii on the malformation and color abnormality of larval Japanese flounder. Fish. Sci. 61: 141–148.

Takeuchi T., Dedi J., Haga Y., Seikai T. & Watanabe T. (1995). Effect of vitamin A compounds on bone deformity in larval Japanese flounder (*Paralichthys olivaceus*). Aquaculture 169: 155–165.

Taki, Y., Kohno, H., Hara, S. (1987). Morphological aspects of the development swimming and feeding functions in the Milkfish *Chanos chanos*. Jap. J. Ichthyol. 34: 198-208.

Tanaka, M., Kawai, S., Seikai, T. & Burke, J. S. (1996). Development of the digestive organ system in Japanese flounder in relation to metamorphosis and settlement. Marine and Freshwater Behaviour and Physiology 28: 19–31.

Taylor, W.R. and Van Dyke, G.C. (1985). Revised procedures for staining and clearing small fishes and other vertebrates for bone and cartilage study. Cybium 9(2): 107-119.

Taylor, L.H., Hall, B.K., Miyake, T., Cone, D.K. (1994). Ectopic ossicles associated with metacercariae of *Apophallus brevis* (Trematoda) in yellow perch, *Perca flavescens* (Teleostei): development and identification of bone and chondroid bone. Anat. Embryol. (Berl). 190: 29-46.

Taylor, B.C., Schreiner, P.J., Doherty, T.M., Fornage M., Carr J.J., Sidney, S. (2005). Matrix Gla protein and osteopontin genetic associations with coronary artery calcification and bone density: the CARDIA study. Human genetics 32: 1258-1270

Tintut, Y., Parhami, F., Bostrom, K., Jackson, S.M., Demer, L.L.(1998). cAMP stimulates osteoblast-like differentiation of calcifying vascular cells: potential signaling pathway for vascular calcification. J. Biol. Chem. 273: 7547-7553.

Tintut, Y. and Demer, L.L. (2001). Recent advances in multifactorial regulation of vascular calcification. Curr. Opin. Lipidol. 12: 555-560.

Urist, M.R., Huo, Y.K., Brownell, A.G., Hohl, W.M., Buyske, J., Lietze, A., Tempst, P., Hunkapiller, M., DeLange, R.J. (1984). Purification of bovine bone morphogenetic protein by hydroxyapatite chromatography. Proc. Natl. Acad. Sci. USA 81: 371–375.

Van der heyden, C. and Huysseune, A. (2000). Dynamics of Tooth Formation and Replacement in the Zebrafish (*Danio rerio*) (Teleostei, Cyprinidae). Dev. Dyn. 219: 486–496.

Van der heyden, C., Wautier, K., Huysseune, A. (2001). Tooth succession in the zebrafish (*Danio rerio*). Arch. Oral Biol. 46: 1051–1058.

Vergnaud, P., Garnero, P., Meunier, P.J., Breart, G., Kamihagi, K., Delmas, P.D. (1997) Undercarboxylated osteocalcin measured with a specific immunoassay predicts hip fracture in elderly women: the EPIDOS study. J. Clin. Endocrinol. Metab.82: 719-224.

Vermeer, C. (1984). The binding of Gla-containing proteins to phospholipids. FEBS letters 173: 169-172.

Vermeer, C. (1990). Gamma-carboxyglutamate-containing proteins and the vitamin K-dependent carboxylase. Biochem. J. 266: 625–636.

Vermeer, C., Soute, B.A.M., Hendrix, H., de Boer van der Berg, M.A.G. (1984). Decarboxylated bone gla protein as a substrate for hepatic vitamin k-dependent carboxylase. FEBS lett. 165: 16-20.

Vermeer, C. and Braam, L. (2001). Role of K vitamins in the regulation of tissue calcification. J. Bone Miner. Metab. 19: 201–206.

Viegas, C.S.V., Pinto, J.P., Conceição, N., Simes, D.C., Cancela, M.L. (2002). Cloning and characterization of the cDNA and gene encoding *Xenopus laevis* osteocalcin. Gene 289: 97–107.

Vogel, G. (2000). Zebrafish earns its stripes in genetic screens. Science 288: 1160–1161.

Wajih, N., Borras, T., Xue, W., Hutson, S.M, Wallin, R. (2004). Processing and transport of matrix Gla protein (MGP) and bone morphogenetic protein-2 (BMP-2) in cultured human vascular smooth muscle cells: evidence for an uptake mechanism for serum fetuin. J. Biol. Chem. 282: 154-166.

Walker, W.F. Jr and Liem, K.F. (1994). Functional anatomy of the vertebrates. An evolutionary perspective 2nd ed. Saunders College Publications, Philadelphia, USA. 788p.

Wallin, R., Cain, D., Sane, D.C. (1999). Matrix Gla protein synthesis and gamma-carboxylation in the aortic vessel wall and proliferating vascular smooth muscle

cells. A cell system which resembles the system in bone cells. Thromb. Haemost. 82: 1764–1767.

Wallin, R., Cain, D., Hutson, S.M., Sane, D.C., Loeser, R. (2000). Modulation of the binding of matrix Gla protein (MGP) to bone morphogenetic protein-2 (BMP-2). Thromb. Haemost. 84: 1039–1044.

Wallin, R., Wajih, N., Greenwood, G.T., Sane, D.C. (2001). Arterial calcification: A review of mechanisms, animal models, and the prospects for therapy. Med. Res. Rev. 21(4): 274-301.

Wang, X., Ford, B.C., Praul, C.A., Leach Jr., R.M. (2005). Characterization of the non-collagenous proteins in avian cortical and medullary bone. Comp. Biochem. Physiol., Part B 140: 665–672

Wassersug, R.J. (1976). A procedure for differential staining of cartilage and bone in whole formalin-fixed vertebrates. Stain Technol. 51:131-134.

Wautier, K., Van der heyden, C., Huysseune, A., 2001. A quantitative analysis of the pharyngeal tooth shape in the zebrafish (*Danio rerio*) (Teleostei, Cyprinidae). Arch. Oral Biol. 46: 67–75.

Webb, G.N., Byrd, R.A.(1994). Simultaneous differential staining of cartilage and bone in rodent fetuses: an alcian blue and alizarin red S procedure without glacial acetic acid. Biotech. Histochem. 69: 181-185.

Weiss, R.E. and Watabe, N. (1979). Studies on the bilogy of fish bone. III.Ultrastructure of osteogenesis and resorption in osteocytic (cellular) and anosteocytic (acelular) bones. Calcif. Tissue Int. 28 (1): 43-56.

Witten, P.E. (1997). Enzyme histochemical characteristics of osteoblasts and mononucleated osteoclasts in a teleost fish with acellular bone (*Oreochromis niloticus*, Cichlidae). Cell Tissue Res. 287: 591–599.

Witten, P.E., Villwock, W. (1997). Growth requires bone resorption at particular skeletal elements in a teleost fish with acellular bone (*Oreochromis niloticus*, Teleostei: Cichlidae). J. Appl. Ichthyol. 13: 149–158.

Witten, P. E., Hansen, A., Hall, B.K. (2001). Features of Mono- and Multinucleated Bone Resorbing Cells of the Zebrafish *Danio rerio* and Their Contribution to Skeletal Development, Remodeling, and Growth. J. Morphol. 250: 197–207

White, C., Gardiner, E., Eisman, J. (1998).Tissue specific and vitamin D responsive gene expression in bone. Mol. Biol. Rep. 25: 45–61.

Wiedemann, M., Trueb, B., Belluoccio, D. (1998). Molecular cloning of avian matrix Gla protein. Biochim. Biophys. Acta 1395: 47–49.

Wu, S.M., Morris, D.P., Stafford, D.W. (1991). Identification and purification to near homogeneity of the vitamin K-dependent carboxylase. Proc. Natl. Acad. Sci. USA 88: 2236–2240.

Yagami, K., Suh, J. Y., Enomoto-Iwamoto, M., Koyama, E., Abrams, W. R., Shapiro, I. M., Pacifici, M., and Iwamoto, M. (1999). Matrix GLA protein is a developmental regulator of chondrocyte mineralization and, when constitutively expressed, blocks endochondral and intramembranous ossification in the limb. J. Cell Biol. 147: 1097–1108.

Yin, Z.F. Huang, Z.F., Cui, J., Fiehler, R., Asky, N., Ginsburg, D., Brooze, G.J.J. (2000). Prothrombotic phenotype of protein Z deficiency. Proc. Natl. Acad. Sci. USA 97: 6734-6738.

Zebboudj, A.F., Imura, M., Bostrom, K. (2002). Matrix GLA protein, a regulatory protein for bone morphogenetic protein-2. J. Biol. Chem. 277: 4388–4394.

Zebboudj, A.F., Shin, V. Bostrom, K. (2003). Matrix GLA Protein and BMP-2 Regulate Osteoinduction in Calcifying Vascular Cells. J. Cell. Biochem. 90: 756–765

Zhang, R., Ducy, P., Karsenty, G. (1997). 1,25-Dihydroxyvitamin D_3 inhibits osteocalcin expression in mouse through an indirect mechanism J. Biol. Chem. 272 (1): 110–116.

Zhang, Y., Cui, F.Z., Wang, X.M., Feng, Q.L., Zhu, X.D. (2002). Mechanical properties of skeletal bone in gene-mutated *stöpsel*^{dtl28d} and wild-type zebrafish (*danio rerio*) measured by atomic force microscopy-based nanoindentation. Bone 30: 541–546.

Zofková, I., Hill, M., Palicka, V. (2003). Association between serum undercarboxylated osteocalcin and bone density and/or quality in early postmenopausal women. Nutrition 19: 1001–1005.

ANNEX I

Annex I

Stock solutions

Solutions for detection of acid phosphatase activity

Pararosanilin-HCL Stock

- Pararosanilin 1g (Sigma P3750), CI 42500)
- Distilled water 20ml
- HCl Conc 5ml

The pararosanilin was dissolved in distilled water and the hydrochloric acid added slowly. The solution was heated gently, cooled, filtered and stored in aliquots in a refrigerator.

Sodium Nitrite

- Sodium nitrite 2g
- Distilled water 50ml

This solution was prepared and immediately separated into 0.4ml aliquots and stored at -30°C.

Veronal-Acetate Buffer Stock

- Sodium Acetate ($3H_20$) 3.88g
- Sodium Barbitone 5.88g
- Distilled water 200ml

Naphthol ASBI Phosphate Stock

- Naphthol ASBI Phosphate 50mg
- Dimethyl formamide 5ml

This solution is separated into 0.5ml aliquots and stored at -30°C.

Incubating solution

- Pararosanilin - HCL 0.4ml
- Sodium nitrite (40mg/ml) 0.4ml

The pararosanilin was added drop by drop to the thawed sodium nitrite, shaking well after each addition until the solution became corn-colored. After prepared this solution was kept in ice.

- Naphthol ASBI phosphate 0.5ml
- Veronal Acetate Buffer Stock 2.5ml
- Distilled water 6.5ml

These were well mixed together and then the pararosanilin/sodium nitrite solution was added. After adjusting the pH to 4.7-5.0, the solution was filtered and used immediately.

Solutions for detection of alkaline phosphatase activity

Incubating Medium

- Naphtol AS-MX phosphate, di-sodium salt (Sigma) - 5 mg
- N,N - dimethylformamide - 0.25 ml
- Fast Blue BB (Sigma) - 30 mg
- Distilled Water - 25 ml
- 0.2M Tris (pH 8.9) - 25 ml
- 10% Magnesium Sulfate Solution. - 2 drops

The solution was prepared freshly and filtered before use.

Nuclear Fast Red

- To 0.2 gm of Nuclear Fast Red it was added 200 ml of boiling 0.5% aluminum sulfate solution and kept boiling for 5 - 10 minutes
- The solution was allowed to cool and filtered before use.

Solutions for whole mount double staining of the skeleton

<u>Ethanol solutions</u>:

- 100%; 96%; 90%; 70%; 50%; 30%; 15%, with distilled water.
- 50 ml of 100% ethanol to which is added 50µl of 1% KOH

Potassium hydroxide (KOH)

- 5 g KOH
- 100 ml distilled water.

Caution: The solution reaction is exothermic.

Alizarin red stock solution

- 100 mg Alizarin red S (Sigma C.I. 58005)
- Dissolve in 100 ml of 1% KOH.

The stock solution was stirred to dissolve and paper filtered prior to use or storage.

Alcian blue 8GX solution

- 10 mg Alcian blue 8GX (Sigma. C.I. 74240)
- 70 ml Absolute ethanol
- 30 ml glacial acetic acid.

The solution (final pH < 1.0) was filtered before use or storage. The dye must be discarded when the pH ≥ 2.5. The solution can be stored for a maximum of 3 months at 4°C.

Preparation of slides for histology and in situ hybridization

TESPA coating

- Wash slides O/N in a 70% ethanol / 10% HCL if they are not clean.
- 2 h in several changes of distilled water
- Fast immersion in absolute ethanol
- 30 s in a solution of 2% TESPA (3-aminopropyltriethoxysilane, Sigma) in acetone
- 2 fast immersions in acetone
- Wash briefly in distilled water

Dry at 37°C and store in slide boxes at 4°C.

Poly-L-lysine coating

- Wash slides O/N in a 70% ethanol / 10% HCL if they are not clean.
- 2 h in several changes of distilled water
- Immerse the slides in a 0.1 % poly-L-lysine solution in sterile water for 15 min.
- Wash twice in absolute ethanol and

Dry at 37°C and store in slide boxes.

Electrophoresis of DNA and RNA

Solutions

50X TAE (per liter)

- 175 g NaCl
- 57.1 ml glacial acetic acid
- 100 ml 0.5 M EDTA (pH 8.0)

10X MOPS (per liter)

- 41.6 g MOPS (3-[N-Morpholino] propanesulphonic acid)
- 4.1 g Na acetate anhydrous
- 12.5 ml 0.4 M EDTA (pH 8.0)
- Bring volume to 900 ml and adjust pH to 7.0 with NaOH. Adjust volume to 1 liter and filter by 0.22 μm filter. Store protected from light.

2% agarose gel preparation (100 ml)

- Prepare a gel adding by the appropriate amount of agarose to 100 ml of 1x TAE buffer to have a final concentration of 1-2% as desired.
- Heat on a microwaves until completely dissolved
- Cool under moderate agitation
- Add ethidium bromide immediately before pouring
- Load DNA samples with 10% 6x loading dye and run in 1x TAE at 60-100 volts to fractionate the DNA.

Southern blot protocol

Solutions

Denaturing Solution

- 1.5 M NaCl
- 0.5 M NaOH

Neutralizing Solution

- 1.5 M NaCl

- 1.0 M Tris base
- pH to 8.0 with HCl (conc.)

20X SSC

- 3.0 M NaCl
- 0.5 M Na Citrate
- Adjust pH to 7.2.

Buffers and stock solutions

DEPC treated water (RNase free water)

- Add 1 ml DEPC (dy-ethil pirocarbonate) to 999 ml ddH_2O
- Stir over night until all DEPC is dissolved
- Autoclave to neutralize the DEPC.

TE (pH 8.0)

- 0.1 M Tris
- 1 mM EDTA

10x PBS (pH 7.4)

- 1.5M NaCl
- 3M KCl
- 40 mM $Na_2HPO_4.12H_2O$
- 20 mM KH_2PO_4
- Dissolve in 950 ml ddH_2O, adjust pH to7.4 and complete volume to 1 liter.
- Autoclave.

4% paraformaldehyde (PFA), pH 7.4

- Weigh 40 g paraformaldehyde into a sterile bottle
- Add 900 ml sterile water and stir on a heated plate until the solution clear
- Allow the solution to cool and add 100 ml of 10x PBS
- Store at 4°C, protected from light.

ANNEX II

Submitted April 26, 1999, revised Nov. 1, 1999, accepted Nov. 2, 1999

Detection of Mineralized Structures in Early Stages of Development of Marine *Teleostei* Using a Modified Alcian Blue-Alizarin Red Double Staining Technique for Bone and Cartilage

Paulo J. Gavaia[1], Carmen Sarasquete[2] and M. Leonor Cancela

[1]*Center for Marine Sciences, CCMar, University of Algarve, Campus de Gambelas, 8000-810-Faro, Portugal, and* [2]*Institute of Marine Sciences of Andalucia, Spanish Council for Scientific Research, CSIC, Pol. Rio San Pedro s/n, Apdo. Oficial, 11510 Puerto Real (Cádiz), Spain*

ABSTRACT. We have developed a procedure for staining cartilage and bone in fish larvae as small as 2 mm (notochord length), for which standard alcian blue/alizarin red procedures did not give positive and/or consistent results. Small calcified structures only 100–200 μm in length can be clearly visualized. The method is suitable for both ontogenic studies during early stages of skeletal development in most marine fishes (e.g., *Sparus aurata* L., *Solea senegalensis* Kaup), whose larvae at hatching are often only a few millimeters long and for detecting skeletal abnormalities in small larvae. This procedure can also be used for specimens that have been preserved in 100% ethanol for up to two years.

Correspondence should be addressed to: M. Leonor Cancela, Ph.D., Associate Professor, Molecular Biology and Biotechnology, Center for Marine Sciences, University of Algarve—UCTRA, Campus de Gambelas, Faro 8000-810, Portugal. Tel: 351.289.800971, Fax: 351.289.818353, E-mail:lcancela@ualg.pt

BIOTECHNIC & HISTOCHEMISTRY © by Lippincott Williams & Wilkins, Inc.
1052-0295/98/079–84 Volume 75, Number 2

Key words: alcian blue, alizarin red, bone, cartilage, *Diplodus sp.*, *Halobatrachus didactilus*, larvae, skeleton, *Solea senegalensis*, *Sparus aurata*

Techniques using alcian blue to stain cartilage and alizarin red to stain bone have been described by several authors for many purposes and species (e.g., Inouye 1976, Wassersug 1976, Dingerkus and Uhler 1977, Kimmel and Trammel 1981, Taylor and Van Dyke 1985, Francillon and Meunier 1985, Parenti 1986, Klymkowsky and Hanken 1991, Webb and Byrd 1994, Song and Parenti 1995). This technique has been used for marine fish larvae both to study skeletal development and to detect skeletal abnormalities in red seabream *Pagrus major* (Matsuoka 1985), seabass *Dicentrarchus labrax* (Daoulas et al. 1991, Boglione et al. 1993, Marino et al. 1993) and in gilthead seabream *Sparus aurata* (Koumoundouros et al. 1997, Faustino and Power 1998). Because most marine teleostei larvae at hatching and during early developmental stages are only

a few millimeters long, with skeletal structures in the micron range, one of the problems encountered with this technique is the loss of calcified material and subsequent absence of staining with alizarin red. This is due to prior cartilage staining in acidic solution, which causes rapid demineralization of small structures undergoing calcification.

Alcian blue at low pH (0.5–1.0) has a high affinity for sulfated mucopolysaccharides, which are major components of cartilage, thereby permanently staining these structures. At higher pH (≥ 2.5), however, alcian blue looses its specificity for sulfated mucopolysaccharides. On the other hand, alizarin red binds calcium and stains bone and other calcified structures in alkaline media (Pearse 1985, Kiernan 1990).

We describe here several improvements to previously described techniques, and these were used to double stain cartilage and bone in larvae and juveniles of marine teleost fishes such as sole (*Solea senegalensis*), gilthead seabream (*Sparus aurata*), white seabream (*Diplodus sp.*) and toadfish (*Halobatrachus didactylus*, Schneider) and to detect mineralization in 2.6 mm recently hatched larvae.

MATERIALS AND METHODS

For this study, we used larvae and juveniles of marine teleost fish currently used in our Center for Marine Sciences including sole (*Solea senegalensis*), gilthead seabream (*Sparus aurata*), white seabream (*Diplodus sp.*) and toadfish (*Halobatrachus didactylus*). Specimen sizes ranged from 2.6 mm for larvae of *S. aurata* and *S. senegalensis* to 78 mm for juveniles. All reagents were purchased from Sigma Chemical Co. Madrid, Spain.

Stock Solutions

Fixative. 4% formalin buffered to pH 7.2–7.4 with 0.1 M phosphate buffer.

TBST. 50 mM Tris, pH 7.4; 150 mM NaCl; 0.1% (v/v) Triton X-100.

Alcian blue 8GX solution. 10 mg Alcian blue 8GX (C. I. 74240), 70 ml absolute ethanol, 30 ml glacial acetic acid. The solution (final pH ≤ 1.0) was filtered before use or storage. The stock stain was discarded when its pH reached 2.5–3.0. The solution can be stored for a maximum of 3 months at 4 C.

Alizarin red S solution. One gram of alizarin red S (C.I. 58005) in 100 ml 0.5% KOH. The stock solution was filtered through paper prior to use of storage.

Ethanol solutions. 100, 96, 90, 70, 50, 30, and 15% with distilled water.

KOH. 0.5 to 2.0% in distilled water.

H_2O_2, 30.

0.5% KOH + Glycerol. Increasing glycerol baths 3:1, 1:1, 1:3.

Double Staining Procedure

Fixation. Specimens were anesthetized in 3-aminobenzoic acid ethyl ester (MS-222) (Sigma A5040), then fixed in buffered formalin prepared as described above. The samples were kept in the dark for 1–2 hr at room temperature or overnight at 4 C when working with larvae from 2.5 to 5.0 mm. When working with larger specimens, the fixation time was extended up to one week at room temperature to ensure proper fixation. Adequate times must be adjusted for each specimen. The container was gently shaken during fixation to avoid a decrease in pH around the specimens.

Washing. Larvae were washed for 3–4 min with TBST immediately after fixation followed by a 5 min wash in distilled water. This step was important for the elimination of residual fixative and for degreasing the tissues, which allows improved dye penetration and clearing.

Preservation. Museum specimens can be preserved in 70–100% ethanol and processed later for cartilage/bone staining, if desired.

Cartilage staining. Specimens were transferred directly from wash water to alcian blue solution. When using museum specimens, larvae were hydrated prior to staining through a decreasing alcohol se-

ries (see stock solutions). Larvae then were stained only long enough for alcian blue to penetrate the tissues. In our hands, larvae 3 mm long stained in 10 min while larvae 6 mm long required 20 min to incorporate the stain adequately.

Neutralization. Immediately after staining cartilage, specimens were transferred for a few minutes to an absolute ethanol bath containing freshly added 1% KOH (approximately 100 µl of 1% KOH in 100 ml ethanol) to neutralize remaining acidity within the tissues.

Maceration. Specimens were transferred to an absolute ethanol bath, hydrated through a decreasing alcohol series to distilled water, then placed in a 0.5–2.0% KOH bath until tissues started to clear. A few hours are usually required.

Bone staining. Specimens were placed in alizarin red staining solution for 30 min. The staining solution was prepared by adding enough Alizarin red stock solution to 1% KOH to turn it deep purple (approximately 1:50 dilution of alizarin red stock solution in 1% KOH).

Final clearing. Final clearing was achieved by incubating specimens at room temperature and with illumination in a bath of 1% KOH to which we added a drop of H_2O_2 if the specimen was strongly pigmented or opaque. The quantity of H_2O_2 must be very small (under 0.1% of total clearing solution) and specimens should be removed if bubbles start to form around them owing to oxidation of the tissues. If larvae become too soft, further clearing can be done in a 3:1 KOH:glycerol solution. The clearing time depends on the size, pigmentation and type of tissue and therefore must be optimized for each case. If clearing time is prolonged, dissociation of the tissues can occur.

Preservation. The stained and cleared specimens were moved through a series of KOH:glycerol baths to a final bath of absolute glycerol, where they were preserved. As described for stock solutions, the time in each bath depends on the time required for glycerol penetration into the sample; normally the specimens are ready when they sink. A few crystals of phenol were added to prevent microbial growth. If specimens are completely cleared before passage to glycerol, the KOH solution can be replaced with distilled water.

RESULTS AND DISCUSSION

The double staining procedure presented here has been used for samples of fish larvae (*Sparus aurata, Solea senegalensis, Diplodus sp, Halobatrachus didactylus*) with good reproducibility. The short fixation period (1–2 hr) was sufficient to preserve the samples without noticeable dissociation of the specimen tissues during staining and preservation. No differences in the visualization of calcified structures were observed between newly fixed and two-year-old museum specimens that had been stored for two years in 100% ethanol, indicating that no significant loss of stainable mineralized tissue occurs when samples are preserved as described above for up to two years. In our hands, structures stained with alcian blue did not lose quality for up to three years after processing, and it has been reported earlier that there is no change in this staining with time (Taylor and Van Dyke 1985). Alizarin red staining, however, has been reported to fade over time (Taylor and Van Dyke 1985, Klymkowsky and Hanken 1991), although it did not occur in our specimens even after three years of preservation after staining. Nevertheless, if fading occurs, the specimens can be brought back to KOH by reversing the preservation procedure described above and re-stained.

Figure 1 shows that our technique can reveal even slight amounts of cartilaginous and calcified tissues, as shown in the 2.6 mm (notochord length) larvae where the calcified *cleithrum* is approximately 260 µm long (Fig. 1a), and in the forming hypurals of a 5.5 mm (standard length) larva (Fig. 1b). Our method is also suitable for studying skeletal development since it allows

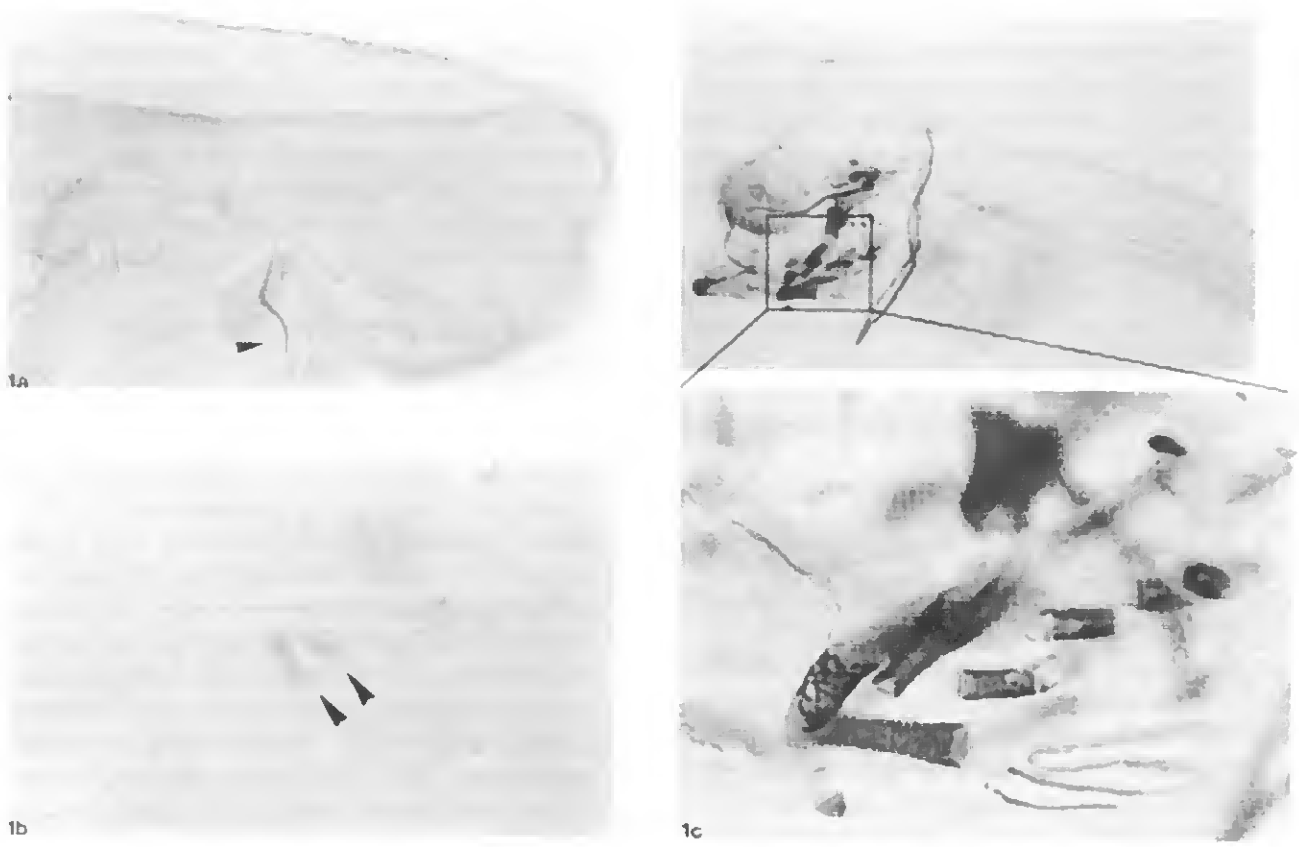

Fig. 1. *Solea senegalensis* larvae at two days after hatching (2.6 mm notochord length) with no visible cartilaginous or calcified structures except for the red stained parietal, calcified cleithrum, approximately 260 µm long in a median position between the head of the larvae (arrows). 100 ×. b) First cartilaginous hypurals appearing in the caudal region of an 8-day-old larva after hatching, 7.8 mm standard length. *Solea senegalensis* larvae (arrows). 200 ×. c) Nine days after hatching (8.4 mm standard length) showing the head structures undergoing calcification. 50 ×. Inset: detail of branchial arches undergoing calcification (ceb). 200 ×.

the detection of small structures undergoing mineralization such as the jaw apparatus and branchial arches of a 9-day-old sole larva (Fig. 1c, inset), and in small larvae undergoing calcification such as the seabream larva in Figs. 2a and the sole in Fig. 2b. In addition, our technique has also proved useful for early detection of skeletal malformations in very young larvae (Fig. 3).

The best results for cartilage staining were obtained at low pH. The specificity of alcian blue for sulfated mucopolysaccharides is greatest near pH 1.0 while at pH greater than 2.0 the dye stains mostly groups of mucopolysaccharides/glycoproteins (Pearse 1985). By contrast to alcian blue incorporated into soft tissues, however, which can be eliminated, dye incorporated into cartilage mucopolysaccharides cannot be washed out (Dingerkus and Uhler 1977).

Staining with alcian blue is the most critical step in this double staining technique because the acidity of the solution can rapidly demineralize small structures undergoing calcification, such as those observed in recently hatched fish larvae where their thickness may be only a few microns. The staining time in alcian blue is, therefore, a critical parameter because adequate dye penetration must be achieved without significant loss of mineralized structures. Staining times of 12–24 hr as proposed by Taylor and Van Dyke (1985) led to complete decalcification in our specimens, whereas 10–15 min were sufficient to stain 3–4 mm larvae adequately. The staining

2a

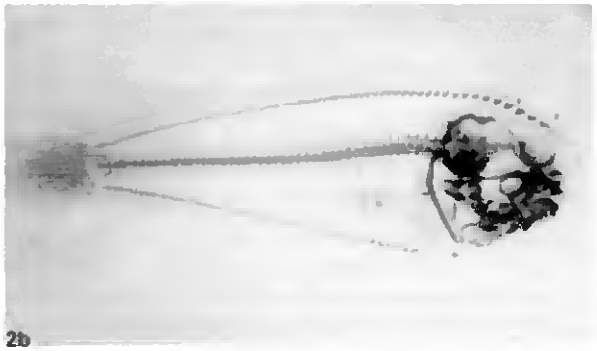

2b

Fig. 2a. *Sparus aurata* (7.8 mm standard length) undergoing calcification of the skeleton. Mineralized structures are stained red; cartilaginous structures are stained blue. 25 ×.
Fig. 2b. *Solea senegalensis*, 45 days after hatching (8.2 mm standard length) with an almost completely formed skeleton. Structures undergoing calcification are stained red; cartilaginous are stained blue. 20 ×.

time must be adjusted for each case by continuous observation of the specimens during alcian blue staining, taking care not to allow the specimens to dry. Furthermore, larvae dehydrated in 100% ethanol prior to staining with alcian blue, or those transferred to the staining solution directly from the fixative showed greater nonspecific staining than those that remained hydrated.

The use of a KOH:ethanol solution to neutralize alcian blue rather than KOH alone (Taylor and Van Dyke 1985) or 100% ethanol alone (Hanken and Wassersug 1981) helps prevent further decalcification by acidity remaining within the specimen without allowing precipitation of the dye. If the neutralization is accomplished using KOH alone, the specimens may show a large amount of nonspecific staining because alcian blue precipitates at pH > 6 and is retained within the sample, resulting in a more difficult and extended clearing process. On the other hand, using 100% ethanol washes removes the dye, but does not neutralize the samples.

The alcohol dehydration step that follows neutralization helps fix alcian blue to cartilage while dissolving excess dye in surrounding soft tissues, as suggested by Hanken and Wassersug (1981).

Clearing the tissues and elimination of alcian blue-stained soft tissues in larvae of the sizes described here is better achieved

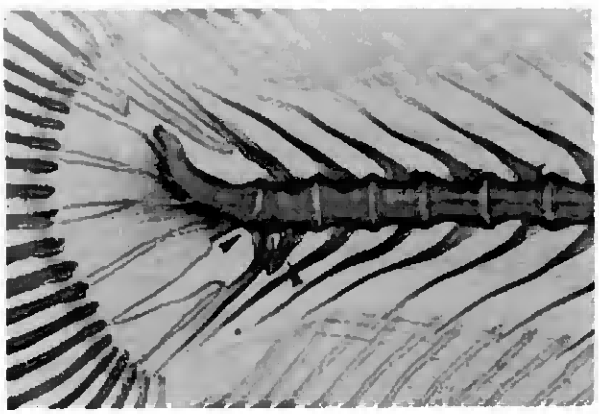

Fig. 3. Abnormal vertebra and processes (arrows) in the vertebral column of *Solea senegalensis* 45 days after hatching (9.8 mm standard length). 100 ×.

with KOH solution alone. The trypsin treatments described by Dingerkus and Uhler (1977), Hanken and Wassersug (1981) and Taylor and Van Dyke (1985) are not applicable to small larvae because they cause rapid dissociation and degradation of the tissues. These treatments remain suitable, however, for larger, more difficult to clear specimens for which they originally were described.

Our technique has produced good results for detecting both cartilage and bone in *Solea senegalensis*, *Sparus aurata*, *Diplodus sp.* and *Halobatrachus didactylus* larvae and juveniles, as small as 2.6 mm (notochord length); thus it is suitable for ontogenic studies of the skeleton in very early development stages (Figs. 1 and 2) and for the detection of skeletal abnormalities in small larvae (Fig. 3).

ACKNOWLEDGMENTS

This work was supported in part by Praxis Bia 469/94 and NATO SA.5.2/ CRG940-751. PJG was the recipient of a fellowship (BTL/2987/96) from the Portuguese Foundation for Science and Technology. The authors thank "Indigo- Inovações digitais, Lda" for expert assistance with image digitalization.

REFERENCES

Boglione, C., Martino, G., Bertolini, B., Rossi, A., Ferreri, F. and Cataudella, S. 1993. Larval and postlarval monitoring in seabass: morphological approach to evaluate finfish seed quality. Production, Environment and Quality. Bordeaux Aquaculture '92. European Aquaculture Society special publication 18: 1–16.

Daoulas, Ch., Economou, N. A., and Bantavas, I. 1991. Osteological abnormalities in laboratory reared sea-bass (*Dicentrachus labrax*) fingerlings. Aquaculture 97: 169–180.

Dingerkus, G., and Uhler, L. D. 1977. Enzyme clearing of alcian blue stained whole small vertebrates for demonstration of cartilage. Stain Technol. 52: 229-232.

Faustino, M. and Power, D. M. 1998. Development of osteological structures in the sea bream: vertebral column and fin complex. J. Fish Biol. 52: 11–22.

Francillon, H. and Meunier, F. J. 1985. Conservation et présentation des préparations colorées au bleu alcian et a l'alizarine. Cybium 9: 121-126.

Hanken, J. and Wassersug, R. 1981. A new double stain technique reveals the nature of the hard tissues. Visible Skeleton 16: 22–44.

Inouye, M. 1976. Differential staining of cartilage and bone in fetal mouse skeleton by alcian blue and alizarin red. S. Congen. Anom. 16: 171–173.

Kiernan, J. A. 1990. *Histological & Histochemical Methods: Theory and Practice*. 2nd ed. Pergamon press. Oxford. pp. 170–197.

Kimmel, C. A. and Trammell, C. 1981. A rapid procedure for routine double staining of cartilage and bone in fetal and adult animals. Stain Technol. 56: 271–273.

Klymkowsky, M. W. and Hanken, J. 1991. Whole mount staining of *Xenopus* and other vertebrates. Methods Cell Biol. 36: 419–441.

Koumoundouros, G., Gagliardi, F., Divanach, P., Boglione, C., Cataudella, S. and Kentouri, M. 1997. Normal and abnormal osteological development of caudal fin in *Sparus aurata* L. fry. Aquaculture 149: 215–226.

Marino, G., Boglione, C., Bertolini, B., Rossi, A., Ferreri, F. and Cataudella, S. 1993. Observations on development and anomalies in the appendicular skeleton of seabass, *Dicentrarchus labrax* L. 1758, larvae and juveniles. Aquacult. Fish. Manage. 24: 445–456.

Martínez, I., Alvariz, R., Herraez, I. and Herraéz, P. 1992. Skeletal malformation in hatchery reared *Rana perezi* tadpoles. Anat. Rec. 233: 314–320.

Matsuoka, M. 1985. Osteological development in the red sea bream, *Pagrus major*, Jpn. J. Ichthol. 32: 35–51.

Parenti, L. R. 1986. The phylogenetic significance of bone types in euteleost fishes. Zool. J. LINN. SOC. 87(1):37–51.

Pearse, A. G. E. 1985. *Histochemistry: Theoretical and Applied*. Vol 2. *Analytical Technology*. 4th ed., Churchill-Livingstone, Edinburgh. pp. 441-1055.

Song, J. and Parenti, L. R. 1995. Clearing and staining whole fish specimens for simultaneous demonstration of bone, cartilage and nerves. Copeia 1: 114–118.

Taylor, W. R. and Van Dyke, G. C. 1985. Revised procedures for staining and clearing small fishes and other vertebrates for bone and cartilage study. Cybium 9: 107–119.

Wassersug, R. J. 1976. A procedure for differential staining of cartilage and bone in whole formalin-fixed vertebrates. Stain Technol. 51: 131–134.

Webb, G. N. and Byrd, R. A. 1994. Simultaneous differential staining of cartilage and bone in rodent fetuses: an alcian blue and alizarin red S procedure without glacial acetic acid. Biotechnic & Histochem. 69: 181–185.

ELSEVIER

Aquaculture 211 (2002) 305–323

Aquaculture

www.elsevier.com/locate/aqua-online

Osteological development and abnormalities of the vertebral column and caudal skeleton in larval and juvenile stages of hatchery-reared Senegal sole (*Solea senegalensis*)

P.J. Gavaia, M.T. Dinis, M.L. Cancela*

Center for Marine Sciences—CCMAR, University of Algarve, Campus de Gambelas 8000-810, Faro, Portugal

Received 26 July 2001; received in revised form 9 April 2002; accepted 9 April 2002

Abstract

The Senegal sole is a species recently adapted to aquaculture for which little information on larval development is available. This study was designed to describe normal skeletal development and the occurrence of skeletal malformations in Senegal sole reared in captivity. Eggs were collected from natural spawning, incubated until hatching and larvae reared to the juvenile stage in a closed recirculating system. Samples were collected throughout development at regular intervals from hatching to fully formed juveniles. Specimens were stained with alcian blue and alizarin red and observed for skeletal development and detection of anomalies. A high number of malformations were detected, both in the caudal complex and the vertebral column. About 44% of the individuals observed showed at least one malformation and the highest occurrence of deformities was observed in the caudal region and in the vertebral column. Accordingly, 28% of the total deformities identified in this study were detected at those sites and in adjacent arches and spines. The causes were not identified in this study, but the high incidence of malformations may reflect culture problems due to rearing and/or feeding conditions that affect skeletal development.

Keywords: *Solea senegalensis*; Larvae; Development; Skeleton; Deformities

1. Introduction

The Senegal sole is a marine species recently adapted to aquaculture with high commercial value in the south of Portugal and Spain and in the Mediterranean basin.

* Corresponding author. Tel.: +351-289-800971; fax: +351-289-818353.
E-mail address: lcancela@ualg.pt (M.L. Cancela).

0044-8486/02/$ - see front matter
PII: S0044-8486(02)00167-9

Despite the interest in this species, only few studies have been reported on larval development and skeletal calcification (Dinis, 1986, 1992; Ribeiro et al., 1999; Gavaia et al., 2000a,b). There is no description of the normal skeletal morphology in the adult fish nor on the onset of these structures during Senegal sole development.

The quality of aquaculture-produced fish depends on organoleptic and morphological characteristics that are directly related to the quality of the fry and its diet (Dinis and Soares, 1993). In aquaculture, skeletal abnormalities are a serious economical problem, as they reduce the market value of produced fish by affecting their morphology and survival (Koumoundouros et al., 1997a). Since manual sorting is required to discard deformed individuals, there is also a negative effect on growth and conversion rates as well as in susceptibility to disease (Koumoundouros et al., 1997b; Boglione et al., 2001). High frequencies of deformities, often associated with reduced growth and viability, have been reported in hatchery-produced fish (Hilomen-Garcia, 1997; Kitajima et al., 1994) and may be caused by either genetic (Bengtsson et al., 1998) or external factors. The most probable causes seem to be the existence of unfavorable abiotic conditions (Polo et al., 1991; Pavlov, 1997; Pavlov and Moksness, 1997; Faustino and Power, 1999) but nutritional deficiencies (Estevez and Kanazawa, 1995; Takeuchi et al., 1995; Dedi et al., 1998), environmental factors (Boglione et al., 1993; Lindesjoo et al., 1994; Divanach et al., 1997; Haaparanta et al., 1997) and rearing conditions (Koumoundouros et al., 2001), have also been reported to play a role in this process. Previous studies suggest that malformations are induced in early stages during the embryonic and larval periods of life, although the causes and mechanisms responsible are not well understood (Daoulas et al., 1991; Koumoundouros et al., 1997a).

Several studies on skeletal deformities have been reported for larvae and juvenile European sea bass (Chatain, 1987; Daoulas et al., 1991; Boglione et al., 1993; Marino et al., 1993) and gilthead sea bream (Paperna, 1978; Andrades et al., 1994, 1996; Koumoundouros et al., 1997a,b; Faustino and Power, 1999) as well as for other commercially produced fish like fourhorn skulpin (Bengtsson et al., 1998), red sea bream, Japanese sea bass and amberjack (Kitajima et al., 1994) and the flat fish Japanese flounder (Hosoya and Kawamura, 1995, 1998). However, to be able to analyze the appearance of malformations throughout development, knowledge of the normal onset of skeletal structures was required (Kohno et al., 1983; Boglione et al., 1993; Marino et al., 1993; Kohno, 1997; Faustino and Power, 1998, 1999). In this work, we describe the normal vertebral and caudal skeleton of Senegal sole, as well as the most commonly observed skeletal deformities occurring in the early stages of development when reared under aquaculture conditions.

2. Materials and methods

2.1. Rearing conditions

Eggs were collected from natural spawning of a Senegal sole (*Solea senegalensis*) brood stock adapted to captivity in a closed recirculating system without water temper-

ature control, fed squid and polychaets. About 50 g of fertilized eggs (≈ 50000) were transferred to 80 l cylindroconical tanks in a closed recirculating system and incubated at a density of 350 eggs l^{-1} with continuous air supply and a 40 l/h water turnover. Incubation was done under the same environmental conditions of the broodstock tank. Hatching took place 36 to 48 h after spawning. The newly hatched larvae were maintained in the incubation tanks for larval rearing until eye migration was completed, and transferred to flat bottom tanks when benthic lifestyle was acquired. Light was controlled with fluorescent lamps, maintaining a 12:12 h light–dark photoperiod throughout the incubation stage and during larval and juvenile rearing periods. Temperatures were maintained between 16 and 18 °C throughout all the rearing stages. Developing larvae were fed with newly hatched *Artemia* nauplii from day 3 to day 10, 24 h metanauplii from day 11 to metamorphosis, and 48 h metanauplii until the end of the experiment. The metanauplii were enriched with the phytoplankton *Tetraselmis suesica* and *Isochrisys galbana*, clone T-Iso.

2.2. Sample collection

Specimens were randomly collected throughout all the developmental period, from hatching through metamorphosis and up to juvenile stages. Ten specimens were collected every 2 days from hatching until day 30 after hatching (DAH) and then every 5 days until 75 DAH. One individual was also collected at 5 months. Individuals were anesthetized with 0.1% phenoxyethanol and fixed in phosphate buffered saline (PBS)-buffered 10% formalin (pH 7.4) for 24 h, rinsed in distilled water and washed in PBS (pH 7.4). Specimens were immediately processed or preserved in 100% ethanol for later use.

2.3. Histological procedures

Skeletal development in Senegal sole was followed from hatching to juvenile stages by detecting the appearance of calcified and cartilaginous structures through specific staining, following a previously described protocol (Gavaia et al., 2000a). Alcian Blue 8 GX (Sigma) was used to stain cartilage in blue followed by Alizarin Red S (Sigma) to stain calcified structures in red, in combination with KOH and peroxide treatment to increase transparency of soft tissues and allow clear observation. The stained specimens were preserved in glycerol with a crystal of phenol to prevent development of bacteria or fungi contamination.

2.4. Observation and measurements

Observations and photographs of individuals were made with a light microscope ZEISS equipped with a RICOH KR-10 M photographic camera or a WILD Heerbrugg M9A binocular microscope equipped with a Kodak photographic camera. Total length (Lt) was measured from the tip of the snout to the end of the caudal fin. Standard length (Lst) was measured from the tip of the snout to the end of the notochord before and during the urostyle flexion, and from the tip of the snout to the end of hypuralia after

notochord flexion. All lengths were measured to the nearest 0.05 mm with an ocular micrometer using a binocular microscope. The anatomical terminology relating to the skeletal structures followed that used by Hosoya and Kawamura (1995, 1998) to describe the axial skeleton of the Japanese flounder. In counting vertebrae, abdominal and caudal vertebrae were defined based on the presence of parapophyses or haemal spines, respectively. The urostyle was counted as a caudal vertebra. Drawings were based on digital photographs of stained individuals using the software Paint Shop Pro 7.02.

3. Results

In this study, 179 individuals ranging from 3.1 to 59.2 mm standard length were stained for cartilage and bone, measured, observed and photographed.

3.1. General morphology of the adult Senegal sole

In the largest individual observed (5 months of age, 59.2 mm Lt), the vertebral and caudal skeleton were totally formed and mineralized, except for the distal extremities of the hypurals, epural and spines that articulated with fin rays, which remained cartilaginous (Fig. 1). No free uroneurals were observed. The structures that articulated with fin rays in the caudal complex (Fig. 2F) were typically five hypurals, one parhypural, one epural, one neural spine from the first preural centrum and two haemal spines from preural centrum 1 and 2. The hypurals 1–4 were fused to the urostyle by

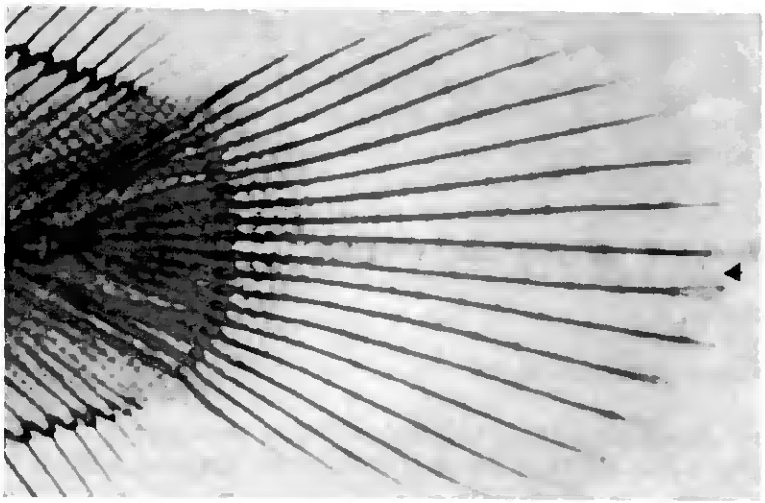

Fig. 1. Caudal fin complex of a juvenile sole with 59.2 mm total length. Full development of skeletal structures and scales has been achieved. The caudal fin is exclusively composed of soft rays and symmetrically divided by the lateral line scales (arrow head). The hypural plates are fused and present branching.

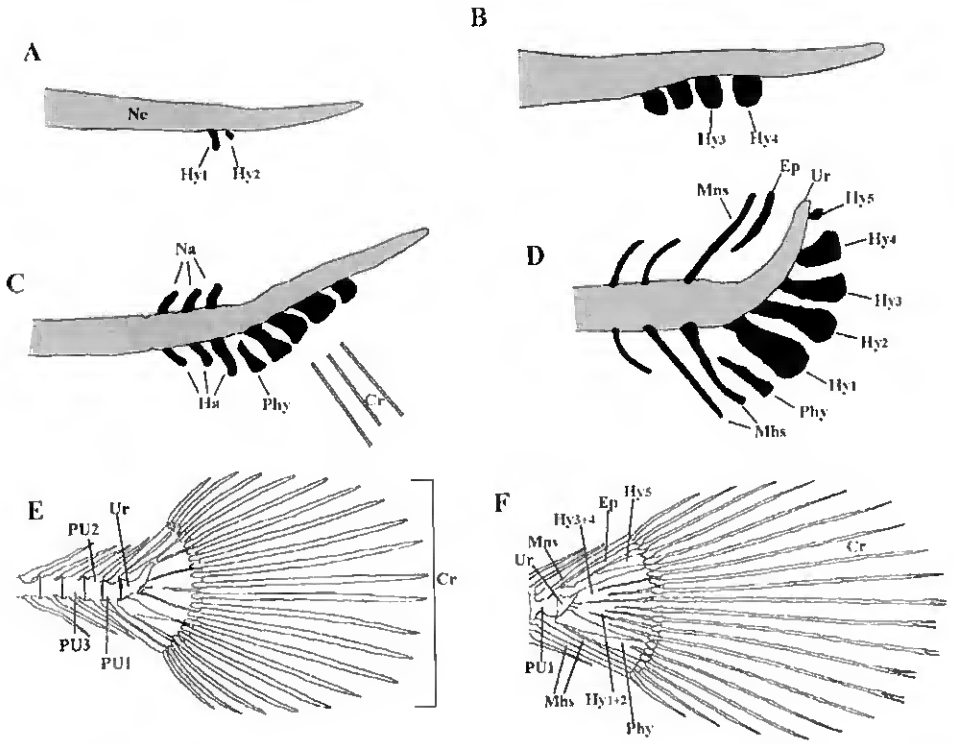

Fig. 2. Schematic representation of the caudal fin complex development in Senegal sole. Calcified structures are presented in white and cartilaginous structures in black. Notochord is shown in gray. (A) 13 DAH specimen (4.4 mm Lst). (B) 15 DAH specimen (4.55 mm Lst). (C) 18 DAH specimen (4.7 mm Lst). (D) 18 DAH specimen (5.6 mm Lst). (E) 34 DAH specimen (7.8 mm Lst). (F) 6-month-old juvenile specimen (59.2 mm Lst). Cr—Caudal fin rays; DAH—days after hatching; Ep—epural; Hy—hypural; Lst—standard length; Mhs—modified haemal spine; Mns—modified neural spine; Nc—notochord; Phy—parhypural; PU—preural vertebra; Ur—urostile.

their proximal bases, which in turn were fused with the base of each adjacent hypural, forming a unique plate (Figs. 1 and 2F). As clearly shown in Fig. 2F, hypural 5, parhypural and epural remained separated from the urostyle, while hypural plates 1–4 and parhypural presented branching through vertical ridges that extended from the distal to the proximal region, almost to the base of the plates. No branching was observed on hypural 5, epural or on the modified spines. The caudal fin had a total number of 20 soft rays. From these, the epural and the neural spines articulated with 3 rays, the hypural 5 with 2 rays, hypurals 1–4 with 10 rays and the parhypural and the haemal spines with 5 rays (Fig. 2F). The caudal fin was symmetrical, with 10 rays on each side of the lateral line (Fig. 1, arrowhead), which extended almost to the posterior tip of the caudal fin.

The vertebral column was composed of 45 vertebrae, separated in 8 abdominal and 37 caudal, including the urostyle (Fig. 3F). Each abdominal vertebra (Figs. 3F and 4A) was equipped dorsally with a neural arch and neural spine and ventrally with a pair of

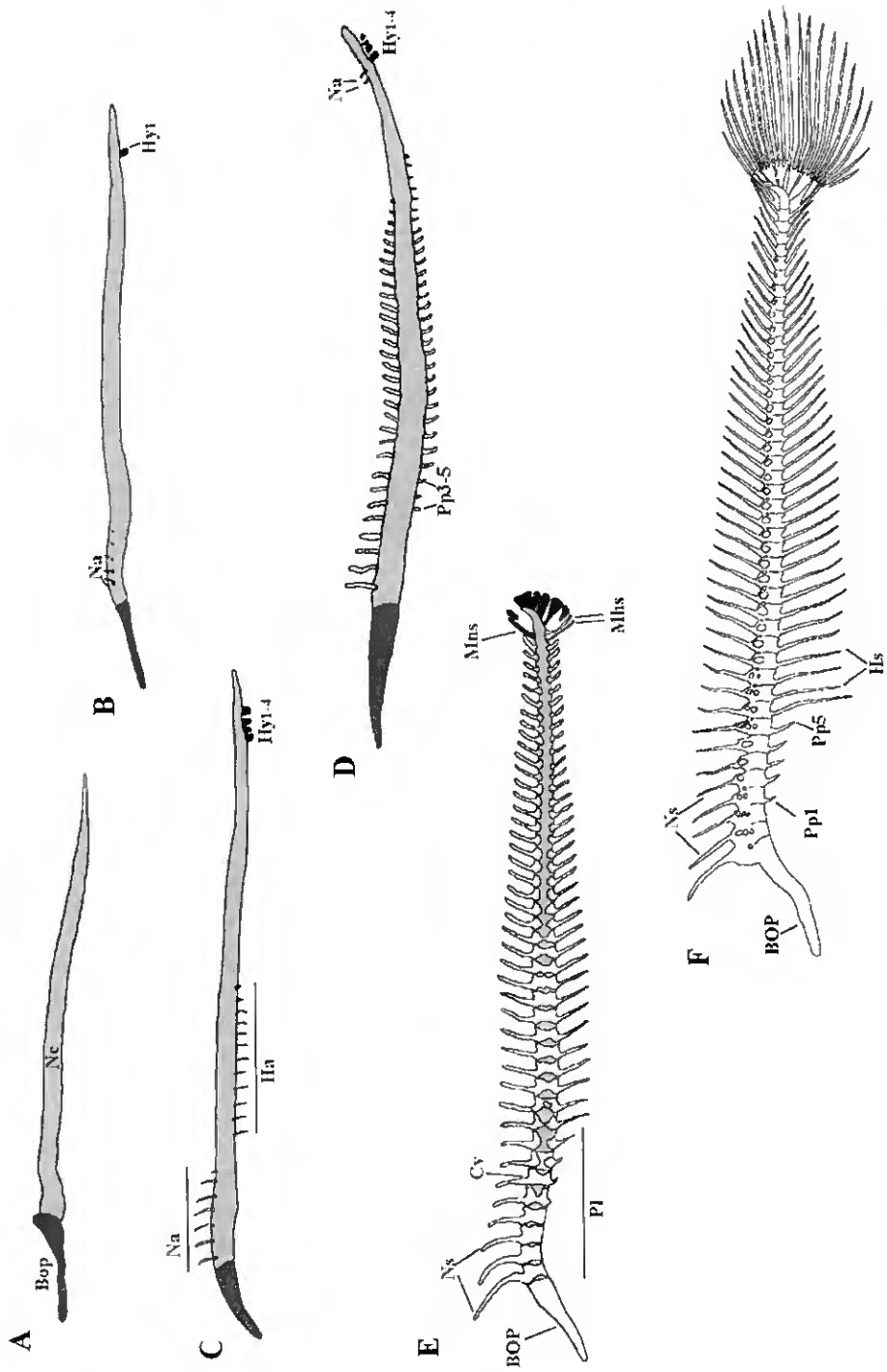
A
Bop
Nc
B
Na
Hy1
C
Na
Hy1-4
Ha
D
Na
Hy1-4
Pp3-5
E
Ns
BOP
Cv
Pl
Mns
Mls
F
Ns
BOP
Pp1
Pp5
Hs

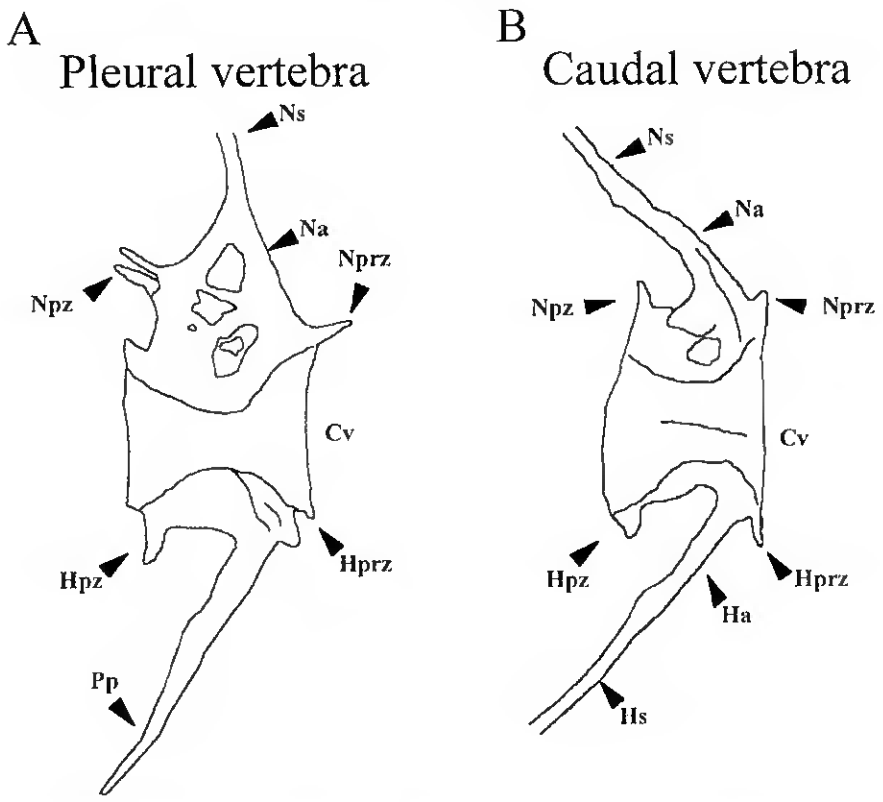

Fig. 4. Schematic representation of an abdominal vertebra (A) and a caudal vertebra (B) from a Senegal sole juvenile. Ha—haemal arch; Hpz—haemal poszigapophysis; Hprz—haemal prezigapophysis; Npz—neural poszigapophysis; Nprz—neural prezigapophysis. For other abbreviations, see Fig. 3.

parapophysis from the fourth to the eighth vertebrae. The first abdominal vertebra was articulated with the basioccypital articulatory process that connects the vertebral column to the skull (Fig. 3). The first five neural spines were generally thicker than the others. The caudal vertebra (Fig. 4B) was equipped dorsally with a neural arch and neural spine and ventrally with a haemal arch and haemal spine. The neural spines of preural vertebrae 1 and 2 and the haemal spine of the first preural vertebra were elongated and modified to help support the caudal fin rays (Fig. 2F). Both abdominal and caudal vertebrae exhibited

Fig. 3. Schematic representation of the vertebral column development in Senegal sole. Calcified structures are presented in white and cartilaginous structures in black. Notochord is shown in gray. (A) 0 DAH larva (3.4 mm Lst). (B) 13 DAH Lst larva (4.3 mm Lst). (C) 15 DAH specimen (4.55 mm Lst). (D) 18 DAH specimen (4.7 mm Lst). (E) 18 DAH specimen (5.65 mm Lst). (F) 45 DAH specimen (8.3 mm Lst). Bop—basioccypital articulatory process; Cv—Vertebral centra; Hs—haemal spine; Pl—pleural vertebra; Pp—parapophysis; Na—neural arch; Ns—neural spine. For other abbreviations, see Fig. 2.

in the neural arch an anterior neural prezygapophysis and a posterior neural poszygapophysis. The haemal arches similarly exhibited an anterior haemal prezygapophysis and a posterior haemal poszygapophysis (Fig. 4).

3.2. Skeletal development

At the yolk sac and early larval stages, Senegal sole presented a straight notochord that extended for the entire length of the body, being the only visible support structure (Fig. 3A). At these early stages, the only fin structures present were the primordial marginal fin fold and the pectoral cartilaginous plates (results not shown). The caudal fin was the first to differentiate, followed by the formation of fin rays by intramembranous ossification. Development of vertebral column elements occurred in parallel with caudal fin structures and eye migration. By the time development of the vertebral column and formation of the caudal fin were completed, eye migration had also occurred.

Major morphological changes during metamorphosis imply acquisition of asymmetry and occur in parallel with changes in life style from pelagic to benthonic. These changes are (1) eye migration from left to right side and concomitant bending of the urostyle; (2) torsion of internal organs that starts during the process of eye migration; this process initiated in larvae around 4.1 mm Lst and ended when larvae were approximately 8 mm Lst (circa 27 DAH).

3.2.1. Vertebral column development

Vertebral column was formed by the vertebral centra, the neural and haemal arches and spines, the parapophyses and the ventral ribs. They were all formed by intramembranous ossification except for the arches and spines of the four preural centra, which appeared initially as cartilaginous structures and calcified by endochondral ossification. No vertebral elements were observed at hatching and in early stages of development, where the notochord was the only axial suspension structure present (Fig. 3A).

The first elements of the vertebral column to be observed were neural arches 2–6 in the first abdominal vertebrae of a 4.3 mm Lst larvae (Fig. 3B), at 13 DAH. Arch development initiated with two buds formed latero-dorsally by intramembranous ossification on each side of the notochord. The buds elongated dorsally until they joined together forming the arch (Fig. 3B). After the arch was formed, the spine also appeared by intramembranous ossification and elongated dorsally. Vertebral development continued *caudad* for all the remaining neural arches except for the first, which formed *cephalad*. Haemal arches also developed *caudad* as observed for neural arches.

The first haemal arches were observed in a 4.55 mm Lst larvae, showing neural arches 2–8 and haemal arches 1–12 (Fig. 3C). In an 18 DAH, 4.7 mm Lst specimen, 28 neural arches and 17 haemal arches were visible and the first neural arch was already completely formed (Fig. 3D). The development of the arches in caudal vertebrae was faster than in trunk vertebrae, where the arches were still not closed. The cartilaginous buds of the arches in preural vertebra were already present near the urostyle, which had not yet begun its bending upwards. Parapophyses 3–5 were visible on trunk centra at this stage (Fig.

3D). Calcification extended from the base of the arches, beginning to form the centra surrounding the notochord.

At 5.65 mm (Fig. 3E), the anterior vertebrae and arches were nearly formed with the notochord completely surrounded by calcified tissue, while in the posterior caudal vertebrae, the calcified tissue was starting to spread around the notochord from the site of insertion of the arches. The urostyle had started its upward bending, and was partially calcified. Only the modified arches and spines from preural vertebra 1 and 2 and the hypuralia were still present as cartilaginous structures.

In an 8.3 mm Lst 45 DAH individual, with metamorphosis and flexion of the urostyle completed, all vertebral elements were formed and calcified (Fig. 3F). The vertebral centra completely surrounded the notochord and the adjacent arches were all closed around the ventral aorta in the haemal side and around the nervous chord in the neural side. The arches exhibited a spine that formed in the median plan of the body, and elongated from the proximal to the distal region. The parazygapophyses were still forming and the characteristic holes in the neural arches were not yet visible in the posteriomost caudal vertebrae.

In larger animals, the vertebral elements and processes only increased in complexity and size, and the spines elongated distally. The first two neural spines in the pleural vertebrae increased in thickness compared to the other spines.

3.2.2. Caudal fin complex

The caudal elements were formed either by endochondral or by intramembranous ossification. The first group included the hypurals and epural, the preural arches and modified spines; the second group included the urostyle, the preural centra and the caudal fin rays (dermatotrichia).

Hypural 1 was the first visible element, appearing in a cartilaginous form at 13 DAH in preflexion larvae ranging in size from 4.3 to 4.65 mm Lst. It was followed by hypural 2 (Fig. 2A) at 4.4 mm Lst and hypural 3 at 4.45 mm Lst, circa 15 DAH. Hypural 4 appeared generally in larvae larger than 4.5 mm Lst, at 15 to 18 DAH (Fig. 2B). At this stage, the parhypural and the cartilaginous buds of the arches were visible. From the bases of these arches began to form the preural centra 1, 2 and 3, on each latero-dorsal face of the notochord, as seen in larvae with 4.7 mm Lst (Fig. 2C). At this stage, the upward flexion of the urostyle is initiated and the caudal rays started to form by intramembranous ossification within the primordial fin, in the area adjacent to the forming cartilaginous hypurals. Three ossifying rays that articulated with hypural 2 and 3 were visible, with mineralization starting in the median zone and extending to the extremities of the soft rays (Fig. 2C). The epural appeared during flexion of the urostyle, between 5.2 and 5.65 mm Lst. The hypural 5 was the last structure to appear ventrally, next to the tip of the notochord, in 18 DAH larvae larger than 5.5 mm Lst (Fig. 2D), when flexion of the urostyle was almost concluded.

At 6.6 mm Lst, all the caudal plates had increased in size and calcification was visible in the urostyle, extending to the proximal bases of hypurals 1–4, which began to fuse with the urostyle (results not shown). The neural and haemal arches of the preural vertebrae started to calcify, as well as the corresponding centrum, which gradually surrounded the notochord, starting from the area of insertion of the arches. At this stage, all fin rays were

already present, with alizarin red staining decreasing in intensity from the longer central to the shorter lateral rays. The caudal fin was still connected to the anal and dorsal fins by the primordial fin tissue (results not shown).

In a 7.8 mm Lst 34 DAH larvae (Fig. 2E), all the plates were largely ossified, with greater intensity of alizarin red staining observed in the proximal parts, and progressively decreasing in intensity towards the distal parts. The posterior end was still cartilaginous and thus stained in blue. Calcification also extended to the spines in the preural vertebrae. At this stage, the caudal rays were all ossified and articulated with hypuralia. The caudal fin was totally separated from the anal and dorsal fins.

At 12.8 mm Lst, all the caudal fin elements were totally calcified and hypurals 1–4 were fusing to the urostyle and to each other by their proximal bases (results not shown). At 19.8 mm Lst, vertical fissures had appeared in the posterior regions of the parhypural and hypural 4, indicating the beginning of branching. Hypurals 1–4 were totally fused to the urostyle (results not shown). At the juvenile stage, in a 59.1 mm Lst individual, hypurals 1–4 and parhypural showed one vertical fissure each, extending from the posterior to the median zone of the plates (Fig. 2F). At this stage, reduction of the urostyle size in proportion to all other structures and branching of the caudal fin rays were evident (Fig. 1).

3.3. Skeletal malformations

A large number of deformities were observed in the individuals used for this study, from larvae at the initial developmental stages to juveniles with fully developed skeletal structures. Incidence of malformations ranged from fish with only one small anomaly to fish displaying multiple deformities with different degrees of severity. From a total of 179 specimens observed, 79 (44%) presented at least one deformity in the skeletal structures analyzed. From these, more than half (25.6% of the individuals analyzed) showed only one

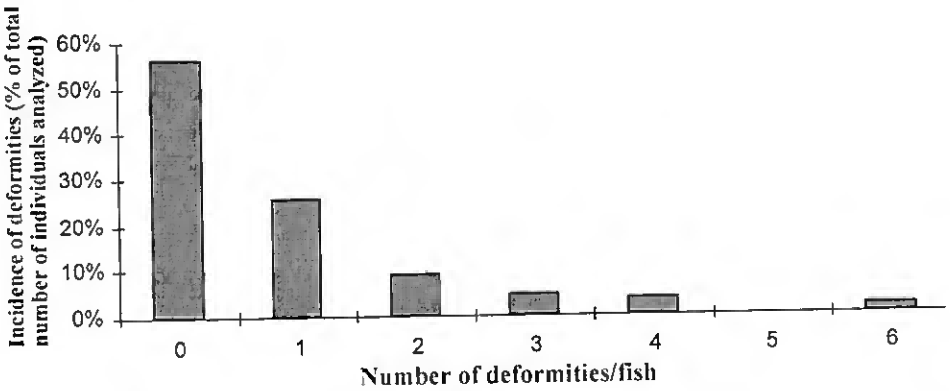

Fig. 5. Distribution of analyzed fish according to the number of deformities observed in each individual.

deformity while 33 specimens (18.4% of the individuals) presented multiple deformities (Fig. 5).

Malformations were divided into nine categories according to the place of incidence, as follows: trunk vertebra, caudal vertebra, arches, neural spines, haemal spines, parapophysis, caudal fin rays, hypurals and epural. The frequency of each type of deformity encountered in the total number of specimens observed is shown in Fig. 6. Caudal vertebra showed higher frequency of malformations (28% of the observed cases) but they also occurred in the neural (11%) and haemal spines (9%), trunk vertebra (7%), and vertebral arches (10%). In Fig. 7, some examples of the most frequent deformities observed are shown. Fig. 7A shows the caudal complex of a young larva (24 DPH) still presenting a large number of cartilaginous structures. It is visible the appearance of a supernumerary hypural (arrow) and the abnormal formation of the parhypural fused to hypurals 1 and 2, all still at a cartilaginous stage. The vertebral deformities observed were frequently the result of partial or total vertebral fusions (arrow in Fig. 7B,C) and asymmetries to the vertebral axis (Fig. 7D). In some cases, abnormal compressions in the vertebra were also observed. Structures related to the abnormal centra, like the arches, were also found to present malformations, either in their general conformation or by fusing to adjacent structures (Fig. 7C).

A schematic representation of the most common deformities encountered and described in this article is shown in Fig. 8. The skeletal changes are shown in a diagram representing the axial skeleton of a 45 DAH individual, as follows: (1) fusion of caudal fin rays by their proximal portion; (2) malformation of neural arch and spine of the preural vertebra 3; (3) fusion of hypurals 1–2, resulting in only one structure; (4) malformation of preural vertebra 2 with fusion of the correspondent haemal arch and spine with those of preural vertebra 3 (this type of deformity is also very common in preural vertebra 1 and 2); (5) malformation in a caudal vertebra partially fused with the adjacent vertebrae,

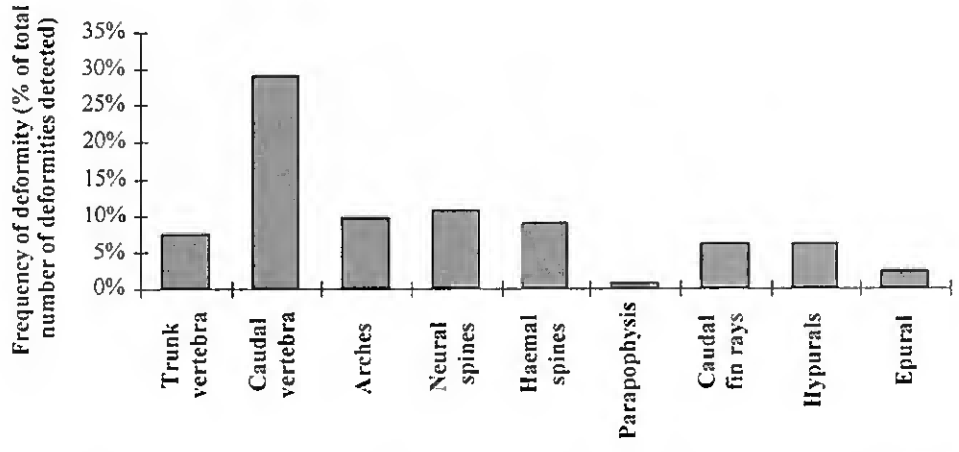

Fig. 6. Distribution of the abnormalities detected according to the affected structures. All the skeletal structures studied are affected by deformities, with special incidence in the caudal vertebra and associated structures.

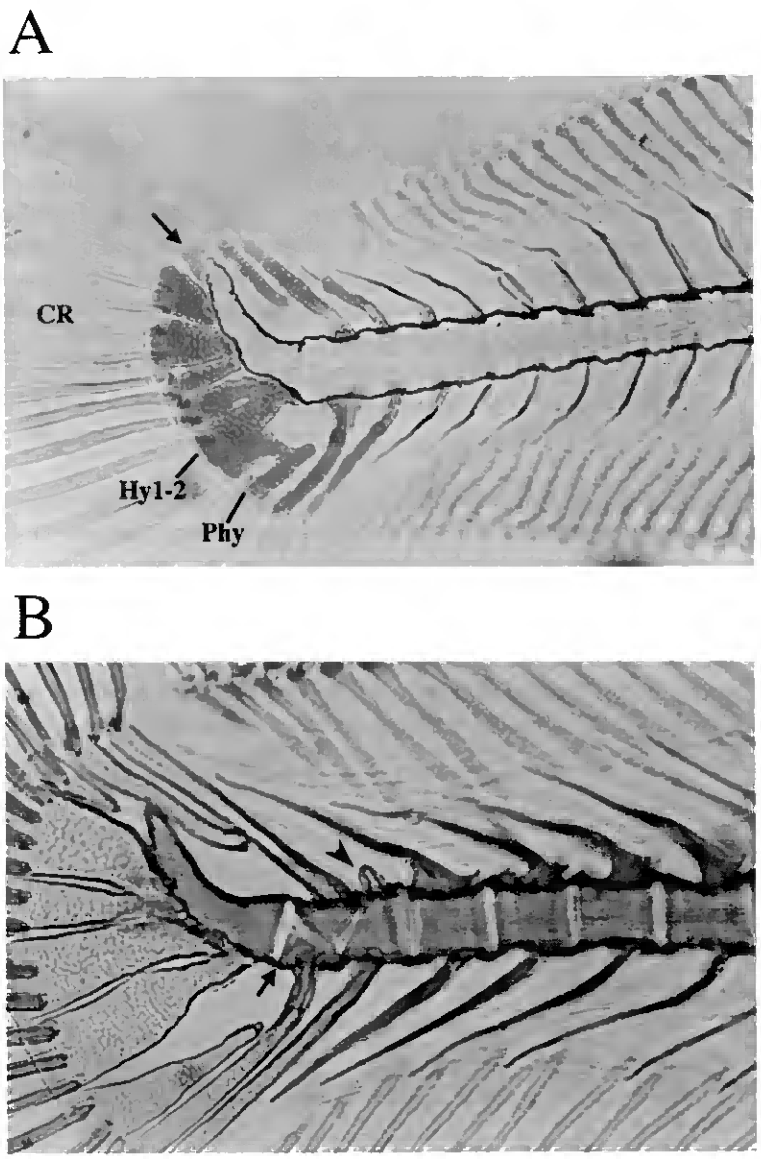

Fig. 7. Some examples of the most frequently observed malformations. (A) Fusion of the parhypural with the hypural plates 1 and 2, still in a cartilaginous form. Extra hypural plate near the tip of the urostyle (arrow). (B) Abnormal formation and partial fusion of the preural vertebrae 1–3 (arrow) with an atrophied neural arch (arrow head) forming in PU3. (C) Malformation of the pleural vertebrae and associated arches, spines and parapophysis. Partial fusion of pleural vertebrae 4–6 (arrow). (D) Severe abnormality affecting the caudal vertebrae and adjacent arches and spines and the symmetry of the vertebral column. For abbreviations, see Figs. 2 and 3.

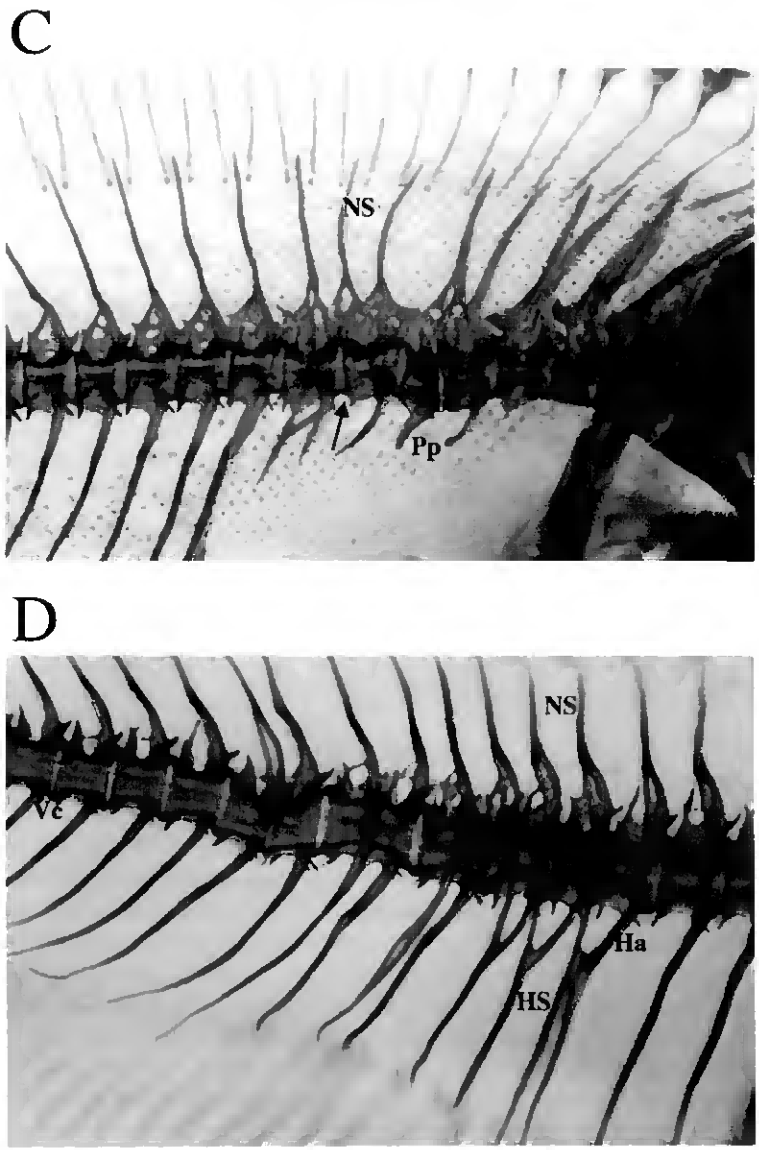

Fig. 7 (*continued*).

resulting in absence of the haemal arch and spine and with the corresponding neural arch malformed and fused with the arch of the following vertebra, exhibiting an atrophied neural spine; (6) fusion of the neural arches of two vertebras surrounding one that is deformed; (7) malformed caudal vertebra exhibiting no neural processes and an atrophied haemal spine; (8) compression of caudal vertebrae and of their corresponding processes (this type of deformity is sometimes associated with deviations from the normal axis as

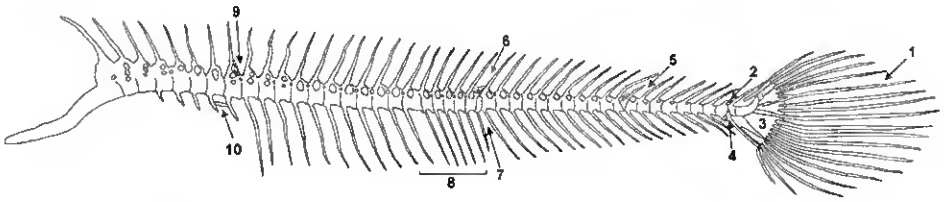

Fig. 8. Schematic representation of the axial skeleton of a 45 DAH individual, presenting the major types of deformities described in this work. (1) Fusion of the proximal portion of caudal fin rays. (2) Malformation of neural arch and spine of preural vertebra 3. (3) Fusion of hypurals 1–2. (4) Malformation of preural vertebra 2 with fusion of the haemal arches of preural vertebra 2–3, resulting in one spine only. (5) Malformation in caudal vertebra associated with partial fusion with adjacent vertebrae resulting in absence of the corresponding haemal arch and spine. The corresponding neural arch is malformed and fused with the arch of the following vertebra, exhibiting an atrophied neural spine. (6) Fusion of the neural arches of two adjacent vertebrae. (7) Abnormal caudal vertebra with atrophied haemal spine. (8) Compression in caudal vertebrae and corresponding processes. (9) Malformation in neural arch of the last pleural vertebra. (10) Abnormal presence of bony element connecting parapophysis.

shown in Fig. 7D); (9) malformation in the neural arch of the last pleural vertebra; (10) abnormal extra-numerary bony element connecting the parapophysis of the two last pleural vertebrae.

4. Discussion

In this work, the osteological development of the caudal complex and vertebral column in Senegal sole is described. In this species, we have previously shown that the first calcified structures to appear are the appendicular elements (cleithrum) at 2 DAH (Gavaia et al., 2000a). Development of both caudal complex and vertebral column begins at 12–13 DAH, accompanying the urostyle torsion and acquisition of asymmetry by migration of the left eye. At this stage, larvae progressively change to a benthonic life style. Similar observations were made in the Japanese flounder, where the flexion of the notochord is closely related to the development of hypuralia (Hosoya and Kawamura, 1998). This parallelism can be explained by the importance of the described structures in the swimming and feeding capabilities of the larvae, especially in early stages of their development as reported for other species like red sea bream, rabbit fish or Asian sea bass (Kohno et al., 1983, 1986, 1996). Knowledge of the normal pattern of development of skeletal structures is essential prior to identification of the factors responsible for the onset of skeletal deformities.

The caudal fin of Senegal sole is the first to develop, acquiring full meristic count after 6.1 mm Lst, followed by anal and dorsal and then paired fins. This same sequence of fin development has also been observed in the red sea bream (Kohno et al., 1983), the milkfish (Taki et al., 1987), the common dentex (Koumoundouros et al., 1999) and the Japanese flounder (Hosoya and Kawamura, 1998). In Senegal sole, there is a large variation in size and stage of development of larvae of the same age as can be seen in Figs. 1D,E and 3C,D. This occurrence has also been reported for the gilthead seabream (Faustino and Power, 1998). The caudal structure of the Senegal sole is less complex than in the majority of species already reported, lacking the uroneural processes visible in

some sparid species (Matsuoka, 1985; Taki et al., 1986, 1987; Koumoundouros et al., 1997a, 1999). In addition, only one epural is found in the Senegal sole, a finding common only to the yellowtail, with all other species studied to date presenting two or more epurals, including the pleuronectiform Japanese flounder (Hosoya and Kawamura, 1998).

The alizarin red-alcian blue double staining method for cartilage and bone allows the visualization of the entire skeleton throughout vertebrate development and the easy detection of any deformities that may occur. Similar techniques have been used to localize bone and cartilage in froglets (Martínez et al., 1992), fetal mice (Webb and Byrd, 1994), and larvae and juveniles from sea bass (Boglione et al., 1993; Marino et al., 1993) and gilthead sea bream (Faustino and Power, 1998; Gavaia et al., 2000a).

According to previous reports, the observation of deformities in wild specimens of teleost fish is rare (Hosoya and Kawamura, 1998) either because they are less abundant or due to decreased viability of the abnormal fish in their natural habitat. Nevertheless, skeletal malformations have been described in captured larval specimens of wild sea bass (Marino et al., 1993), gilthead sea bream (Boglione et al., 2001), common dentex (Koumoundouros et al., 2001) and Japanese flounder (Hosoya and Kawamura, 1995, 1998), revealing, in all cases, a significantly lower incidence of deformities, when compared to those observed in specimens of the same species reared in hatchery conditions. The meristic characteristics also presented a higher variability in hatchery-reared than in wild captured specimens (Boglione et al., 1993, 2001; Marino et al., 1993; Koumoundouros et al., 2001). These observations indicate that deviations to normal development are correlated to rearing conditions and may even be induced by them.

Our results show an overall incidence of deformities of 44% in hatchery-reared Senegal sole, a value that is comparable to those observed in species already well adapted to intensive aquaculture conditions (Table 1). Accordingly, in seedlings of the flatfish Japanese flounder reared in captivity, malformations such as increase of hypural branches, fused spines and central fusions have been detected with an incidence of 30–60% of the total number of malformations observed in the caudal complex (Hosoya and Kawamura, 1995, 1998). For the gilthead sea bream, samples from individuals reared under intensive culture conditions presented a frequency of deformities of up to 100% while under semi-intensive culture conditions, this frequency decreased to 55% (Boglione et al., 2001). In aquaculture-reared sea bass, a high number of deformities were also encountered in the axial skeleton and fins, with frequencies of incidence of up to 75% in the vertebrae and 45% in the fins. In contrast, for common dentex it was found that only 6% of the individuals presented deformities, and from these the caudal fin region was not more affected than other regions of the skeleton (Koumoundouros et al., 1999). The reason for such a discrepancy between species is not known and additional work is required in order to explain this fact.

Among the abnormalities observed in Senegal sole, the most common were vertebral fusions (Fig. 6), indicating that the development of these structures may be the most susceptible to rearing conditions in captivity. These deformities are among the most visible, since they can alter the shape and length of the fish depending on the severity and number of structures affected and consequently make it less attractive for the consumer. Nutritional factors such as levels of vitamin A and its precursors or of vitamin C in the diet have also been shown to affect the development of skeletal structures. Low levels of dietary vitamin C were implicated in the development of severe deformities in rainbow

Table 1
Axial skeleton deformities detected in other fish species

Affected area	Type of deformity	Species	References
Pleural vertebra	Fused vertebra	Sea bream	Boglione et al., 2001
		Sea bass	Boglione et al., 1993
		Japanese flounder	Dedi et al., 1995
		Rainbow trout	Madsen and Dalsgaard, 1999
	Shortening in vertebra	Sea bream	Boglione et al., 2001
		Sea bass	Boglione et al., 1993
		Japanese flounder	Dedi et al., 1995
		Rainbow trout	Madsen and Dalsgaard, 1999
		Atlantic salmon	Kvellestad et al., 2000
	Abnormal vertebra	Sea bream	Boglione et al., 2001
		Sea bass	Boglione et al., 1993
		Japanese flounder	Dedi et al., 1995
		Rainbow trout	Madsen and Dalsgaard, 1999
	Abnormal neural arches and spines	Sea bream	Boglione et al., 2001
		Sea bass	Boglione et al., 1993
	Abnormal parapophises	Sea bream	Boglione et al., 2001
		Sea bass	Boglione et al., 1993
Caudal vertebra	Fused vertebra	Sea bream	Boglione et al., 2001
		Sea bass	Boglione et al., 1993
		Japanese flounder	Dedi et al., 1995
		Rainbow trout	Madsen and Dalsgaard, 1999
	Shortening in vertebra	Sea bream	Boglione et al., 2001
		Sea bass	Boglione et al., 1993
		Japanese flounder	Dedi et al., 1995
		Rainbow trout	Madsen and Dalsgaard, 1999
		Atlantic salmon	Kvellestad et al., 2000
	Abnormal vertebra	Sea bream	Boglione et al., 2001
		Sea bass	Boglione et al., 1993
		Japanese flounder	Dedi et al., 1995
		Milkfish	Hilomen-Garcia, 1997
		Rainbow trout	Madsen and Dalsgaard, 1999
	Abnormal neural arches and spines	Sea bream	Boglione et al., 2001
		Sea bass	Boglione et al., 1993
	Abnormal haemal arches and spines	Sea bream	Boglione et al., 2001
		Sea bass	Boglione et al., 1993
Caudal fin	Fused preural vertebra	Sea bream	Boglione et al., 2001
		Japanese flounder	Dedi et al., 1998
		Rainbow trout	Madsen and Dalsgaard, 1999
	Abnormal preural vertebra	Sea bream	Boglione et al., 2001
		Japanese flounder	Dedi et al., 1998
		Rainbow trout	Madsen and Dalsgaard, 1999

Table 1 (*continued*)

Affected area	Type of deformity	Species	References
Caudal fin	Fused modified arches and spines	Sea bream	Boglione et al., 2001
		Japanese flounder	Dedi et al., 1998
	Abnormal hypurals	Sea bream	Boglione et al., 2001
		Japanese flounder	Dedi et al., 1998
	Fused elements of hypuralia	Sea bream	Boglione et al., 2001
		Japanese flounder	Dedi et al., 1998
	Supernumerary elements	Sea bream	Boglione et al., 2001
		Japanese flounder	Dedi et al., 1998
	Abnormal caudal fin rays	Sea bream	Boglione et al., 2001

trout (Madsen and Dalsgaard, 1999) while the number of malformations affecting the caudal region and vertebra of Japanese flounder larvae treated with vitamin A palmitate during metamorphosis were shown to increase with increasing dietary levels of vitamin A (Dedi et al., 1995, 1998). Similar effects of vitamin A over vertebral column elements were observed in turbot (Estevez and Kanazawa, 1995). Parasite infection has also been reported to be a possible factor in development of skeletal malformations (Taylor et al., 1994). Shortness of the vertebral column described in Atlantic salmon was suspected to be related to an infectious etiology (Kvellestad et al., 2000).

This work represents the first description of the skeletal structures in Senegal sole and their appearance during normal development. It provides therefore the basic knowledge required to easily identify the presence of skeletal malformations in this species, being of relevance for future studies. Since nearly half of the fishes observed had at least one deformity and given the very high commercial value of sole, it would be important to analyze the molecular events underlying the onset of such a high percentage of deformities when sole is reared in captivity. Establishment of both nutritional and abiotic parameters involved in the mechanisms leading to the appearance of these deformities must be determined in order to prevent a high incidence of malformations particularly under intensive culture conditions.

Acknowledgements

This work was supported in part by grants from the Portuguese Science and Technology Foundation (PRAXIS/BIA/469/94) and NATO/SA.5.2/CRG940751. PJG was the recipient of a fellowship (PRAXIS XXI/BD/19665/99) from the Portuguese Science and Technology Foundation.

References

Andrades, J.A., Becerra, J., Fernández-Llebrez, P., 1994. Skeletal deformities of the gilthead sea bream (*Sparus aurata*, L.): study of the subcommissural organ (SCO) and Reissner's fiber (RF). Ann. Anat. 176, 381–383.

Andrades, J.A., Becerra, J., Fernández-Llebrez, P., 1996. Skeletal deformities in larval, juvenile and adult stages of cultured gilthead sea bream (*Sparus aurata*, L.). Aquaculture 141, 1–11.

Bengtsson, Å., Bengtsson, B.E., Lithner, G., 1998. Vertebral defects in fourhorn sculpin, *Myoxocephalus quadricornis* L., exposed to heavy metal pollution in the Gulf of Bothnia. J. Fish Biol. 33, 517–529.

Boglione, C., Marino, G., Bertolini, B., Rossi, A., Ferreri, F., Cataudella, S., 1993. Larval and post larval monitoring in sea bass: morphological approach to evaluate finfish seed quality. In: Barnabé, G., Kestmont, P. (Eds.), Aquaculture 92. Production, Environment and Quality. Eur. Aquacult. Soc. Spec. Publ. 18, 189–204.

Boglione, C., Gagliardi, F., Scardi, M., Cataudella, S., 2001. Skeletal descriptors and quality assessment in larvae and post-larvae of wild-caught and hatchery-reared gilthead sea bream (*Sparus aurata* L. 1758). Aquaculture 192, 1–22.

Chatain, B., 1987. La vessie natatoire chez *Dicentrachus labrax* et *Sparus aurata*: II. Influence des anomalies de développement sur la croissance de la larve. Aquaculture 65, 175–181.

Daoulas, C.H., Economou, N.A., Bantavas, I., 1991. Osteological abnormalities in laboratory reared sea bass (*Dicentrachus labrax*) fingerlings. Aquaculture 97, 169–180.

Dedi, J., Takeuchi, T., Seikai, T., Watanabe, T., 1995. Hypervitaminosis and safe levels of vitamin A for larval flounder (*Paralicthys olivaceus*) fed *Artemia* nauplii. Aquaculture 133, 135–146.

Dedi, J., Takeuchi, T., Hosoya, K., Watanabe, T., Seikai, T., 1998. Effect of vitamin A levels in *Artemia* nauplii on the caudal skeleton formation of Japanese flounder *Paralicthys olivaceus*. Fish. Sci. 64, 344–345.

Dinis, M.T., 1986. Quatre soleidae de l'estuaire du Tage. Reproduction et croissance. Essai d'élevage de *S. senegalensis*, Kaup. Thèse de Doctorat des Sciences Naturelles, Université de Bretagne Occidentale.

Dinis, M.T., 1992. Aspects of the potential of *S. senegalensis* Kaup, for aquaculture: larval rearing and weaning to artificial diet. Aquac. Fish. Manage. 23, 515–520.

Dinis, M.T., Soares, F., 1993. Skeleton abnormalities in farmed fish. World aquaculture—from discovery to commercialization. World Aquac. Soc., Spec. Publ. 19, 349.

Divanach, P., Papandroulakis, N., Anastasiadis, P., Koumoundouros, G., Kentouri, M., 1997. Effect of water currents on the development of skeletal deformities in sea bass (*Dicentrarchus labrax* L.) with functional swimbladder during postlarval and nursery phase. Aquaculture 156, 145–155.

Estevez, A., Kanazawa, A., 1995. Effect of (n-3) PUFA and vitamin A *Artemia* enrichment on pigmentation success of turbot, *Scophthalmus maximus* (L). Aquac. Nutr. 1, 159–168.

Faustino, M., Power, D.M., 1998. Development of osteological structures in the sea bream: vertebral column and caudal fin complex. J. Fish Biol. 52, 11–22.

Faustino, M., Power, D.M., 1999. Development of the pectoral, pelvic, dorsal and anal fins in cultured sea bream. J. Fish Biol. 54, 1–17.

Gavaia, P.J., Sarasquete, M.C., Cancela, M.L., 2000a. Detection of mineralized structures in very early stages of development of marine teleostei using a modified Alcian blue-Alizarin red double staining technique for bone and cartilage. Biotech. Histochem. 75, 79–84.

Gavaia, P.J., Dinis, M.T., Cancela, M.L., 2000b. Skeletal development as an assessment criteria for larval *Solea senegalensis* (Kaup) quality. In: Flos, R., Cresswell, L. (Eds.), AQUA 2000—Responsible Aquaculture in the New Millennium. Eur. Aquacult. Soc. Spec. Publ. 28, 233.

Haaparanta, A., Valtonen, E.T., Hoffmann, R.W., 1997. Gill anomalies of perch and roach from four lakes differing in water quality. J. Fish Biol. 50, 575–591.

Hilomen-Garcia, G.V., 1997. Morphological abnormalities in hatchery-bred milkfish (*Chanos chanos*, Forsskal) fry and juveniles. Aquaculture 152, 55–166.

Hosoya, K., Kawamura, K., 1995. Osteological evaluation in artificial seedlings of *Paralichthys olivaceus* (Temminck and Schlegel). In: Keller, B., Park, P., McVey, J., Takayanagi, K., Hosoya, K. (Eds.), Interactions Between Cultured Species And Naturally Occurring Species In The Environment, vol. 24. Corpus Christi, Texas, pp. 107–114.

Hosoya, K., Kawamura, K., 1998. Skeletal formation and abnormalities in the caudal complex of the Japanese flounder, *Paralichthys olivaceus* (Temminck and Schlegel). Bull. Natl. Res. Inst. Fish. Sci. 12, 97–110.

Kitajima, C., Watanabe, T., Tsukashima, Y., Fujita, S., 1994. Lordotic deformation and abnormal development of swim bladders in some hatchery-bred *Physoclistous* fish in Japan. J. World Aquac. Soc. 25, 64–77.

Kohno, H., 1997. Osteological development of the caudal skeleton in the carangid, *Seriola lalandi*. Ichthyol. Res. 44, 219–221.

Kohno, H., Taki, Y., Ogasawara, Y., Shirojo, Y., Taketomi, M., Inoue, M., 1983. Development of swimming and feeding functions in larval *Pagrus major*. Jpn. J. Ichthyol. 30, 47–60.

Kohno, H., Hara, S., Gallego, A.B., Duray, M.N., Taki, Y., 1986. Morphological development of the swimming and feeding apparatus in larval rabbitfish, *Signatus guttatus*. In: Maclean, J.L., Dizon, L.B., Hosillos, L.V. (Eds.), The First Asian Fisheries Forum. Asian Fisheries Society, Manila, Philippines, pp. 173–178.

Kohno, H., Ordonio-Aguillar, R., Ohno, A., Taki, Y., 1996. Osteological development of the feeding apparatus in early stage larvae of the sea bass, *Lates calcarifer*. Ichthyol. Res. 43, 1–9.

Koumoundouros, G., Gagliardi, F., Divanach, P., Boglione, C., Cataudella, S., Kentouri, M., 1997a. Normal and abnormal osteological development of caudal fin in *Sparus aurata* L. fry. Aquaculture 149, 215–226.

Koumoundouros, G., Oran, G., Divanach, P., Stefanakis, S., Kentouri, M., 1997b. The opercular complex deformity in intensive gilthead sea bream *Sparus aurata* L. larviculture. Moment of appearance and description. Aquaculture 156, 165–177.

Koumoundouros, G., Divanach, P., Kentouri, M., 1999. Osteological development of the vertebral column and of the caudal complex in *Dentex dentex*. J. Fish Biol. 54, 424–436.

Koumoundouros, G., Divanach, P., Kentouri, M., 2001. The effect of rearing conditions on development of saddleback syndrome and caudal fin deformities in *Dentex dentex* (L.). Aquaculture 200, 285–304.

Kvellestad, A., Høie, S., Thorud, K., Tørud, B., Lyngøy, A., 2000. Platyspondyly and shortness of vertebral column in farmed Atlantic salmon *Salmo salar* in Norway-description and interpretation of pathologic changes. Dis. Aquat. Org. 39, 97–108.

Lindesjoo, E., Thulin, J., Bengtsson, B.E., Tjarnlund, U., 1994. Abnormalities of a gill cover bone, the operculum, in perch *Perca fluviatilis* from a pulp mill effluent area. Aquat. Toxicol. 28, 189–207.

Madsen, L., Dalsgaard, I., 1999. Vertebral column deformities in farmed rainbow trout (*Oncorhynchus mykiss*). Aquaculture 171, 41–48.

Marino, G., Boglione, C., Bertolini, B., Rossi, A., Ferreri, F., Cataudella, S., 1993. Observations on development and anomalies in the appendicular skeleton of sea bass, *Dicentrarchus labrax* L. 1758, larvae and juveniles. Aquac. Fish. Manage. 24, 445–456.

Martinez, I., Álvarez, R., Herraéz, I., Herraéz, P., 1992. Skeletal malformations in hatchery reared *Rana perezi* tadpoles. Anat. Rec. 233, 314–320.

Matsuoka, M., 1985. Osteological development in the red sea bream, *Pagrus major*. Jpn. J. Ichthyol. 32, 35–51.

Paperna, I., 1978. Swimbladder and skeletal deformations in hatchery bred *Sparus aurata*. J. Fish Biol. 12, 109–114.

Pavlov, D.A., 1997. Development of head skeleton and paired fin girdles in wolffish, *Anarhichas lupus*, at different temperature regimes. J. Ichthyol. 37, 294–303.

Pavlov, D.A., Moksness, E., 1997. Development of the axial skeleton in wolffish, *Anarhichas lupus* (Pisces, Anarhichadidae), at different temperatures. Environ. Biol. Fishes 49, 401–416.

Polo, A., Yufera, M., Pascual, E., 1991. Effects of temperature on egg and larval development of *Sparus aurata* L. Aquaculture 92, 367–375.

Ribeiro, L., Zambonino-Infante, J.L., Cahu, C., Dinis, M.T., 1999. Development of digestive enzymes in larvae of *Solea senegalensis*, Kaup 1858. Aquaculture 179, 465–473.

Takeuchi, T., Dedi, J., Ebisawa, C., Watanabe, T., Seikai, T., Hosoya, K., Nakazone, J.I., 1995. The effect of beta-carotene and vitamin A enriched *Artemia* nauplii on the malformation and color abnormality of larval Japanese flounder. Fish. Sci. 61, 141–148.

Taki, Y., Kohno, H., Hara, S., 1986. Early development of fin-suports and fin-rays in the Milkfish *Chanos chanos*. Jpn. J. Ichthyol. 32, 413–420.

Taki, Y., Kohno, H., Hara, S., 1987. Morphological aspects of the development swimming and feeding functions in the Milkfish *Chanos chanos*. Jpn. J. Ichthyol. 34, 198–208.

Taylor, L.H., Hall, B.K., Miyake, T., Cone, D.K., 1994. Ectopic ossicles associated with metacercariae of *Apophallus brevis* (Trematoda) in yellow perch, *Perca flavescens* (Teleostei): development and identification of bone and chondroid bone. Anat. Embryol. (Berl.) 190, 29–46.

Webb, G.N., Byrd, R.A., 1994. Simultaneous differential staining of cartilage and bone in rodent fetuses: an alcian blue and alizarin red S procedure without glacial acetic acid. Biotech. Histochem. 69, 181–185.

ELSEVIER

Bone 32 (2003) 201–210

BONE

www.elsevier.com/locate/bone

Matrix Gla protein gene expression and protein accumulation colocalize with cartilage distribution during development of the teleost fish *Sparus aurata*

J.P. Pinto,[1] N. Conceição,[1] P.J. Gavaia, and M.L. Cancela*

University of Algarve-CCMAR, 8005-139 Faro, Portugal

Received 20 August 2002; revised 30 October 2002; accepted 30 October 2002

Abstract

Matrix Gla protein (MGP) is a member of the family of extracellular mineral-binding Gla proteins, expressed in several tissues with high accumulation in bone and cartilage. Although the precise molecular mechanism of action of this protein remains unknown, all available evidence indicates that MGP plays a role as an inhibitor of mineralization. We investigated the sites of gene expression and protein accumulation of MGP throughout development of the bony fish *Sparus aurata*, by in situ hybridization, Northern and RT-PCR Southern hybridization, and immunohistochemistry. The results obtained were compared with the patterns of developmental appearance of cartilaginous and mineralized structures in this species, identified by histological techniques and by detection of mRNA presence and protein accumulation of osteocalcin (Bone Gla protein), a marker for osteoblasts known to accumulate in bone mineralized extracellular matrix. The expression of MGP mRNA was first detected at 2 days posthatching (dph) by Northern analysis, RT-PCR amplification, and in situ hybridization, and thereafter continuously detected at various levels of intensity, until 130 dph. In situ hybridization analysis performed in parallel with immunohistochemistry indicated that until ca. 45 dph, the MGP gene was highly expressed in a number of different tissues including skull, jaw, neural and hemal arches, and heart and the protein accumulated in cartilaginous tissues. At 85 dph, a stage when most skeletal structures are mineralized, MGP gene expression and protein accumulation were restricted to the remaining cartilaginous structures, whereas osteocalcin gene expression and protein accumulation were localized in most mineralized structures. MGP gene expression was also detected in heart and kidney, although in situ hybridization only detected MGP mRNA in heart, located in the arterial bulbus and not in the cardiac muscle. Our results are in agreement with those recently described for MGP localization in adult tissues of another teleost fish, as well as available data from higher vertebrates, strengthening the hypothesis of a conserved function for MGP from teleost fish to human, a period of more than 200 million years of evolution. In addition, *Sparus aurata*, a marine teleost fish routinely grown in captivity, appears to be a good model to further analyze MGP gene expression and regulation.

Keywords: Matrix Gla protein; Development; Bone and cartilage appearance; Osteocalcin; *Sparus aurata*

Introduction

Matrix Gla protein (MGP) is a 10-kDa secreted protein containing five residues of the vitamin K-dependent calcium-binding amino acid γ-carboxyglutamic acid (Gla) [1,2]. Recent evidence indicates that MGP functions as an inhibitor of mineralization [3–5] and is synthesized in vivo mainly in cartilage [6] and in the vascular system [7]. The presence of MGP mRNA in the wall of major arterial blood vessels, both in mammals [8] and in fish [8a] may contribute to its previous detection in a variety of soft tissues such as lung, heart, and kidney in mammals [9] and in amphibians [10].

The accumulation of MGP protein in mineralized bone and calcified cartilage seems to be due to its calcium-binding properties related to the presence of γ-carboxylated residues and greatly exceeds that of the soft tissues, which fail to accumulate MGP under normal conditions [9] but can do so when subjected to abnormal mineralization [5,11].

* Corresponding author. Fax: +351-289-818353.
E-mail address: lcancela@ualg.pt (M.L. Cancela).
[1] Both authors contributed equally to this work.

8756-3282/03/$ – see front matter
doi:10.1016/S8756-3282(02)00981-X

Following the purification of the MGP protein from a lower vertebrate and the subsequent cDNA and gene cloning [8a,10,12], we have shown that the primary sequence of the MGP protein and its gene structure have been highly conserved between lower and higher vertebrates. These results indicate that lower vertebrates are adequate models for studying the early events underlying MGP onset of gene expression and fish in particular represent an easy model system to follow gene expression and protein accumulation during development.

In this work we report the onset of MGP gene expression and protein accumulation during development of the marine fish *Sparus aurata* and relate its timing of appearance with the development of the skeletal structures, as assessed by histological techniques. A comparison between higher and lower vertebrates is established and some hypotheses are advanced concerning the function(s) of the protein in this species.

Materials and methods

1. Cloning of the Sparus MGP cDNA

1.1. Amplification and molecular cloning of a partial Sparus MGP cDNA

Total RNA was extracted from a *Sparus* (spp.) bone-derived cell line [12a], following established procedures [13]. One microgram of total RNA was reverse-transcribed at 42°C for 1 h, using M-MLV reverse transcriptase (GibcoBRL, Grand Island, NY), followed by polymerase chain reaction (PCR) amplification, using a forward primer (corvMGP3F, 5′-AGGCGTGCAGAGACCTGCGAG-3′) designed according to the *Argyrosomus regius* MGP cDNA sequence previously obtained (GenBank Accession No. AF334473) and a reverse universal adapter (5′-ACGCGTCGACCTCGAGATCGATG -3′). PCR was conducted for 30 cycles (1 cycle: 30 s at 94°C, 1 min at 60°C, and 1 min at 68°C), followed by a 10-min final extension at 68°C with *Taq* DNA polymerase (Promega). PCR products of the expected size were visualized following 1% agarose gel electrophoresis and ethidium bromide staining, excised from the gel, and eluted from the agarose slice using the CONCERT rapid gel extraction kit (GibcoBRL). Resulting DNA fragments were cloned into the pGEM-T-Easy vector (Promega, Madison, WI) and final identification was achieved by DNA sequence analysis of several clones by the dideoxy chain termination method [14].

1.2. Amplification of the 5′ end of the spMGP cDNA

Poly $A^{(+)}$ RNA was purified from 600 μg of total RNA extracted from a mixture of *Sparus* tissues (vertebra, heart, kidney, and branchial arches), using the QuickPrep Micro mRNA purification kit (Pharmacia Laboratories, Piscataway, NJ) The mRNA was used to obtain the 5′ end of spMGP cDNA by 5′-RACE PCR with the Marathon cDNA amplification kit (Clontech, Palo Allo, CA). Amplification of the 5′-RACE PCR products thus obtained was accomplished with Advantage cDNA polymerase mix (Clontech), using the AP1 oligo (Clontech, 5′-CCATCCTAATACGACTCACTATAGGGC-3′) and a specific reverse primer, MGP2R (5′-AAGCCGTGGCGATAGGCGTAGAAGC-3′), designed according to the partial spMGP cDNA sequence previously obtained. Amplification conditions were those suggested by the supplier. The resulting amplified DNA fragments were cloned in pGEM-T-Easy vector and further identified by DNA sequence analysis.

Two specific primers were then designed according to the sequence obtained, spanning from nucleotides 30 to 55 (spMGPcDNA1F) and from 414 to 442 (spMGP1R), respectively, and used to amplify by PCR (same conditions as used in 1.1) the complete spMGP cDNA coding region, which was later used as a probe for Northern and Southern blot hybridization.

2. Northern blot analysis

Total RNA was extracted from *Sparus* tissues (heart, branchial arches, kidney, and liver) and from *Sparus* embryos and whole larvae collected at different developmental stages [2, 5, 7, 9, and 18 days posthatching (dph)] and size-fractionated by electrophoresis on a 1.4% formaldehyde-containing agarose gel. The RNA in the gel was transferred onto N^+ Nylon membranes (Schleicher & Schuell, Keene, NH) by a capillary method [15] and prehybridized at 42°C in ULTRAhyb (Ambion, Austin, TX) solution for 2 h. A spMGP cDNA probe (spanning from nucleotides 30 to 442 of the spMGP mRNA) was labeled with [α-^{32}P]dCTP using the Prime-It II random primer labeling kit (Stratagene, La Jolla, CA) and separated from unincorporated nucleotides on a MicroSpin S-200 HR column (Pharmacia). The purified labeled probe was added to the prehybridization solution and incubated with the membrane overnight under the same conditions described for prehybridization. Blots were washed twice in 2× SSC [1× SSC is 150 mM NaCl, 15 mM sodium citrate (pH 7.0)], 0.1% SDS at 42°C for 5 min and twice in 0.1× SSC, 0.1% SDS at 42°C for 15 min, and a final wash was performed with 0.1× SSC, 0.1% SDS, for 30 min at 55°C. Autoradiography was performed with Kodak X-Omat AR film with two intensifying screens, at −80°C, for up to 1 week.

3. RT-PCR amplification of MGP message in developmental stages of Sparus and Southern hybridization

One microgram of total RNA, extracted from whole *Sparus* specimens from various developmental stages (1, 2, 3, 5, 7, 8, 10, 20, 27, 37, 47, 61, 82, 91, and 130 dph), was treated with RNase-free DNase I for 3 h (37°C) and reverse-transcribed using the same conditions described above. One-twentieth of each reaction was amplified by PCR, using two specific oli-

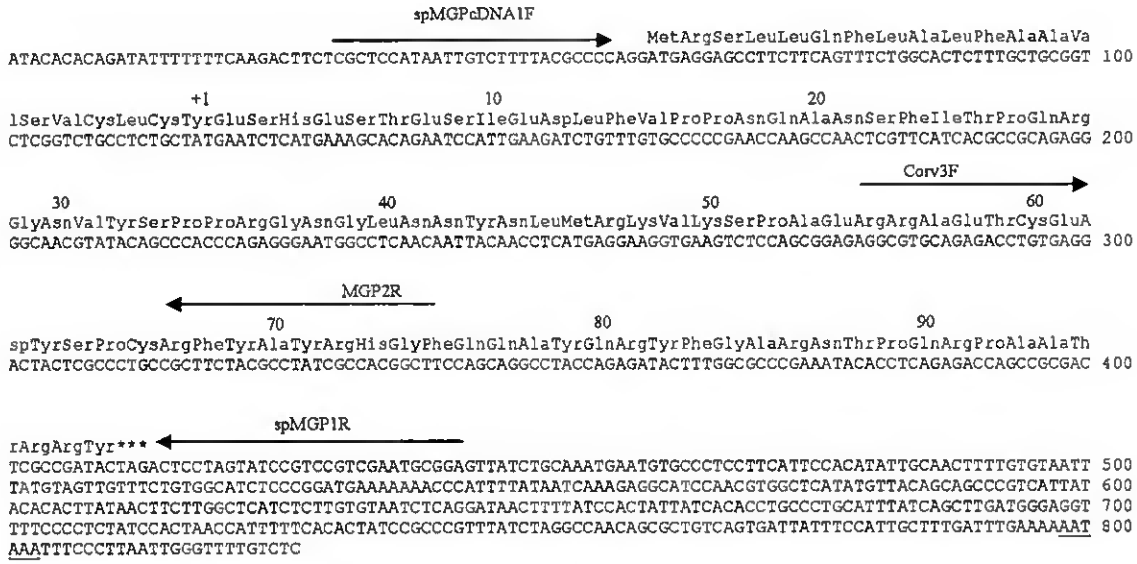

Fig. 1. Complete nucleotide sequence of the cDNA encoding *Sparus* MGP. Numerical positions in the nucleotide sequence are shown at the right end of the sequence. Localization of spMGPcDNA1F, Corv3F, MGP2R, and spMGP1R oligonucleotides are denoted by horizontal arrows. Amino acid residues are numbered according to residue 1 of the mature protein and are shown above the respective sequence. The stop codon is indicated by asterisks and the polyadenylation signal is underlined.

gonucleotide primers designed according to the spMGP cDNA sequence obtained previously (spMGPcDNA1F: 5′-TCGCTCCATAATTGTCTTTTACGCCC-3′ and spMGP1R: 5′-TCCGCATTCGACGGACGGATACTAGGAGT-3′). PCR was carried out with *Taq* DNA polymerase (Promega) for 20 cycles (one cycle: 30 s at 94°C, 1 min at 60°C, and 1 min at 68°C), followed by a final extension period of 12 min at 68°C. Positive and negative controls were made by amplifying, respectively, a clone of spMGP cDNA and a sample without DNA template with the same primers. As a control for the integrity of the RNA used for each sample amplification, *Sparus* β-actin was amplified from the same amount of RT reaction, using two specific primers designed according to the published *Sparus* β-actin cDNA (GenBank Accession No. X89920; forward primer: 5′-TTCCTCGGTATGGAGTCC-3′; reverse primer: 5′-GGACAGGGAGGCCAGGA-3′). Resulting PCR products were Southern transferred onto a N^+ Nylon membrane (Schleicher & Schuell) and prehybridized at 42°C for 2 h using UltraHyb solution (Ambion). A spMGP cDNA probe (spanning from nucleotides 30 to 442 of the spMGP mRNA) was labeled with [α-^{32}P]dCTP, as described above, and hybridization was performed in the same solution, for 15 h at 42°C. Membranes were washed first with 2× SSC, 0.1% SDS (2× 5 min, 42°C), followed by 0.1× SSC, 0.1% SDS (2× 15 min) at 42°C. Autoradiography was performed with Kodak X-Omat AR film and two intensifying screens at −80°C.

4. Animals and tissue preparation for histological analysis

Sparus specimens with ages ranging from 2 to 85 dph were collected and fixed with freshly made 4% paraformaldehyde in 0.1 M sodium phosphate buffer, at 4°C, from 24 h to 7 days, according to size. Specimens were then washed for 3 × 10 min in TBST buffer (50 mM Tris, pH 7.4; 150 mM NaCl; 0.1% Triton X-100) and stored in methanol at 4°C. Specimens ranging from 27 to 90 dph were rinsed with 10 mM PBS (pH 7.4) after fixation, decalcified in 15% EDTA in PBSS (10 mM PBS, 5% sucrose) for 3 to 7 days at 4°C, and rinsed in PBSS. Samples were dehydrated in increasing methanol concentrations and embedded in paraffin. Tissues were cut into longitudinal 5-μm-thick sections and mounted on slides precoated with 3-aminopropyltriethoxy-silane (Sigma, St. Louis, Mo), dried for 48 h at 42°C, and kept at room temperature (R/T) until use.

5. Alcian blue/alizarin red histological staining

Fixed specimens were hydrated by bathing in a 50% ethanol solution for 30 min (60 min for 90-dph specimens), in a 25% ethanol solution for 3 × 30 min and, finally, in ddH_2O for 3 × 30 min. Detection of cartilaginous and mineralized tissues was performed by histological staining with alcian blue 8GX (Sigma) and alizarin red S (Sigma), as previously described [16].

6. In situ hybridization

6.1 Probe preparation

Eight micrograms of the spMGP (from 30 to 442 bp; Fig. 1) and *Sparus* osteocalcin (spOC; from 322 to 587 bp [16]) cDNAs cloned in pGEM-T-Easy vector were linearized with restriction enzymes *Sal*I and *Apa*I (for spMGP) or with *Apa*I and *Pst*I (for spOC), in order to generate sense and antisense riboprobes, respectively. The resulting digestion

products were separated by electrophoresis in a 1% agarose gel, and the DNA fragments of interest excised from the gel and purified from agarose with the Qiaex II gel extraction kit (Qiagen, Chatsworth, CA). Linearized cDNAs were used to prepare digoxigenin-11-UTP-labeled single-strand RNA probes, with the DIG RNA labeling kit (Boehringer-Mannheim Biochemica, Mannheim, Germany), following the manufacturer's instructions.

6.2 Pretreatment of the sections

Sections were deparaffinized, rehydrated, digested with proteinase K (40 μg/ml in 1 M Tris, pH 7.4) for 15 min at R/T, washed for 3 min with PBS/Tween (PTW: 1× PBS + 0.1% Tween 20), and fixed in 4% formaldehyde (in PTW) for 30 min, followed by two 5-min washes with PTW.

6.3 Hybridization, washing, blocking, and immunodetection of hybridized probe

In situ hybridization was performed as described previously [16]. Photos were taken with a C-3030 Olympus digital camera coupled to a BX-41 Olympus microscope.

7. Immunohistochemistry

Antibodies were developed for fish (*Argyrosomus regius*) MGP (α*Ar*MGP) and osteocalcin (α*Ar*OC) as previously described [8a] and affinity-purified. Specificity of these antibodies for *Sparus* antigen was confirmed by Western blot (results not shown).

Sections were dewaxed in xylene and hydrated in a decreasing methanol series and endogenous phosphatases were blocked by incubation for 15 min in a 15% glacial acetic acid solution. Following two 10-min washes in Coons buffer [10 mM 5,5-diethylbarbituric acid sodium salt (Merck & Co., Rahway, NJ), 145 mM sodium chloride (Sigma), pH 7.4], sections were incubated for 30 min in Coons + 0.5% bovine serum albumin, at R/T, and overnight with α*Ar*OC or α*Ar*MGP antibodies, at R/T, in a moisture chamber saturated with 20× SSC. Sections were then washed twice in Coons, for 10 min, at R/T, and incubated with diluted (1:1000 in Coons) anti-rabbit IgG alkaline phosphatase conjugate (Sigma), for 2 h, at R/T. Antibody was removed by washing twice with Coons for 10 min, at R/T, and sites of antibody retention revealed by incubation with fast red TR/naphtol AS-MX (Sigma) in Tris buffer (Sigma). Mounting was performed in Aquatex aqueous mounting media (Merck & Co.). Photos were taken with a C-3030 Olympus digital camera coupled to a BX-41 Olympus microscope.

Results

1. Cloning of the spMGP cDNA

Total RNA extracted from *Sparus* bone-derived cells was used for the reverse transcription and amplification of a partial spMGP cDNA as described under Materials and Methods. The 569-bp band encoded a partial amino acid sequence highly homologous to the *Ar*MGP in the region of the heterologous primer used (ArMGP3F [8a]). This DNA fragment spun from amino acid 55 of the mature protein to the stop codon, and extended an additional 414 bp to the site of insertion of the poly $A^{(+)}$ tail, 24 bp after a consensus polyadenylation signal (Fig. 1). The 5′-end of the spMGP cDNA was obtained by 5′-RACE PCR, using the Marathon cDNA amplification kit (Clontech) and a specific spMGP reverse primer (MGP2R; Fig. 1). The spMGP cDNA thus obtained spans 827 bp and comprises a 5′-untranslated region (UTR) of 59 bp, an open reading frame of 351 bp, coding for a polypeptide with 117 amino acid residues, and a 417-bp 3′-UTR, from the stop codon to the site of insertion of the poly -A tail (Fig. 1).

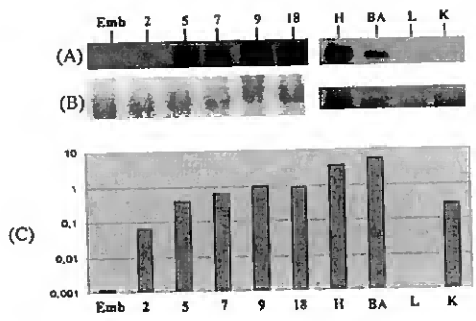

Fig. 2. Developmental appearance and tissue distribution of *Sparus* MGP mRNA, as detected by Northern blot hybridization. Total RNA was extracted from various developmental stages [embryo (Emb), 2 to 18 dph] and tissues [heart (H), branchial arches (BA), liver (L), and kidney (K)], fractionated in a denaturing agarose gel, transferred to a nylon membrane and hybridized with a ^{32}P-labeled spMGP cDNA (A), as described under Materials and Methods. β-Actin transcript levels were determined (B) and used to normalize those of spMGP transcripts (C) using the Quantity One 4.2.1 (Bio-Rad). A logarithmic scale was used in C to account for major differences between values of the different samples.

2. Developmental expression of the spMGP gene

2.1. Detection of spMGP gene expression by Northern and RT-PCR Southern blot hybridization

Northern blot hybridization showed the presence of spMGP mRNA already at 2 dph, with no signal being detected in the embryo at the neurula stage (Figs. 2A and C). The spMGP mRNA was always clearly present in the subsequent developmental stages analyzed, with an increase in signal intensity observed during the first stages of development until 9 dph. The levels of expression detected at 18 dph were comparable to those at 9 dph. Analysis of tissue distribution showed that the spMGP gene was expressed in the branchial arches, heart, and kidney (Fig. 2A), with the strongest signal detected for branchial arches and heart (Fig. 2C). No positive signal was detected in liver tissue (Figs. 2A and C).

RT-PCR followed by Southern blot hybridization con-

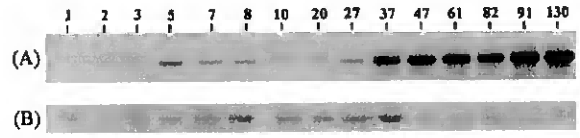

Fig. 3. Detection of *Sparus* MGP mRNA by RT-PCR. Total RNA was extracted from developmental stages (1 to 130 dph) of *Sparus* and used to amplify MGP mRNA by RT-PCR, as described under Materials and Methods. The resulting PCR products were size-fractionated by agarose gel electrophoresis, transferred to a nylon membrane, and hybridized with a ^{32}P-labeled spMGP cDNA (A). *Sparus* β-actin transcript levels were determined (B) to assess for RNA integrity.

firmed that the spMGP gene was being transcribed at 2 dph, with no RT-PCR amplification occurring for 1-dph larvae (Fig. 3A). A positive signal was always clearly detected in subsequent developmental stages, up to 130 dph.

2.2. Detection of spMGP gene expression and protein accumulation by in situ hybridization and immunohistochemistry

Transcripts of the *Sparus* MGP gene were detected by in situ hybridization at 2 dph in the branchial arches (Fig. 4A1) and accumulation of MGP protein at these sites was confirmed by immunohistochemistry (Fig. 4A2). In addition to branchial arches, the only other cartilaginous structures at this age are the lower jaw (Fig. 4A4), the otic capsula (Fig. 4A3), the hypural 1, and a small ventral cartilaginous formation, the coracoid–scapula complex (data not shown). Mineralization at this age is detected solely in the cleitrum and in the upper jaw (Fig. 4A4).

At 9 dph, a stage when the mouth of the larvae has already opened (exogenous feeding is possible), the lower jaw is in the process of mineralization (Fig. 4B4), and structures such as the basioccipital process and the trabeculae have become cartilaginous (Fig. 4B3). At this stage a significant increase in the spMGP gene expression was observed, with a strong signal detected by in situ hybridization in the branchial arches, trabeculae, Meckel's cartilage, and the basioccipital process (Fig. 4B1). Accumulation of MGP protein was detected at the same general locations at this age (Fig. 4B2 and data not shown).

Between 9 and 27 dph, *Sparus* larvae show a dramatic increase in the number of cartilaginous structures, namely at the level of the axial skeleton (most neural and hemal arches are formed; data not shown) and of the skull bones (Figs. 4C3 and C4). All these structures show signs of spMGP mRNA and protein accumulation, which can be clearly delimited to chondrocyte-like cells, included in cartilaginous capsules, with signal being detected in the branchial arches and preopercular cartilage (Fig. 4C1), hemal and neural arches, basioccipital process, ethmoid plates, jaw, Meckel's cartilage, and generalized in the skull bones (Fig. 4C2 and data not shown). No spMGP gene expression and protein accumulation was detected in any soft tissues until this stage (data not shown).

Between 27 and 45 dph spMGP gene expression reaches a peak in terms of number of tissues where it is detected (Figs. 4D1 and D2), concomitant with the development of cartilage in all the remaining tissues (Fig. 4D3). This period is also characterized by a strong increase in the ossification process, either intramembranous or endochondral (i.e., bone formation by direct mineralization from the matrix secreted by osteoblasts or by deposition of an osseous matrix in a preexisting cartilaginous matrix, respectively [17]) (Fig. 4D4). At 45 dph the localization of spMGP mRNA closely resembles what is seen at 27 dph, mainly detected throughout the entire juvenile body, including the branchial arches, ethmoid plate, opercular and preopercular cartilages, skull and jaw bones (Figs. 4D1 and D2), and hemal and neural arches (data not shown). Protein accumulation was detected in the same locations (data not shown). However, and in contrast with results at 27 dph, MGP mRNA was now easily detected in the cardiac chamber known as bulbus arteriosus, mainly composed of smooth muscle cells and endothelial cells, while no MGP mRNA was detected in the cardiac ventricle, mainly consisting of striated muscle cells (Fig. 4F1). No protein was found to accumulate in any of the heart compartments. This period corresponds to the end of the larval stage, when the specimens develop scales and the fins are fully differentiated.

At 85 dph ossification is nearly complete (Fig. 4E3), with only the structures necessary for the continuous growth of the fish remaining in the cartilaginous state [16]. All the fin soft rays, the vertebra, and almost every bone from the head and the jaw are ossified. The only structures that remain cartilaginous are the branchial arches (Fig. 4E2), some skull bones, the accessory cartilage, the last ventral and dorsal pterigiophores, and the pectoral distal radials (data not shown). The presence of spMGP mRNA and accumulation of MGP protein are restricted to these tissues (e.g., Fig. 4E1 and data not shown), with no signal being observed in the previously MGP mRNA-positive cartilaginous tissues, which presumably have by now become bone structures. In general, the results obtained indicate that in the *Sparus* skeleton MGP mRNA production occurs mainly in cartilaginous tissues, where it is located in chondrocyte-like cells associated with regions containing a mucopolysaccharide-rich extracellular matrix, revealed by alcian blue staining. No hybridization was observed when we used the MGP sense probe (data not shown).

Discussion

In this work we describe the molecular cloning of Matrix Gla protein cDNA in the marine teleost fish *S. aurata* and analyze the developmental appearance and tissue distribution of MGP mRNA and protein through the use of *Sparus*-specific molecular probes and functional antibodies. These findings are correlated with cartilage formation and sites of tissue mineralization during larval development.

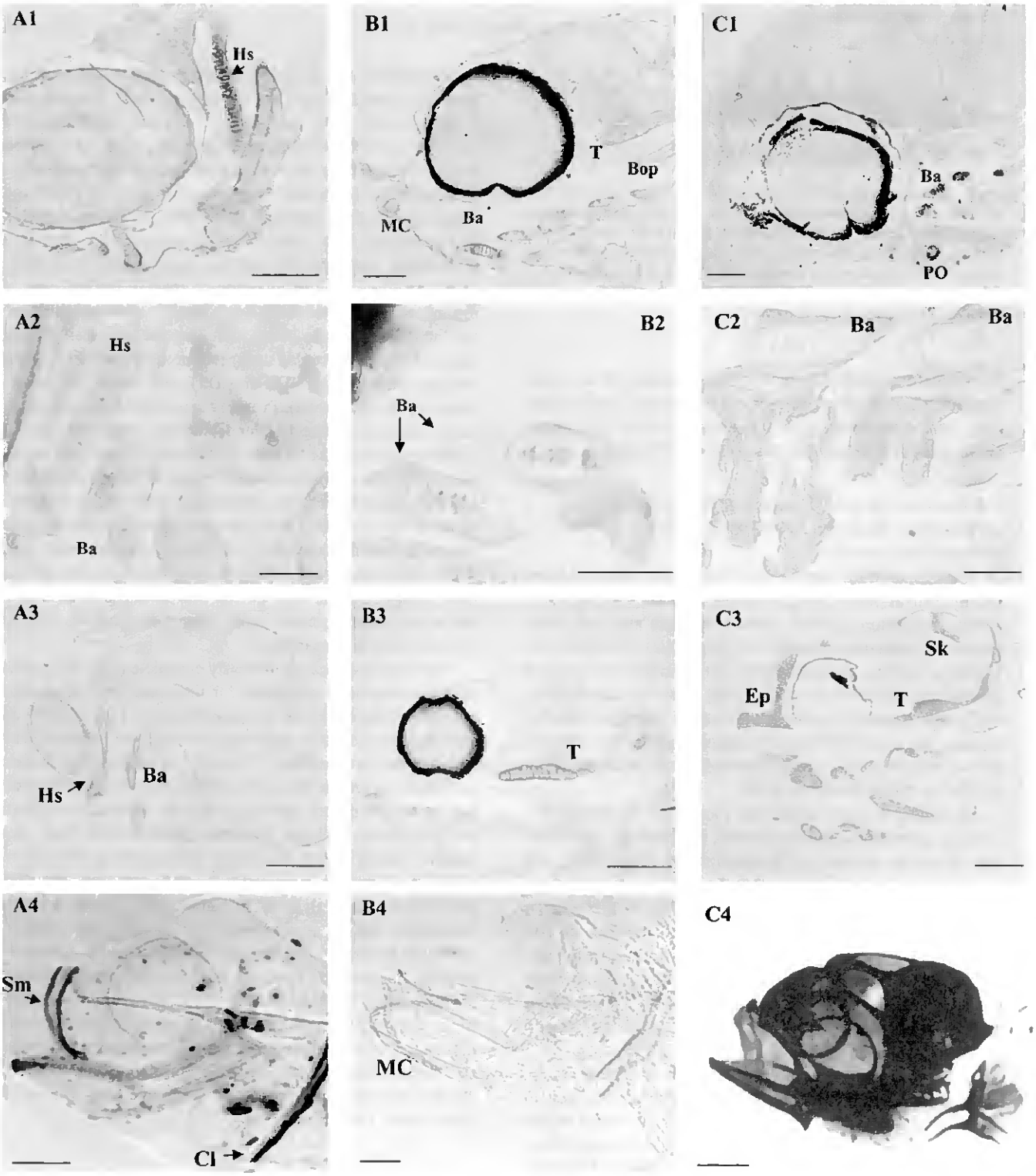

Fig. 4. Developmental analysis of MGP gene expression (A1–C1, D1–F1), MGP protein accumulation (A2–C2), appearance of cartilaginous and mineralized structures (A3–C4; D3–G1), osteocalcin accumulation (G2 and H1), and osteocalcin gene expression (H2) in *Sparus*. A1–A4, 2 dph; B1–B4, 9 dph; C1–C4, 27 dph; D1–D4 and F1, 45 dph; E1–E3, G1, G2, H1, and H2, 85 dph. (A1) spMGP gene transcription is detected, by *in situ* hybridization, at 2 dph in the hyosymplectic (Hs). (A2) spMGP protein is detected, by immunohistochemistry, in the hyosymplectic and branchial arches (Ba). (A3) Branchial arches are one of the first structures to acquire a cartilaginous nature. (A4) Mineralization is detected (red) by alizarin red staining in the cleitrum (Cl) and in the supramandibulars (Sm). (B1) At 9 dph the spMGP mRNA is detected in the cartilaginous branchial arches (Ba), trabeculae (T), Meckel's cartilage (MC), and in the basioccipital process (Bop). (B2) Detection of spMGP accumulation in the branchial arches (Ba). (B3) Structures such as the basioccipital articulatory process and the trabeculae (T) still have a cartilaginous nature and (B4) the Meckel's cartilage (MC) is under a process of perichondral calcification. (C1) Detection of spMGP gene expression in the branchial arches (Ba) and at the preoperculum (PO) at 27 dph. (C2) Detection of spMGP accumulation in the branchial arches (Ba). (C3) Most head structures [e.g., skull (Sk), trabeculae (T), and ethmoid plate (Ep)] still have a cartilaginous nature. (C4) Mineralization of lower and upper jaws is almost complete. (D1 and D2) At 45 dph spMGP mRNA is present in most head structures, like skull (Sk).

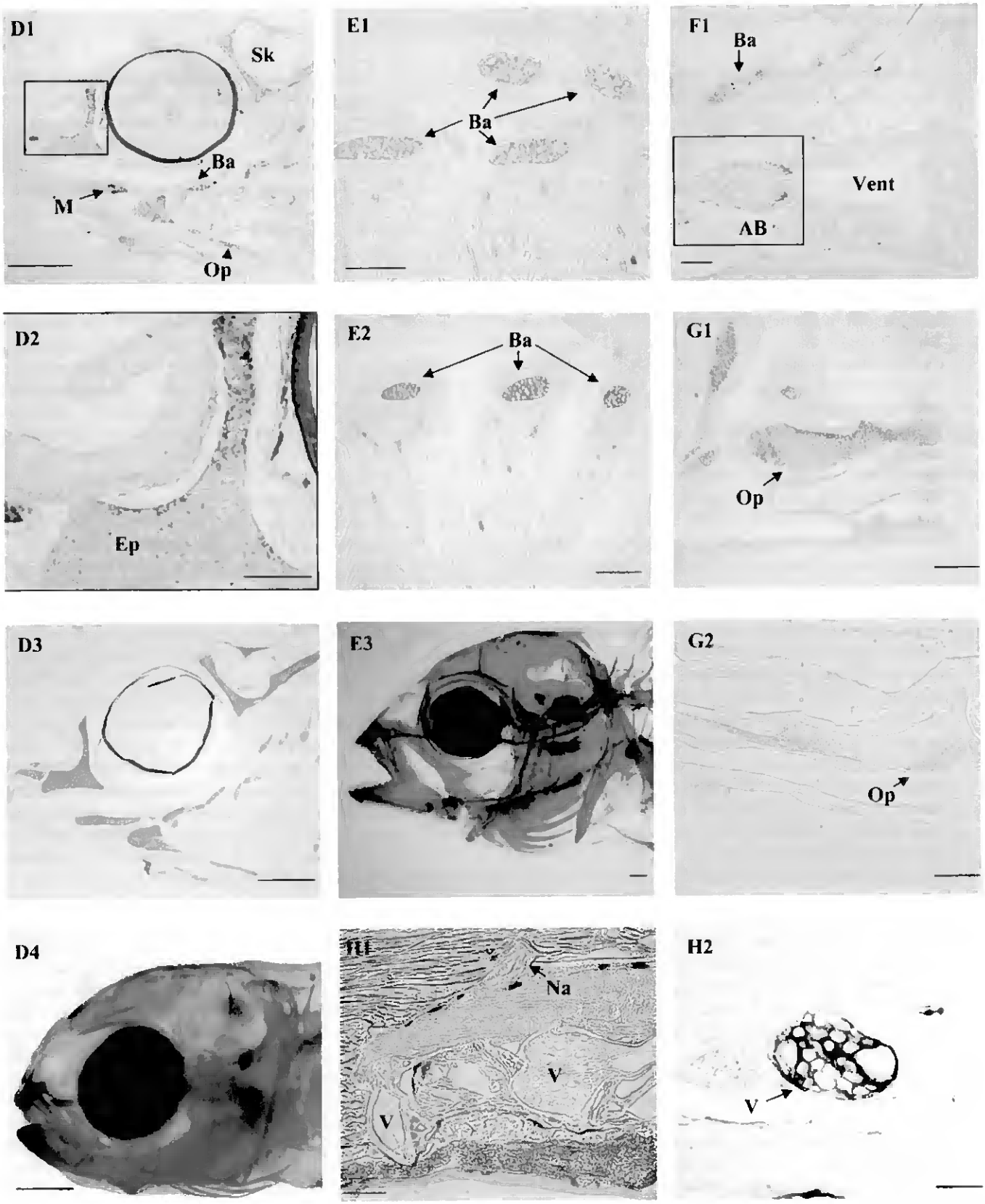

branchial arches (Ba), operculum (Op), and mandibula (M). (D3) Most hard head structures remain in a cartilaginous state, while others, like mandibula, ceased to stain with alcian blue. (D4) Mineralization of hard head structures is ubiquitously detected. (E1) spMGP mRNA is still present in branchial arches, which remain partially cartilaginous (E2). (E3) Most head structures are mineralized at this stage. (F1) spMGP mRNA is present in the arterial bulbus (AB) at 45 dph, but not in the cardiac muscle (Vent, ventricle). Osteocalcin protein (G2 and H1; red) and mRNA (H2; blue) accumulate at 85 dph in mineralized structures like vertebra (V) and neural arches (Na) and at the border of cartilaginous structures such as opercular bones (Op) undergoing calcification (G1 and G2). Magnification bars, 25 μm (A2 and B2), 50 μm (B1, B4, C2, and F1), 100 μm (A1, A4, C1, D2, H1, and H2), 200 μm (A3, B3, C3, C4, E1, E2, G1, and G2), and 400 μm (D1, D3, D4, and E3).

Analysis by Northern blot and RT-PCR coupled with Southern hybridization identified the temporal and spatial pattern of expression of the spMGP gene throughout *Sparus* development, from day 1 post-hatching to the juvenile stage. The MGP gene was expressed as early as 2 dph (Fig. 2 and 3) and its transcripts were subsequently detected in all stages of larval development analyzed. A significant (10-fold) increase in the relative amounts of MGP mRNA was observed between 2 and 9 dph, whereas at 18 dph the relative amounts of this mRNA were no different from those seen at 9 dph. These results may be the reflection of the large number of cartilaginous structures appearing between 2 and 9 dph in the body structure of the larvae and the corresponding increase in MGP mRNA-positive cells, a hypothesis that was further analyzed by in situ hybridization techniques coupled with immunohistochemistry.

In situ hybridization confirmed the presence of spMGP mRNA and protein at 2 dph (Figs. 4A1 and A2) in the first skeletal structures of *Sparus* known to develop a cartilaginous matrix (Fig. 4A3). In the next few days, the larvae body acquires a morphology that is indicative of its final phenotype, with the acquisition of more cartilaginous structures in the head skeleton, as seen by alcian blue staining. The 10-fold increase in MGP mRNA detected between 2 and 9 dph and the observed restricted location of this transcript in chondrocyte-like cells could therefore reflect the onset of chondrogenesis with the differentiation of cells from the chondrocytic lineage involved in the formation of different skeletal structures. Comparable morphological changes have been shown, in higher vertebrates, to be associated with a strong induction of MGP gene transcription [26]. These authors have shown by in situ hybridization that, in mouse, MGP mRNA was consistently more abundant in the periphery of the zone of resting and prolipherative chondrocytes than in the central area. This same pattern of MGP mRNA production is observed in *Sparus* (e.g., Fig. 4D2), indicating that the biosynthesis of spMGP is more active in the peripheral zone, where newly differentiated chondrocytes arise, than in the central zone, where the chondrocytes may be more mature. A recent work[18] suggests that MGP may be required for chondrocyte maturation in mammals. Our finding that in *Sparus* MGP mRNA is preferentially produced by newly differentiated chondrocytes may signify that in fish this important putative function is also accomplished by MGP.

Synthesis of spMGP mRNA production seemed to decrease once cartilage was fully mineralized, a result that mimics the pattern of expression that has been reported for higher vertebrates, where MGP mRNA has been detected prior to calcification, mainly associated with cartilage [6] or in hypertrophic chondrocytes adjacent to fronts of mineralization [19]. In addition, we have recently shown that in *Xenopus laevis* MGP gene expression is first detected at the time of chondrocranium development, i.e., concomitant with the appearance of cartilage [10].

Decalcification of the specimens used for this work hinders the detection of mineralized tissue and mineralization fronts in histological sections by histochemical techniques. We have used the pattern of gene expression and protein accumulation of osteocalcin (an osteoblast-specific vitamin K-dependent protein found to accumulate in bone extracellular matrix in mammals [20] and in fish [16]) to detect the presence of bone-derived calcified structures in the same specimens used for MGP studies, since the presence of osteocalcin mRNA or protein accumulation has never been observed in cartilaginous matrix or chondrocytes. Osteocalcin gene expression and protein accumulation in 85-dph *Sparus* was detected in all mineralized tissues that also stained with alizarin red in nondecalcified *Sparus* specimens of the same age, including vertebra (Figs. 4H2 and H1, respectively) and jaw and skull bones (data not shown), consistent with our previous findings [16]. We have detected cartilage- and bone-specific cells in the same skeletal structures in fish (unpublished results) and a similar cartilage–bone location within the same skeletal structure in fish has been described by others [21], showing a chondrocyte-rich matrix that does not mineralize involved with a growing bone capsula calcifying independently of the cartilage. These data also confirm recent results from our laboratory with a different marine fish, *A. regius* [8a], where both MGP and osteocalcin were found in the same skeletal structures (branchial arches) but clearly produced by different cell types. In this work MGP mRNA-positive staining was never detected in the same cells as osteocalcin mRNA, and sites of MGP accumulation were always distinct from those found to accumulate osteocalcin. Moreover, when MGP and osteocalcin were indeed detected in the same skeletal structures, MGP was always associated with cartilage (data not shown) whereas osteocalcin accumulated in the periphery of the cartilaginous structure (Fig. 4G1 and G2), suggesting a mechanism of endochondral ossification, where both proteins play their roles, albeit at different locations of the same structure. It seems, therefore, that, like in higher vertebrates, MGP in *Sparus* is required early in development and is tightly associated with chondrocyte differentiation and cartilage formation, presumably involved in prevention or regulation of its rate of calcification. It is still unclear how MGP fulfills its calcification inhibitory activity, but an attractive hypothesis was recently postulated by Bostrom et al. [22], who proposed that MGP may, at least partially, fulfill its function by complexing BMP-2, an important inductor of osteogenesis. In addition, previous studies have proven MGP to be a potent inhibitor of mineralization in vitro via its γ-carboxylated Gla residues [23]. In any case, it seems that the presence of Gla residues is required for MGP to fulfill its function as calcification inhibitor since when functional Gla residues are abolished by warfarin treatment there is a clear increase in abnormal cartilage and vascular calcification [4,5,24].

Northern blot hybridization has revealed the presence of spMGP cDNA in juvenile soft tissues such as heart and kidney. In situ hybridization results confirmed the presence

of spMGP mRNA in heart (Fig. 4F1), localized in the bulbus arteriosus, which is rich in smooth muscle fibers and endothelial cells, with no signal being detected in the striated muscle forming the heart ventricle. MGP gene expression in the heart has been reported for other species [9,10] and its synthesis by smooth muscle and endothelial cells from the vascular system has been proven [5,8]. Several studies also account for the presence of protein in the aortic vessel wall of mammals and not in the cardiac muscle itself, which is composed mainly of striated cardiac fibers [25]. Additionally, both functional and genetic MGP depletion studies in rodents [3,5] have shown a rapid calcification of the lamellae of coronary artery and aortic heart valve, suggesting that MGP is important in these tissues to prevent calcification. The presence of spMGP mRNA in heart and its expression pattern in this tissue suggests that this protein is also important in fish to prevent arterial calcification. In addition, the fact that, as in mammals [9], spMGP protein is not accumulated in the heart (data not shown), despite the relatively high level of MGP mRNA production, suggests that one of the protein functions, like in higher vertebrates, might be the clearance of excess calcium from tissues into the circulation, thus protecting against calcification.

In situ hybridization did not confirm the presence of spMGP mRNA in kidney, with no clear signal above the background noise being detected in this tissue (not shown). Since the Northern blot signal was already relatively weak, it is possible that the spMGP gene expression in kidney can be due to the presence of vascular tissues that irrigate this organ. The detection of MGP mRNA was also weak (only detected by RT-PCR) in another lower vertebrate, *X. laevis* [10], a result confirmed by our data and further suggesting the involvement of the arterial vessels in the positive signal detected.

In conclusion, this study represents the first comprehensive analysis of the pattern of gene expression and protein accumulation of MGP throughout development of a marine teleost, *S. aurata*. We have identified the pattern of MGP gene expression and protein accumulation throughout the first stages of *Sparus* development, in relation to skeletal development, and shown the existence of a similarity at this level between this lower vertebrate and previous results published for mammals. Several implications arise from these results: (1) matrix Gla protein might have the same function(s) in all organisms where it is present, a result further emphasized by the previously described evolutionary conservation of MGP amino acid residues thought to be required for normal function [10; and references therein], suggesting that the need for its function arose more than 200 million years ago; (2) fish in general can be considered as a valuable model for the study of this protein, both in structure and in function; and (3) *S. aurata* is a valid model for analyzing gene expression and regulation in marine fish.

Acknowledgments

This work was partially funded by research grants (PRAXIS/BIA/469/94 and BIA/11159/98) from the Portuguese Science and Technology Foundation (FCT) and research funds from CCMAR/University of Algarve. We thank D. Simes for her contribution of polyclonal antibodies against fish MGP and osteocalcin. J.P. Pinto, N. Conceição, and P.J. Gavaia were the recipients of a postdoctoral fellowship (PRAXIS XXI/BPD/20229/99) and two PhD fellowships (PRAXIS BD/11567/97 and PRAXIS BD/19665/99), respectively.

References

[1] Price PA, Williamson MK. Primary structure of bovine Matrix Gla protein, a new vitamin K-dependent bone protein. J Biol Chem 1985;260:14971–5.

[2] Price PA, Urist MR, Otawara Y. Matrix Gla protein, a new gamma-carboxyglutamic acid-containing protein which is associated with the organic matrix of bone. Biochem Biophys Res Commun 1983;117:765–71.

[3] Luo G, Ducy P, McKee MD, Pinero GJ, Loyer E, Behringer RR, Karsenty G. Spontaneous calcification of arteries and cartilage in mice lacking matrix Gla protein. Nature 1997;386:78–81.

[4] Price PA, Faus SA, Williamson MK. Warfarin-induced artery calcification is accelerated by growth and vitamin D. Arterioscler Thromb Vasc Biol 2000;20:317–27.

[5] Price PA, Faus SA, Williamson MK. Warfarin causes rapid calcification of the elastic lamellae in rat arteries and heart valves. Arterioscler Thromb Vasc Biol 1998;18:1400–7.

[6] Hale JE, Fraser JD, Price PA. The identification of matrix Gla protein in cartilage. J Biol Chem 1988;263:5820–4.

[7] Shanahan CM, Proudfoot D, Farzaneh-Far A, Weissberg PL. The role of Gla proteins in vascular calcification. Crit Rev Eukaryot Gene Express 1998;8:357–75.

[8] Shanahan CM, Cary NRB, Salisbury JR, Proudfoot D, Weissberg PL, Edmonds M. Medial localization of mineralization-regulating proteins in association with Monckeberg's Sclerosis; evidence for smooth cell-mediated vascular calcification. Circulation 1999;100:2168–76.

[8a] Simes DC, Williamson MK, Ortiz-Delgado JB, Viegas CS, Price PA, Cancela ML. Purification of matrix Gla protein from a marine teleost fish, *Argyrosomus regius*: calcified cartilage and not bone as the primary site of MGP accumulation in fish . J Bone Miner Res 2003;18:244–59.

[9] Fraser JD, Price PA. Lung, heart and kidney express high levels of mRNA for the vitamin K-dependent matrix Gla protein. J Biol Chem 1988;263:11033–6.

[10] Cancela ML, Ohresser MC, Reia JP, Viegas CS, Williamson MK, Price PA. Matrix Gla Protein in *Xenopus laevis*– molecular cloning, tissue distribution and evolutionary considerations. J Bone Miner Res 2001;16:1611–21.

[11] Shanahan CM, Cary NRB, Metcalfe JC, Weissberg P. High expression of genes for calcification-regulating proteins in human atherosclerotic plaques. J Clin Invest 1994;93:2393–402.

[12] Conceição N, Henriques NM, Ohresser MC, Hublitz P, Schule R, Cancela ML. Molecular cloning of the Matrix Gla Protein gene from *Xenopus laevis*. Functional analysis of the promoter identifies a calcium sensitive region required for basal activity. Eur J Biochem 2002;269:1947–56.

[12a] Laizé V, Pombinho AR, Cancela ML. Development of bone-derived cell lines from a marine teleost: establishment of the first in vitro

model system from fish suitable to analyse regulatory pathways of Matrix Gla protein and osteocalcin gene expression. J Bone Miner Res 2002;17(Suppl 1):S406.

[13] Chomczynski P, Sacchi N. Single step method of RNA isolation by acid guanidinium thiocyanate–phenol–chloroform extraction. Analyt Biochem 1987;162:156–9.

[14] Sanger F, Donelson JE, Coulson AR, Kossel H, Fischer D. Use of DNA polymerase I primed by a synthetic oligonucleotide to determine a nucleotide sequence in phage fl DNA. Proc Natl Acad Sci USA 1973;70:1209–13.

[15] Sambrook J, Fritsch EF, Maniatis T. Molecular cloning: A laboratory manual. 2nd ed. Cold Spring Harbor, NY: Laboratory Press, 1989, 7.46.

[16] Pinto JP, Ohresser M, Cancela ML. Cloning of the Bone Gla Protein Gene from the teleost fish *Sparus aurata*. Evidence for overall conservation in molecular structure and pattern of expression from fish to man. Gene 2001;270:77–91.

[17] Jee WSS. The skeletal tissues. In: Weiss L, editor. Cell and tissue biology. Munich: Urban & Schwarzenberg, 1988. p. 211–54.

[18] Yagami K, Suh J-Y, Enomoto-Iwamoto M, Koyama E, Abrams WR, Shapiro IM, Pacifici M, Iwamoto M. Matrix Gla protein is a developmental regulator of chondrocyte mineralization and, when constitutively expressed, blocks endochondral and intramembranous ossification in the limb. J Cell Biol 1999;147:1097–108.

[19] Ikeda T, Nomura S, Yamaguchi A, Suda T, Yoshiki S. In situ hybridization of bone matrix proteins in undecalcified adult rat bone sections. J Histochem Cytochem 1992;40:1079–88.

[20] Price PA, Otsuka AS, Poser JW, Kristaponis J, Raman N. Characterization of a γ-carboxyglutamic acid-containing protein from bone. Proc Natl Acad Sci USA 1976;73:1447–51.

[21] Witten PE, Villwock W. Growth requires bone resorption at particular skeletal elements in a teleost fish with acellular bone (*Oreochromis niloticus*, Teleostei: Cichlidae). J Appl Ichthyol 1997;13:149–58.

[22] Bostrom K, Tsao D, Shen S, Wang Y, Demer LL. Matrix Gla protein modulates differentiation induced by bone morphogenetic protein-2 in C3H10T1/2 cells. J Biol Chem 2001;276:14044–52.

[23] Alagao FC, Patel R, Price PA. Matrix Gla protein specifically inhibits calcification of human aortic elastin in vitro. J Bone Miner Res 2000;15(Suppl 1):S208.

[24] Howe AM, Webster WS. Warfarin exposure and calcification of the arterial system in the rat. Int J Exp Path 2000;81:51–6.

[25] Wallin R, Cain D, Sane DC. Matrix Gla protein synthesis and gamma-carboxylation in the aortic vessel wall and proliferating vascular smooth muscle cells. Thromb Haemost 1999;82:1764–7.

[26] Luo G, Dsouza R, Hougue D, Karsenty G. The matrix Gla protein is a marker of the chondrogenesis cell lineage during mouse development. J Bone Miner Res 1995;10:325–34.

Calcif Tissue Int (2004) 74:170–180
DOI: 10.1007/s00223-003-0079-4

Calcified Tissue International

Characterization of Osteocalcin (BGP) and Matrix Gla Protein (MGP) Fish Specific Antibodies: Validation for Immunodetection Studies in Lower Vertebrates

D. C. Simes,[1] M. K. Williamson,[2] B. J. Schaff,[1] P. J. Gavaia,[1] P. M. Ingleton,[3] P. A. Price,[2] M. L. Cancela[1]

[1]CCMAR-University of Algarve, Faro 8005-139, Portugal
[2]Division of Biology, University of California San Diego, La Jolla, CA 92093-0368, USA
[3]Division of Musculo-Skeletal Medicine, Institute of Endocrinology, University of Sheffield, Beech Hill Rd, Sheffield S10 2RX, UK

Received: 4 April 2003 / Accepted: 2 June 2003 / Online publication: 15 December 2003

Abstract. In fish species the basic mechanisms of bone development and bone remodeling are not fully understood. The classification of bone tissue in teleosts as cellular or acellular and the presence of transitional states between bone and cartilage and the finding of different types of cartilage in teleosts not previously recognized in higher vertebrates emphasizes the need for a study on the accumulation of the Gla-containing proteins MGP and BGP at the cellular level. In the present study, polyclonal antibodies developed against BGP and MGP from *A. regius* (a local marine teleost fish) and against MGP from *G. galeus* (a Pacific Ocean shark), were tested by Western blot for their specificity against BGP and MGP from several other species of teleost fish and shark. For this purpose we extracted and purified both proteins from various marine and freshwater teleosts, identified them by N-terminal amino acid sequence analysis and confirmed the presence of gamma-carboxylation in the proteins with the use of a stain specific for Gla residues. Each antibody recognized either BGP or MGP with no cross-reaction between proteins detected. All purified fish BGPs and MGPs tested were shown to be specifically recognized, thus validating the use of these antibodies for further studies.

Matrix Gla Protein (MGP) and Bone Gla Protein (BGP, osteocalcin) belong to the family of vitamin K-dependent (VKD), γ-carboxyglutamic acid (Gla)-containing proteins that have been unequivocally associated with bone formation and mineralization [1–4], and more recently, with vascular calcification [5–10].

MGP is a 10–15 kDa-secreted protein, containing 4–5 residues (depending on the species) of the Ca^{2+} binding Gla residue [11–15] while BGP is a small secreted protein with approximately 6 kDa molecular weight and includes three Gla residues. Although there is little information about the regulation of expression of these proteins in teleosts, BGP in teleost fish has been shown to be associated with bone-like mineralized tissues present in branchial arches, jaw, vertebra and scales [15, 16] while MGP was only recently found to accumulate, mainly in the extracellular matrix of calcified cartilage [15]. In this previous work, the MGP gene was found to be predominantly expressed in chondrocytes from branchial arches, with no expression detected in the different bone-like mineralized tissues analyzed while BGP mRNA was mainly located in bony tissues associated with osteoblast-like cells, as expected [15]. As previously seen in mammals and *Xenopus*, MGP mRNA was also found to be present in teleost soft tissues, predominantly in heart and kidney [15], with the expression of MGP in heart tissue mainly associated with two specific cell types, smooth muscle and endothelial cells [15].

We have recently developed specific polyclonal antibodies against BGP and MGP from the teleost fish *A. regius* [15] as well as against MGP purified from soupfin shark (*Galeorhinus galeus*) (our unpublished results). The purpose of the present work was to demonstrate the usefulness of these antibodies for studies of BGP/MGP accumulation and tissue distribution in marine and fresh water fish and amphibians. To achieve this goal we purified and characterized MGP and BGP from various fish species and from *Xenopus* and compared the ability of our antibodies to recognize these specific antigens.

Correspondence to: M. L. Cancela; E-mail: lcancela@ualg.pt

Material and Methods

Extraction of MGP and BGP from Fish and Amphibian Tissues

Vertebra from *Sparus aurata*, *Solea senegalensis* and *Prionace glauca*, branchial arches from *Halobatrachus didactylus* and the entire skeleton of *Xenopus laevis* and *Danio rerio* were cleaned from adhering soft tissues and the Gla-containing proteins were extracted based on previously described procedures [14, 15, 17]. Briefly, the mineralized material was ground in a mortar with liquid nitrogen to less than 1 mm in diameter.

extensively washed with 6 M guanidine HCl and water and dried with acetone. The resulting powder was demineralized with 10% formic acid, dialyzed (SpectraPor 3) against 50 mM HCl, freeze-dried, re-suspended in 6 M guanidine-HCl, 0.1 M Tris-HCl pH 9, 10 mM EDTA, further dialyzed (SpectraPor 3; Spectrum, Gardena, CA, USA) against 5 mM ammonium bicarbonate and freeze-dried [15]. *P. glauca* dialyzed extract showed a precipitate that was separated, dissolved in 50 mM HCl and stored at −80°C. Samples were then analyzed by SDS-PAGE as described in "Electrophoresis and Blotting."

For all the other preparations, the crude extracts were ultrafiltrated using a Centricon-10 with 10 kDa molecular weight cut-off (Amicon, Millipore, Bedford, MA, USA). The combined final filtrates containing BGP (lower than 10 kDa) were further desalted and concentrated using a Centricon-3 (3 kDa cut-off) (Amicon).

Both the filtrate and filter-retained samples were collected and their protein content was determined as described in "Protein Quantification." Proteins in each fraction were further analyzed by SDS-PAGE.

Protein Quantification

Total protein concentration in crude acid extracts was determined using the Commassie plus protein assay reagent (Pierce, Rockford, IL, USA) according to the manufacturer's protocol. For the determination of protein concentration of purified BGP samples, the value of $E^{0.1\%\ 1\ cm} = 1.33$ at 280 nm [18] was used. For MGP concentration determination the value of $E^{0.1\%\ 1\ cm} = 1.0$ at 280 nm was used (P.A. Price, personal communication).

N-Terminal Protein Sequence Analysis

*Dr*BGP (*D. rerio* BGP) and *Hd*BGP (*H. didactylus* BGP) purified proteins were directly deposed on a polybrene-coated glass fiber filter. *Pg*MGP (10 µg) (*P. glauca* MGP) containing samples were loaded onto 4 lanes and fractionated on a 18% SDS-polyacrylamide gel, then transferred onto a PVDF membrane filter (Applied Biosystems, Foster City, CA, USA) and stained with Commassie Brilliant Blue in order to visualize protein bands. The band corresponding to *Pg*MGP (around 18 kDa) detected in each lane was cut for further identification by protein sequence analysis. Automatic Edman degradations were performed as described [13] using an Applied Biosystems Model 494 sequenator equipped with an on-line HPLC and employing the standard program supplied by the manufacturer. Phenylthiohidantoin (PTH) amino acid derivatives were separated by a 2.1 mm × 22 cm C-18 reverse-phase HPLC column (Applied Biosystems) and the gradient conditions were those recommended by Applied Biosystems.

Electrophoresis and Blotting

Total protein (20–30 µg) was dissolved in SDS sample buffer containing reducing agent (NuPage, Invitrogen, La Jolla, CA, USA), applied to a 12% or 4–12% gradient polyacrylamide precast gel containing 0.1% SDS (NuPage, Invitrogen) and fractionated at a constant 140 volts. The gels were stained either with 0.2% Commassie Brilliant Blue R-250 (C.I. 42660, Bio-Rad, Richmond, CA, USA), 10% trichloroacetic acid, 10% 5-sulfosalicylic acid or with a DBS-staining solution specific for Gla-containing proteins [(8.5 mM 4-diazobenzene sulfonic acid (DBS); Sigma, Spain; 6.4 mM $NaNO_2$ in 2 M acetate buffer, pH 4.6)] as described in [19]. Lysozyme (Sigma) and protease factor Xa (New England Biolabs) were used, respectively, as negative and positive controls for the DBS-staining method. Blotting onto nitrocellulose (Invitrogen) was performed for 1 h at constant 80 mA using a Bio-Rad Mini Trans-Blot Cell system (Bio-Rad) and a Bis-Tris transfer buffer (NuPage, Invitrogen). The membranes were blocked for 2 h with 5% (w/v) non-fat dried milk powder in TBST (15 mM NaCl, 10 mM Tris-HCl buffer, pH 8, 0.05% Tween 20; Blotto) and then incubated overnight with 0.04 µg/ml anti-*Ar*MGP or anti-*Ar*BGP affinity-purified antiserum in Blotto or with anti-*Gg*MGP polyclonal antibody diluted 1:100 in the same solution. Immunoreactive protein bands were detected using alkaline phosphatase-labeled goat anti-rabbit IgG antibody (Gibco-BRL, Paisley, UK) diluted 1:20,000 in TBST and visualized using NBT/BCIP substrate solution (Sigma) as described [20]. Negative controls consisted in the substitution of the primary antibody with phosphate-buffered saline (150 mM NaCl, 15 mM sodium phosphate buffer, pH 7.2; PBS) in the experiments with the purified antibody and with normal rabbit serum when using the non-purified antibody. Controls also included pre-incubation of the primary antibody for 1 h at room temperature with purified *Ar*MGP and *Ar*BGP purified protein (1:10 weight ratio).

Dot-blot Analysis

Purified protein samples were deposited in 1 µl aliquots (0.5 µg total protein) onto a nitrocellulose membrane (Invitrogen). Membranes were allowed to dry for 1 h and blocked for 2 h with 5% (w/v) dried milk powder in TBST. Incubation with anti-*Ar*MGP, anti-*Ar*BGP affinity-purified antibodies and anti-*Gg*MGP polyclonal antiserum and detection of immunoreactive protein spots was performed as described in "Electrophoresis and blotting."

ArBGP, ArMGP and GgMGP Antiserum

MGP and BGP were purified from formic acid extracts of *A. regius* branchial arches as described [15]. Rabbit polyclonal antibodies against MGP and BGP from *A. regius* were obtained from Strategic BioSolutions (Ramona, CA, USA) using the purified protein adsorbed to polyvinylpyrrolidone (PVP-40), as described [11, 15]. *Gg*MGP (MGP from *Galeorhinus galeus*) antiserum was raised against purified *Gg*MGP [21] using a described method [11].

Specificity of the antiserum was determined by Dot-blot and Western-blot immunoassays as described in "Electrophoresis and Blotting" using either the purified proteins (*Ar*MGP and *Ar*BGP) [15] or the characterized MGP obtained from a crude extract of *P. glauca* calcified cartilage.

Affinity Purification of ArBGP and ArMGP Antiserum

Purified protein samples [15] (5 mg of *Ar*BGP dissolved in 0.1 M $NaHCO_3$, 0.5 M NaCl, pH 8.3 and 1.2 mg of *Ar*MGP resuspended in 0.2 M $NaHCO_3$, 4 M urea) were coupled to the CNBr-activated Sepharose 4B resin (Amersham-Pharmacia, Piscataway, NJ) overnight at 4°C. Adsorption of the *Ar*BGP and *Ar*MGP polyclonal antibodies was performed according to the manufacture's instructions. Bound antibodies were eluted with 100 mM glycine pH 2.5 followed with 100 mM triethylamine, pH 11.5 and samples (1 ml) were immediately neutralized by adding 100 µl of 1 M Tris-HCl, pH 7. Absorption of the effluent at 280 nm was monitored. The resulting peak fractions were dialyzed against phosphate-buffer saline and stored at −20°C.

Determination of BGP Theoretic Isoelectric Point

Isoelectric point of BGPs from *A. regius*, *S. aurata*, *D. rerio*, *X. laevis* and *B. taurus* were calculated using the Peptide Statistics Tool (PEPSTATS) from biotools (http://biotools.umassmed.edu). The complete mature sequence derived from cDNA was used in each case and values were calculated in the absence of either hydroxylation of proline or γ-carboxylation of glutamic acid residues.

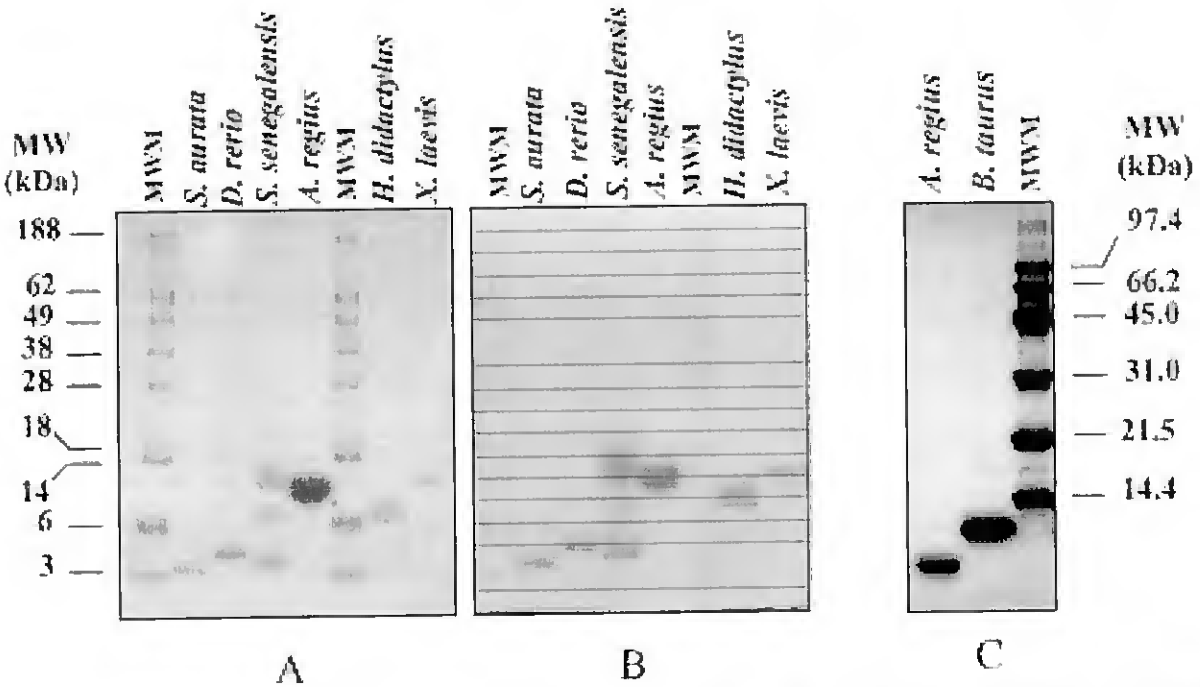

Fig. 1. Comparison of migration behavior on SDS-PAGE of Gla-containing BGPs from different teleosts (*S. aurata*, *D. rerio*, *S. senegalensis*, *H. didactylus*, *X. laevis* and *B. taurus*. (**A**) and (**B**) Each lane of 12% SDS-PAGE (Nupage, Invitrogen) was loaded with 10 µg of protein. One gel was stained using the CBB-staining method for total protein detection (**A**) and the other with DBS-staining method specific for Gla-containing proteins (**B**); MWM, SeeBlue pre-stained molecular weight markers (Invitrogen). (**C**) Protein 10 µg either *A. regius* or *B. taurus* purified BGP was loaded per lane on a 18% SDS-PAGE gel (Novex, Invitrogen) and stained with CBB; MWM, low range molecular weight markers from BioRad. Corresponding molecular weights (in kDa) are indicated on the margins of the figure.

Results

Identification of Gla-containing Proteins from Mineralized Tissues of Teleost and Cartilaginous Fishes and from Xenopus

BGP and MGP were separated from the acid extract of *S. aurata*, *H. didactylus*, *S. senegalensis*, *D. rerio* and *X. laevis* mineralized tissues by ultrafiltration, as described in Material and Methods. SDS-PAGE results depicted in Figure 1A demonstrate that most of the protein in BGP-containing filtrates from *S. aurata*, *D. rerio* and *H. didactylus* migrated as a single component with higher mobility than BGP purified from *A. regius* branchial arches, a migration behavior similar to *X. laevis* BGP (Fig. 1A). Only *S. senegalensis* BGP sample showed more than one band, and the reason for this discrepancy remains to be clarified. In addition, all fish and *Xenopus* BGPs showed a higher migration behavior than bovine BGP (Fig. 1A, C). Positive reaction (red-orange) obtained with the DBS-staining method (Fig. 1B) following SDS-PAGE clearly indicated that the purified proteins from all species were gamma-carboxylated.

Comparison of the migration behavior between fish (*S. aurata*, *S. senegalensis*, *A. regius*, *D. rerio*), *Xenopus* and bovine BGPs in non-denaturing conditions over a 18% Tris-Glycine native gel is depicted in Figure 2. The results confirm the purity of the fractions analyzed since in this type of gel all protein samples tested migrated

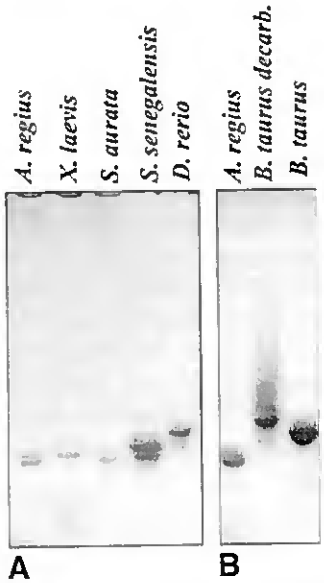

Fig. 2. Comparison of native electrophoresis migration behavior of BGPs from different fish species (*A. regius*, *S. senegalensis*, *S. aurata* and *D. rerio*), *X. laevis* and *B. taurus* applied to 18% Tris-glycine polyacrylamide gel (Novex, Invitrogen). Each lane was loaded with 10 µg of protein and the gel was stained using the CBB staining method. *B. taurus* decarb - *B. taurus* BGP decarboxylated (Poser and Price, 1979).

essentially as a major band although a second less intense band is also seen that could be explained by the

Table 1. Detection and characterization of BGP protein purified from bone and calcified cartilage acid extracts obtained from several teleost fishes (*A. regius*, *S. senegalensis*, *S. aurata*, *H. didactylus*, *D. rerio*) and *X. laevis*

	Specimen (tissue)	SDS-PAGE[a] CBB	SDS-PAGE[a] DBS	Immunodetection[b] (antibody)	N-terminal sequence[c]
BGP	*A. regius* (vertebra)	10 kDa	Positive	Western blot (anti-*Ar*BGP)	AAKELTLAQTE*SLRE*VCE* TNMACDEMADAQGIVAAY
	S. aurata (vertebra)	4 kDa	Positive	Western blot (anti-*Ar*BGP)	n.d.
	S. senegalensis† (vertebra)	4 kDa	Positive	Western blot (anti-*Ar*BGP)	n.d.
	D. rerio (skeleton)	5 kDa	Positive	Western blot (anti-*Ar*BGP)	AGTAXGDLTPFQLE*SLRE*VCE*
	H. didactylus (branchial arches)	8 kDa	Positive	Dot blot (anti-*Ar*BGP)	AAAELSLVQLE*SLRE*VCE*Q
	X. laevis (skeleton)	10 kDa	Positive	—*	n.d.

[a] The proteins were electrophoresed on a 18% SDS-PAGE (NuPage, Invitrogen) stained with CBB and DBS and the molecular weights were estimated by plotting the log versus relative migration distance using the pre-stained molecular weight markers (SeeBlue, Invitrogen) over a linear range

[b] Immunodetection of the proteins was performed by Western blot or Dot blot analysis using anti-*Ar*BGP affinity purified antibodies as primary antibody (0.1 µg) and alkaline phosphatase-labeled goat anti-rabbit IgG antibody with the NBT/BCIP substrate solution as secondary antibody

[c] N-terminal sequence was obtained as described in Materials and Methods section and is numbered from the first amino acid residue identified from sequence determination, E*, Gla residue. X, non-identified amino acid residue, (n.d.) not determined

† Besides this one band (3–6 kDa) there were 2 extra bands both coloring with CBB- and DBS-staining (SDS-PAGE, Figure 1) and recognized by the same antibody (Western blot, Figure 3)

* Affinity purified antibodies (anti-*Ar*BGP and anti-*Ar*MGP) as well as anti-*Gg*MGP polyclonal antiserum were tested and gave negative results

presence of a BGP with a different degree of carboxylation. In fact, the effect of carboxylation of BGP is quite clear once we compare, over a native gel, the migration of *B. taurus* BGP with a sample of decarboxylated protein (Fig. 2B) obtained using a described procedure [23].

N-terminal amino acid sequence analysis was obtained for *Dr*BGP and *Hd*BGP (Table 1) and their identity was confirmed based on the fact that the first 21 (*Dr*BGP) and 19 (*Hd*BGP) amino acid residues sequenced showed high homology with previously sequenced BGPs [15, 17]. The assignment of the three Gla residues in the N-terminal sequence (Table 1) was based on comparison with other BGP sequences [17] where these residues are highly conserved, and also on the fact that in the standard sequence analysis no PTH derivative could be identified at these positions. Western- blot analysis of the fish BGP-containing filtrates from *S. aurata*, *D. rerio*, *H. didactylus* and *S. senegalensis* using the anti-*Ar*BGP purified antibody (Fig. 3) also confirmed the identification of these bands as BGP.

Analysis by SDS-PAGE of the centricon 30 filter-retained contents of each sample followed by CBB and DBS staining permitted the identification of a Gla-containing protein in *X. laevis*, *S. aurata* and *S. senegalensis* sample extracts (Fig. 4) with a migration behavior (14–18 kDa) similar to that previously obtained for *Ar*MGP (Fig. 4). The *P. glauca* sample showed a clearly defined band (Fig. 4) that was sufficiently pure and abundant to obtain a N-terminal amino acid sequence (30 amino acids residues were obtained, see Table 2) and confirmed its identity to be *Pg*MGP based on its high homology with the previously sequenced

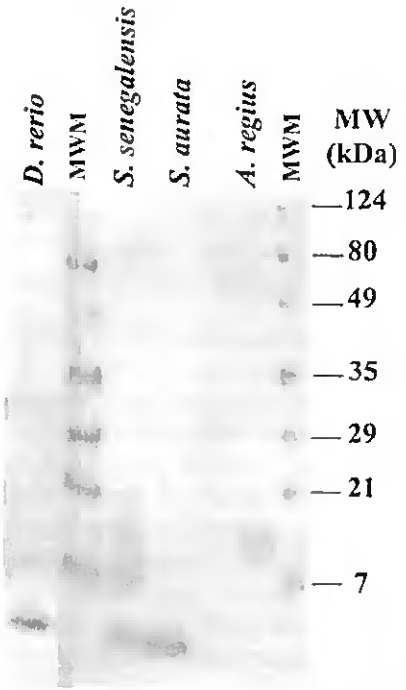

Fig. 3. Western blot analysis of BGPs from several teleost fish. 1 µg of each protein was electrophoresed on 18% SDS-PAGE (Novex, Invitrogen). Following electrophoresis, proteins were blotted onto nitrocellulose, and membranes were incubated with 0.04 µg/ml of anti-*Ar*BGP affinity purified antibody. Alkaline phosphatase-labeled goat anti-rabbit IgG wasused as secondary antibody and NBT/BCIP as substrate solution. MWM, pre-stained molecular weight markers from Bio-Rad. Corresponding molecular weight (in kDa) are indicated on the right margin of the figure.

soupfin shark MGP [21]. Western-blot analysis of the filter-retained content in each sample using either the

Table 2. Detection and characterization of MGP protein in crude or purified bone and calcified cartilage acid extracts obtained from several teleost fish (*A. regius*, *S. senegalensis*, *S. aurata*, *D. rerio*), *X. laevis* and blue shark (*P. glauca*)

	Specimen (tissue)	SDS-PAGE[a]		Immunodetection[b] (antibody)	N-terminal sequence[c]
		CBB	DBS		
MGP	*A. regius* (branchial arches)	14–18 kDa	Positive	Western blot (anti-*Ar*MGP)	YE*SHESXESAEDLFVPXQ XANSFMTPXRG
	D. rerio (skeleton)	14–18 kDa	Positive	Western blot (anti-*Ar*MGP)	n.d.
	S. senegalensis (vertebra)	14–18 kDa	Positive	Western blot (anti-*Ar*MGP)	n.d.
	S. aurata (vertebra)	14–18 kDa	Positive	Western blot (anti-*Ar*MGP)	n.d.
	X. laevis (skeleton)	14–18 kDa	Positive	Western blot (anti-*Gg*MGP)	n.d.
	P. glauca (vertebra, jaw, branchial arches)	14–18 kDa	Positive	Western blot (anti-*Gg*MGP)	DSSESNEIDDVLFLGRRDA NSFMKYPQLGN

[a] The proteins were electrophoresed on a 4–20% SDS-PAGE (NuPage, Invitrogen), stained with CBB and DBS and the relative molecular weight estimated by comparison with pre-stained molecular weight markers (SeeBlue, Invitrogen)
[b] Immunodetection of the protein was performed by Western blot or Dot blot analysis using the anti-*Ar* MGP purified antibodies (0.1 µg) or anti-*Gg* MGP polyclonal antiserum (1:100 dilution) as primary antibody and alkaline phosphatase-labeled goat anti-rabbit IgG antibody with the NBT/BCIP substrate solution as secondary antibody
[c] The N-terminal sequence presented in this table was obtained as described in Materials and Methods section and is numbered from the first amino acid residue obtained from sequence determination. X, non-identified amino acid residue. E*, Gla residue, (n.d.) not determined

anti-*Ar*MGP purified antibody or the anti-*Gg*MGP polyclonal antiserum (Table 2) also confirmed the identification of these bands as MGP.

For the *S. aurata* and *S. senegalensis* retentate samples a single band with positive immunoreaction with anti-*Ar*MGP purified antibody was obtained (Fig. 4, A2, B2). These results together with the DBS-staining results performed on the same SDS-PAGE that also gave positive coloration for a band with the same migration behavior (Fig. 4, A1, B1) confirmed that the protein was γ-carboxylated and that there was no evidence of MGP aggregation. The presence of a second band in the same filter-retained extract (and a third band in the case of *S. senegalensis* sample) with a positive coloration by the DBS-staining but with a higher migration behavior suggested that BGP was present in both *S. aurata* and *S. senegalensis* filter-retained samples (Fig. 4, A1, B1). Western blot using anti-*Ar*BGP purified antibody as a control in these samples, gave positive immunoreaction for BGP confirming the hypothesis of the presence of BGP in *S. aurata* and *S. senegalensis* filter-retained samples (results not shown).

Western-blot analysis of *X. laevis* filter-retained content identified a band around 14–18 kDa with positive immunoreaction with anti-*Gg*MGP polyclonal antiserum that also gave positive coloration with DBS-staining performed on the same SDS-PAGE, confirming that the protein was γ-carboxylated (Fig. 4, A3, A1). In the case of *D. rerio*, the results obtained by Western blot showed three bands that positively immunoreacted with anti-*Ar*MGP antibody with a pattern of migration behavior similar to *Ar*MGP (Fig. 4, A2). The absence of any detectable band around 14–18 kDa is possibly due to protein aggregation during the ultrafiltration procedure performed using 5 mM ammonium bicarbonate. This phenomenon is characteristic of MGP especially when stored in non-denaturing buffers as previously referred to [23, 24]. A comparable result was also observed, although to a less extent, for the *Ar*MGP sample (Fig. 4, A2). However, and in agreement with results obtained for *A. regius* (results not shown), no coloration by DBS-staining was observed for this *Dr*MGP sample (result not shown) probably because of the protein aggregation limiting the exposure of the Gla residues to the staining, an essential feature to obtain a positive result with this staining procedure.

Given the complexity of the protein mixture content in *X. laevis*, *S. senegalensis*, *S. aurata* and *D. rerio* filter-retained samples, the low efficiency obtained on the separation over a 4–12% gradient SDS-PAGE (Fig. 4) and also the low MGP content and the aggregation phenomenon, it was not possible to obtain a clear N-terminal amino acid sequence for these samples.

*Pg*MGP sample analysis by Western blot with anti-*Gg*MGP polyclonal antiserum showed a positive immunoreaction for the 14 kDa band but a second band was also identified in the precipitant fraction with a higher migration behavior (around 6 kDa) (Fig. 4, C1, C2). This band probably represents fragments of MGP,

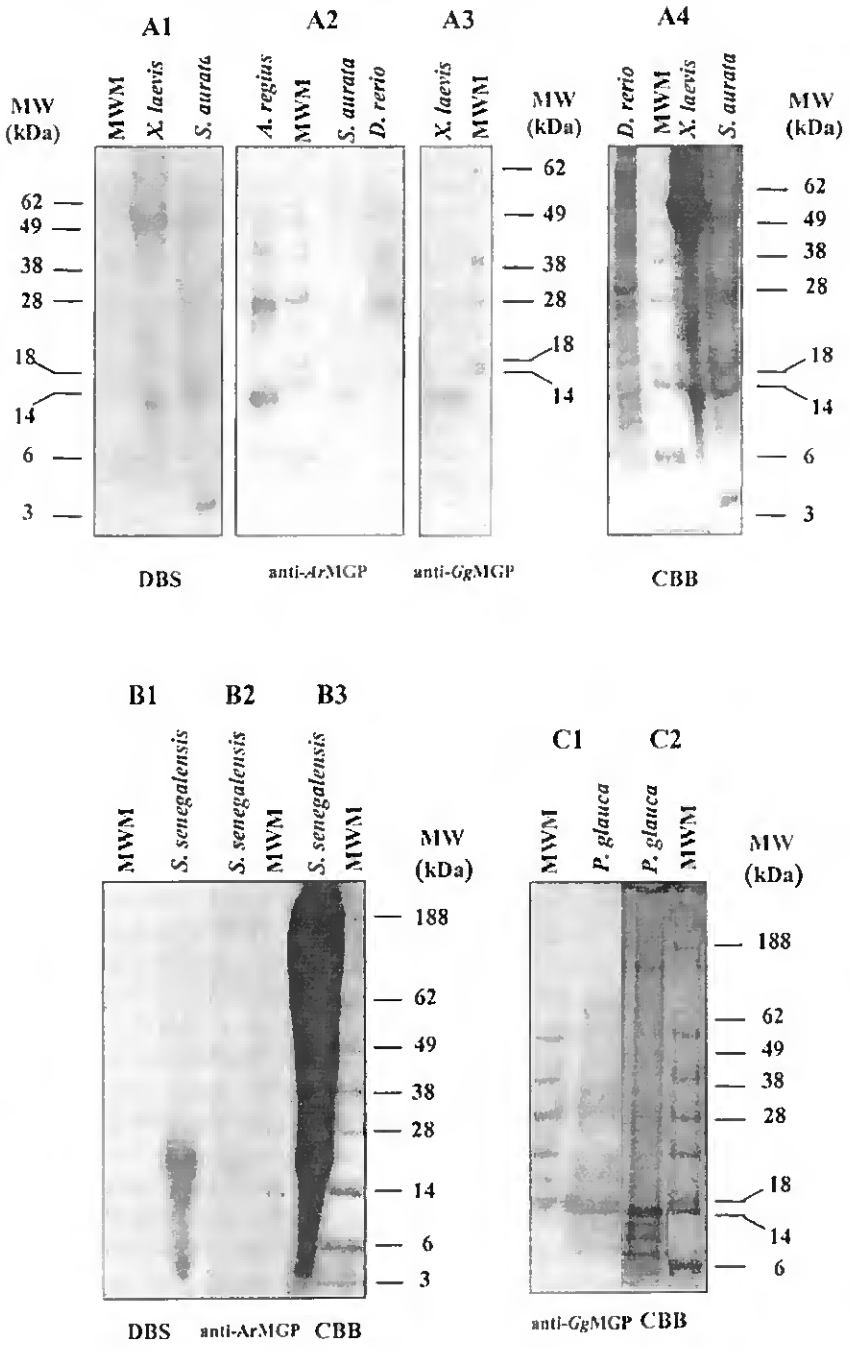

Fig. 4. SDS-PAGE and Western-blot analysis of several teleost fish (*S. aurata*, *S. senegalensis*, *D. rerio*, *A. regius*), *X. laevis* and *P. glauca* dialyzed acid extracts containing MGP. Electrophoresis was performed using 4–12% SDS-PAGE gels (Nupage, Invitrogen). Each lane was loaded with 30–50 µg of total protein. CBB: Gels were stained using the CBB staining method for total protein detection (A4, B3, C2). DBS: Gels were stained using the DBS staining method specific for Gla residues (A1, B1). anti-*Ar*MGP and anti-*Gg*MGP: for Western blot analysis, a 1:10 dilution of the samples was used to load the gel. Following electrophoresis, proteins were blotted onto nitrocellulose, and the membranes were incubated either with 0.04 µg/ml of anti-*Ar*MGP purified antibody (A2, B2) or 1:100 dilution of anti-*Gg*MGP polyclonal antiserum (A3, C1). Alkaline phosphatase-labeled goat anti-rabbit IgG was used as secondary antibody and NBT/BCIP as substrate solution as described in the Materials and Methods. MWM, SeeBlue pre-stained molecular weight markers (Invitrogen).

a result previously obtained in *Ar*MGP purification from teleost fish-calcified cartilage [15]. Western blot analysis of the insoluble and the soluble dialyzed fraction using the anti-*Ar*BGP antibodies gave negative results (results not shown).

Antiserum Purification and Characterization

For use in immunohistochemistry and in the analysis of cell protein extracts, *Ar*BGP and *Ar*MGP polyclonal antisera were affinity-purified, as described in Materials and Methods, using *Ar*BGP and *Ar*MGP purified from *A. regius* branchial arches [15]. As shown in Figures 5A and 5B, the affinity purification elution profile of both antisera permitted the separation of two different antibody entities, anti-*Ar*BGP-1 and anti-*Ar*BGP-2 in *Ar*BGP polyclonal antiserum (5A) and anti-*Ar*MGP-1 and anti-*Ar*MGP-2 in *Ar*MGP polyclonal antiserum (5B). Comparing the relative amount of the elution peaks obtained, anti-*Ar*BGP-2 (5A) and anti-*Ar*MGP-1 (5B) purified antibodies seemed to be the most abundant in the unpurified anti-*Ar*BGP and anti-*Ar*MGP antiserum, respectively. Dot blot analysis

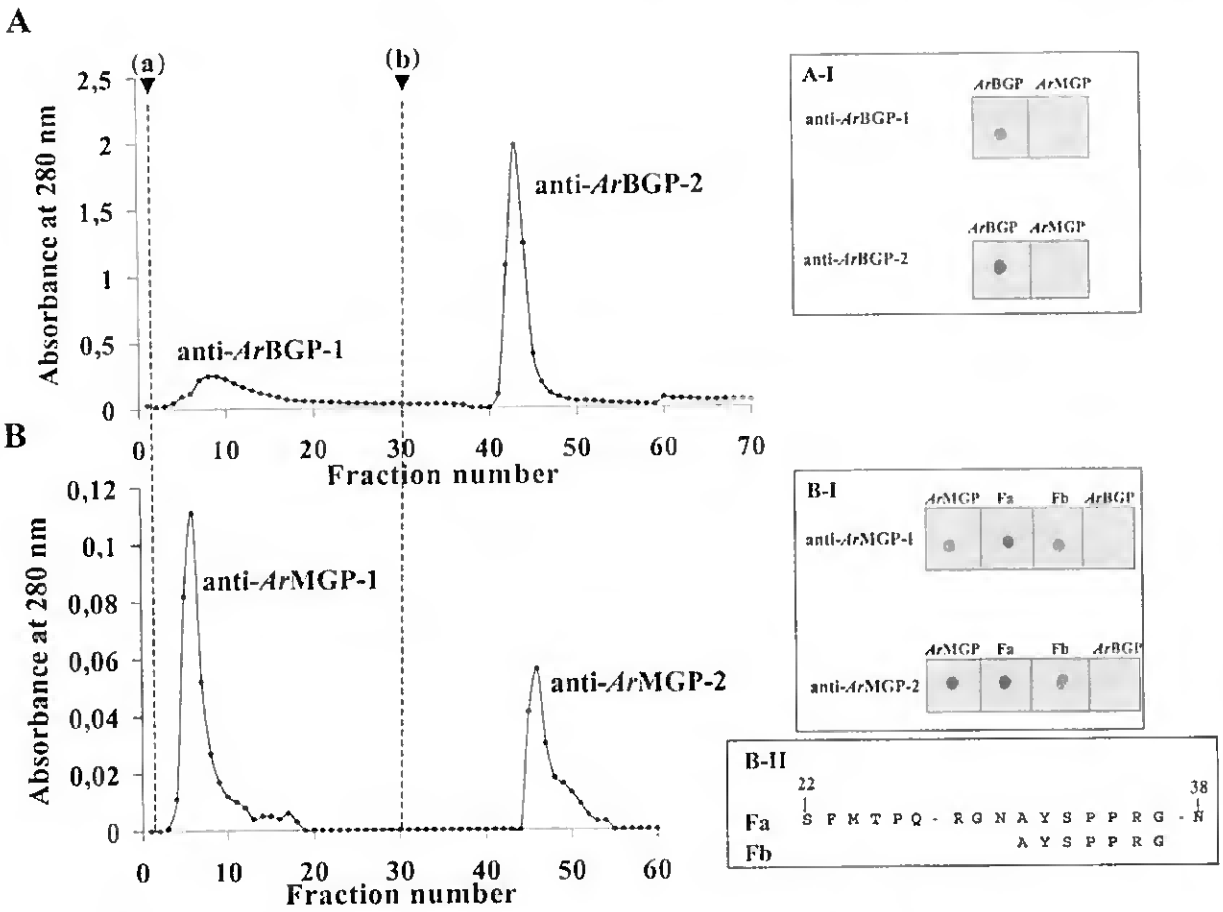

Fig. 5. Affinity purification of anti-*Ar*BGP (**A**) and anti-*Ar*MGP (**B**) polyclonal antiserum using CNBr-activated Sepharose 4B resin coupled with the corresponding antigen. Bound antibodies were eluted with approximately 100 mM glycine pH 2.5 (**a**), followed with 100 mM triethylamine, pH 11.5 (**b**). Fractions of approximately 1 ml were collected every 5 minutes. Elution profile was obtained by measuring absorbance of effluent fractions at 280 nm. Peak fractions were collected and dialyzed with phosphate buffer saline (PBS). Immunoreaction of 0.1 µg of *Ar*MGP, *Ar*BGP or polypeptide *Ar*MGP fragments (Fa and Fb, B-II) upon treatment with 0.04 µg/ml of anti-*Ar*BGP purified antibodies (A-I) and anti-*Ar*MGP purified antibodies (B-I) obtained by Dot-blot analysis, as described in Materials and Methods.

using different anti-*Ar*BGP purified antibody dilutions against various concentrations of the pure antigen showed that anti-*Ar*BGP-1 and -2 recognized the BGP antigen with the same degree of sensitivity (results not shown).

Characterization of anti-*Ar*MGP-purified antibodies by Dot-blot analysis also showed that anti-*Ar*MGP-1 and -2 recognized both *Ar*MGP antigen and the purified *Ar*MGP fragments [15] with the same degree of sensitivity, as tested by Dot blot analysis (Fig. 5B-I, B-II). Relative specificity of these antibodies was further tested using different antibody dilutions against various concentrations of purified MGP and polypeptide fragments and shown to be both equally specific for the fragments and the mature protein (results not shown).

Our results also indicate that the anti-*Ar*MGP and anti-*Ar*BGP purified antibodies were 100 times more sensitive than the unpurified antiserum since a dilution of 1:10,000 (corresponding to the same total protein concentration of originally unpurified antiserum) could detect 10 ng of purified antigen (results not shown).

Immunodetection of BGP and MGP Proteins from Different Teleost Fish, X. laevis and P. glauca Using ArBGP, ArMGP and GgMGP Antibodies

Specificity of both the affinity-purified anti-*Ar*BGP and anti-*Ar*MGP and the non-purified anti-*Gg*MGP antibodies was confirmed by Western blot analysis. The specificity was further tested by comparing its reaction with BGP and MGP proteins extracted from several teleost, a cartilaginous fish and *Xenopus*.

Recognition of *S. aurata, S. senegalensis and D. rerio* BGPs by anti-*Ar*BGP purified antibodies was assessed

Table 3. Immunodetection results for MGP and BGP extracted from several teleost fishes (*A. regius*, *S. aurata*, *S. senegalensis*, *D. rerio*), *X. laevis* and *P. glauca* using the affinity purified anti-*Ar*MGP (0.1 µg) and anti-*Ar*BGP antibodies (0.5 µg) and the anti-*Gg*MGP polyclonal antiserum (1:100 dilution). Relative specificity was deduced from Western blot and Dot blot analysis (as described in Materials and Methods) using the same concentration of antigen and primary antibody

Antibody	Antigen	Species	Relative specificity
		A. regius	+ + +
anti-*Ar*BGP	BGP	*S. aurata*	+ +
		S. senegalensis	+ +
		H. didactylus	+ +
		D. rerio	+ +
		X. laevis	–
anti-*Ar*MGP	MGP	*A. regius*	+ + +
		S. aurata	+ +
		S. senegalensis	+ +
		P. glauca	+
		D. rerio	+ +
		X. laevis	–
anti-*Gg*MGP	MGP	*P. glauca*	+ + +
		X. laevis	+ +
		A. regius	+ +

by Western blot (Fig. 3) using the proteins purified from acid extracts of calcified tissues (Table 1). A positive reaction with anti-*Ar*BGP antibodies was seen by Dot blot assay with *H. didactylus* BGP while no positive reaction was observed for *Xl*BGP (Table 1).

Positive immunoreaction of *S. aurata*, *S. senegalensis* and *D. rerio* MGPs was seen by Western blot analysis using the anti-*Ar*MGP purified antibodies as depicted in Figure 4. However, this antibody did not recognize *X. laevis* MGP whereas *P. glauca* MGP was recognized but with a lower specificity than teleost fish MGPs (Table 3). However, both *P. glauca* and *X. laevis* MGPs were immunodetected by Western blot using anti-*Gg*MGP polyclonal antiserum (Table 3).

Discussion

Based on previous results obtained in higher vertebrates (*B. taurus*) [25], in *X. laevis* and the teleost fishes *Xiphias gladius*, *S. aurata* and *A. regius* [15, 17, 26], we were able to purify and characterize BGP from the vertebra and jaw of several other marine teleost fishes (*S. senegalensis* and *H. didactylus*), and from the entire mineralized skeleton of a fresh water teleost (*D. rerio*). In contrast with mammals, two major histological types of bone can be found in teleost fish (cellular and acellular bone) [27, 29]. Despite these structural differences, our results indicate that in fish, as in mammals [26], fish bone-like mineralized tissue is the major site of accumulation for BGP [14, 15, 17] supporting the hypothesis that BGP function is likely to be associated with bone in all vertebrates. Comparison of *A. regius* BGP SDS-PAGE migration profile with those from other teleosts (*S. senegalensis*, *S. aurata*, *H. didactylus* and *D. rerio*), as well as from *X. laevis* and *B. taurus*, showed clear differences. While *X. laevis*, *H. didactylus* and *A. regius* BGPs had a similar behavior and migrated more like the *B. taurus* protein, the *S. aurata* and *D. rerio* BGPs migrated as smaller entities (Fig. 1). This result cannot be explained solely by the known molecular weight difference between the proteins, or by the differences in gamma-carboxylation, since the results of N-terminal sequence obtained (*A. regius* [15], *H. didactylus* and *D. rerio*, (this study), *S. aurata* and *X. laevis* [17], and *B. taurus* [29]) showed that BGP was always fully gamma-carboxylated at each of the three Gla residues. Comparison between calculated isoelectric points (pI) (Table 4) also does not reflect the anomalous migration behavior in SDS-PAGE since they all have low pIs. In contrast, the relative migration behavior of these BGPs on native polyacrylamide gels (Fig. 2) correlates better with the differences observed between their calculated pIs (Table 4), suggesting the presence of different levels of gamma-carboxylation.

Comparing the gel filtration purification profiles for BGP from different fishes (swordfish [26], *S. aurata* [17], *L. macrochirus* [16] and *A. regius* [15]) and considering the different levels of purity achieved in each reported experiment using similar techniques, we conclude that the BGP content in bone-like mineralized tissues seems to be dependent not only on the origin of the tissue but also on the fish species and stage of development. Different contents of BGP in vertebra may reflect not only the cellular versus acellular nature of the bone (depending on the species analyzed) but also on the requirement for this protein, which may vary depending on growth stage in teleosts.

This study reports for the first time the identification of MGP in acid extracts of teleosts vertebra. The identification of MGP in the teleosts *S. senegalensis*, *S. aurata* and *D. rerio* suggests that the level of MGP accumulation in teleost fishes mineralized tissues is also probably dependent on the stage of development since previous experiments failed to purify MGP from teleost fish vertebra acid extracts [15, 17]. This evidence is further supported by our previous immunohistochemistry results where we found that MGP can accumulate in *A. regius* neural arch vertebra in regions counterstaining with Alcian Blue (stains positive for mucopolyssacarides) [15]. The full characterization of this extracellular matrix by *in situ* hybridization and immunohistochemistry will be the subject of future studies once additional specific molecular markers are available for this fish, a work presently ongoing in our laboratory. Differences between the levels of MGP accumulation in vertebra of young and adult fishes may also

Table 4. Comparison of descriptive information based on BGP amino acid sequences of *B. taurus*, *X. laevis*, *A. regius*, *S. aurata* and *D. rerio* obtained using Peptide Statistics Tool (PEPSTATS) from biotools (http://biotools.umassmed.edu)[a]

		B. taurus	*X. laevis*	*A. regius*	*S. aurata*	*D. rerio**
	Molecular weight (Da)	5704.33	5359.79	4868.49	4950.63	5209.89
	Isoelectric point (pI)	4.21	4.08	3.76	3.87	4.10
	Number of residues	49	49	45	45	48
Types of residues	Aliphatic	8	8	7	10	8
	Aromatic	9	6	4	5	6
	Non-polar	31	28	28	29	30
	Polar	18	21	17	16	18
	Charged	16	12	9	8	9
	Basic	6	4	2	2	3
	Acidic	10	8	7	6	6

Sequence GenBank accession numbers are: AF459030 for *Argyrosomus regius*; AF048703 for *Sparus aurata* (seabream); AF055576 for *Xenopus laevis*; X53699 for bovine (*Bos taurus*); AY078413.1 for *Danio rerio*

* The complete mature sequence derived from nucleotic analysis was used for this comparison obtained from AY078413.1 (Gavaia, Simes et al., 2003 submitted)

[a] Values were calculated for BGP in the absence of hydroxyproline and γ-carboxylation of glutamic acid residues

reflect changes in the degree of mineralization found throughout development and in adult life and could be related to variable MGP synthesis rates at different periods of life or different requirement for MGP as the fish grows. These results are in contrast with data obtained in mammals in which it was shown that MGP accumulates at similar levels in bone of fetus or adult rats [11]. The presence in teleost fish MGPs of an extended C-terminus enriched in basic amino acids also found in shark [15, 21] and never found in mammalian MGPs, could be one of the reasons for the apparent higher affinity of the MGP for the mucopolisacaride-rich extracellular matrix found in branchial arches calcified cartilage and vertebra of fish.

Following the purification of MGP and BGP from *A. regius* mineralized tissues, the generation of specific polyclonal antibodies was successfully accomplished, as seen when tested for specificity and sensitivity for each specific antigen by Western blot analysis. The results obtained clearly showed that the anti-*Ar*MGP polyclonal antiserum only recognized fish MGP and not fish BGP and that anti-*Ar*BGP polyclonal antiserum was also specific for BGP [15].

To increase antibody specificity for use in immunohistochemistry studies, both polyclonal antisera were affinity-purified. Analysis of their purification profile suggested the presence of different antigen recognition sites in these antibodies, resulting in the purification of two separate peaks, each one in different elution conditions (acid and basic) (Fig. 5A, B). Both antibody-containing fractions resulted in comparable results when tested for immunoreactivity at different dilutions against the purified mature proteins. In the case of anti-*Ar*MGP antibodies, immunoreactivity against the purified MGP polypeptide fragments was also tested and both purified anti-*Ar*MGP antibody entities gave comparable results (Fig. 5B-I, B-II). Based on these results and since the two *Ar*MGP fragments comprised most of the mature protein (fragment Fa extended from residue 22 to the C-terminal residue, fragment Fb from residue 31 to the C-terminal residue) the possibility that the two antibodies recognize different epitopes cannot be inferred.

Immunodetection results obtained by Western blot using the affinity purified anti-*Ar*MGP and anti-*Ar*BGP antibodies showed that anti-*Ar*MGP specifically identified MGPs extracted from *S. senegalensis*, *S. aurata*, *D. rerio* and to a lower extent from *P. glauca* but did not immunoreact with *X. laevis* MGP (Table 3), a result that can be explained by the higher degree of sequence homology of the *X. laevis* sequence with MGPs from mammals and birds than with *A. regius* MGP [15]. Interestingly, the *X. laevis* MGP was found to immunoreact with another MGP polyclonal antiserum previously developed against shark MGP (anti-*Gg*MGP), a result that is not surprising given the features that shark and *X. laevis* MGPs have in common, namely the presence of an aspartic acid at position 2 and not a Gla residue which is seen in all other MGP sequences including *A. regius* [15]. However, this reaction was not as strong as was seen with MGP purified from a different shark (*Prionace glauca*) as expected.

Immunoreactivity of BGPs isolated from *S. senegalensis*, *S. aurata*, *D. rerio* and *H. didactylus* was also tested by Western blot and the results clearly showed that the purified anti-*Ar*BGP polyclonal antibodies were able to specifically recognize BGP purified from each of these different teleosts. As seen for MGP, the purified *Ar*BGP polyclonal antibody did not recognize BGP extracted from *Xenopus* bone (*Xl*BGP) (Table 3). This result has some consistency after comparison with the presently known fish BGP sequences [15, 30] since amphibian BGP is more closely related to bird and mammalian BGPs than to the fish proteins. The most notable

features are the conserved N-terminal insertion in bird, mammalian and *Xenopus* that is absent in teleosts and a homologous C-terminal in all *Xenopus*, bird and mammalian BGPs that is not conserved in fish BGPs.

The validation of these important biochemical tools in the recognition of either BGP or MGP antigen from different teleosts species, as well as from *X. laevis* and *P. glauca*, which are currently being studied in our laboratory, should be useful to further understand the deposition, distribution and developmental appearance of these proteins in non-mammalian vertebrates, thus providing further insight into its function throughout vertebrate evolution. The purified antibodies can now allow the establishment of specific immunoassays to adequately measure circulating levels of fish BGP and MGP, as already seen in the mammalian system. Another potential use of these tools may be to simplify purification procedures since they can be used to affinity purify these Gla-containing proteins from bone and calcified cartilage demineralized extracts.

Acknowledgments. This work was partially funded by grants from the Portuguese Science and Technology Foundation (Praxis BIA 469/94; BIA 11159/98; POCTI/CVT/42098/2001) and US Public Health Service, Grant AR25921 from the National Institutes of Health. DC Simes was the recipient of a PRODEP fellowship awarded by the Portuguese Ministry of Education. N-terminal amino acid sequences for *Dr*BGP, *Hd*BGP and *Pg*MGP were submitted to SWISS-PROT database and were assigned accession numbers P83238, P83473 and P83347, respectively.

References

1. Hauschka PV, Lian JB, Cole DEC, Gundberg CM (1989) Osteocalcin and matrix Gla protein: vitamin K-dependent proteins in bone. Physiol Rev 69:990–1047
2. Ducy P, Desbois C, Boyce B, et al. (1996) Increased bone formation in osteocalcin-deficient mice. Nature 382:448–452
3. Luo G, Ducy P, McKee MD, Pinero GJ, Loyer E, Behringer RR, Karsenty G (1997) Spontaneous calcification of arteries and cartilage in mice lacking matrix gla protein. Nature 386:78–81
4. Yagami K, Suh J-Y, Enomoto-Iwamoto M, Koyama E, Abrams WR, Shapiro IM, Pacifici M, Iwamoto M (1999) Matrix gla protein is a developmental regulator of chondrocyte mineralization and, when constitutively expressed, blocks endochondral and intramembranous ossification in the limb. J Cell Biol 147:1097–1108
5. Shanahan CM, Proudfoot D, Farzaneh-Far A, Weissberg PL (1998) The role of Gla proteins in vascular calcification. Crit Rev Eukaryotic Gene Express 8:357–375
6. Price PA, Faus SA, Williamson MK (1998) Warfarin causes rapid calcification of the elastic lamellae in rat arteries and heart valves. Arterioscler Thromb Vasc Biol 18:1400–1407
7. Shanahan CM, Cary NRB, Salisbury JR, Proudfoot D, Weissberg PL, Edmonds M (1999) Medial localization of mineralization-regulating proteins in association with monckeberg's sclerosis, evidence for smooth cell-mediated vascular calcification. Circulation 100:2168–2176
8. Price PA, Faus SA, Williamson MK (2000) Warfarin-induced artery calcification is accelerated by growth and vitamin D. Arterioscler Thromb Vasc Biol 20:317–327
9. Shanahan CM, Proudfoot D, Tyson KL, Cary NRB, Edmonds M, Weissberg PL (2000) Expression of mineralization-regulating proteins in association with human vascular calcification. Z Kardiol 89:63–68
10. Spronk HMH, Soute BAM, Schurgers LJ, Cleutjens JPM, Thijssen HHW, De Mey JGR, Vermeer C (2001) Matrix gla protein accumulates at the border of regions of calcification and normal tissue in the media of the arterial vessel wall. Biochem Biophys Res Commun 289:485–490
11. Otawara Y, Price PA (1986) Developmental appearance of Matrix gla protein during calcification in rat. J Biol Chem 261:10828–10832
12. Hale JE, Mattew KW, Price PA (1991) Carboxyl-terminal proteolytic processing of matrix gla protein. J Biol Chem 266:21145–21149
13. Price PA, Rice JS, Williamson MK (1994) Conserved phosphorylation of serine in the Ser-X-Glu/Ser(P) sequences of the vitamin K-dependent matrix gla protein from shark, lamb, rat, cow and human. Protein Sci 3:822–830
14. Cancela ML, Williamson MK, Ohresser MCP, Reia JP, Price PA (2001) Matrix gla protein in *Xenopus laevis:* molecular cloning, tissue distribution and evolutionary considerations. J Bone Miner Res 16:1611–1621
15. Simes DC, Williamson MK, Ortiz-Delgado JB, Viegas CSB, Cancela ML, Price PA (2003) Purification of Matrix Gla Protein (MGP) from a marine teleost fish, *Argyrosomus regius*: calcified cartilage and not bone as the primary site of MGP accumulation in fish. J Bone Miner Res 18:244–259
16. Nishimoto SK, Araki N, Robinson FD, Waite JH (1992) Discovery of bone γ-carboxyglutamic acid protein in mineralized scales. The abundance and structure of *Lepomis macrochirus* bone γ-carboxyglutamic acid. J Biol Chem 267:11600–11605
17. Cancela ML, Williamson MK, Price PA (1995) Amino-acid sequence of Bone Gla Protein from the African clawed toad *Xenopus laevis* and the fish *Sparus aurata*. Int J Peptide Protein Res 46:419–423
18. Delmas PD, Christiansen C, Mann KG, Price PA (1990) Bone Gla Protein (osteocalcin) assay standardization report. J Bone Miner Res 5:5–11
19. Jie K-SG, Gijsbers BLMG, Vermeer C (1995) A specific colorimetric staining method for γ-carboxyglutamic acid-containing proteins in polyacrylamide gels. Anal Biochem 224:163–165
20. Sambrook J, Fritsch EF, Maniatis T (1989) Molecular cloning: a laboratory manual. Cold Spring Harbor Laboratory Press, New York
21. Rice JS, Williamson MK, Price PA (1994) Isolation and sequence of the vitamin K-dependent Matrix Gla Protein from the calcified cartilage of the soupfin shark. J Bone Miner Res 9:567–576
22. Poser JW, Price PA (1979) A method for decarboxylation of the γ-carboxyglutamic acid in proteins. J Biol Chem 254:431–436
23. Fraser JD, Price PA (1990) Induction of Matrix Gla Protein synthesis during prolonged 1,25-Dihydroxyvitamin D_3 treatment of osteosarcoma cells. Calcif Tissue Int 46:270–279
24. Fraser JD, Otawara Y, Price PA (1988) 1,25-Dihydroxyvitamin D_3 stimulates the synthesis of matrix γ-carboxyglutamic acid protein by osteosarcoma cells. J Biol Chem 263:911–916
25. Price PA, Otsuka AS, Poser JW, Kristaponis J, Raman N (1976) Characterization of a γ-carboxyglutamic acid-containing protein from bone. Proc Natl Acad Sci USA 73:1447–1451
26. Price PA, Otsuka AS, Poser JW (1977) Comparison of gamma-carboxyglutamic acid-containing proteins from bovine and swordfish bone: primary stucture and Ca^{2+} binding. In: Wasserman RH, Corradino RA, Carafoli E, Kretsinger RH, Mac-Lennan DH, Siegel FL (Eds.) Cal-

cium-binding proteins and calcium function. Elsevier North-Holland, Amsterdam, pp 333–337
27. Witten PE (1997) Enzyme histochemical characteristics of osteoblasts and mononucleated osteoclasts in a teleost fish with acellular bone (*Oreochromis niloticus*, Cichlidae). Cell Tissue Res 287:591–599
28. Witten PE, Hansen A, Hall BK (2001) Features of mono- and multinucleated bone-resorbing cells of the Zebrafish *Danio rerio* and their contribution to skeletal development, remodeling and growth. J Morph 250:197–207
29. Price PA, Poser JW, Raman N (1976) Primary structure of the gamma-carboxyglutamic acid-containing protein from bone. Proc Natl Acad Sci USA 73:3374–3375
30. Viegas CS, Pimto JP, Conceicao N., Simes DC, Cancela ML (2002) Cloning and characterization of the cDNA and gene encoding **Xenopus laevis** osteocalcin Gene 289: 97–107

Elsevier Editorial System(tm) for Gene Expression Patterns

Manuscript Draft

Manuscript Number:

Title: Molecular cloning of osteocalcin and Matrix Gla Protein from zebrafish (Danio rerio) and Senegal sole (Solea senegalensis): Comparative gene and protein expression analysis from larval development through adulthood

Article Type: Normal Submission

Section/Category:

Keywords: Matrix Gla protein; Bone Gla protein; zebrafish; Senegal sole; expression patterns

Corresponding Author: Dr. Paulo J. Gavaia,

Corresponding Author's Institution: CCMar, Universidade do Algarve

First Author: Paulo Jorge Gavaia, PhD

Order of Authors: Paulo Jorge Gavaia, PhD; Paulo J. Gavaia; Dina C. Simes; Juan-Bosco Ortiz-Delgado; Carla S.B. Viegas; Jorge P. Pinto; Robert N. Kelsh; Carmen Sarasquete; Leonor Cancela

Manuscript Region of Origin:

Abstract: In this study the tissue distribution and accumulation of bone Gla protein (Bgp or osteocalcin) and matrix Gla protein (Mgp) were determined during larval development and in adult tissues of the zebrafish (Danio rerio) and throughout metamorphosis in Senegal sole (Solea senegalensis) following cloning of the corresponding cDNAs. Mineral deposition was investigated in parallel using Alizarin red. In zebrafish, the presence of bgp and mgp mRNA was revealed by in situ hybridization in all mineralized tissues during and after calcification, including bone and the calcified cartilage of branchial arches. This expression was confirmed by Real Time PCR in specimens of same age and developmental stages. Immunolocalization of Bgp and Mgp demonstrated that these proteins accumulate mainly in the matrix of skeletal structures

already calcified or in the process of calcifying, confirming in situ hybridization results. Interestingly, some accumulation of Bgp was also observed in kidney, which could be due to the presence of a related protein, nephrocalcin. Chromosomal localization of bgp and mgp using a zebrafish radiation hybrid panel indicated that both genes are located on the same zebrafish chromosome, in contrast to their mapping in mammals. Results obtained in Senegal sole further indicate that, during metamorphosis, there is an increase in expression of both bgp and mgp, in parallel with the calcification of axial skeleton structures.
In contrast with results obtained for previously studied marine fishes, in sole as in the fresh water Zebrafish, Mgp accumulates in both calcified tissues and in vessel walls of the vascular system, as also seen previously in higher vertebrates. These results suggest a major difference in the pattern of Mgp accumulation between marine and freshwater fishes, the latter being more reminiscent of those results obtained in mammals. From an evolutionary point of view, these results further indicate that zebrafish is a suitable model to conduct studies on mgp gene expression and function.

Molecular cloning of osteocalcin and Matrix Gla Protein from zebrafish (*Danio rerio*) and Senegal sole (*Solea senegalensis*): Comparative gene and protein expression analysis from larval development through adulthood.

Paulo J. Gavaia [(1)], Dina C. Simes[(1)], J.B. Ortiz Delgado[(1)], Carla S.B. Viegas[(1)], Jorge P. Pinto[(1)*], Robert N. Kelsh[(2)], M. Carmen Sarasquete[(3)], M. Leonor Cancela[(1)]

[(1)] CCMar, Universidade do Algarve, Campus de Gambelas, 8005-139 Faro, Portugal.

[(2)]Centre for Regenerative Medicine, Department of Biology and Biochemistry, University of Bath, Claveston Down, Bath BA2 7AY, UK.

[(3)] Superior Council for Scientific Investigation - Andalusia Institute of Marine Sciences. Pol. Rio San Pedro s/n, Apdo. Oficial 11510, Puerto Real (Cadiz), Spain.

* Present address: Institute for Molecular and Cell Biology. Laboratory of Molecular Immunology. Rua do Campo Alegre, 823. 4150-180 Porto- Portugal

Running title: Expression of *bgp* and *mgp* genes in *D. rerio* and *S. senegalensis*

Corresponding author: M. Leonor Cancela,

Email: lcancela@ualg.pt

Fax: (+351) 289 818353

Phone: (+351) 289 800971

Abstract

In this study the tissue distribution and accumulation of bone Gla protein (Bgp or osteocalcin) and matrix Gla protein (Mgp) were determined during larval development and in adult tissues of the zebrafish (*Danio rerio*) and throughout metamorphosis in Senegal sole (*Solea senegalensis*) following cloning of the corresponding cDNAs. Mineral deposition was investigated in parallel using Alizarin red. In zebrafish, the presence of *bgp* and *mgp* mRNA was revealed by *in situ* hybridization in all mineralized tissues during and after calcification, including bone and the calcified cartilage of branchial arches. This expression was confirmed by Real Time PCR in specimens of same age and developmental stages. Immunolocalization of Bgp and Mgp demonstrated that these proteins accumulate mainly in the matrix of skeletal structures already calcified or in the process of calcifying, confirming *in situ* hybridization results. Interestingly, some accumulation of Bgp was also observed in kidney, which could be due to the presence of a related protein, nephrocalcin. Chromosomal localization of *bgp* and *mgp* using a zebrafish radiation hybrid panel indicated that both genes are located on the same zebrafish chromosome, in contrast to their mapping in mammals. Results obtained in Senegal sole further indicate that, during metamorphosis, there is an increase in expression of both *bgp* and *mgp*, in parallel with the calcification of axial skeleton structures.

In contrast with results obtained for previously studied marine fishes, in sole as in the fresh water Zebrafish, Mgp accumulates in both calcified tissues and in vessel walls of the vascular system, as also seen previously in higher vertebrates. These results suggest a major difference in the pattern of Mgp accumulation between marine and freshwater fishes, the latter being more reminiscent of those results obtained in

mammals. From an evolutionary point of view, these results further indicate that zebrafish is a suitable model to conduct studies on *mgp* gene expression and function.

1. Introduction

Matrix γ-carboxyglutamic acid (Gla) protein (Mgp) and bone Gla protein (also known as Bgp or osteocalcin) are small extracellular matrix proteins originally isolated from vertebrate bone (Price et al 1976, Price et al 1983, Price and Williamson, 1985) and belong to the family of Ca^{2+} binding vitamin K-dependent proteins. In mammals, genetic studies have provided evidence that Bgp and Mgp function as inhibitors of tissue calcification (Ducy *et al.*, 1996; Lou *et al.*, 1997), with expression of *bgp* being specific to bone tissue and dentine (Price 1990) while expression of *mgp* is mainly associated with cartilage and soft tissues (heart, kidney and lung) (Fraser & Price, 1988, Cancela *et al.*, 1990, Cancela *et al.*, 2001), as well as the vascular system (Hao *et al*, 2004). Furthermore, Mgp has been proven to be a decisive factor for differentiation and maturation of chondrocytes and a key regulator of endochondral and intramembranous ossification (Yagami *et al.*, 1999, Newman *et al.*, 2001). However, much remains to be elucidated concerning the roles played by these two proteins at the molecular level.

Price *et al* (1977) identified Bgp in fish bone (swordfish, *Xiphias gladius*). Later, Nishimoto *et al* (1992) purified Bgp from the scales of bluegill (*Lepomis macrochirus*) while Cancela *et al.* (1995) and Roy *et al.* (2001) isolated Bgp from bone of the seabream (*Sparus aurata*) and carp (*Ciprinus carpio*) respectively, and found that Bgp is present in fish bone in amounts comparable to those extracted from mammalian bone. The first nucleotide sequences for fish *bgp* cDNA and gene were obtained for *Sparus aurata* indicating a comparable gene structure with mammalian genes and a similar expression pattern following the onset of calcification (Pinto *et al* 2001). The *bgp* cDNA was also cloned from another marine fish, *Argyrosomus regius*, and specific antibodies developed against the purified protein (Simes *et al.*, 2003). More recently,

these antibodies were validated for various marine and freshwater fishes including zebrafish and Senegal sole (Simes *et al* 2004).

In fish, Mgp was first purified from the vertebra of a cartilaginous fish, the soupfin shark (*Galeorhinus galeus*) (Rice et al 1994). However, its purification from a teleost fish was only achieved very recently in *Argyrosomus regius*, a fish with large calcified branchial arches, the only tissue where Mgp was found to accumulate (Simes et al 2003), in contrast with results obtained for mammals, chicken and amphibian, which accumulate Mgp in bone tissue. The cloning of its cDNA and development of specific antibodies allowed identification of sites of *mgp* gene expression and protein accumulation in this fish (Simes et al 2003). Its subsequent cloning from *Sparus aurata*, which can be grown in aquaculture conditions, provided for the first time insight into the tissue distribution and expression of *mgp*, demonstrating that the protein accumulates mainly in cartilage and gene expression is restricted to cartilage and arterial system during larval developmental of this marine fish (Pinto *et al.*, 2003).

Despite this recent information obtained for fish Bgp and Mgp, not much is known about their function in non-mammalian organisms and in particular, during the early formation of fish skeletal elements. Since these proteins are known to be endogenous calcification inhibitors, we chose to work in two different teleost fishes living in environments with very different calcium concentrations, fresh water and sea water. Zebrafish (*Danio rerio)*, is a fresh water teleost with cellular (osteocyte containing) bone, which is an accepted model organism for vertebrate development. The cells involved in bone formation and remodelling are described as being similar in many aspects to those found in the mammalian system, with the presence of osteoblasts (bone forming cells) and both mononucleated and multinucleated osteoclasts (bone resorbing cells) (Witten *et al.*, 2001) although little is known of how these cells interact to

modulate bone matrix formation and remodelling (Witten *et al.*, 2001). In contrast, the Senegal sole (*Solea senegalensis*) is an important marine fish for aquaculture and was chosen because it undergoes a radical change in skeletal morphology during larval stages, which is crucial for its later survival and life style. The skeletal development for this species has been previously described (Gavaia *et al.*, 2002). The first bony structure reported is the cleithrum that forms early after hatching, while the remaining skeletal structures appear as cartilage. Sole undergoes a metamorphosis with eye migration from left to right side and concomitant bending of the urostyle and torsion of internal organs that starts in larvae around 4.1 mm standard length (Lst) and ends at approximately 8 mm Lst. Development of both caudal complex and vertebral column begins at 12–13 days after hatching, accompanying the urostyle torsion and acquisition of asymmetry by migration of the left eye and changing to a benthic life style (Gavaia *et al.*, 2002).

In this article we report for the first time the cloning of full length *bgp* and *mgp* cDNAs from zebrafish and provide a comprehensive description of the onset of *bgp* and *mgp* gene expression throughout larval development and into adulthood. These findings are related to the sites of Bgp/Mgp protein accumulation and the appearance of bone and cartilaginous structures as detected by histological techniques. These results are compared with those obtained for Senegal sole, and analyzed in light of the recent information obtained in the literature for fish Bgp and Mgp. Furthermore, these results provide the essential basal knowledge required to further study the role exerted by Bgp and Mgp on the molecular mechanisms associated with onset and mineralization of skeletal structures in the two species analyzed.

2. Materials and Methods

2.1 Larval rearing and maintenance

S. senegalensis eggs were collected from natural spawning of a broodstock adapted to captivity and incubated in 80 l cylindro-conical tanks at a density of 350 eggs per liter, under the same environmental conditions of the broodstock tank. Newly hatched artemia nauplii were supplied from day 3 to day 10, 24 h metanauplii from day 11 to metamorphosis and 48 h metanauplii until juvenile stage. The metanauplii were enriched with the phytoplankton *Tetraselmis suessica* (clone T Chui) and *Isochrisys galbana* (clone T Iso).

D. rerio eggs were obtained from natural spawning of wild type breeding fish, maintained at 28.5°C on a 14 hour light/10 hour dark photoperiod. Larvae were maintained and raised by standard methods, according to Westerfield et al (1995) in the zebrafish book.

2.2 Sample collection

Samples of larval and juvenile individuals were randomly collected at regular intervals throughout the developmental period, from hatching through metamorphosis and up to juvenile stages. For histological analysis, individuals were anaesthetized with 0.1% 2-phenoxyethanol (Sigma, St Louis, MO) and fixed in buffered 4% paraformaldehyde (pH 7.4 in PBS) for 24 h at 4°C. After fixation, samples were washed in PBS and immediately processed for skeletal double staining or conserved in methanol at –20°C until further processing. For RNA preparation, individuals were frozen in liquid nitrogen and either immediately processed or stored at –80°C for later use.

2.3 Histological procedures

Whole mount staining of the skeleton: Development of *Danio rerio* and *Solea senegalensis* skeletal structures was followed from hatching to juvenile stages through specific staining according to Gavaia *et al* (2000).

Histological slides: Some individuals of the same age and developmental stage of those used for whole mount skeletal staining were included either in paraffin or in Historesin Plus (Jung). Paraffin sections of 6-8 μm were prepared in a microtome, floated in sterile distilled water, collected in TESPA (3-aminopropyltriethoxysilane, Sigma) -coated slides and dried over night at 37°C. Historesin Plus sections with 2-5 μm were obtained in a JUNG supercut 2065 microtome and collected in TESPA coated slides. The sections were stored at 4°C in a dry box with silica gel until processing for *in situ* hybridization or immunostaining. Some sections were stained for mineral deposits with Alizarin red S and haematoxylin or with silver nitrate by the von Kossa's method to confirm presence of mineral. Adjacent sections were stained with haematoxylin-eosin (HE) or toluidine blue to identify physiological structures.

Staining for acid phosphatase activity: Tartrate resistant acid phosphatase (TRAP) detection was performed using a modification of a previously established method (Burstone 1959). Plastic sections of mineralizing larvae and juveniles were incubated in a working solution containing naphthol-ASBI-phosphate, sodium nitrite, hexazotized pararosanilin and 50 mM sodium tartrate in veronal acetate buffer at pH 5, for 1 hour at 37°C. Counterstaining was performed with haematoxilin. After staining, the sections were dehydrated and mounted with EUKIT (Merck).

Staining for alkaline phosphatase activity: Alkaline phosphatase activity was demonstrated by incubating samples for 1 hour at 37°C in a solution containing naphthol AS-MX phosphate, Fast blue BB, and magnesium sulfate, in 0.1M Tris buffer

(pH 8.0). Counter staining was performed with nuclear fast red for 10 minutes. After staining, the sections were dehydrated by air drying and mounted with EUKIT.

2.4 Molecular cloning of *D. rerio* and *S. senegalensis bgp* cDNAs

Partial cDNAs for *Danio rerio* and *Solea senegalensis bgp* (*Danio rerio bgp* AY078413; *Solea senegalensis bgp* AF059349) were cloned from total RNA extracted from the vertebral columns and heads of adult wild-type fishes by RT-PCR amplification. 1μg of total RNA was reverse transcribed using the Universal oligo-(dT) primer and MMLV-Reverse transcriptase (Gibco, BRL) and amplified by PCR with Taq DNA polymerase (Promega) in a Perkin Elmer DNA thermal cycler (Perkin Elmer, Foster City, CA, USA). Amplification of *D. rerio bgp* was achieved using a forward primer (ZbBGP 6F) designed based on the N-terminal amino acid sequence obtained (Simes *et al.*, 2004) and the universal adapter as reverse primer. For the cloning of *Solea senegalensis bgp* the forward primer (SBG5F) was designed from a concensus region based on alignments of all fish *bgp* sequences previously known and the universal adapter was used as reverse primer. PCR products were resolved in a 1.5% agarose gel by electrophoresis and expected size fragments extracted from the gel, inserted into the plasmid pGem T-easy (Promega), cloned and sequenced (T7 sequencing kit, Amersham-Pharmacia Biotech, USA). For the identification of the 5' ends of the two cDNAs, poly(A+) RNA was purified from 300 μg of total RNA extracted from either a whole zebrafish specimen or from the vertebral column, branchial arches, kidney and heart of a juvenile sole, with Quick Prep Micro messenger RNA (mRNA) purification Kit (Amersham-Pharmacia Biotech, USA). The 5′ends of *D. rerio* and *S. senegalensis bgp* cDNAs were amplified by 5′rapid amplification of cDNA ends (5'-RACE) with the MarathonTM cDNA Amplification Kit (Clontech), and

specific reverse primers (ZbBGP1R and SseBGP1R) designed within the corresponding partial *bgp* cDNA sequences previously obtained. Amplification conditions used were those indicated by the supplier. Sequences of all primers are shown in Table 1.

2.5 Molecular cloning of *D. rerio* and *S. senegalensis mgp* cDNAs

A partial cDNA sequence for *Danio rerio mgp* (BF938148) was obtained by TblastN search on the NCBI gene bank (EST: fm73a11.y1). One forward primer was designed based on this sequence (*Dr*MGP1F) and used to amplify the 3' end of *Danio rerio mgp* sequence using 1 μg of reverse transcribed total RNA obtained from zebrafish heads and vertebral columns and the universal adapter as reverse primer.

A partial *Solea senegalensis mgp* sequence was amplified from 1 μg of total RNA isolated from Senegal sole head and vertebral column by RT-PCR using a forward primer designed from a consensus region based on alignments of all fish *mgp* sequences previously known (CorvMGP3F, Simes *et al.*, 2003) and the universal adapter as reverse primer. PCR products were resolved in a 1.5 % agarose gel by electrophoresis and expected size fragments extracted from the gel, inserted into the plasmid pGem T-easy (Promega), cloned and sequenced (T7 sequencing kit, Amersham-Pharmacia Biotech, USA).

The 5'-end of *Danio rerio mgp* and *Solea senegalensis mgp* cDNAs were amplified by 5-RACE with specific reverse primers constructed based on the previously obtained partial *mgp* cDNAs sequences (DrMGP1R) and (SseMGP1R) and using the same Marathon libraries and PCR conditions described for *Danio rerio mgp* and *Solea senegalensis bgp* 5'-end amplification. Sequence of all primers is indicated in Table 1.

2.6 Detection of *D. rerio bgp* and *mgp* gene expression by quantitative Real-time PCR

Total RNA was isolated with TRIZOL reagent from different larval and juvenile stages of *D. rerio*, ranging from 32 hours post-fertilization (hpf) to 47 days post-fertilization (dpf). 1 μg of total RNA was reverse transcribed using an oligo (dT) adapter.

Real-time PCR was performed in a iCycler iQ real-time PCR detection system (Bio-Rad), using the following primer sets: ZBGP8F and ZBGP2R to amplify *D. rerio bgp*; DrMGP4F and DrMGP2R for *D. rerio mgp*, Dr28SRIB1F and Dr28SRIB to amplify *D. rerio* 28S ribosomal RNA and, SsBGP3F and SsBGP2R to amplify *S. senegalensis bgp*, SsMGP2F and SsMGP2R for *S. senegalensis mgp*, SsACT1F and SsACT1R to amplify *S. senegalensis* β-actin (based on a partial sequence previously obtained - AF059350). Sequence of all primers is indicated in Table 1.

The PCR reactions were set up in triplicates by adding 2μl of a 1:10 cDNA dilution to 18μl reaction mix containing 0.5 μM of each primer, and 10 μl of iQ SYBR green Supermix (Bio-Rad). The PCR program contained an initial cycle of 3 min at 95°C followed by 50 cycles comprising an initial denaturation step at 95°C for 30 sec, followed by annealing and extension at 68°C for 30 sec. The fluorescence was measured at the end of each extension cycle in the FAM-490 channel. Relative levels of expression were determined using as control levels those found for the youngest specimen analyzed in each species (29 hpf for zebrafish and 72 hpf for Senegal sole).

2.7 Immunohistochemistry

Immunohistochemistry was performed as described using rabbit polyclonal primary antibodies developed against Bgp and Mgp from *A. regius* and previously

validated for *D. rerio* and *S. senegalensis* Bgp and Mgp (Simes *et al.*, 2004). To confirm the specificity of the immunostaining, controls were performed by replacement of primary antibody with pre immune serum or BSA and by omission of primary and secondary antibodies.

2.8 *In situ* hybridization

Partial cDNAs for both *D. rerio* and *S. senegalensis bgps* and *mgps* were cloned into pGem T-Easy. After linearization of the plasmid with appropriate endonucleases, Digoxigenin (DIG)-labelled sense and antisense RNA-probes were synthesized according to the manufacturer's specifications using either bacteriophage T7 or SP6 RNA polymerases (Boehringer Mannheim). Probe synthesis was analyzed by agarose (1.2%) gel electrophoresis. Sections were prepared and *in situ* hybridization performed as described (Simes *et al.*, 2003).

2.9 Mapping of *mgp* and *bgp* genes on the Zebrafish LN54 panel.

The radiation hybrid panel LN54 (Loeb, NIH, 5000rad, 4000rad) was constructed by Marc Ekker's group (Hukriede *et al.*, 1999) and used to map *mgp* and *bgp* genes from zebrafish. One microliter of each of the 93 radiation hybrid DNA samples (100 ng/µl) and three controls, consisting of DNA from the two individual parental cell lines (zebrafish AB9 and mouse B78) and a 1:10 mixture of the later two, were amplified by PCR, using 1 µM of primer pair ZFMGPMAP1F / ZFMGPMAP1R or ZFBGPMAP1F / ZFBGPMAP1R (Table 1). Reaction mixture included 1x PCR Buffer (Invitrogen), 2 mM $MgCl_2$, 0.2 mM each dATP, dCTP, dGTP and dTTP, and 1 unit of Taq DNA polymerase (Invitrogen) in a total volume of 20 µl. PCR was performed for 35 cycles (one cycle: 30 sec at 94°C, 40 sec at 68°C and 45 sec at 72°C)

with a pre-dwell of 3 min at 94°C and a post-dwell of 12 min at 72°C. PCR products were separated on 1.5% agarose gels and the images captured with a Gel Doc 2000 using the Quantity One 4.2.1 software (BioRad). All PCR assays were performed at least in duplicate.

3. Results

3.1 Zebrafish skeletal development: The nomenclature used for description of head structures follows and extends that presented by Piotrowski *et al.* (1996) and Schilling *et al.* (1996) for the description of early branchial arches and skeletal development in the cranium. Specimens of zebrafish collected during the hatching period (between 48-52 hours post fertilization, hpf) present an underdeveloped skeleton, composed only of cartilaginous elements and the otolyths. Structures present in the head skeleton are the basihyal and the first branchial arches, ceratohyal and ceratobranchials 1, 2 and 3, Meckel's cartilage, palatoquadrate, hyosymplectic, ethmoid plate and trabeculae. The notochord is the only axial support element and the paired pectoral fins appear as cartilaginous plates, attached to a cartilaginous coraco-scapular complex. No calcified structures are visible at this stage, beside the otolyths. At 72 hpf the larvae present a similar distribution of skeletal elements, although an elongation of the structures is observed and the number of ceratobranchials has increased to 5. Meckel's cartilage has migrated forward and the mouth is already opened. At this stage a calcified cleithrum becomes visible, supporting the coraco-scapular complex. The first calcified pharyngeal teeth appear at 96 hpf (**Figure 1A**) attached to the fifth pair of ceratobranchials as ventral elements. At this same age the process of perichordal calcification of the basioccipital articulatory process (BOP) has started, and this is the first structure of the axial support skeleton to mineralise. At 5 days post fertilisation (dpf) calcification continues to increase in the cleithrum, pharyngeal teeth and BOP and extends to the opercular bones (**Figure 1B**). At 6 dpf the hyosymplectic starts to mineralize in a perichondral manner (**Figure 1C**), and the zones on the periphery of the opercula start to calcify. The ceratohyal cartilage begins to mineralize in a median region at 8 dpf (**Figure 1D**) extending subsequently to both extremities. The first two cartilaginous

hypural plates appear ventrally at the posterior extremity of the notochord (**Figure 1E**). The first forming vertebrae are observed at 9 dpf as a mineral deposition over the notochord (**Figure 1F**), starting on the dorsal zone and then extending ventrally. The first vertebrae to form are 3, 4, 5 and 6, followed shortly by vertebrae 1 and 2. Calcification continues in the head structures and the cartilaginous hypural 3 appears. Vertebral formation continues towards the posterior end and at 12 dpf all individuals showed vertebrae surrounding the notochord to the level of caudal vertebrae 20-25 (**Figure 1G**). The five hypurals, parhypural and modified haemal arches are already present (**Figure 1H**) and the first calcified rays of the caudal fin are forming by intramembranous calcification. The ceratobranchial 5 is almost completely calcified and the first mineral deposits appear in the basihyal, palatoquadrate and Meckel's cartilage. The first neural arches appear at 14 dpf on the fourth vertebra, already with visible calcification (**Figure 1I**) while the cartilaginous elements of the hypuralia are beginning endochondral mineralization (**Figure 1J**). An almost completely formed vertebral column is visible at 19 dpf (**Figure 1K**), with all structures calcified, except for the two most posterior vertebra that form the urostile, still undergoing calcification, and in the process of upwards inflexion. The caudal fin has achieved the total number of structures with all rays, hypurals, epurals and modified arches and spines. The dorsal and anal fins are already formed and largely mineralized while in pectorals, mineralization of the rays is just beginning. The head is largely mineralized although skull bones forming by intramembranous calcification and cartilage undergoing endochondral ossification are continuing to develop until late juvenile stages.

3.2 Cloning of zebrafish and Senegal sole *bgp* and *mgp* cDNAs

D. rerio and S. senegalensis bgp cDNAs: Taking advantage of the N-terminal amino acid sequence obtained for purified *Danio rerio* Bgp (P83238) (Simes *et al.*, 2004), the complete nucleotide sequence of the corresponding cDNA was obtained by a combination of RT-PCR and 5'RACE-PCR using total RNA extracted from fully calcified individuals. The *Danio rerio bgp* cDNA (AY178836) spans 406 bp and contains an open reading frame (ORF) of 315 bp (**Figure 2**) encoding a polypeptide with 104 aminoacids (AA), comprising a 56 residue pre-propeptide and a 48 residue mature peptide. The nucleotide sequence of the *Solea senegalensis* (*Sse*) *bgp* cDNA, obtained by a similar approach, spans 629 bp and encodes a 45 residue mature protein, preceded by a 55 residue pre-propeptide (**Figure 2**). All pre-pro cleavage sites were deduced by comparison with other known Bgp sequences from mammals, birds, fish and amphibian (**Figure 2**). The first amino acid of the mature form was identified by comparison with results obtained following protein sequence analysis of Bgp purified from zebrafish and sole bone (Simes *et al.*, 2004). In both cases, the deduced N-terminal region was in full agreement with the sequence previously deduced by amino acid sequence analysis.

Zebrafish Bgp was found to contain three more amino acids then *S. senegalensis* Bgp at the N-terminus of its mature form. Out of the 45 AA present in the common region of the mature protein common between the two species, 36 residues were 100% conserved, including the three Gla residues and the two cysteines required for the disulphide bridge. This high level of identity contrasted with that observed between the pre-pro regions, where only 18 out of 55 residues were conserved. Comparison of the two cDNAs also identified a larger 3'-untranslated region (UTR) in *S. senegalensis bgp* cDNA with two consensus polyadenylation signals while the shorter 3'-UTR in

zebrafish *bgp* contained a CA repeat, four nucleotides downstream from the stop codon, and only one polyadenylation signal.

***D. rerio* and *S. senegalensis mgp* cDNAs**: The *Danio rerio mgp* cDNA (*Dr*MGP-AY072811), cloned by a combination of RT- and 5'-RACE PCR, spans 625 bp (**Figure 3**) and comprises an ORF with 318 bp coding for a polypeptide of 105 residues comprising a pre-peptide of 21 residues and a mature protein of 84 residues. The 3'UTR includes a dinucleotide repeat motif (GT) and one canonical polyadenylation site. The *Solea senegalensis mgp* cDNA (AY113679), cloned similarly, spans 799 bp and contains a 435 bp ORF encoding 144 residues (**Figure 3**) from which the first 19 constitute the pre-peptide. At the 3'-end is located a motif repeated two times within the coding region (consensus: CAGAGACCCCAGATACCCCAG, coding for Gln-Arg-Pro-Gln-Ile-Pro-Gln). Comparison between the two sequences show the conservation of the phosphorylation motif in the N-terminal region (Ser-Xxx-Glu-Ser-Xxx-Glu-Ser), the Ala-Asn-Xxx-Phe motif and the three putative Gla residues located within the region containing the two cysteines responsible for the disulphyde bridge (Gla-Xxx-Xxx-Xxx-Gla-Xxx-Cys-Gla-Xxx-Xxx-Xxx-Xxx-Cys). There is also a C-terminal extension in both fish sequences compared with mammalian Mgps, which is longer in Senegal sole than in zebrafish (**Figure 3**).

3.3 Detection of *bgp* and *mgp* gene expression in *D. rerio* and *S. senegalensis* developing larva

3.3.1 Detection of *bgp* and *mgp* gene expression by quantitative Real Time -PCR

Expression levels for *bgp* and *mgp* were determined in RNA samples from *D. rerio* and *S. senegalensis* larvae and juveniles, covering the main skeletal development

stages for both species. *bgp* and *mgp* mRNA expression was observed at all developmental stages analyzed, but with a different pattern of expression for each species (Figure 4). In *D. rerio*, *bgp* levels increase 13 fold from somitogenesis stage (29 hpf) to complete embryo at 48 hpf followed by a strong upregulation at 120 hpf and returning to levels comparable to the reference sample or even moderately suppressed at 9 dpf (Figure 4A). At 13 dpf and all stages thereafter *bgp* levels were 60 to 90 fold higher than the reference sample. *mgp* expression levels closely parallel the *bgp* expression, being up-regulated and down-regulated at the same developmental stages. For *S. senegalensis*, *bgp* expression levels are stable from 72 hpf until 7 dpf but then increase by c.100 fold from10 dpf to 14 dpf. A further dramatic increase in expression is observed at 15 dpf corresponding to the stage of metamorphosis, but by20 dpf, as metamorphosis ends, *bgp* expression levels return to the pre-metamorphic stages, but again an increase of 1000 fold is observed in juveniles. *mgp* is expressed at lower levels at all developmental stages until 14 dpf but then dramatic increase is observed at 15 dpf. Levels remain high throughout metamrphosis and in juveniles.

In the zebrafish, *mgp* and *bgp* gene expression levels increased in parallel throughout larval development, and showed a stable expression level at late larval and juvenile stages. In Senegal sole *bgp* expression started to increase after 10 dpf, and was observed to be highly up-regulated around the time of metamorphosis (13-16 dpf). In contrast, *mgp* is down-regulated in larval stages before metamorphosis and highly up-regulated during metamorphosis.

3.3.2 Time-course of *bgp* gene expression by *in situ* hybridization

Using mRNA in situ hybridisation on sections of larval fish, we examined the time-course of *bgp* expression in both zebrafish and Senegal sole. Here we highlight the

stages when expression is first seen in individual skeletal elements. In *D. rerio*, *bgp* gene expression was first observed by *in situ* hybridization at 7 dpf on the fifth ceratobranchial cartilage, by which stagethe calcified pharyngeal teeth are already present. At 11 dpf both BOP and otic capsules presented *bgp*-positive cells, as well as the Meckell`s cartilage (**Figure 5A**). At 13 dpf vertebrae were developing around the notochord and hypertrophic cells in the forming vertebral arches showed positive signal for *bgp* expression (**Figure 5B**). At the same age, *bgp* expression was also observed in other structures undergoing calcification like opercular bones, BOP and the ceratobranchials (**Figure 5C**). As the calcification of the BOP increased, expression appeared within the cells adjacent to the calcifying zones of the structure (**Figure 5D**). At 24 dpf, *bgp* mRNA was observed in cells associated with the mineralizing cartilaginous pterigophores of the dorsal fin (**Figure 5E**). As the number of structures undergoing mineralization increased in the head region, a more generalized expression was observed in the skeletal structures, as seen in the ceratobranchials, opercula, ceratohyal, BOP and jaw of a 24 dpf sample (**Figure 5F**). In the adult fish, the proportion of matrix greatly increased relative to the number of cells, and the positive signal indicating *bgp* expression became restricted to areas containing cells with a hypertrophic phenotype. Localization of *bgp* gene expression in *Solea senegalensis* by *in situ* hybridization was first detected after the beginning of mineralization and in parallel with the onset of metamorphosis in the head structures, a process that initiated at around 12-13 dpf in the studied individuals. In 15 dpf larvae, *bgp* expression was detected in the first vertebra forming over the notochord (**Figure 5G**), and later, *bgp* expression was detected in cells within forming neural arches. It was also detected in head structures such as endochondral bones from skull as shown in the hyosymplectic and basioccipital process and in the branchial arches (**Figure 5H**). At 20 dpf larvae

showed expression in the forming skeletal elements of the fins such as the dorsal pterigophores and distal radials (**Figure 5I**). At 58 dpf osteoblasts expressing *bgp* are clearly visible in the mandibula of a juvenile sole (**Figure 5J**).

3.4 Time-course of *mgp* gene expression by *in situ* hybridization

Using mRNA in situ hybridisation on sections of larval fish, we examined the time-course of *mgp* expression in both zebrafish and Senegal sole. Here we highlight the stages when expression is first seen in individual skeletal elements. In *D. rerio*, *mgp* expression was first detected at 96 hpf on chondrocytes of the ethmoid plate (**Figure 6A**). At 9 dpf, *mgp* expression was located in chondrocytes both from trabecular cartilage and ceratobranchial arches (**Figure 6B**) as well as in the Meckel's cartilage and quadrate (**Figure 6C**). At 10 dpf, in cartilage from pectoral fin, *mgp* mRNA was detected in chondrocytes but was not observed in the cleithrum (**Figure 6D**). At 13 dpf *mgp* gene expression was observed in ceratobranchials, mainly in hypertrophic chondrocytes and in the BOP (**Figure 6E**). In addition, *mgp* mRNA was also observed in hypertrophic chondrocytes from Meckel's cartilage and in chondrocytes of the hyaline cartilage from the basibranchial cartilage (**Figure 6F**). At 16 dpf *mgp* mRNA was observed in chondrocytes from the BOP (Figure 6**G**), within the cytoplasm of hypertrophic chondrocytes from the Meckel's cartilage and within chondrocytes of the ethmoid plate (**Figure 6H**). At 17 dpf *mgp* expression was detected in chondrocytes of the optic capsules (**Figure 6I**) and at 20 dpf in chondrocytes from the Zellknorpel cartilage in the branchial filaments (**Figure 6J**). At 25 dpf, the vertebrae were nearly formed with the notochord completely surrounded by calcified cartilage. At this stage, *mgp* expression was located in endosteal cells surrounding the vertebral centra. These cells were elongated in shape, with strong staining for *mgp* (**Figures 6K and 6L**). *mgp*

expression was also located in chondrocytes from the pterigophores (**Figure 6L**). In the adult fish, as mineralization of the skeleton increased, expression of *mgp* was only detected in chondrocytes within the remaining cartilage islands.

In *S. senegalensis*, *mgp* gene expression was observed mainly in skeletal structures both cartilaginous and calcified. At 7 dpf *mgp* mRNA was first observed in the branchial arches. At 11 dpf *mgp* mRNA was clearly observed in the chondrocytes of the branchial arches, trabeculae and hyosymplectic (**Figure 6M**), an. At 17 dpf when vertebral structures are forming, *mgp* mRNA was observed in the chondrocyte-like cells at the base of the vertebral arches, and in the developing internal skeleton of the fins, as seen in the dorsal pterigophores in **Figure 6N**. In juveniles, *mgp* expression was present only in non-calcified skeletal structures, like the cartilaginous growth zones or the cartilage in the base of the vertebra arches, as observed in a 47 dpf sole (**Figure 6O**).

3.5 Time-course of Bgp accumulation

To confirm and extend the studies of Bgp mRNA expression, we used a well-characterised antibody that specifically detects Bgp in teleost fish to characterise the distribution of accumulated protein. *Danio rerio* Bgp was found to accumulate in the matrix of tissues undergoing calcification as determined by immunolocalization studies. This accumulation was first detected at 8 dpf in the BOP and calcified teeth of the branchial arch 5 and in the otolyths (**Figure 7A**). At 9 dpf accumulation was also observed in the cleithrum and in the BOP undergoing intra-membranous mineralization (**Figure 7B**). At 13 dpf, Bgp accumulation was observed in the calcified upper jaw and in the mineralized matrix deposited by osteoblasts on the surface of Meckels cartilage undergoing perichondral mineralization (**Figure 7C**). At this age Bgp was detected in the inthe mineralized matrix of the forming vertebrae and arches on the surface of the

notochord sheath, as observed in **Figure 7D** for vertebra and haemal arches. At 20 dpf the skeletetal elements of the fin and of fin support were mineralizing, and presented positive signal for Bgp accumulation, as observed in the coraco-scapular complex (**Figure 7E**). In the last vertebral element, the urostile, strong Bgp signal was observed by immunofluorescence within sites undergoing perichordal mineralization (arrows in **Figure 7F**). The developing vertebrae, arches and spines of a 20 dpf specimen showed a strong Bgp accumulation associated with a noticeable thickening of the mineralized tissue surrounding the notochord (**Figure 7G**). At 31 dpf all the structures that compose the caudal fin, including hypurals, lepidotrichia and the last vertebrae clearly showed accumulation of Bgp associated with the mineralized matrix. A strong increase in signal was observed as vertebra and arches became thicker (**Figure 7H**). Bgp accumulated strongly in juvenile and adult calcified tissues, as seen in the supramandibular, trabeculae and skull bones (**Figure 7I**) as well as in the branchial arches of a juvenile by immunofluorescence (**Figure 7J**). A clear signal was also observed on the kidney of juveniles and adults, associated with the glomerulii (**Figure 7K**).

In *S. senegalensis*, Bgp was found to accumulate in mineralized skeletal structures but with a slight delay in respect to the appearance of mineralization. At 15 dpf larvae showed Bgp accumulation in the mineralized vertebrae forming around the notochord (**Figure 7L**). At 17 dpf Bgp was found in the calcifying caudal vertebrae, and associated neural and haemal arches and at 25 dpf Bgp was observed in all the vertebral elements as revealed by immunofluorescence (**Figure 7M**), showing strong accumulation of Bgp in calcified vertebral column and parapophysis of 25 dpf individuals with a completed metamorphosis. At this same age Bgp accumulation was also detected in the cartilaginous distal radials undergoing endochondral calcification (**Figure 7N**). 41 dpf juveniles presented strong Bgp accumulation in all calcified

structures, as observed in the calcified cartilages of the branchial arches (**Figure 7O**). All the structures are formed at juvenile stage and Bgp is observed to accumulate in all bones, both from endochondral or intramembranous origin, and in all cartilages that present calcification.

3.6 Detection of sites of Mgp accumulation by immunohistochemistry

Using a previously validated polyclonal antibody for Mgp we examined the accumulation of Mgp in both zebrafish and Senegal sole structures throughout development by immunohistochemistry. Here we report the stages when accumulation was first seen in individual skeletal elements. Mgp was first observed in the mineralized otolyths at 96 hpf and the intensity of staining increased as the structure grew, as observed in a 6 dpf larvae (**Figure 8A**). As new calcified structures appeared (see Figure 1), accumulation of Mgp was observed in the mineralized matrix as soon as it formed as can be observed in a 8 dpf larvae in the mineralized otolyth and cleithrum (**Figures 8B and 8C**). At 13 dpf when vertebrae and arches are forming, Mgp was observed to accumulate in pleural vertebrae where mineralization of neural arches initiated, as seen in vertebrae 3-5 of a 13 dpf larva (**Figure 8D**). At this same age, accumulation of Mgp was observed in the mineralizing branchial arches and pharyngeal teeth (**Figure 8E**). At 20 dpf Mgp accumulation was present in the mineral layer over cranial cartilages undergoing endochondral ossification (**Figure 8F**) and in the forming caudal vertebra and associated arches (**Figure 8G**). In juveniles at 40 dpf a strong signal for Mgp accumulation was observed in the pre-opercular bones undergoing endochondral ossification (**Figure 8H**) and in skull bones undergoing intra-membranous ossification (**Figure 8I**). In *S. senegalensis*, Mgp accumulation was first detected at 8 dpf in the cartilaginous otic capsules (**Figure 8J**) but not in the otoliths. As

calcification initiated, Mgp accumulation was observed in the mineralizing matrix of forming endochondral and intramembranous bones such as vertebrae and cranial structures, as can be observed in the the calcified matrix below the trabecula of a 17 dpf larvae (**Figure 8K**). In 26 dpf post larvae, Mgp accumulation was observed mainly in calcified structures including mineralizing branchial arches, but also in the aorta and cardiac arterial bulbus (arrowhead in **Figure 8L**).

3.7 Detection of ALP and TRAP enzymatic activity

The nature of the cells responsible for bone deposition was verified by determining the activity of alkaline phosphatase (ALP) required for the correct formation of the mineralized extracellular matrix, in order to identify bone forming cells, and tartrate resistant acid phosphatase (TRAP), required to degrade the mineralized matrix, to detect bone resorbing cells both in *D. rerio* and in *S. senegalensis*. ALP is consistently detected in structures undergoing mineralization throughout skeleton development. In 13 dpf *D. rerio*, ALP activity is present in the mineralizing vertebrae (**Figure 9A**), and at 17 dpf is detectable in pre-opercular bones (**Figure 9B**) undergoing intracartilaginous ossification and the opercular bone undergoing intramembranous ossification. At the same age, TRAP activity indicative of ongoing resorption of mineralized matrix was detected in mineralizing branchial arches (**Figure 9C**) and in skull bones undergoing intramembranous ossification at 26 dpf (**Figure 9D**). Only mononuclear cells were observed in sites where TRAP activity was detected. In *S. senegalensis*, ALP is also observed in various calcified structures like in forming neural arches vertebrae of a 17 dpf individual (**Figure 9E**). Resorption was observed in the vertebrae but not in head structures at this age (results not shown). Interestingly, although calcified structures were present in the head region, no

resorption sites were detected by TRAP staining in individuals undergoing metamorphosis at the stage in which ocular migration occurs (15 dpf). In a 32 dpf juvenile, TRAP activity was strongly detected in the areas surrounding vertebrae, arches and spines (**Figure 9F**).

3.8 Chromosomal mapping of *D. rerio mgp* and *bgp* genes using the LN54 panel.

The *D. rerio mgp* and *bgp* genes were mapped on the radiation hybrid panel LN54 by PCR amplification in order to determine in which chromosome they were located and to check for the presence or not of synteny with mammals. Using the *D. rerio* mapping program at http://mgchd1.nichd.nih.gov:8000/zfrh/beta.cgi a best lod score of 12.5 for the marker Z1209, located on LG3, 9.54 cR was obtained for *Danio rerio mgp* (**Figure10**).

Amplification of the radiation hybrid panel with the *bgp* primers resulted in a product with approximately 350 bp. Amplification with the same set of primers in the cDNA would give a product of 251 bp due to the presence of a small intron in the region encompassed by this set of primers. This has recently been confirmed by the identification of *D. rerio bgp* gene structure (Laize *et al.*, JBC, in Press). The mapping program showed that *Danio rerio bgp* is also located on LG3, with a best LOD score of 12.1 for the marker Z15479, located at 3.87 cR from the *bgp* gene (**Figure 10**).

No amplification was detected when *mgp* and *bgp* specific primers sets were used in the control reaction containing mouse genomic DNA (B78), while high levels of product were derived from *D. rerio* genomic DNA (AB9) and from the 1:10 mix of *D. rerio* versus mouse genomic DNA (Mix).

Discussion

In this work we have cloned, for the first time, complete cDNAs for *bgp* and *mgp* in zebrafish and Senegal sole. We made a comprehensive study of gene expression and protein accumulation for these two important mineralization-related proteins during development of the skeleton in these fish species with different ecologies. These data, summarized in Tables 2 and 3, make an interesting comparison with our previous data for other fishes and with preexisting information for mammals.

Expression of *bgp* and *mgp* during skeletal development. Zebrafish has an accelerated development compared with other teleosts and, in general, structures develop earlier and faster than for the marine fish species examined here and elsewhere (Pinto *et al.*, 2003). In our work we used an improved histological procedure to detect sensitively development of the calcified and cartilaginous structures that compose the zebrafish skeleton by detecting both calcium deposition and cartilage with the histological markers alizarin red and alcian blue. This method allowed us to follow the onset of skeletogenesis in more detail compared with previous studies using calcein as a fluorescent marker for calcium (Du *et al*, 2001) which do not allow cartilage visualization.

The skeletal development in zebrafish larval stages is described in detail up to the juvenile stage, when most skeletal elements are already present, and thus complements earlier studies describing the development of skeletal structures during specific periods. Schilling *et al.*, (1996), Piotrovsky *et al.*, (1996) and Schilling and Kimmel (1996) have described the chondrocranium in embryos up to 120 hours focusing in particular on the development of pharyngeal arches. Cubbage and Mabee (1996) describe skeletal development in larval and adult individuals, with special

reference to the cranium and paired fins. Du *et al.* (2001) used calcein to describe the axial skeleton, in larvae up to 23 days post fertilization (dpf). Although their study only allowed visualization of calcified structures, our results concerning mineralisation are in good general agreement with those obtained by Du *et al* (2001). We detect calcification one day sooner in the head region, although this may perhaps result from differences in the feeding regimes employed, but the timing of subsequent events of skeletal development remain similar. .

As observed for other species like mouse (Desbois *et al.*, 1994a) and seabream (Pinto *et al.*, 2001) the accumulation of Bgp protein in zebrafish is detected soon after the appearance of the first calcified structures. Although Bgp accumulation was clearly observed at 8 dpf in the otolyths, cleithrum and pharyngeal teeth, some was detectable at 96 hpf. in the mineralized pharyngeal teeth. Thus Bgp is detected here within around a day of the onset of mineralisation although we note that Huysseune *et al.* (1998) and Van der heyden *et al.* (2000) report mineralisation slightly earlier than this.

The presence of *Danio rerio bgp* mRNA is first observed at 5 dpf by *in situ* hybridization in the pharyngeal teeth of the fifth ceratobranchial arch and in the cleithrum, consistent with RT-PCR amplification of *Danio rerio bgp* at this age and with these structures being the first to become mineralized. . In *Solea senegalensis*, *bgp* is observed much later, at 15 dpf, and at a more advanced stage of skeletal development, when calcified structures are prominent in both the head and axial skeleton. At this age, sole were already mineralizing the vertebral column (Gavaia *et al*, 2002) and there is extensive calcification in the head region. We suggest that in this slower growing species, *bgp* expression appears to initiate later than in the faster growing zebrafish. This is consistent with results obtained by others for *Sparus aurata* (Pinto *et al.*, 2001), where presence of mRNA is only detected at relatively late stages (39 dpf). *bgp*

expression in *Danio rerio* is restricted to cells of mineralized structures or stuctures undergoing calcification like the cartilages undergoing endochondral calcification, in agreement with results obtained for other fish species (Pinto *et al.*, 2001; Simes et al 2003). Expression of *bgp* was mainly observed in hypertrophic chondrocytes during the early skeletogenesis events, when the cartilaginous structures are starting to present deposits of mineral (as observed by histological staining) and becoming calcified cartilages or bones. Although Bgp has been widely accepted as a bone marker and referred to as expressed mainly in osteoblastic and odontoblastic cells (Price, 1990), some references describe the presence of Bgp in cultures of hypertrophic chondrocytes from chicken (Neugebauer *et al.*, 1995) and from mouse (Strauss *et al.*, 1990). The observation of *bgp* gene expression in chondrocytes at a stage when cartilage calcification is occurring is in agreement with those observations and may reflect the fact that during cartilage calcification a number of structures calcify before osteoblasts have been observed. Bgp is thought to be required for the correct formation of hydroxyapatite crystals in the mineralizing matrix of developing skeletal structures, as previously described in mouse (Boskey *et al*, 1998), a function that is consistent with the data obtained from fish and which suggesting evolutionary conservation of gene function.

Relationship between expression of *bgp* and *mgp* mRNAs and the onset of metamorphosis: The analysis of mRNA transcripts for *bgp* and *mgp* by quantitative real time PCR revealed expression of both transcripts in all developmental stages investigated, but with different patterns for the two species. *bgp* transcripts showed a tendency to increase in both species with a peak for *D. rerio* at 120 hpf, corresponding to the periods when calcification of cranial bones and initial formation of axial skeleton

elements take place. The pattern of *mgp* levels closely matches that of *bgp* in zebrafish. In contrast, in *S. senegalensis* the levels of *mgp* are proportionately much lower until the beginning of metamorphosis at 14 dpf. In *S. senegalensis* a dramatic increase of *bgp* and *mgp* expression is observed at 14-16 dpf when metamorphosis is initiated, coincident with the time of dramatic rotation of the skeletal structures to the ocular (right) side. This increase may be related both to the high number of structures that form *de novo* and calcify during the metamorphosis and to the corresponding need for rearrangement of pre-existing structures, which must rotate and change morphology.

Sites of Mgp accumulation in fish versus mammals: Our results show that Mgp in zebrafish and Senegal sole is accumulating mainly in sites where a calcified matrix is present, either bone or calcified cartilage, in contrast to the observations in *A. regius* where Mgp accumulates in cartilage matrix and in chondrocytes (Simes *et al*, 2003). The results obtained for zebrafish are thus more in agreement to those found in mammals, where Mgp protein was found to accumulate only in the extracellular matrix of bone, cartilage and tooth cementum (Price *et al.*, 1983; Hashimoto *et al.*, 2001), despite the fact that *mgp* mRNA was present in cartilage and various soft tissues as described in rats particularly in heart, kidney, and arterial vessel wall (Fraser and Price, 1988).

Previous studies carried out in mammals reported that Bgp appears to be absent during early stages of osteoblast maturation, being undetectable in undifferentiated or recently differentiated osteoblasts near the growth plate but clearly detectable in mature osteoblasts (Mark *et al*, 1988; Ikeda *et al*, 1992; Liu *et al*, 1994). Likewise, studies of the accumulation of Bgp protein in osteoblastic cells by immunolabeling could only detect this protein in cuboidal cells with a clear osteoblastic phenotype (Liu *et al*, 1994). The relationship between Bgp and mineralization remains unclear even within the same

species, since some authors detect Bgp prior to mineralization (Bronckers *et al*, 1987; Gerstenfield *et al*, 1987; Mark *et al.*, 1988; Liu *et al.*, 1994) and others at the onset or after the beginning of mineralization (Groot *et al*, 1986; Boivin *et al*, 1990; Owen *et al*, 1990, 1991; Pockwinse *et al*, 1992, Pinto *et al.*, 2001). This discrepancy remains to be explained and is likely to be linked to the still unclear function played by Bgp during bone formation and/or mineralization. For the species described in this study Bgp was detected after the onset of mineralization in all the structures annalized as summarized in Table 2.

Chomosomal localization of *bgp* and *mgp* in zebrafish: *Danio rerio mgp* and *bgp* were found to be located on the same chromosome (LG3) in zebrafish, a result that differs from what is known in mammals, where the two genes are located in different chromosomes [chromosome 12 for *mgp* (Cancela *et al.*, 1990) and chromosome 1 for *bgp* (Puchacz *et al.*, 1989), in human; chromosome 6 for *mgp* and chromosome 3 for *bgp* in mouse (Johnson *et al.*, 1991; Desbois *et al.*, 1994b)]. Studies showing the existence of conserved synteny groups between zebrafish and human (eg.: Barbazuk *et al.*, 2000) have raised the possibility that significant portions of the zebrafish genome are uninterrupted by rearrangements since the divergence of the teleost and tetrapod ancestors. Indeed, analysis of LG3 shows a considerable degree of synteny with human chromosomes 17, 19 and 22. However, other genes are present in this Linkage Group that locates in different chromosomes in human, suggesting the existence of considerable differential chromosome rearrangement in the lineages that originated teleosts and mammals. However, several events are supposed to have occurred in the teleost genome since this divergence. One of these events may have been whole genome duplication in the teleost lineage or, alternatively, a more restricted duplication, rather

than a single, whole-genome event (Amores *et al.*, 1998; Gates *et al.*, 1999). Recent examination of the pufferfish genome sequences gives strong evidence for the whole genome duplication scenario in early teleost differentiation (Jaillon *et al.*, 2004). However, we found no evidences of gene duplication, either for *mgp* or *bgp*, which is in agreement with our previous findings for both genes in other lower vertebrate species (Pinto *et al.*, 2001; Viegas *et al.*, 2002; Conceição *et al.*, 2002). In 1995 Cancela *et al.*, based on structure similarity, suggested that Bgp and Mgp may share a common ancestor, which, by gene duplication and/or exon shuffling, would have originated two distinct, however related, proteins. The location of the two proteins only 2Mb away in the same chromosome, reinforces this hypothesis. More studies on the location of the two genes in other low vertebrates are, however, necessary to further test this hypothesis.

Acknowledgements

This work was partially funded by research grants POCTI/CVT/42098/2001 (FISHDEV) from the Portuguese Foundation for Science and Technology (FCT) and MCYT/AGL2003-03558 from the Spanish Ministry of Science and Technology. Part of this work was performed as luso-british collaboration between L. Cancela and R. Kelsh, funded by the C.R.U.P.-British council protocol. P.J. Gavaia and J.P. Pinto were the recipients respectively of PhD (PRAXIS XXI/BD/19665/99) and post-doctoral (PRAXIS XXI/BPD/20229/99) fellowships from FCT. The authors would like to thank Dr. Marie-André Akimenco from the Loeb Research Institute in Ottawa for reviewing and comments. We thank Dr. Marc Ekker, from the Center for Advanced Research in Environmental Genomics, University of Ottawa, for kindly providing the LN54 radiation hybrid panel.

REFERENCES

Amores, A., Force, A., Yan, Y.L., Joly, L., Amemiya, C., Fritz, A., Ho, R.K., Langeland, J., Prince, V., Wang, Y.L., *et al.* (1998). Zebrafish hox clusters and vertebrate genome evolution. Science 282: 1711–1714.

Barbazuk, W.B., Korf, I., Kadavi, C., Heyen, J., Tate, S., Wun, E., Bedell, J.A., McPherson, J.D., Johnson, S.L. (2000). The Syntenic Relationship of the Zebrafish and Human Genomes. Genome Research 10: 1351–1358.

Boivin, G., Morel, G., Lian, J.B., Anthione-Terrier, C., Dubois, P.M., Meunier, P.J. (1990). Localization of endogenous osteocalcin in neonatal rat bone and its absence in articular cartilage: effect of warfarin treatment. Pathol. Anat. 417:505–512.

Boskey, A.L., Gadaleta, S., Gundberg, C., Doty, S.B., Ducy, P., Karsenty, G. (1998). Fourier transform infrared microspectroscopic analysis of bones of osteocalcin-deficient mice provides insight into the function of osteocalcin. Bone 23(3): 187–196.

Bronckers, A.L., Gay, S., Finkelman, R.D., Butler, W. T. (1987). Developmental appearance of Gla proteins (osteocalcin) and alkaline phosphatase in tooth germs and bones of the rat. Bone Miner. 2 (5): 361-373.

Burstone, M.S. (1959). Histochemical demonstration of acid phosphatase activity in osteoclasts. J. Histochem. Cytochem. 7: 39-41.

Cancela, L., Hsieh, C.L., Francke, U., Price, P.A. (1990). Molecular structure, chromosome assignment and promoter organization of the Human matrix gla protein gene. J. Biol. Chem. 265: 15040-15048.

Cancela, M.L., Williamson, M.K., Price, P.A. (1995). Amino-acid sequence of bone Gla protein from the African clawed toad *Xenopus laevis* and the fish *Sparus aurata*. Int. J. Peptide Protein Res. **46**: 419-423.

Cancela, M.L., Ohresser, M.C.P., Reia, J.P., Viegas, C.S.B., Williamson, M.K., Price, P.A. (2001). Matrix Gla Protein in Xenopus laevis: molecular cloning, tissue distribution and evolutionary considerations. J. Bone Miner. Res. 16: 1611-1622.

Conceição, N., Henriques, N.M., Ohresser, M.C., Hublitz, P., Schule, R., Cancela, M.L. (2002). Molecular cloning of the Matrix Gla Protein gene from Xenopus laevis. Functional analysis of the promoter identifies a calcium sensitive region required for basal activity. Eur. J. Biochem. 269: 1947-1956.

Cubbage, C.C. and Mabee, P.M. (1996). Development of the cranium and paired fins in the zebrafish *Danio rerio* (Ostariophysi, Cyprinidae). J. Morphol. 229: 121–160.

Desbois, C., Hogue, D.A., Karsenty, G. (1994a). The mouse osteocalcin gene cluster contains three genes with two separate spatial and temporal patterns of expression. J. Biol. Chem. 269: 1183-1190.

Desbois, C., Seldin, M.F., Karsenty, G. (1994b) Localization of the osteocalcin gene cluster on mouse chromosome 3. Mamm. Genome 5: 321-322.

Du, S.J., Frenkel, V., Kindschi, G., Zohar, Y. (2001). Visualizing normal and defective bone development in zebrafish embryos using the fluorescent chromophore Calcein. Dev. Biol. 238: 239-246.

Ducy, P., Desbois, C., Boyce, B., Pinero, G., Story, B., Dunstan, C., Smith, E., Bonadio, J., Goldstein, S., Gundberg, C., Bradley, A., Karsenty, G. (1996). Increased bone formation in osteocalcin-deficient mice. Nature 382: 448 –452

Fraser, J.D. and Price, P.A. (1988). Lung, heart, and kidney express high levels of mRNA for the vitamin K-dependent Matrix Gla Protein. J. Biol. Chem. 23, 11033-11036.

Gates, M.A., Kim, L., Egan, E.S., Cardozo, T., Sirotkin, H.I., Dougan, S.T., Lashkari, D., Abagyan, R., Schier, A.F., Talbot, W.S. (1999). A genetic linkage map for zebrafish: Comparative analysis and localization of genes and expressed sequences. Genome Res. 9: 334–347.

Gavaia, P.J., Sarasquete, C., Cancela, M.L. (2000). Detection of mineralized structures in early stages of development of marine *Teleostei* using a modified alcian blue-alizarin red double staining technique for bone and cartilage. Biotech. Histochem. 75(2): 79-84.

Gavaia, P.J., Dinis, M.T., Cancela, M.L. (2002). Osteological development and abnormalities of the vertebral column and caudal skeleton in larval and juvenile stages of hatchery-reared Senegal sole (*Solea senegalensis*). Aquaculture 211: 305–323.

Gerstenfeld, L.C., Chipman, S.D., Glowacki, J., Lian, J.B. (1987). Expression of differentiated function by mineralizing cultures of chicken osteoblasts. Dev. Biol. 122: 49–60.

Groot, C.G., Danes, J.K., Blok, J., Hoogendijk, A., Hauschka, P.V. (1986). Light and electron microscopic demonstration of osteocalcin antigenicity in embryonic and adult rat bone. Bone 7: 379–385.

Hao, H., Hirota, S., Ishibashi-Ueda, H., Kushiro, T., Kanmatsuse, K. Yutani, C. 2004. Expression of matrix Gla protein and osteonectin mRNA by human aortic smooth muscle cells. Cardiovasc. Pathol. 13: 195– 202.

Hashimoto, F., Kobayashi, Y., Kobayashi, E.T., Sakai, E., Kobayashi, K., Shibata, M., Kato, Y., Sakai, H. (2001). Expression and localization of MGP in rat tooth cementum. Arch. Oral Biol. 46: 585–592.

Hukriede, N., Joly, L., Tsang, M., Miles, J., Tellis, P., Epstein, J., Barbazuk, W., Li, F., Paw, B., Postlethwait, J., Hudson, T., Zon, L., McPherson, J., Chevrette, M., Dawid, I., Johnson, S., Ekker, M. (1999). Radiation hybrid mapping of the zebrafish genome. Proc. Natl. Acad. Sci. USA 96: 9745-9750.

Huysseune, A., Van der heyden, C., Sire, J.Y. (1998). Early development of the zebrafish (*Danio rerio*) pharyngeal dentition (Teleostei, Cyprinidae). Anat. Embryol. 198: 289–305.

Ikeda, T., Yamaguchi, A., Icho, T., Tsuchida, N., Yoshiki, S. (1991). cDNA and deduced amino acid sequence of mouse Matrix Gla Protein: One of five glutamic acid residues potentially modified to gla is not conserved in the mouse sequence. J. Bone. Miner. Res. 6: 1013–1017.

Jaillon, O., Aury, J. M., Brunet, F., Petit, J. L., Stange-Thomann, N., Mauceli, E., Bouneau, L., Fischer, C., Ozouf-Costaz, C., Bernot, A., Nicaud, S., Jaffe, D., Fisher, S., Lutfalla, G., Dossat, C., Segurens, B., Dasilva, C., Salanoubat, M., Levy, M., Boudet, N., Castellano, S., Anthouard, V., Jubin, C., Castelli, V., Katinka, M., Vacherie, B., Biémont, C., Skalli, Z., Cattolico, L., Poulain, J., de Berardinis, V., Cruaud, C., Duprat, S., Brottier, P., Coutanceau, J.-P., Gouzy, J., Parra, G., Lardier, G., Chapple, C., Mckernan, K.J., Mcewan, P., Bosak, S., Kellis, M., Volff, J.-N., Guigó, R., Zody, M.C., Mesirov, J., Lindblad-Toh, K., Birren, B., Nusbaum, C., Kahn, D., Robinson-Rechavi, M., Laudet, V., Schachter, V., Quétier, F., Saurin, W., Scarpelli, C., Wincker, P., Lander, E.S., Weissenbach J., Crollius, H.R. (2004). Genome duplication in the

teleost fish Tetraodon nigroviridis reveals the early vertebrate proto-karyotype. Nature 431, 946-57.

Johnson, T.L., Sakaguchi, A.Y., Lalley, P.A., Leach, R.J. (1991). Chromosomal assignment in mouse of matrix GLA protein and bone GLA protein genes. Genomics 11: 770-772.

Kiefer, M.C., Bauer, D.M., Young, D., Hermsen, K.M., Masiarz, F.R, and Barr, P.J. (1988). The cDNA and derived amino acid sequences for human and bovine Matrix Gla Protein. Nucleic Acids Res. 16: 5213–5213.

Lawton, D.M., Andrew, J.G., Marsh, D.R., Hoyland, J.A., Freemont, A.J. (1999). Expression of the gene encoding the matrix gla protein by mature osteoblasts in human fracture non-unions. J. Clin. Pathol.: Mol. Pathol. 52: 92–96.

Liu, F., Malaval, L., Gupta, A.K., Aubin, J.E. (1994). Simultaneous detection of multiple bone-related mRNAs and protein expression during osteoblast differentiation: polymerase chain reaction and immunocytochemical studies at the single cell level. Dev. Biol. 166: 220-234.

Luo, G., D'Souza, R., Hogue, D., Karsenty, G. (1995). The matrix Gla protein gene is a marker of the chondrogenesis cell lineage during mouse development. J Bone Miner Res 10: 325–34.

Luo, G., Ducy, P., McKee, M.D., Pinero, G.J., Loyer, E., Behringer, R.R., and Karsenty, G. (1997). Spontaneous calcification of arteries and cartilage in mice lacking matrix Gla protein. Nature 386: 78–81.

Mark, M.P., Butler, W.T., Prince, C.W., Finkelman, R.D., Ruch, J.V. (1988). Developmental expression of 44-kDa bone phosphoprotein (osteopontin) and bone gamma-carboxyglutamic acid (Gla)-containing protein (osteocalcin) in calcifying tissues of rat. Differentiation 37: 123-36

Newman, B., Gigout, L.I., Sudre, L., Grant, M.E., Wallis, G.A. (2001). Coordinated expression of matrix Gla protein is required during endochondral ossification for chondrocyte survival. J Cell Biol 154 (3): 659–666.

Neugebauer, B.M., Moore, M.A., Broess, M., Gerstenfeld, L.C., Hauschka, P.V. (1995). Characterization of structural sequences in the chicken osteocalcin gene: expresiion of osteocalcin by maturing osteoblasts and by hypertrophic chondrocytes in vitro. J. Bone Miner. Res. 10(1): 157-163

Nishimoto, S.K., Araki, N., Robinson, F.D., Waite, J.H. (1992). Discovery of bone γ-carboxyglutamic acid protein in mineralized scales. The abundance and structure of Lepomis macrochirus bone γ-carboxyglutamic acid. J. Biol. Chem. 267 (16): 11600-11605.

Owen, T.A., Aronow, M., Shalhoub, V., Barone, L.M., Wilming, L., Tassinari, M.S., Kennedy, M.B., Pockwinse, S., Lian, J.B., Stein, G.S. (1990). Progressive development of the rat osteoblast phenotype in vitro: reciprocal relationships in expression of genes associated with osteoblast proliferation and differentiation during formation of the bone extracellular matrix. J. Cell. Physiol. 143: 420–430.

Owen, T.A., Aronow, M.A., Barone, L.M., Bettencourt, B., Stein, G.S., Lian, J.B. (1991). Pleiotropic effects of vitamin D on osteoblast gene expression are related to the proliferative and differentiated state of the bone cell phenotype: dependency upon basal levels of gene expression, duration of exposure, and bone matrix competency in normal rat osteoblast cultures. Endocrinology 128: 1495–1504.

Pinto, J. P., Ohresser, M., Cancela, M. L. (2001). Cloning of the Bone Gla Protein Gene from the teleost fish *Sparus aurata.* Evidence for overall conservation in molecular structure and pattern of expression from fish to man. Gene 270: 77-91.

Pinto, J.P., Conceição, N., Gavaia, P.J., Cancela, M.L. (2003). Matrix Gla protein gene expression and protein accumulation co-localize with cartilage distribution during development of the teleost fish *Sparus aurata*. Bone 32: 201 –210.

Piotrowski, T., Schilling, T. F., Brand, M., Jiang, Y.-J., Heisenberg, C.-P., Beuchle, D., Grandel, H., van Eeden, F.J.M., Furutani-Seiki, M., Granato, M., Haffter, P., Hammerschmidt, M., Kane, D.A., Kelsh, R.N., Mullins, M. C., Odenthal, J., Warga, R.M., Nüsslein-Volhard, C. (1996). Jaw and branchial arch mutants II: anterior arches and cartilage differentiation. Development 123: 345-356.

Pockwinse, S., Wilming, L., Conlon, D., Stein, G.S., Lian, J.B. (1992). Expression of cell growth and bone specific genes at single cell resolution during development of bone tissue-like organization in primary osteoblast cultures. J. Cell Biochem. 49: 310–323.

Price, P.A., Otsuka, A.S., Poser, J.W., Kristaponis, J., Raman, N. (1976). Characterization of a gamma-carboxyglutamic acid-containing protein from bone. Proc. Natl. Acad. Sci. 73 (5): 1447-1451.

Price, P.A., Otsuka, A., Poser, J.W. (1977). Comparation of gamma-carboxyglutamic acid containing proteins from bovine and swordfish bone: primary structure and Ca++ binding. In : R.H. Wasserman *et al.* (eds.) Calcium binding proteins and calcium functions. Elsevier North-Holland, Inc., pp. 333-337.

Price, P.A., Urist, M.R., Otawara, Y. (1983). Matrix Gla protein, a new □-carboxyglutamic acid-containing protein which is associated with the organic matrix of bone. Biochem. Biophys. Res. Commun. 117: 765–771.

Price, P.A. and Williamson, M.K. (1985). Primary structure of bovine matrix Gla protein, a new vitamin K-dependent bone protein. J. Biol. Chem. 260: 14971-14975.

Price, P.A. (1990). Vitamin K-dependent bone proteins. *in* Saito H. and Suttie. J.W. Vitamin K-dependent proteins and their metabolic roles. New York, Elsevier. chapter 3: 49-70.

Puchacz, E., Lian, J.B., Stein, G. S., Wozney, J., Huebner, K., Croce, C. (1989). Chromosomal Localization of the Human Osteocalcin Gene. Endocrinology 124: 2648-2650.

Rice, J.S., Williamson, M.K., Price, P.A. (1994). Isolation and sequence of the vitamin K-dependent matrix Gla protein from the calcified cartilage of the Soupfin shark. J. Bone Min. Res. 9: 567-576.

Roy, M.E., Nishimoto, S.K., Rho, J.Y., Bhattacharya, S.K., Lin, J.S., Pharr, G.M. (2001). Correlations between osteocalcin content, degree of mineralization, and mechanical properties of *C. Carpio* rib bone. J. Biomed. Mater. Res. 54: 547–553.

Schilling, T.F. and Kimmel, C.B. (1997). Musculoskeletal patterning in the pharyngeal segments of the zebrafish embryo. Development 124: 2945-2960.

Schilling, T.F., Piotrowski, T., Grandel, H., Brand, M., Heisenberg, C.-P., Jiang, Y.-J., Beuchle, D., Hammerschmidt, M., Kane, D.A., Mullins, M.C., van Eeden, F.J. M., Kelsh, R.N., Furutani-Seiki, M., Granato, M., Haffter, P., Odenthal, J., Warga, R. M., Trowe, T., Nüsslein-Volhard, C. (1996). Jaw and branchial arch mutants in zebrafish I: branchial arches. Development 123: 329-344.

Simes, D.C., Williamson, M.K., Ortiz-Delgado, J.B., Viegas, C.S.B., Price, P.A., Cancela, M.L. (2003). Purification of Matrix Gla Protein from a marine teleost fish, *Argyrosomus regius*: calcified cartilage and not bone as the primary site of MGP accumulation in fish. J. Bone Min. Res. 18: 244-259.

Simes, D.C., Williamson, M.K., Schaff, B.J., Gavaia, P.J., Ingleton, P.M., Price, P.A., Cancela, M.L. (2004). Characterization of Osteocalcin (BGP) and Matrix Gla

Protein (MGP) Fish Specific Antibodies: Validation for Immunodetection Studies in Lower Vertebrates. Calcif Tissue Int 74: 170 –180.

Strauss, P.G., Closs, E.I., Schimdt, J., Erfle, V. (1990). Gene expression during osteogenic differentiation in mandibular condyles *in vitro*. J. Cell. Biol. 110: 1369-1378.

Van der heyden, C. and Huysseune, A. (2000). Dynamics of Tooth Formation and Replacement in the Zebrafish (Danio rerio) (Teleostei, Cyprinidae). Dev. Dyn. 219: 486–496.

Viegas, C.S., Pinto, J.P., Conceição, N., Simes, D.C., Cancela, M.L. (2002). Cloning and characterization of the cDNA and gene encoding Xenopus laevis osteocalcin. Gene 289: 97-107.

Yagami, K., Suh, J-Y., Enomoto-Iwamoto, M., Koyama, E., Abrams, W.R., Shapiro, M. S., Pacifici, M., Iwamoto, M. (1999). Matrix Gla Protein is a developmental regulator of chondrocyte mineralization and, when constitutively expressed, blocks endochondral and intramembranous ossification in the limb. J. Cell Biol. 147 (5): 1097-1108.

Westerfield, M. (1995). The zebrafish book. Guide for the laboratory use of zebrafish (*Danio rerio*). 3rd ed., University of Oregon Press, Eugene.

Witten, P.E., Hansen, A., Hall. B.K. (2001). Features of mono- and multinucleated bone resorbing cells of the zebrafish *Danio rerio* and their contribution to skeletal development, remodeling, and growth. J. Morphol. 250: 197–207.

FIGURE LEGENDS

Figure 1- Time-course of skeletal development in *Danio rerio* using Alcian blue-Alizarin red double staining

Whole mount double staining of the skeleton was used to follow ontogenic development of cartilaginous and calcified structures.

A- 96 hpf *D. rerio* larvae head skeleton presenting calcified pharyngeal teeth (PT), cleithrum (Cl) and basioccipital articulatory process (BOP) while the remaining structures like Meckel's cartilage (MC) and ceratohyal (CH) remain as cartilage (100X); B- 5 dpf *D. rerio* larva presenting calcification on the opercula (Op) (40x); C- Beginning of the calcification of the hyosymplectic (HS) in a 6 dpf larva (100x); D- Beginning of the calcification of the ceratohyal (CH) in a 8 dpf *D. rerio* (100x); E- First hypurals (Hyp) developing at 8 dpf (100x); F- The formation of the first vertebrae (V) is observed at 9 dpf (100x); G- Calcification of the trabeculae (T) is observed at 11 dpf, vertebrae continue to form (in an anterior-posterior direction) towards the posterior end of the notochord (40x); H- Caudal hypuralia acquires final number of structures and caudal fin rays appear at 12 dpf (100x); I- Formation of the first neural arches (NA) is observed dorsally in the anterior vertebrae at 14 dpf; note that the mandibular is already calcified (M)(40x); J- Beginning of calcification of the hypurals at 14 dpf (40x); K- Composite image of a 19 dpf *D. rerio* with most skeletal structures present and calcified.

Figure 2- *Danio rerio* and *Solea senegalensis bgp* cDNAs

Nucleotide sequence of the cDNAs encoding *D. rerio* and *S. senegalensis* Bgp. The *bgp* cDNAs were obtained by a combination of RT-PCR and 5' RACE-PCR amplification. Numbering on right side corresponds to the nucleotides. Amino acid residues are

numbered according to the first residue of the mature protein and are shown above (for *D. rerio* Bgp) corresponding codon in the DNA sequence. The polyadenylation signals are underlined twice and the stop codons are identified by their three letter code. Conserved Cys residues are boxed. An asterisk is used to show identity between *D. rerio* Bgp and *S. senegalensis* Bgp amino acid sequences. The sequences used for constructing primers are underlined and marked by horizontal arrows next to the name of the primer. Presumed Gla residues are shown in bold (based in homology with other *bgp* sequences). A 16 (AC) repetitive motif on *D. rerio bgp* 3'-UTR region is marked between curved arrows.

Figure 3- *Danio rerio* and *Solea senegalensis mgp* cDNAs

Nucleotide sequence of the cDNAs encoding *D. rerio* and *S. senegalensis mgp*. *Danio rerio mgp* and *Solea senegalensis mgp* cDNA sequences were obtained by a combination of RT-PCR and 5' RACE-PCR amplification. Numbering and labeling as in Figure 2. Amino acid residues are numbered according to the first residue of the mature protein and are shown above the corresponding codon in the DNA sequence, for *D. rerio*. A 13 (GT) repetitive motif on *Danio rerio mgp* 3'-UTR region is marked between curved arrows.

Figure 4- *bgp* and *mgp* gene expression detected by real time PCR

Quantitative detection of *bgp* and *mgp* levels of mRNA transcripts throughout development in *D. rerio* and *S. senegalensis*. The relative expression levels determined with respect to the youngest stage analyzed are presented as bar graphs for *D. rerio* (A) and for *S. senegalensis* (B) using logarithmic scales.

Figure 5- *In situ* localization of *Danio rerio bgp* mRNA. *bgp* gene expression was detected by in situ hybridization in sections of zebrafish larvae collected at different ages and developmental stages.

A- *bgp* expression in the calcifying Meckel's cartilage (arrows) of an 11 dpf larvae (200x). B- Detection of *bgp* expression in a neural arch (arrowhead) at the beginning of formation at 11 dpf (1000x). C- At 13 dpf, *bgp* expression is detected in the branchial arches (BA) (arrowheads), Ceratobranchial (CB) and the calcifying preopercular bones (Pop) (arrow) (100x). D- At 20 dpf, *bgp* expression is detected in chondrocytes of the BOP (arrows) (1000x). E- Expression is visible in the mineralizing internal fin support skeleton, in this case the pterigophores (Pt) of the dorsal fin of a 24 dpf zebrafish (1000x). F- At 24 dpf *bgp* expression is strongly detected in the calcifying preopercular bones (arrows), branchial arches (arrowheads) and trabeculae (small arrow) (100x). G- *bgp* expression in the first vertebra forming over the notochord (arrow), just posterior to the BOP at 15 dpf (400x). H- Head of a 17 dpf larva with *bgp* expression detected in the branchial arches (BA), basioccipital process (BOP) and hyosympletic (Hs) (100x). I- Expression in the dorsal pterigophores (Pt) and distal radials (Dr) of a 20 dpf larvae (200x). J- Osteoblasts (arrow) expressing *bgp* in the mandibula of a 56 DAH juvenile sole (1000x). For other abbreviations see Figure 1.

Figure 6- *In situ* localization of *Danio rerio* and *Solea senegalensis mgp* mRNA. Sites of *mgp* gene expression were detected by in situ hybridization in sections of *D. rerio* larvae (A to L) and *S. senegalensis* larvae (M to O) collected at different ages and developmental stages.

A- *mgp* expression in the ethmoid plate of a 96 hpf larvae (arrow) (200x). B- Detection of *mgp* expression in chondrocytes from the trabecular cartilage (arrowhead) and

ceratobranchial arches from a 9 dpf larvae (arrows) (1000x). C- *mgp* expression in Meckel's cartilage (arrowheads) and quadrate (arrow) in a 9 dpf larvae (100x). D- Cartilage from the pectoral fin of a 10 dpf larvae showing *mgp* expression located within the chondrocytes (arrow). Note absence of signal in the cleithrum (asterisk) (1000x). E- In 13 dpf larvae, *mgp* expression in the ceratobranchials (arrows) and in the BOP (asterisk) (1000x). F- At 13 dpf, *mgp* expression was also evident in the hypertrophic chondrocytes from the Meckel's cartilage (arrowhead), quadrate (arrow) and in chondrocytes from the basibranchial cartilage (asterisk) (200x). G- *mgp* expression in a 16 dpf larvae, showing expression in chondrocytes from the BOP (arrowhead) (1000x). H- At 16 dpf, *mgp* expression is also detected in hypertrophic chondrocytes of the Meckel's cartilage (arrow), and in chondrocytes from the ethmoid plate (arrowheads) (1000x). I- 17 dpf larvae showing *mgp* expression in chondrocytes from the optic capsules (arrowheads) (1000x). J- *D. rerio* gill filaments showing *mgp* expression close to the plasma membrane in chondrocytes from the Zellknorpel (arrow) (1000x). K- *mgp* expression in endosteal cells surrounding the vertebral centra in a 25 dpf larvae (arrows) (1000x). L- *mgp* expression in chondrocytes from the pterigophores in a 25 dpf larvae (arrowheads). Note also the presence of fusiform cells surrounding the central core of a vertebra (arrow) (1000x). M- *mgp* expression at the branchial arches (arrowheads), trabecula (arrow) and hyosymplectic (asterisk) of a larval *S. senegalensis* at 11 dpf (200x). N- *mgp* expression (arrows) in the chodrocytes of the dorsal pterigophores in a 17 dpf *S. senegalensis* (500x). O- *mgp* gene expression in the vertebral cartilage of a 47 dpf *S. senegalensis* (1000x).

Figure 7- Immunohistochemical and immunofluorescent detection of Bgp accumulation in different developmental stages of *Danio rerio* (A-K) and *Solea senegalensis* (L-P).

A- Accumulation of Bgp in the teeth of branchial arch 5 (?Ba) and otolyth (Ot) of a 8 dpf *D. rerio* larvae (200x); counterstaining with toluidine blue. B- Accumulation of Bgp in the teeth of branchial arch 5, otolyth and cleithrum of a 9 dpf *D. rerio* larvae (400x).C- Accumulation of Bgp in Meckel's cartilage of a 13 dpf *D. rerio* larvae (1000x). D- Accumulation of Bgp is first detected in calcifying vertebra and haemal arches at 13 dpf (1000x). E- Accumulation of Bgp in the calcifying pectoral fin (F) and coracoscapular complex (Co) of *D. rerio* at 20 dpf (400x). Notice the accumulation at the periphery of the coracoid undergoing perichondral mineralization. F- Immunofluorescent detection of Bgp accumulation in the mineralizing urostile at 20 dpf (400x). G- Accumulation of Bgp in the vertebral column (V), neural arches (Na), neural spines (Ns) and haemal arches (Ha) at 20 dpf (200x). H- Bgp accumulation in the vertebral column, haemal arches and in the mineralizing matrix of hypural plates (Hy) of the caudal fin and in the mineralized fin rays of a 31 dpf *D. rerio* juvenile (100x). I- Accumulation of Bgp in a juvenile is detected in all the bones and calcifying cartilages of the head region, eg. supramaxilary (arrow) and associated bones, the ethmoid plate (arrowhead) and the supra orbital cartilage that surrounds the eye (100x). J- Accumulation of Bgp is widely detected by immunofluorescence in the branchial arches of a juvenile *D. rerio* (200x). K- Bgp accumulation in epithelial cells from some renal tubules of the kidney in juvenile zebrafish individuals (400x). L- Immunofluorescent detection of Bgp in the forming vertebra (Arrows) surrounding the notochord of a 15 dpf *S. senegalensis* larvae (400x). M- Detection of Bgp accumulation in the vertebra and parapophysis (Pp) of *S. senegalensis* at 25 dpf (M1 brightfield and M2 darkfield)

(250x). N- Accumulation of Bgp in the calcifying distal radials at 25 dpf. O- Bgp is strongly detected in the calcified branchial arches of a 41 dpf *S. senegalensis* juvenile (O1 bright field and O2 dark field) (250x). P- No staining observed in the head bones in a control with pre-immune serum of an 18 DAH larvae.

Figura 8- Immunohistochemical detection of Mgp accumulation in *Danio rerio* (A-I) and *Solea senegalensis* (J-L).

A- Accumulation of Mgp in the otolyth of a 6 dpf larvae (400x); B- Accumulation of Mgp in the otolyth and cleithrum at 8 dpf (400x); C- Consecutive section (to that in B) of the otolyth (arrowhead) and cleithrum (arrow) stained by Alizarin red and counterstained with toluidine blue (400x); D- Accumulation of Mgp at the zones initiating the mineralization of neural arches in pleural vertebrae 3-5 of a 13 dpf larva (1000x); E- Accumulation of Mgp in the mineralizing branchial arches and pharyngeal teeth at 13 dpf; F- Mgp accumulation in the otolyth, BOP and cranial cartilages (arrow) undergoing endochondral ossification at 20 dpf (1000x); G- Mgp accumulation in the forming caudal vertebra and associated arches at 20 dpf (250x); H- Mgp accumulation in the preopercular bones under endochondral ossification (arrows) in a 40 dpf juvenile (1000x); I- Mgp accumulation in skull bones undergoing intramembranous ossification (arrow) at 40 dpf (1000x); J- Mgp accumulation in the otic capsule (OC) of a 8 dpf Senegal sole (200x); K- Mgp accumulation in the mineralizing matrix under the trabecula (T) of a 17 dpf larva (400x); L- Mgp accumulation in the mineralizing branchial arches and pharyngeal teeth of a 26 dpf Senegal sole (200X), but also in the aorta and cardiac arterial bulbus (arrowhead). No staining was observed in control zebrafish vertebrae sections incubated with pre immune serum (results not shown).

Figure 9- Alkaline phosphatase and TRAP activity in the developing zebrafish and Senegal sole skeleton.

A- Alkaline phosphatase activity (in blue) detected in the forming vertebra (arrow) surrounding the notochord (No) of a zebrafish larva at 13 dpf (1000x). B- Alkaline phosphatase activity in observed the calcifying preopercular cartilage (PO) and in the intramembranous opercular bone (OP) (1000x) in zebrafish larvae at 17 dpf. C- Tartrate resistant acid phosphatase (TRAP) activity (in red) is detected in developing, partially calcified, branchial arches and pharyngeal teeth (Te) of a zebrafish at 17 dpf (1000x). D- TRAP activity in the intramembranously forming skull bones (1000x) of zebrafish at 26 dpf. A cell surrounded by TRAP activity is located in a resorption site (arrow). E- Alkaline phosphatase activity (blue) is detected in 17 dpf Senegal sole in the forming neural arches (1000x). F- TRAP activity (red) is detected surrounding the vertebra, arches and spines (arrows) in a 32 dpf Senegal sole (F).

Figure 10- Chromosomal localisation of zebrafish *mgp* and *bgp* using the LN54 panel.

mgp and *bgp* map on LG3, at 9.54cR from Z1209 and 3.87cR from Z15479 markers, respectively. Some synteny was observed between zebrafish LG3 and human chromosomes 1 and 12, as indicated by lines between syntenic homologues.

Figure 1
Click here to download high resolution image

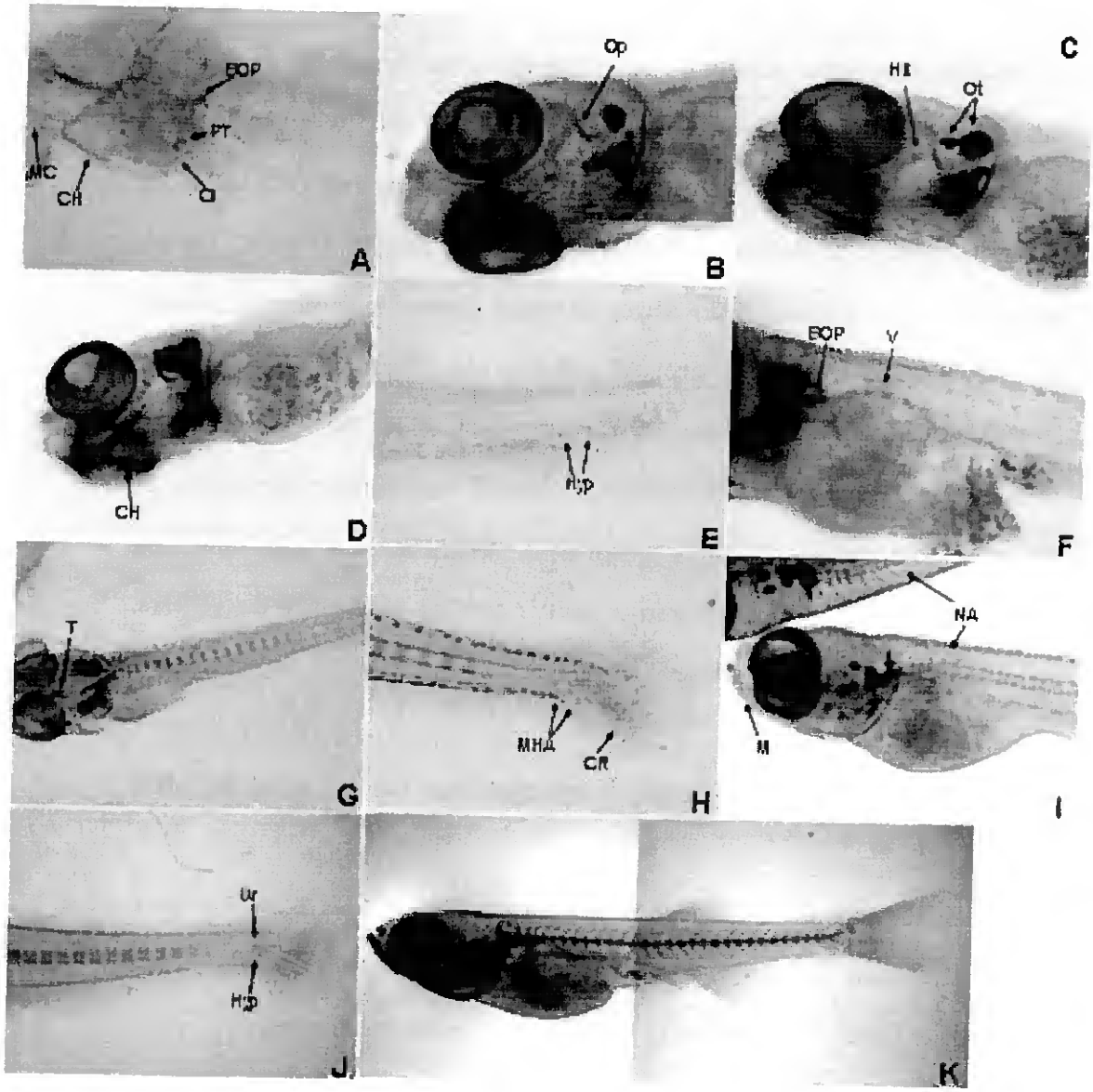

Figure 2

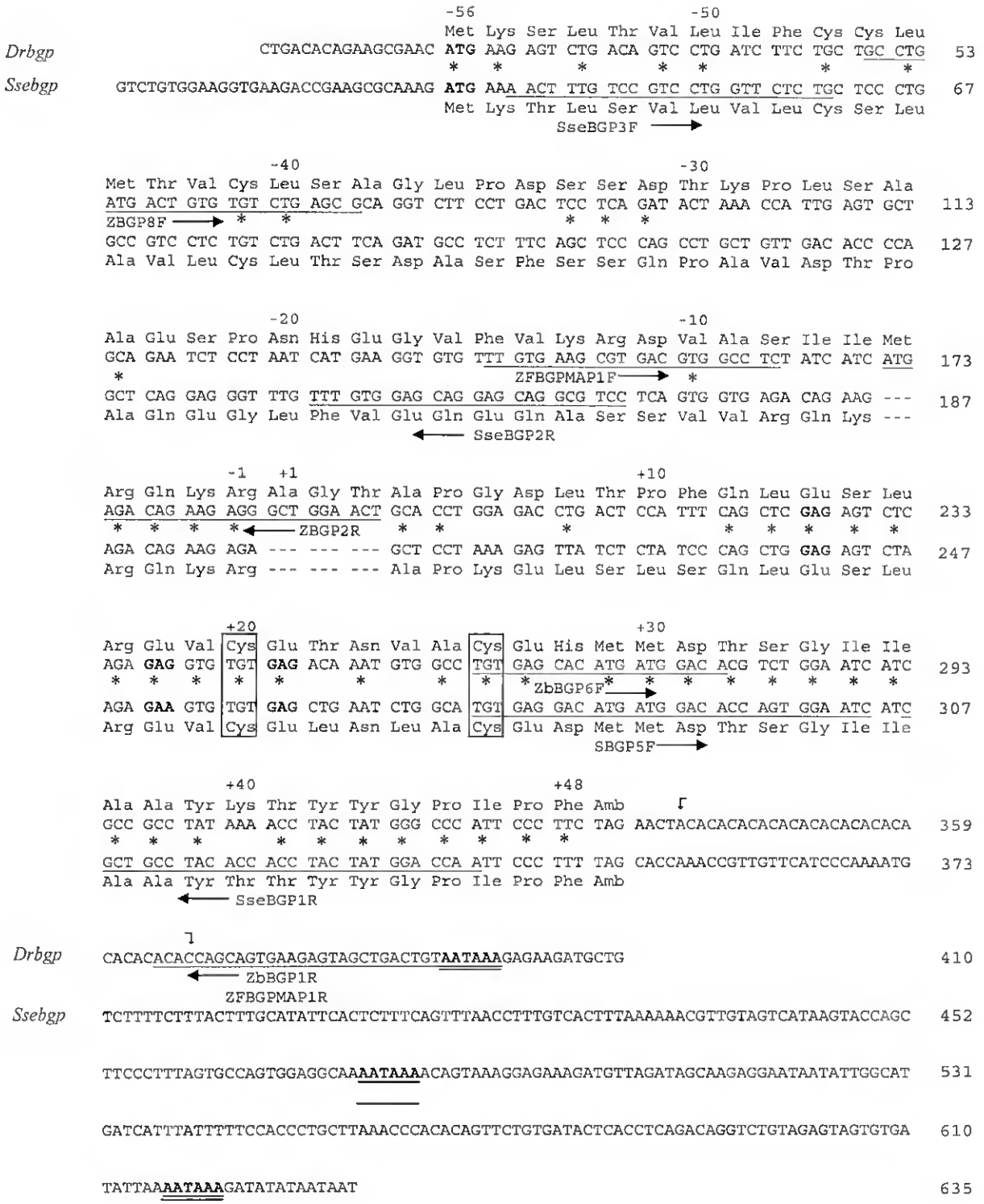
-56
-50
Met Lys Ser Leu Thr Val Leu Ile Phe Cys Cys Leu
Drbgp CTGACACAGAAGCGAAC ATG AAG AGT CTG ACA GTC CTG ATC TTC TGC TGC CTG 53
Ssebgp GTCTGTGGAAGGTGAAGACCGAAGCGCAAAG ATG AAA ACT TTG TCC GTC CTG GTT CTC TGC TCC CTG 67
Met Lys Thr Leu Ser Val Leu Val Leu Cys Ser Leu
SseBGP3F
-40
-30
Met Thr Val Cys Leu Ser Ala Gly Leu Pro Asp Ser Ser Asp Thr Lys Pro Leu Ser Ala
ATG ACT GTG TGT CTG AGC GCA GGT CTT CCT GAC TCC TCA GAT ACT AAA CCA TTG AGT GCT 113
ZBGP8F
GCC GTC CTC TGT CTG ACT TCA GAT GCC TCT TTC AGC TCC CAG CCT GCT GTT GAC ACC CCA 127
Ala Val Leu Cys Leu Thr Ser Asp Ala Ser Phe Ser Ser Gln Pro Ala Val Asp Thr Pro
-20
-10
Ala Glu Ser Pro Asn His Glu Gly Val Phe Val Lys Arg Asp Val Ala Ser Ile Ile Met
GCA GAA TCT CCT AAT CAT GAA GGT GTG TTT GTG AAG CGT GAC GTG GCC TCT ATC ATC ATG 173
ZFBGPMAP1F
GCT CAG GAG GGT TTG TTT GTG GAG CAG GAG CAG GCG TCC TCA GTG GTG AGA CAG AAG --- 187
Ala Gln Glu Gly Leu Phe Val Glu Gln Glu Gln Ala Ser Ser Val Val Arg Gln Lys ---
SseBGP2R
-1 +1
+10
Arg Gln Lys Arg Ala Gly Thr Ala Pro Gly Asp Leu Thr Pro Phe Gln Leu Glu Ser Leu
AGA CAG AAG AGG GCT GGA ACT GCA CCT GGA GAC CTG ACT CCA TTT CAG CTC GAG AGT CTC 233
ZBGP2R
AGA CAG AAG AGA --- --- --- GCT CCT AAA GAG TTA TCT CTA TCC CAG CTG GAG AGT CTA 247
Arg Gln Lys Arg --- --- --- Ala Pro Lys Glu Leu Ser Leu Ser Gln Leu Glu Ser Leu
+20
+30
Arg Glu Val Cys Glu Thr Asn Val Ala Cys Glu His Met Met Asp Thr Ser Gly Ile Ile
AGA GAG GTG TGT GAG ACA AAT GTG GCC TGT GAG CAC ATG ATG GAC ACG TCT GGA ATC ATC 293
ZbBGP6F
AGA GAA GTG TGT GAG CTG AAT CTG GCA TGT GAG GAC ATG ATG GAC ACC AGT GGA ATC ATC 307
Arg Glu Val Cys Glu Leu Asn Leu Ala Cys Glu Asp Met Met Asp Thr Ser Gly Ile Ile
SBGP5F
+40
+48
Ala Ala Tyr Lys Thr Tyr Tyr Gly Pro Ile Pro Phe Amb
GCC GCC TAT AAA ACC TAC TAT GGG CCC ATT CCC TTC TAG AACTACACACACACACACACACACA 359
GCT GCC TAC ACC ACC TAC TAT GGA CCA ATT CCC TTT TAG CACCAAACCGTTGTTCATCCCAAAATG 373
Ala Ala Tyr Thr Thr Tyr Tyr Gly Pro Ile Pro Phe Amb
SseBGP1R
Drbgp CACACACACCAGCAGTGAAGAGTAGCTGACTGTAATAAAGAGAAGATGCTG 410
ZbBGP1R
ZFBGPMAP1R
Ssebgp TCTTTTCTTTACTTTGCATATTCACTCTTTCAGTTTAACCTTTGTCACTTTAAAAAACGTTGTAGTCATAAGTACCAGC 452
TTCCCTTTAGTGCCAGTGGAGGCAAAATAAAACAGTAAAGGAGAAAGATGTTAGATAGCAAGAGGAATAATATTGGCAT 531
GATCATTTATTTTTCCACCCTGCTTAAACCCACACAGTTCTGTGATACTCACCTCAGACAGGTCTGTAGAGTAGTGTGA 610
TATTAAAATAAAGATATATAATAAT 635

Figure 3

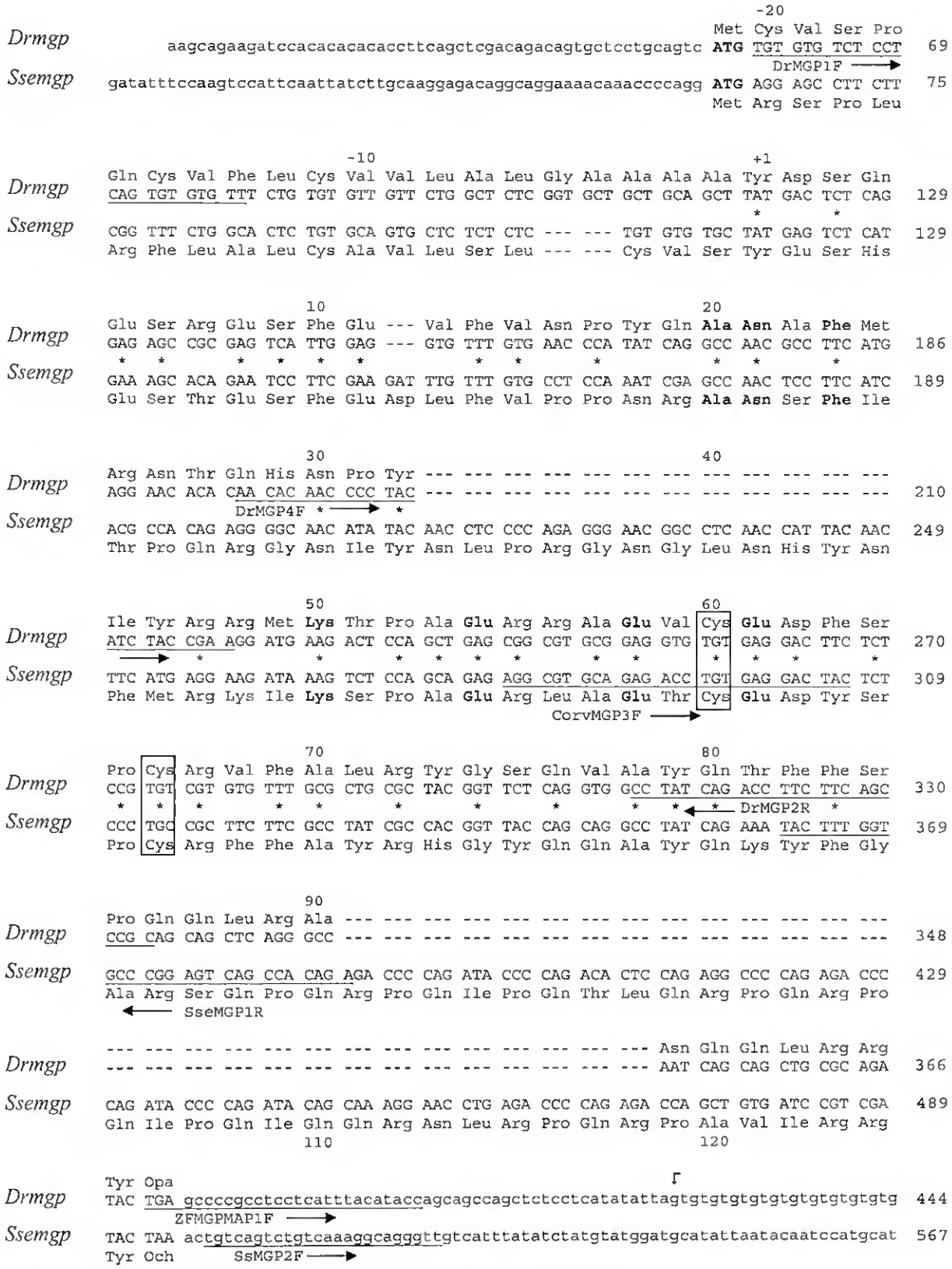
-20
Drmgp
Met Cys Val Ser Pro
aagcagaagatccacacacacaccttcagctcgacagacagtgctcctgcagtc ATG TGT GTG TCT CCT 69
DrMGP1F
Ssemgp
gatatttccaagtccattcaattatcttgcaaggagacaggcaggaaaacaaaccccagg ATG AGG AGC CTT CTT 75
Met Arg Ser Pro Leu
-10
+1
Gln Cys Val Phe Leu Cys Val Val Leu Ala Leu Gly Ala Ala Ala Ala Tyr Asp Ser Gln
Drmgp
CAG TGT GTG TTT CTG TGT GTT GTT CTG GCT CTC GGT GCT GCT GCA GCT TAT GAC TCT CAG 129
Ssemgp
CGG TTT CTG GCA CTC TGT GCA GTG CTC TCT CTC --- --- TGT GTG TGC TAT GAG TCT CAT 129
Arg Phe Leu Ala Leu Cys Ala Val Leu Ser Leu --- --- Cys Val Ser Tyr Glu Ser His
10
20
Glu Ser Arg Glu Ser Phe Glu --- Val Phe Val Asn Pro Tyr Gln Ala Asn Ala Phe Met
Drmgp
GAG AGC CGC GAG TCA TTG GAG --- GTG TTT GTG AAC CCA TAT CAG GCC AAC GCC TTC ATG 186
Ssemgp
GAA AGC ACA GAA TCC TTC GAA GAT TTG TTT GTG CCT CCA AAT CGA GCC AAC TCC TTC ATC 189
Glu Ser Thr Glu Ser Phe Glu Asp Leu Phe Val Pro Pro Asn Arg Ala Asn Ser Phe Ile
30
40
Arg Asn Thr Gln His Asn Pro Tyr --- --- --- --- --- --- --- --- --- --- --- ---
Drmgp
AGG AAC ACA CAA CAC AAC CCC TAC --- --- --- --- --- --- --- --- --- --- --- --- 210
DrMGP4F
Ssemgp
ACG CCA CAG AGG GGC AAC ATA TAC AAC CTC CCC AGA GGG AAC GGC CTC AAC CAT TAC AAC 249
Thr Pro Gln Arg Gly Asn Ile Tyr Asn Leu Pro Arg Gly Asn Gly Leu Asn His Tyr Asn
50
60
Ile Tyr Arg Arg Met Lys Thr Pro Ala Glu Arg Arg Ala Glu Val Cys Glu Asp Phe Ser
Drmgp
ATC TAC CGA AGG ATG AAG ACT CCA GCT GAG CGG CGT GCG GAG GTG TGT GAG GAC TTC TCT 270
Ssemgp
TTC ATG AGG AAG ATA AAG TCT CCA GCA GAG AGG CGT GCA GAG ACC TGT GAG GAC TAC TCT 309
Phe Met Arg Lys Ile Lys Ser Pro Ala Glu Arg Leu Ala Glu Thr Cys Glu Asp Tyr Ser
CorvMGP3F
70
80
Pro Cys Arg Val Phe Ala Leu Arg Tyr Gly Ser Gln Val Ala Tyr Gln Thr Phe Phe Ser
Drmgp
CCG TGT CGT GTG TTT GCG CTG CGC TAC GGT TCT CAG GTG GCC TAT CAG ACC TTC TTC AGC 330
DrMGP2R
Ssemgp
CCC TGC CGC TTC TTC GCC TAT CGC CAC GGT TAC CAG CAG GCC TAT CAG AAA TAC TTT GGT 369
Pro Cys Arg Phe Phe Ala Tyr Arg His Gly Tyr Gln Gln Ala Tyr Gln Lys Tyr Phe Gly
90
Pro Gln Gln Leu Arg Ala --- --- --- --- --- --- --- --- --- --- --- --- --- ---
Drmgp
CCG CAG CAG CTC AGG GCC --- --- --- --- --- --- --- --- --- --- --- --- --- --- 348
Ssemgp
GCC CGG AGT CAG CCA CAG AGA CCC CAG ATA CCC CAG ACA CTC CAG AGG CCC CAG AGA CCC 429
Ala Arg Ser Gln Pro Gln Arg Pro Gln Ile Pro Gln Thr Leu Gln Arg Pro Gln Arg Pro
SseMGP1R
--- --- --- --- --- --- --- --- --- --- --- --- --- --- --- Asn Gln Gln Leu Arg Arg
Drmgp
--- --- --- --- --- --- --- --- --- --- --- --- --- --- --- AAT CAG CAG CTG CGC AGA 366
Ssemgp
CAG ATA CCC CAG ATA CAG CAA AGG AAC CTG AGA CCC CAG AGA CCA GCT GTG ATC CGT CGA 489
Gln Ile Pro Gln Ile Gln Gln Arg Asn Leu Arg Pro Gln Arg Pro Ala Val Ile Arg Arg
110
120
Tyr Opa
Drmgp
TAC TGA gccccgcctcctcatttacataccagcagccagctctcctcatatattagtgtgtgtgtgtgtgtgtgtg 444
ZFMGPMAP1F
Ssemgp
TAC TAA actgtcagtctgtcaaaggcagggttgtcatttatatctatgtatggatgcatattaatacaatccatgcat 567
Tyr Och
SsMGP2F

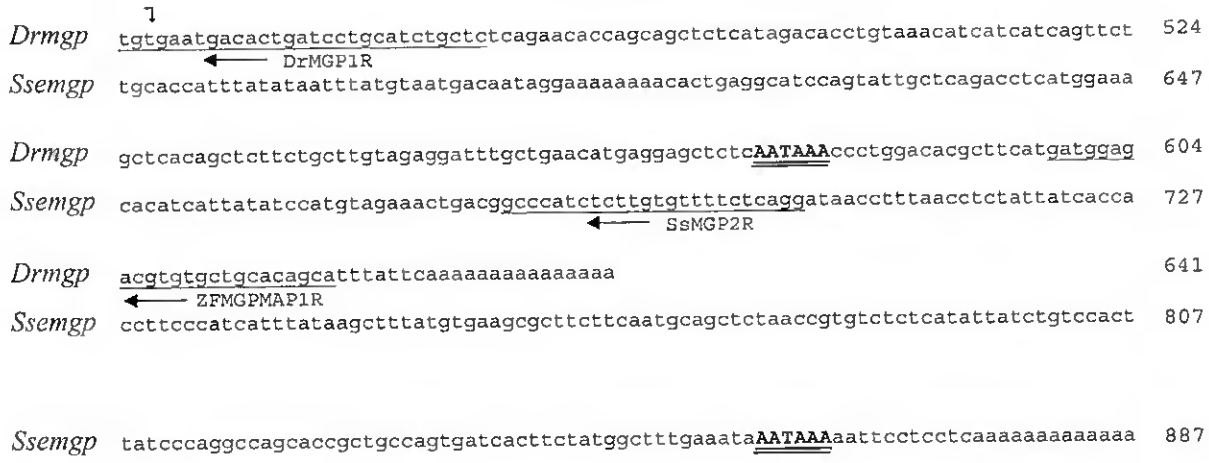
Drmgp
tgtgaatgacactgatcctgcatctgctctcagaacaccagcagctctcatagacacctgtaaacatcatcatcagttct 524
DrMGP1R
Ssemgp
tgcaccatttatataatttatgtaatgacaataggaaaaaaaacactgaggcatccagtattgctcagacctcatggaaa 647
Drmgp
gctcacagctcttctgcttgtagaggatttgctgaacatgaggagctctcAATAAAccctggacacgcttcatgatggag 604
Ssemgp
cacatcattatatccatgtagaaactgacggcccatctcttgtgttttctcaggataacctttaacctctattatcacca 727
SsMGP2R
Drmgp
acgtgtgctgcacagcatttattcaaaaaaaaaaaaaaa 641
ZFMGPMAP1R
Ssemgp
ccttcccatcatttataagctttatgtgaagcgcttcttcaatgcagctctaaccgtgtctctcatattatctgtccact 807
Ssemgp
tatcccaggccagcaccgctgccagtgatcacttctatggctttgaaataAATAAAaattcctcctcaaaaaaaaaaaaa 887

Figure 4
Click here to download high resolution image

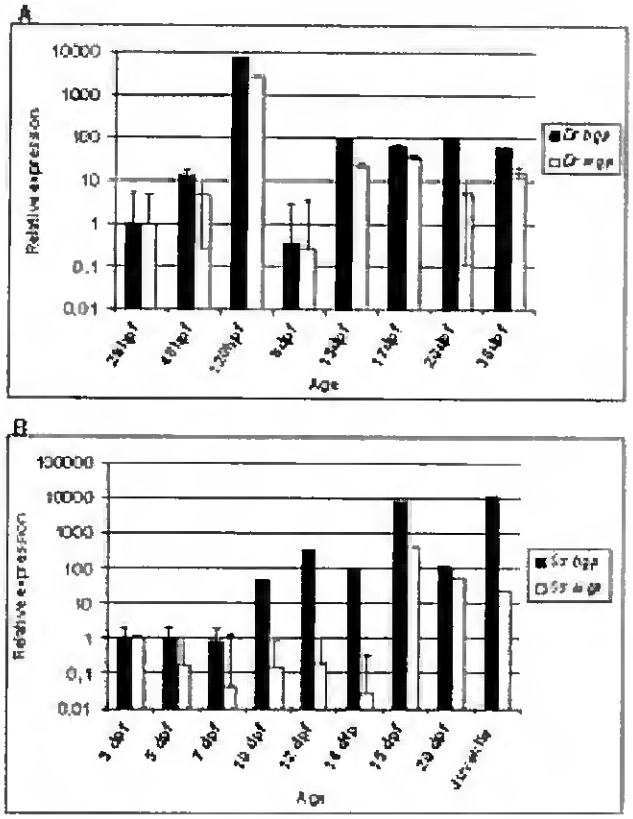

Figure 5
Click here to download high resolution image

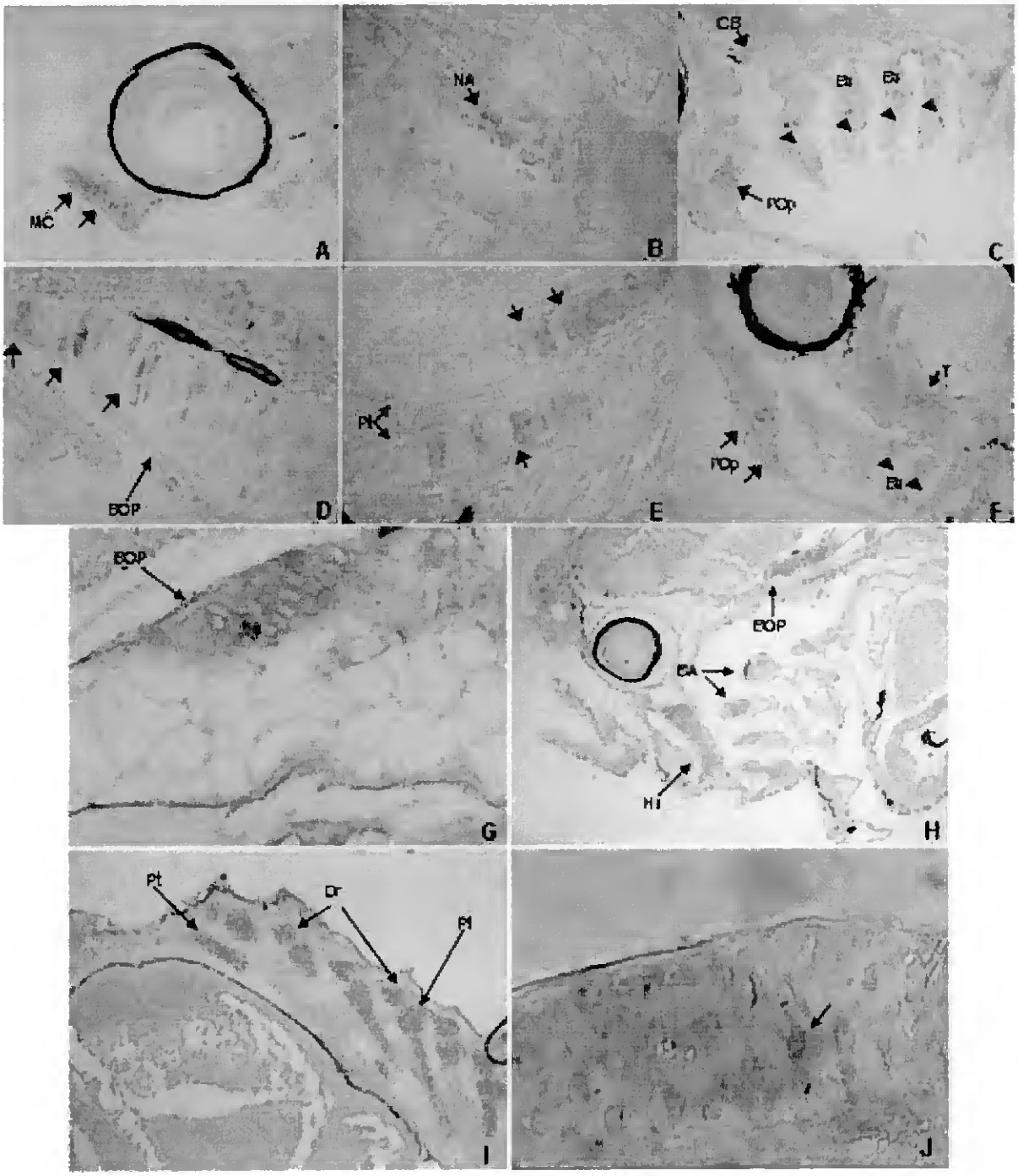

Figure 6
Click here to download high resolution image

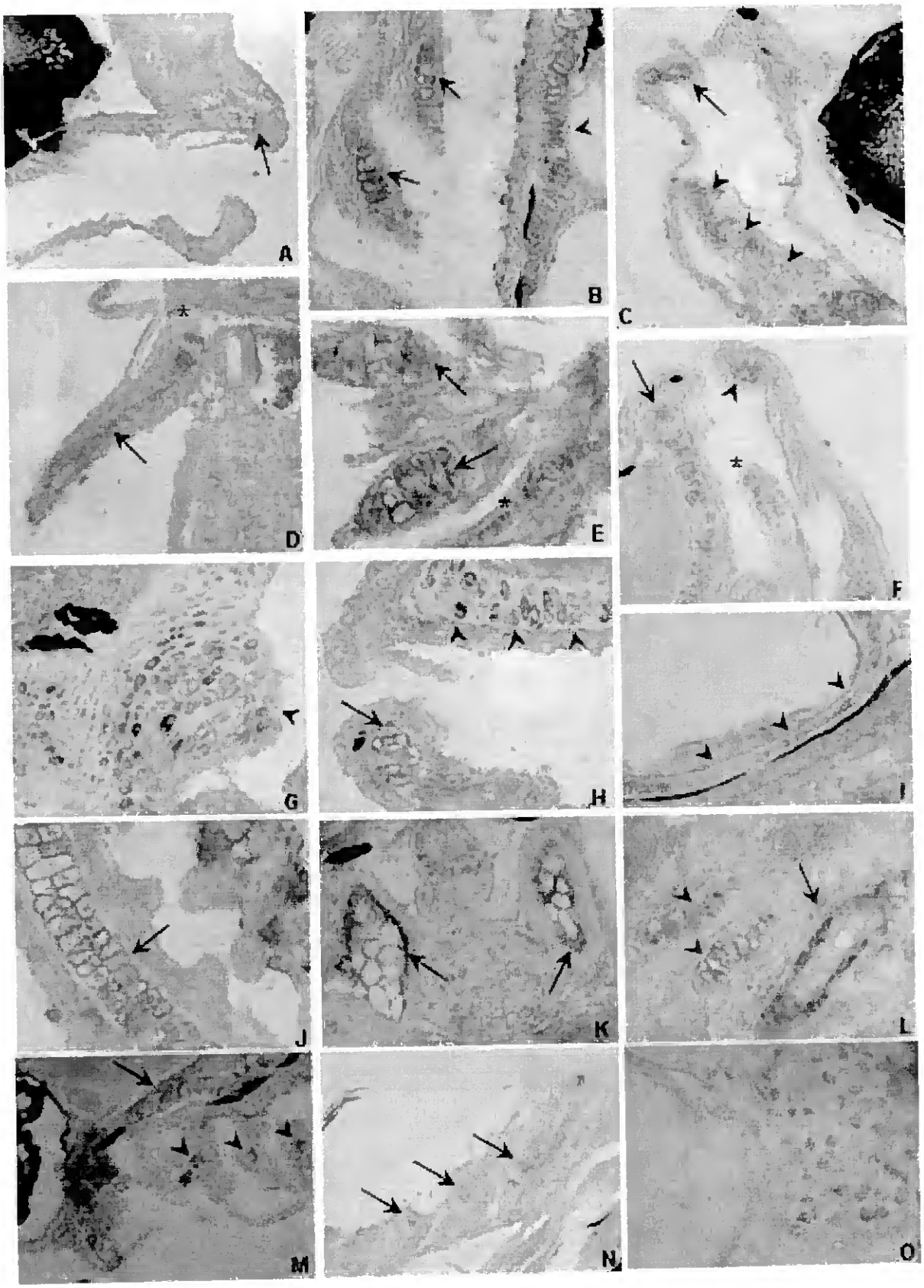

Figure 7
Click here to download high resolution image

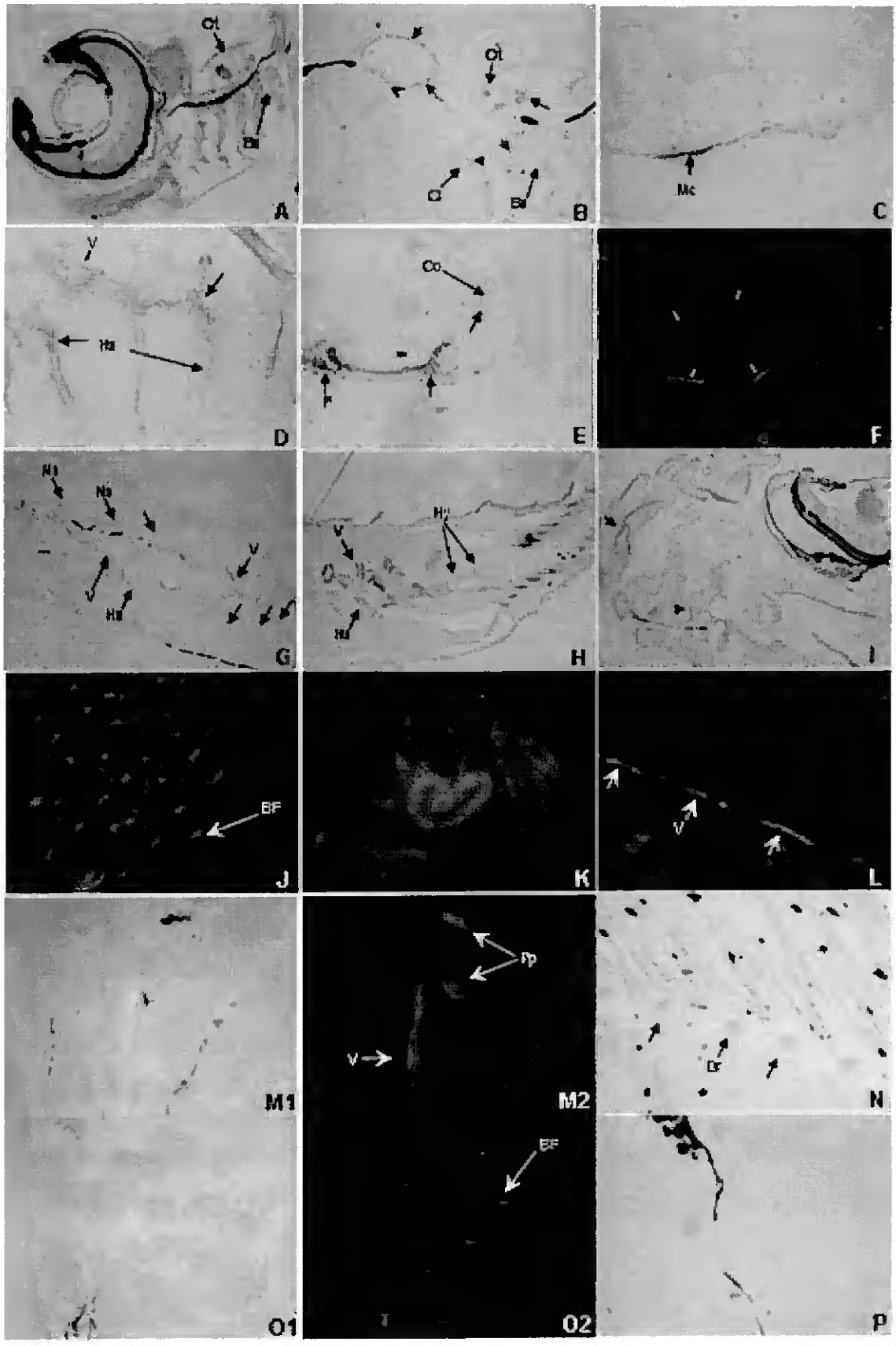

Figure 8
Click here to download high resolution image

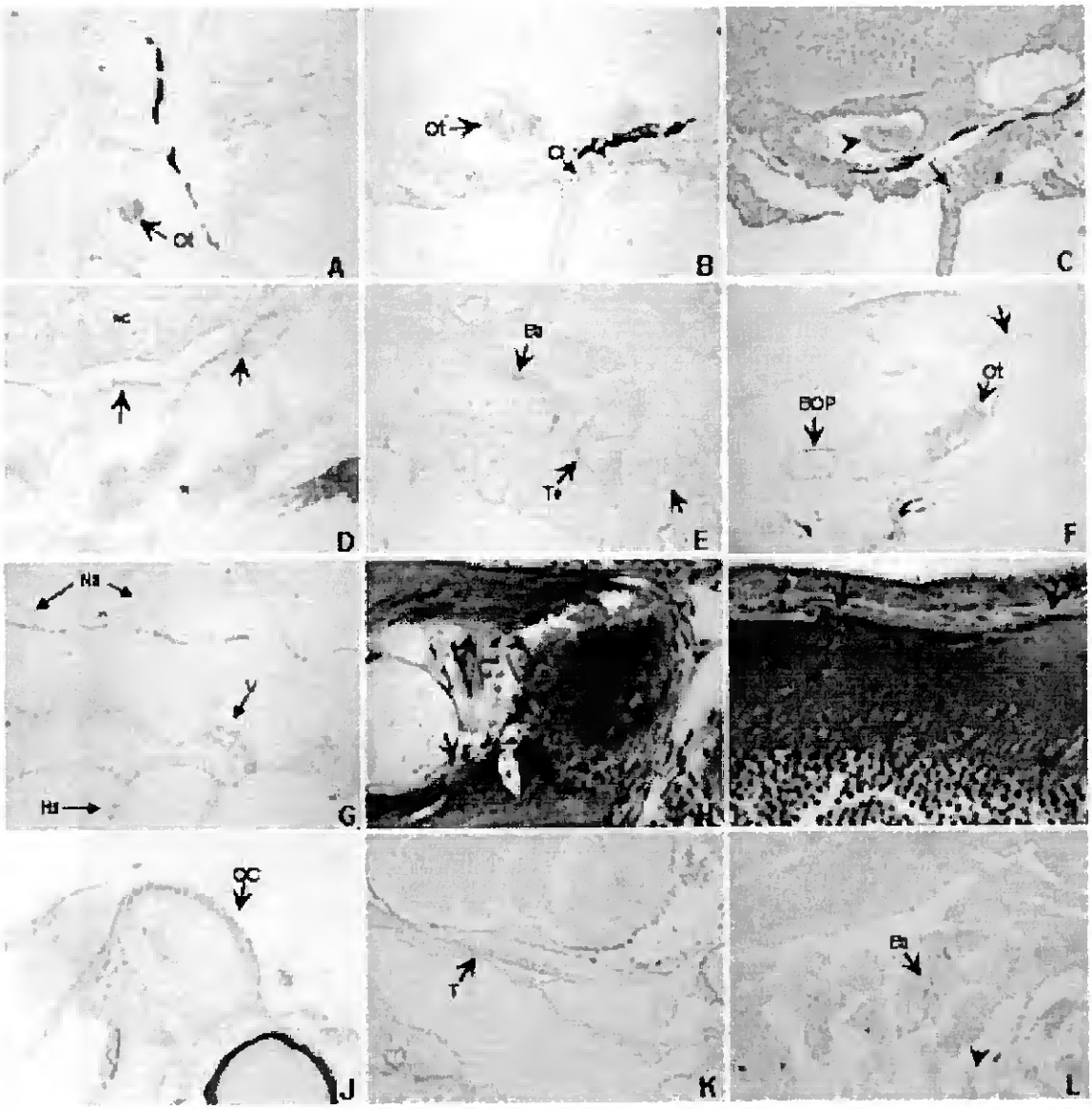

Figure 9
Click here to download high resolution image

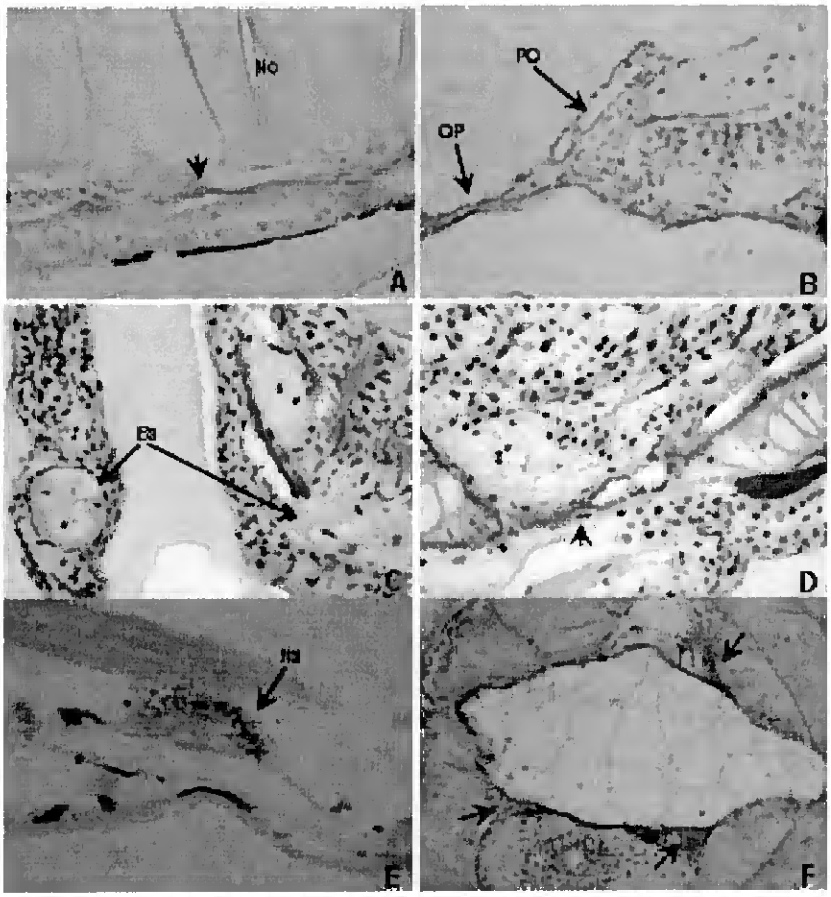

Figure 10

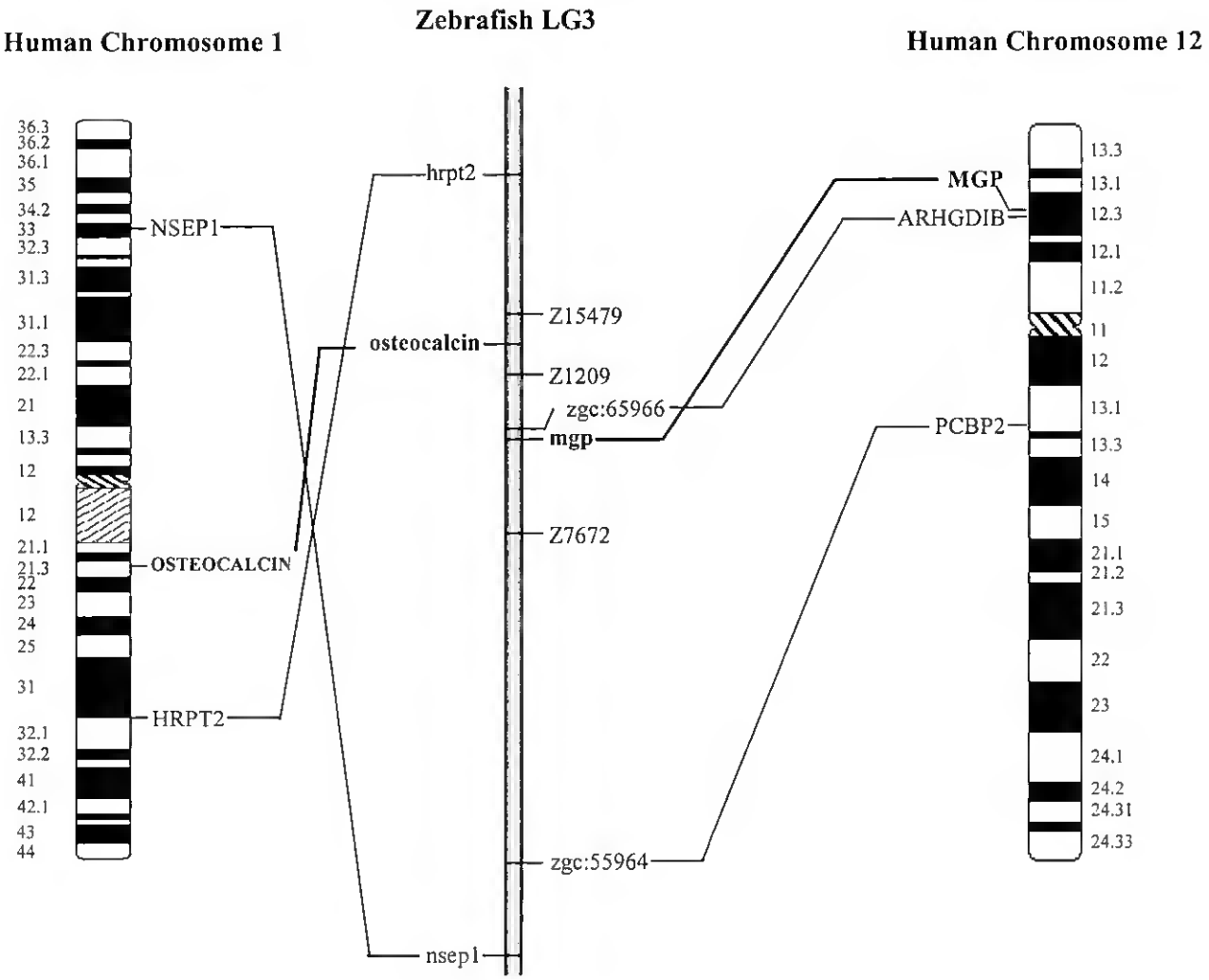
Zebrafish LG3
Human Chromosome 1
Human Chromosome 12
36.3
36.2
36.1
35
34.2
33
32.3
31.3
31.1
22.3
22.1
21
13.3
12
12
21.1
21.3
22
23
24
25
31
32.1
32.2
41
42.1
43
44
NSEP1
OSTEOCALCIN
HRPT2
hrpt2
osteocalcin
nsep1
Z15479
Z1209
zgc:65966
mgp
Z7672
zgc:55964
MGP
ARHGDIB
PCBP2
13.3
13.1
12.3
12.1
11.2
11
12
13.1
13.3
14
15
21.1
21.2
21.3
22
23
24.1
24.2
24.31
24.33

Table 1

Table 1- Sequences for the primers used in this article.

Amplified cDNA	Primer name	Primer Sequence [a]	Base origin
Dr bgp	ZbBGP 6F [b]	TGYGARCAYATGGCNGAYAC	261
Dr bgp	ZbBGP1R	ACAGTCAGCTACTCTTCACTGCTGGTGTG	398
Dr bgp	ZBGP8F	GCCTGATGACTGTGTGTCTGAGCG	49
Dr bgp	ZBGP2R	AGTTCCAGCCCTCTTCTGTCTCAT	194
Dr bgp	ZFBGPMAP1F	TTGTGAAGCGTGACGTGGCCTC	141
Dr bgp	ZFBGPMAP1R	ACAGTCAGCTACTCTTCACTGCTGG	398
Dr mgp	DrMGP1F	TGTGTGTCTCCTCAGTGTGTGTT	58
Dr mgp	DrMGP1R	GAGCAGATGCAGGATCAGTGTCATTCACA	473
Dr mgp	DrMGP4F	AACACAACCCCTACATCTACCGAA	197
Dr mgp	DrMGP2R	GCGGGCTGAAGAAGGTCTGATAGG	334
Dr mgp	ZFMGPMAP1F	TGAGCCCCGCCTCCTCATTTACATACC	370
Dr mgp	ZFMGPMAP1R	TGCTGTGCAGCACACGTCTCCATC	621
Sse bgp	SBG5F	TGTGAGCACATGATGGATACGGAGGGAATC	275
Sse bgp	SseBGP1R	TTGGTCCATAGTAGGTGGTGTAGGCAGCG	335
Sse bgp	SsBGP3F	AACTTTGTCCGTCCTGGTTCTCTG	37
Sse bgp	SsBGP2R	GGACGCCTGCTCCTGCTCCACAAA	166
Sse mgp	CorvMGP3F	AGGCGTGCAGAGACCTGCGAGGACTAT	280
Sse mgp	SseMGP1R	TCTGTGGCTGACTCCGGGCACCAAAGTA	388
Sse mgp	SsMGP2F	TGTCAGTCTGTCAAAGGCAGGGTT	497
Sse mgp	SsMGP2R	CCTGAGAAAACACAAGAGATGGGC	701
Sse β-actin	SsACT1F	GACACTGACATCCGCCAAGACCT	60
Sse β-actin	SsACT1R	CTGCTGGAAGGTGGACAGGGAGG	270
Dr18S Ribosomal [c]	Dr28SRib1F	TCGGTCCTAAGGGATGGG	534
Dr18S Ribosomal [c]	Dr28SRib1R	CCGGGTTGGTTTGCGTCA	691
	Universal adapter	ACGCGTCGACCTCGAGATCGATG	

[a] All sequences are described in the 5' to 3'direction.

[b] Y, pyrimidine; R, purine; N, G + a + T + c.

[c] Based on the available partial sequence for *Danio rerio* 28S ribosomal RNA gene (AF398343)

Table 2

Table 2- Summarized information on the development of skeletal structures of *Danio rerio* with times of cartilaginous appearance, mineralization and detection of *mgp* and *bgp* by *in situ* hybridization (—) and immunolocalization(···). Age is expressed in days post fertilization (dpf).

Structure	Age (DPF)	0 1 2 3 4 5 6 7 8 9 10 11 12 13 14 15 16 17 18 19 20 21 22 23 24 25 26 27 28 29 30 31 32 33 34
Otolith	Cartilage	
	Calcium	
	MGP	·····
	BGP	·····
Branchial arches	Cartilage	
	Calcium	
	MGP	·····
	BGP	·····
Basioccipital articulatory process	Cartilage	
	Calcium	
	MGP	·····
	BGP	·····
Cleithrum	Cartilage	
	Calcium	
	MGP	
	BGP	
Vertebrae and arches	Cartilage	
	Calcium	
	MGP	·····
	BGP	·····
Hypurals	Cartilage	
	Calcium	
	MGP	
	BGP	·····

Table 3

Table 3- Summarized information on the development of skeletal structures of *Solea senegalensis* with times of cartilaginous appearance, mineralization and detection of *mgp* and *bgp* by *in situ* hybridization (▬) and immunolocalization(▪▪▪▪). Age is expressed in days post fertilization (dpf).

Structure	Age (DPF)	0	1	2	3	4	5	6	7	8	9	10	11	12	13	14	15	16	17	18	19	20	21	22	23	24	25	26	27	28	29	30	31	32	33	34
Otolith	Cartilage																																			
	Calcium																																			
	MGP																																			
	BGP																																			
Basioccipital articulatory process	Cartilage																																			
	Calcium																																			
	MGP																																			
	BGP																																			
Cleithrum	Cartilage																																			
	Calcium																																			
	MGP																																			
	BGP																																			
Vertebrae and arches	Cartilage																																			
	Calcium																																			
	MGP																																			
	BGP																																			
Hypurals	Cartilage																																			
	Calcium																																			
	MGP																																			
	BGP